NASA CR 174993

NASA

LARGE SCALE PROP-FAN STRUCTURAL DESIGN STUDY

Volume II
Preliminary Design of SR-7

By: L.C. Billman et al

HAMILTON STANDARD DIVISION
UNITED TECHNOLOGIES

Prepared for
National Aeronautics and Space Administration
NASA-Lewis Research Center
Contract NAS3-22394

CONTENTS

CONTENTS (Continued)

CONTENTS (Continued)

ILLUSTRATIONS

ILLUSTRATIONS (Continued)

ILLUSTRATIONS (Continued)

ILLUSTRATIONS (Continued)

TABLES

SUMMARY

Hamilton Standard, under contract to NASA/Lewis, has conducted the effort to analyze, evaluate and provide structural designs for several advanced propeller configurations. In addition, aeromechanical design requirements were established, blade fabrication concepts were screened, the feasibility of designing a dynamic model was established, the adequacy of current design and fabrication techniques was assessed and a preliminary design of SR-7 established. The specific tasks which were accomplished are:

- A Design Requirements Document which contains the critical operation conditions, was generated for use in the structural design analysis and dynamic model feasibility analysis tasks;
- A Blade Design Concept Definition Document, which defines the blade fabrication concepts for use in the structural design analysis, was generated;
- A Structural Design Analysis was conducted for six blade configuration-fabrication concept combinations. The analysis evaluated stress, deflection, resonant frequency, stall and classical flutter, and FOD;
- The feasibility of designing a dynamic model of a full-size blade configuration was established;
- Based on the structural design analysis task, those items which were unproven or beyond the state-of-the-art were assessed and identified and a technology development plan was prepared;
- The preliminary design of an advanced propeller for turboprop aircraft applications with design cruise speeds of Mach 0.7 to 0.8 was established. This task included: the review of related studies, analyses, and test efforts; an industry survey; a large-scale Prop-Fan preliminary design analysis; the design analysis of a 9-foot diameter Prop-Fan blade and preliminary design of a 14-foot diameter blade.

Volume I of this report covers the effort through the preparation of the technology development plan and Volume II covers the preliminary design of an advanced propeller.

INTRODUCTION

In recent years, considerable attention has been directed toward improving aircraft fuel consumption. Studies have shown that the inherent efficiency advantage that turboprop propulsion systems have demonstrated at lower cruise speeds may now be extended to the higher speed of today's turbofan and turbojet-powered aircraft. To achieve this goal, new propeller designs which feature more blades with thin airfoils and aerodynamic sweep are required.

Since 1975, Hamilton Standard has been deeply involved with the NASA Lewis Research Center in the development of the advanced turboprop or Prop-Fan. Many aircraft system studies have been accomplished for a variety of subsonic air transport applications, and all these studies have shown significant fuel savings with Prop-Fan propulsion. The fuel savings potential of future Prop-Fan powered aircraft is generally 15-20% for commercial applications and 25-35% for military patrol aircraft compared to equal technology turbofan systems, depending upon the specific application, cruise speed, stage length and other requirements.

To date, several small-scale, 0.6223 meter (24.5 inch) diameter models have been designed, manufactured and subjected to a number of tests. Tests have been conducted in both UTRC and NASA wind tunnels and on a modified NASA airplane. These tests have shown that propellers with 8-10 swept blades, high tip speeds and high power loadings can offer increased fuel efficiencies at speeds up to 0.8 Mn.

The purpose of this program was to establish full size structural concepts for such blades; to define their structural properties; to identify any new design, analysis, or fabrication techniques which would be required; to determine the structural trade-offs involved with several blade shapes; to establish the feasibility of fabricating dynamically scaled models of blades for aeroelastic testing and to establish the preliminary design of an advanced propeller for turboprop aircraft applications with design cruise speeds of 0.7 to 0.8 Mn.

The blade configurations for which large-scale designs would be developed in this study were specified at the onset to be SR-2 (8-way), SR-3 (8-way), a 10-way version of SR-3 (same geometry with the chord reduced by the ratio 8/10), and SR-5. The SR-2, SR-3 (8-way), and SR-5 configurations had all been designed and built as models for wind tunnel testing.

Later, the preliminary design of a new configuration, designated SR-7, was developed utilizing the initial results of this study along with other related test and analysis efforts to date. It was intended that the SR-7 design would be built in large-scale (9 ft. diameter) for later ground and flight research tests. The results of the initial design study of the SR-2, SR-3, and SR-5 configurations are covered in Volume I (CR174992) of this report and the preliminary design of SR-7 is covered in Volume II (CR174993).

8.0 TASK VII - PRELIMINARY DESIGN OF SR-7

8.1 DESIGN INPUT PARAMETER SELECTION

8.1.1 Introduction

This effort included the following tasks:

- Review of related studies, analyses and test efforts, an industry study, a trade-off study, a definition of the design requirements,
- Definition of the input for structural design,
- Documentation of the selected design.

The following sections describe these tasks.

8.2 REVIEW OF RELATED STUDIES, ANALYSES AND TEST EFFORTS

8.2.1 Aerodynamic/Acoustic

A number of reports and oral briefings on the studies, analyses and test efforts related to the application of Prop-Fans for high speed airplanes were reviewed. These reports and oral briefings are listed as References 1 through 24. The material was reviewed to assist in the selection of an optimum Prop-Fan configuration from the viewpoints of high efficiency, low noise, high reliability and ease of manufacture. This effort and the aerodynamic, acoustic and structural tradeoff studies reported herein were used to establish a Prop-Fan configuration for a hypothetical airplane application.

The Boeing, Douglas and Lockheed companies conducted several studies respectively (references 1-4, 6-10). These studies showed that Prop-Fan powered airplanes had significant direct operating cost (DOC) and fuel burned reductions relative to turbo-fan powered airplanes. These studies made use of the Hamilton Standard Prop-Fan performance, noise level, maintenance cost and weight data packages (references 12 and 13). Each successive data package, including report SP04A80 (reference 14), published in 1980, incorporates refinements reflecting experience gained through model tests and method development which have occurred over the past six years. Even though the data package performance and noise levels have undergone refinements, the accompanying changes in cabin acoustic treatment and installation losses have resulted in very small changes in fuel burn and DOC (reference 4), relative to estimates using earlier data packs.

Most of the airplanes in the referenced reports cruise at 0.80 Mach number and at an altitude of at least 9144M (30,000 ft.). The airplane benefits afforded by Prop-Fans as compared to turbo-fan propulsion systems range between 6% and 33% improvements in fuel burn and 5% to 15% improvements in direct operating cost. The transport airplanes studied vary between 45,360 Kg (100,000 pounds), 92 passengers to nearly 136,000 Kg (300,000 pounds), 200 passengers. The lower level of improvements were obtained in the Boeing RECAT (Reference 2) study. The smaller benefits were largely due to more conservative estimations of the installed aerodynamic losses and near field noise levels with the Prop-Fan propulsion systems.

The referenced reports generally showed that even larger fuel savings could be achieved with both lower cruise Mach numbers and shorter stage lengths. For example in the DC-9 feasibility study (Reference 8), 0.75 was shown to be the optimum cruise Mach number. The reported DOC Improvements were predominantly reported for fuel prices of 30 and 60 cents per gallon, which are quite low compared to today's prices. The 5% to 15% DOC improvements were reported for the higher fuel price and were at least 2% (two percentage units) higher than with fuel priced at 30 cents per gallon. It was evident that the DOC improvement with Prop-Fans would increase with escalating aviation fuel prices. Since it was also shown (Reference 1) that the optimum cruise Mach number decreased with increasing fuel prices, the advantage of the Prop-Fan would be further increased.

The referenced material helped in the selection of optimum Prop-Fan design parameters in that it linked performance, noise, weight and costs with full scale airplane economy and fuel efficiency. In most instances, the reports (References 4, 6 and 8) showed that practical variations in power loading, tip speed and number of blades had relatively small effects on DOC and fuel burn. This allows the Prop-Fan designer considerable latitude in tailoring full scale Prop-Fans for each airplane and mission.

The amount of blade tip sweep, however, can have a potentially larger effect on the benefits. That is, should the structural integrity of the selected Prop-Fan require a significant reduction in sweep, both the performance and the noise levels would be adversely affected. Experience has shown that the highly swept (48° tip sweep), 10 blade, SR-5 Prop-Fan model (Reference 22) required geometric changes to improve its structural integrity. The changes required for acceptable structure (reduced sweep for example) and their effect on aerodynamic and acoustic performance are now being investigated. The importance of tip sweep for a 10 bladed Prop-Fan for performance and near field noise trends has been shown in the data packages (Reference 12-14). Efficiency falls off by about 3% for a tip sweep angle reduction from about 38° to 20°. For this same change, the near field noise increases by about 4dB. This level of increased noise would increase (Reference 2 and 4) the fuselage sidewall acoustic treatment weight by about 1/2% of the airplane take-off gross weight.

Based on the airplane studies reported here and Hamilton Standard's design experience, the full-scale Prop-Fan is expected to have 8 to 10 blades and 35° to 45° of tip sweep. The cruise rotational tip speed is expected to fall between 213.4 m/s (700 ft/s) and 243.8 m/s (800 ft/s) with a maximum loading (Shaft Horsepower/Diameter^2) between 240.8 kw/m^2 (30 hp/ft^2) and 321.1 kw/m^2 (40 hp/ft^2) at an altitude of 10,668 meters (35,000 feet).

8.2.2 Structural

Various reports, oral briefings, analyses, and test efforts related to the Prop-Fan application to high speed airplanes were reviewed (References 1 through 24). The concern with excitation, stability, and structural design is emphasized in order to assist in the selection of an optimum Prop-Fan configuration with optimum aircraft integration.

This work will be used to affect the design tradeoffs in the areas of structural concern for the full-scale SR-7 Prop-Fan and its companion testbed configuration.

Lockheed California Company, Boeing Aircraft, and McDonnell Douglas Aircraft have conducted studies sizing Prop-Fans for various aircraft configurations in References 1 through 11. In these studies, tradeoffs for performance and structure are made and compared to existing turbo-fan configurations. These studies have used methods developed by Hamilton Standard for sizing the aircraft geometry wherever it effects the interaction between the aircraft and the propeller.

Reference 4 shows the proposed Douglas DC-9 version of the aft-mounted Prop-Fan along with discussions that show reduced drag for this configuration. This configuration is also good for structural reasons, since it has been Hamilton's experience that aft-mounted propellers experience less 1P excitation than forward mount propellers.

References 6 and 7 show Lockheed's proposals for the Prop-Fan testbed. The following aircraft were investigated:

Lockheed C-141A	Grumman Gulfstream II
Lockheed JetStar	Boeing KC-135
Convair 990	Boeing 737

Of these, the KC135 and the Gulfstream II are the recommended candidates for the testbed. From the viewpoint of Prop-Fan excitation, the Gulfstream II is the better choice because of the relative propeller to wing size. It is felt that the propeller is not in proper proportion to the wing on the other proposed testbed aircraft, and are therefore not representative of a final design and will not produce the proper excitation.

Reference 7 recommends 10 blades as opposed to 8 blades and a lower tip speed. Lowering the tip speed could be a benefit depending on frequency placement. For highly swept blades, a lower tip speed would reduce the tendency of the leading edge to buckle, thereby, maintaining better torsional characteristics of the Prop-Fan blade. This might keep the highly swept SR-5 as a contender for the full scale design.

References 8 and 9 are the final oral briefing for the Douglas DC-9 Prop-Fan feasibility and testbed study. These reports indicate that Douglas prefers a propeller location at wing level for a wing mounted nacelle. For minimum excitation, the propeller should be located above the wing. Future measurements should consider shaft moment and hub load measurements on both testbed and final configuration.

Reference 11 is a discussion of wind tunnel results including a simulated slipstream over the wing. This discussion pertains to the SR7 design only by virtue that it could be useful in estimating the lift distribution and flow field of the wing in excitation calculations. Results show that up inboard swirl has less overall drag than up-outboard swirl. This is compatible with Hamilton's knowledge that up-inboard rotation of propellers causes less excitation. It is recommended that up-inboard rotation propellers be considered for all designs.

Reference 15 shows the results of Ames wind tunnel tests on the Prop-Fan, wing, and fuselage combination. The pressure and lift distributions should be useful in calculating flow fields. The effect of a leading edge extension was determined in these tests and found to improve the drag of the aircraft. No notice was taken as to how it might effect blade excitation and/or vibratory loads. It might be necessary to move the nacelle forward as the leading edge is extended. The wing is effectively being moved closer to the propeller and the chord is being increased.

Reference 16 indicates that performance estimates are 10% higher than the calculated values. This could imply that calculated vibratory loads due to the flow field could also be low.

Reference 21 contains results of Boeing's finite element calculations of the wing pressure distribution and propeller swirl and its effects on performance. Again, modifications to the wing may effect blade excitations.

Up to this point, little of the information in the references cited show hard and fast trends as to the structural integrity of the blades as effected by the geometrical and loading parameters. Tip speed, number of blades, disk loading, and blade loading are all adjusted based on design conditions and performance and require that each design be fully investigated within its own envelope. As an example, as the number of blades are increased, the disk loading remaining more or less constant allows the load per blade to be reduced. This allows a smaller blade to be designed to properly match the loads. A parametric study for the Prop-Fan configurations is difficult to generate because of the complexities of the analyses used. The effort then becomes one of designing for optimum performance and acoustics. The design

groups have shown good technique in designing for steady-loads and well understood excitation. But designing in order to keep the Prop-Fan blade stable depends on techniques and analyses that have not as yet been fully developed at Hamilton Standard.

This area of vibratory loading and how it affects the design has not been discussed in the reference literature to any great extent. The importance of flutter was demonstrated in wind tunnel tests of the SR-5 model Prop-Fan. As indicated in Reference 23, areas of high vibratory stress were encountered at high speeds and high RPM. Tests of the SR-2 and SR-3 model Prop-Fans did not give any indication of instabilities; see References 19 and 20.

The results of this review indicate that there will be some radical changes in the design. Specifically, the location of the spar will probably move forward, with an effort to keep the center of mass as far forward as possible. This will tend to reduce the possibility of classical flutter. These trends were indicated in flutter tests on conventional propellers as discussed in Reference 24.

8.3 INDUSTRY SURVEY

An industry survey to determine the mission definition, and possible aircraft configuration for initial applications of a Prop-Fan system was conducted. To accomplish this, a mission definition was established by Hamilton Standard and submitted to major airlines and airframe and engine manufacturers for comment.

The mission definition established by Hamilton Standard was:

twin engine aircraft
2222KM (1200 NM) - 2778KM (1500 NM) design range
926KM (500 NM) - 1111KM (600 NM) average stage length
$1.50/gal fuel (1981 economy)
0.8 M_n cruise at 10668M (35000 FT)

This definition was reviewed by:

Boeing Commercial Airplane Company (BCAC)
Douglas Aircraft Company (DAC)
Lockheed - California Company (LCC)
Lockheed - Georgia Company (LGC)
Detroit Diesel Allison (DDA)
General Electric Company (GE)
Pratt & Whitney Aircraft (P&WA)
American Airlines (AA)
Delta Airlines (DA)
Eastern Airlines (EA)
United Airlines (UA)

A summary of the review is presented in Table 8.1.

Based on the results of this review, an average mission definition was provided to the NASA Project Manager who then provided the Aircraft Sensitivity Coefficients which were used in the trade-off study task (Reference Section 8.4). The selected aircraft configuration and mission definition was the Hamilton Standard (HS) estimate which is very close to the industry survey average.

TABLE 8.1
MISSION DEFINITION REVIEW SUMMARY
PART I

	HS	BCAC	DAC	LCC	LGC	DDA
Engines	2	2	2	2	2	2
Passengers	120	134	120	100	120	80-100
Design Range KM (nm)	2222-2772 (1200-1500)	1852-2222 (1000-1200)	2222-2778 (1200-1500)	1852 (1000)	2222-2778 (1200-1500)	1667-2222 (900-1200)
Stage Length KM (nm)	926-1111 (500-600)	555-926 (300-500)	926-1111 (500-600)	555 (300)	926-1111 (500-600)	463-833 (250-450)
Fuel Cost - Gal.	$1.50	$1.00-1.10	$1.50	-	$1.25	$1.50
Cruise - Mn	.8	.7-.75	.7	.75	.8	.72-.74
Altitude - M (ft)	10,668 (35,000)	10,668 (35,000)	10,668 (35,000)	9,144 (30,000)	10,058 (33,000)	10,668 (35,000)

TABLE 8.1
MISSION DEFINITION REVIEW SUMMARY
PART II

	GE	P&WA	AA	DA	EA	UA
Engines	2	2	2	2	2	2
Passengers	100	120	120	120	120	150
Design Range KM (nm)	1852 (1000)	2222 (1200)	2222-2778 (1200-1500)	2222-2778 (1200-1500)	2222-2778 (1200-1500)	2963 (1600)
Stage Length KM (nm)	596 (322)	741 (400)	926-1111 (500-600)	926-1111 (500-600)	741-926 (400-500)	1296 (700)
Fuel Cost - Gal.	-	$1.50	$1.05-1.10	$1.50	$1.50	-
Cruise - Mn	.75	.8	.8	.8	.8	.8
Altitude - M (ft)	9,754 (32,000)	9,449 (31,000)	10,668 (35,000)	10,668 (35,000)	9,449 (31,000)	10,668 (35,000)

8.4 AERODYNAMIC, ACOUSTIC AND STRUCTURAL TRADE-OFF STUDY

8.4.1 Sensitivity Factors

The baseline airplane and the mission for the SR-7 trade-off study were selected from the findings of a survey of airline, airframe and engine companies described previously. The baseline airplane and mission definitions are summarized in Table 8.2. The economics used in this study are also shown.

The sensitivity factors for examining the fuel burn and Direct Operating Cost (DOC) potential of the Prop-Fan configurations outlined in the trade-off study were provided by the NASA Project Manager and are consistent with the selected mission. The factors are summarized in Table 8.3. The factors were used to estimate the efficiency, weight and cost impacts of the many Prop-Fan configurations on the fuel burned and DOC benefits of the airplane.

TABLE 8.2
SR-7 TRADE-OFF STUDY
BASELINE AIRPLANE AND MISSION DEFINITION

Airplane:	Seats	120
	Design range	2222 KM (1200 nautical miles)
	Design Cruise Speed	Mach 0.8
	Typical Mission	926 KM (500 nautical miles) at 60% load factor
	Design Takeoff Gross Wt.	266,536 kg (120,900 lb.)
	Design Operating Wt. Empty	178,352 kg (80,900 lb.)
Engine:	Type	Scaled STS539-4
	Sizing Condition	10,668 M (35,000 ft.)
	Size	0.893 Thrust Scale
Economics:	Year	1980 Dollars
	Fuel Price	$.396/Liter ($1.50/U.S. Gal.)
	Flight Time	1.35 Hrs.
	Block Time	1.60 Hrs.
	Utilization	2200 Trips/Year

TABLE 8.3
SENSITIVITY FACTORS FOR TYPICAL MISSION OF
120 PAX, TWIN ENGINE TRANSPORT DEFINED IN TABLE 8.2

Change Caused By Prop-Fan Configurations	Effect of Change On: %ΔFuel Burned	%ΔDOC
±1 Pt. Prop-Fan Efficiency for the Airplane Mission	∓1.57%	∓0.74%
±2205 kg (1000 LB)/Engine Δ(Prop-Fan + Gear Box) Weight	±2.10%	±1.30%
±4409 kg (200 LB)/Airplane Δ (Acoustic Treatment + Landing Gear) Weight Penalty	±2.38%	±1.77%
±$100,000 Prop-Fan Price	-	±0.27%
±$1/Flight Hour Prop-Fan Maintenance Cost	-	±0.10%

8.4.2 Prop-Fan and Gear Box Weight Generalizations

The Prop-Fan weights (WPF) used in the SR-7 trade-off study are for advanced technology, double acting propellers. The weights are given by the equation presented below, and include the blades, hub, pitch change and spinner:

$$WPF = (DPF^{1.846})(TAF^{.75})(B^{-.05})(UTO^{.3})(PTO^{.327})WF/104.2$$

where WF is a weight factor dependent upon blade tip sweep (Λ); given by:

$$WF = .091\ (\Lambda/45) + .909$$

The terms in the weight equation are defined in Table 8.4. WPF is the weight in kilograms per propeller.

Gear box weight variations were also included in the trade-off study and are as presented in the Hamilton Standard 1977 data pack (Reference 13). The parametric variations in gear box weights (WGB) expressed by:

$$WGB = 5.34(PTO)(DPF)(GRF^{1/2})/UTO$$

where the gear ratio factor (GRF) is expressed as:

$$GRF = [(BASELINE\ UTO)/UTO][DPF/(BASELINE\ DPF)]$$

TABLE 8.4
List of Symbols

ACGB	-	gear box acquisition cost, $
ACPF	-	Prop-Fan acquisition cost, $
AF	-	blade activity factor = $6250 \int_{SCD}^{1.0} (b/D)(r/R)^3 d(r/R)$
b	-	number of blades
b/D	-	local chord to blade diameter ratio
BPF	-	blade passage frequency, hertz
CLD	-	local blade design lift coefficient
CLi	-	integrated design lift coefficient = $4 \int_{SCD}^{1.0} Cld(r/R)^3 d(r/R)$
db	-	blade passage frequency peak noise level
DOC	-	direct operating cost
DPF	-	Prop-Fan diameter
GBF	-	gear ratio factor = [(BASELINE UTO)/UTO][DPF/(BASELINE DPF)]
h/b	-	local blade thickness to chord ratio
MCBG	-	gearbox maintenance cost, $/flight hour
MCPF	-	Prop-Fan maintenance cost, $/flight hour
PTO	-	take-off power, kilowatts
R	-	blade radius, meters
r/R	-	local blade radius to tip radius ratio
SCD	-	blade innermost r/R
UTO	-	take-off tip speed, meters/sec.
V/Vo	-	local velocity to freestream velocity ratio
TAF	-	B x AF

TABLE 8.4 LIST OF SYMBOLS (CONTINUED)

TAF	-	B x AF
WF	-	weight factor = .091 (Λ/45) = .909
WPF	-	Prop-Fan weight, kilograms
WAT	-	acoustic treatment weight, kilograms
WGB	-	gearbox weight, kilograms
WLG	-	landing gear weight, kilograms
X	-	inplane blade coordinate, meters along pitch change axis
Y	-	inplane blade coordinate, meters perpendicular to pitch change axis. Also clearance between fuselage and blade tip
Z	-	axial blade coordinate, meters positive downstream
θ	-	blade twist angle, degrees
θ^*	-	camber angle, degrees
$\emptyset$	-	cone angle, degrees
Λ	-	sweep angle, degrees
σ	-	acoustic treatment weight parameter

8.4.3 Fuselage Acoustic Treatment Penalty

Each Prop-Fan configuration incurred an acoustical treatment weight penalty to the airplane in order to meet the 80 dBA interior noise level established for the trade-off study. A theoretical treatment analysis was developed by Revell, Balena and Koval at the Lockheed California Company. This acoustical treatment analysis, with LCC's approval and assistance, was adapted for use in this study. The equations are presented below, and are based upon blade passage frequencies (BPF) and the BPF noise levels for each Prop-Fan configuration:

ACOUSTICAL TREATMENT WEIGHT PENALTY FORMULATION

Definition:

Reference acoustic treatment weight (WAT) parameter = σ_{ref}

Adaptation of the LCC Analysis

The theoretical results obtained by Lockheed were found to be represented very well by a mass law and BPF scaling. These scaling laws state that a 6dB near-field noise reduction or a doubling of BPF halves WAT. Therefore, the following generalization was developed:

$$WAT = (4.88(BPF_{REF}/BPF)[10(dB - dB_{REF})/20](\sigma_{REF}(N)(DPF)(DF)$$

where WAT is the acoustic treatment weight penalty in kilograms.

From the number of theoretically defined points provided, the acoustical treatment weight generalization represent LCC's results best with these reference (REF) quantities:

BPF_{ref} = 212

dB_{ref}	= 142.9	@	Y/DPF = 0.2
	= 138.9		= 0.4
	= 136.9		= 0.6
	= 134.9		= 0.8
	= 133.9		= 1.0

where Y is the clearance between the fuselage and the blade tips, and Y/DPF normalizes this clearance to the Prop-Fan diameter. For this parametric study, the distance from the propeller centerline to the fuselage was fixed at 4.92 meters (16.14 ft). Lockheed's theoretical analysis showed that a smaller portion of the fuselage required treatment as the noise source was moved closer. This was generalized as:

$$\sigma_{REF} = 1.25\ (Y/DPF) + 4.6 \quad (0.4 \leq Y/DPF \leq 0.8)$$
$$= 5.1 \quad (0.0 < Y/DPF < 0.4)$$
$$= 5.6 \quad (0.8 < Y/DPF < 1.0)$$

Each of the reference (REF) values are used in the acoustical treatment weight equation.

A benefit of 5dB was assigned to precision synchrophasing and dynamic damping such that the treatment penalty was reduced. The 5 dB, which reduces the fuselage vibration level and thus the dB level, was subtracted from the near field noise levels in the calculation of acoustical treatment weights.

8.4.4 Airplane Landing Gear Weight Penalty

A preliminary design concept which accounts for the effect of varying Prop-Fan diameter on the weight of the airplane landing gear was obtained from the Lockheed California Company (LCC). The Prop-Fan centerline location on the wing was the same for all Prop-Fan diameters investigated. Accordingly, it was not necessary to account for other airplane weight changes (tail surface for engine out and wing structure) which would be affected by Prop-Fan diameter changes. The landing gear weight penalty is expressed as:

$$WLG = 787.4 \text{ (DPF - Baseline DPF)}$$

The weight is expressed in kilograms with the Prop-Fan diameter expressed in meters.

8.4.5 Prop-Fan Gearbox Acquisition and Maintenance Cost Generalization

The airplane DOC is slightly influenced by the various propeller system costs. The influence is shown by the sensitivity factors presented in Table 8.3. These costs are summarized by the following four equations:

8.4.5.1 Prop-Fan Unit Acquisition Cost (ACPF)

$$ACPF = X(DPF - .3048)$$

This is the trend of the sell price in dollars for original equipment manufacture (OEM) customers in the 1981 economy based upon a production rate of approximately 300 units per year. It includes the hub, blades, pitch change, spinner and deicing. The Prop-Fan diameter in the ACPF equation is expressed in meters and covers 8, 10 and 12-blade Prop-Fans with tip sweeps up to 45°.

8.4.5.2 Prop-Fan Maintenance Cost (MCPF):

$$MCPF = 0.479\ DPF + .672, \$/\text{flight hour}$$

The Prop-Fan maintenance cost, based upon the 1981 economy, is fully burdened (maintenance labor and material costs plus overhead and administration) and is applicable for 8, 10 and 12-blade Prop-Fans with tip sweeps up to 45°.

8.4.5.3 Gearbox Acquisition (ACGB) and Maintenance Cost (MCGB)

The gearbox acquisition and maintenance cost generalizations are shown in Figure 8.1. These are unit costs in the 1981 economy and are proportional to Prop-Fan torque. The unit gearbox costs for the baseline Prop-Fan (noted in Figure 8.1) are acquisition of 1.0 and maintenance of 2.114 dollars. These are shown at the torque ratio of 1.0 for the baseline Prop-Fan. The torque ratio is equal to the product of the indicated constant (59.5) and the ratio of diameter and takeoff tip speed. The units for the torque ratio are independent of the system of units as long as both the diameter and the length units used in defining tip speed are consistent.

8.4.6 Trade-off Study Parameters

The parametric variables studied fall into two categories, flight condition definition, and blade geometric properties. The aircraft is designed to operate at a cruise Mach number of 0.8 at an altitude of 10668M (35000 FT) with an average cruise power of 4312 KW (5782 HP). The combination of power/diameter^2 and the Prop-Fan tip speed are optimized for three speeds using the aircraft sensitivity parameters discussed in section 8.4.1.

The Prop-Fan and blade geometric parameters investigated include number of blades, and variations in the radial distributions of blade sweep, thickness ratio, design integrated lift coefficient, twist and blade stacking. Each geometric variable was systematically varied, changing only one variable at a time, to assess the effect of each variable on net efficiency, noise level, percentage change of fuel burned and percentage change of direct operating cost.

The blade geometric radial distributions used in the SR-7 trade-off study are shown in Figures 8.2 through 8.7. Figure 8.2 presents the family of blade sweep distributions studied, including the baseline blade which has a tip sweep of 39.6°.

The sweeps range from 0 up to 48 degrees at the blade tip. The latter sweep is similar to that of the SR-5 design. The case numbers shown refer to the trade-off case numbers discussed later in the text.

The three blade thickness ratio distributions assessed are shown in Figure 8.3. The baseline T1 distribution was used for the previous SR-1, SR-2, SR-3, and SR-5 blade designs. Thickness ratios T1A and T1B have greater thickness ratios inboard to provide potential structural benefits.

The blade planform shapes are shown in Figure 8.4. Two tip chord changes from a baseline are shown. In addition, a blade with a wider chord in the inboard area has been included because of its better structural characteristics.

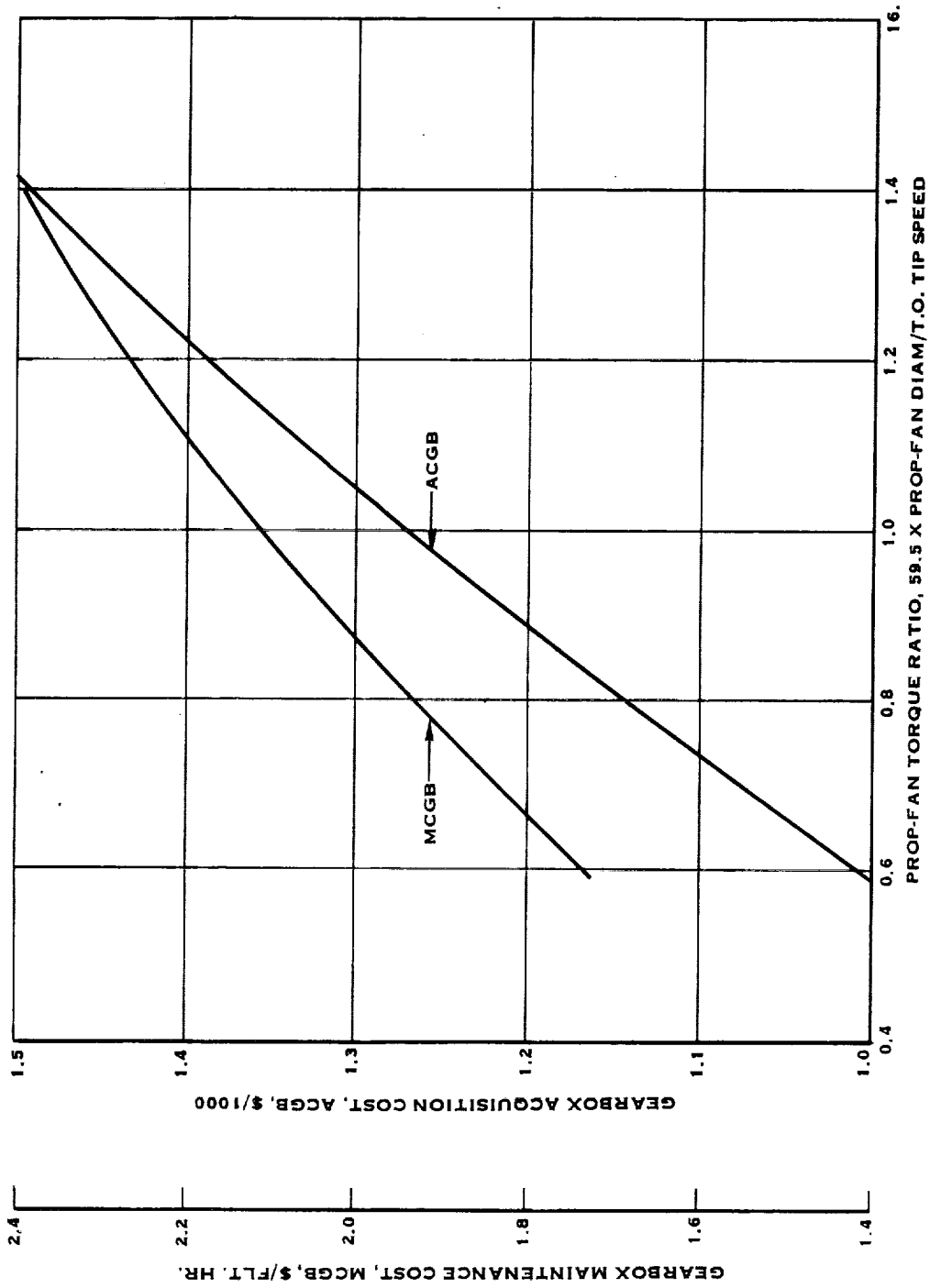

FIGURE 8.1 GEARBOX ACQUISITION AND MAINTENANCE COST VARIATIONS WITH PROP-FAN TORQUE RATIO. 1981 ECONOMY, UNIT COSTS.

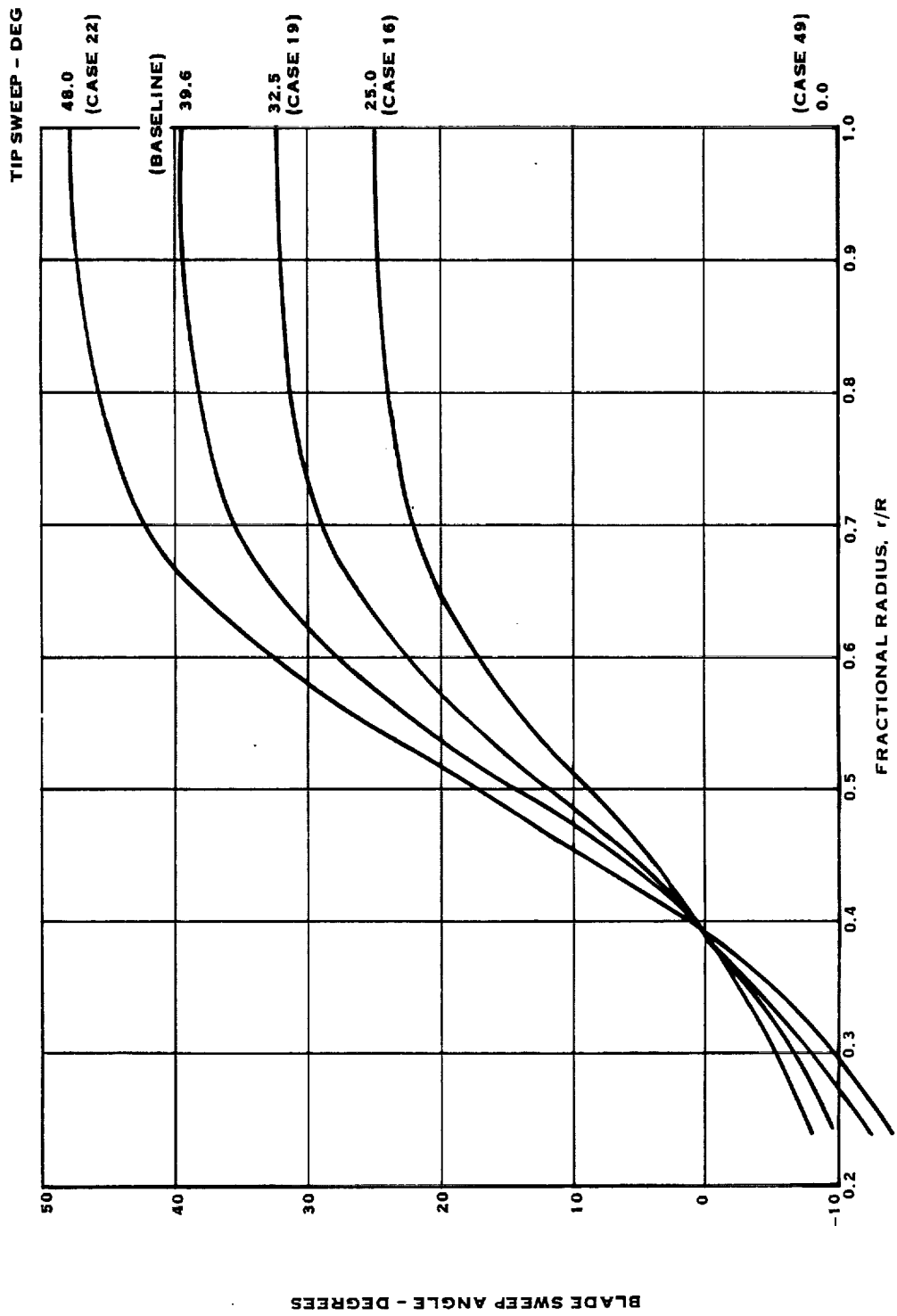

FIGURE 8.2 SWEEP ANGLE DISTRIBUTION

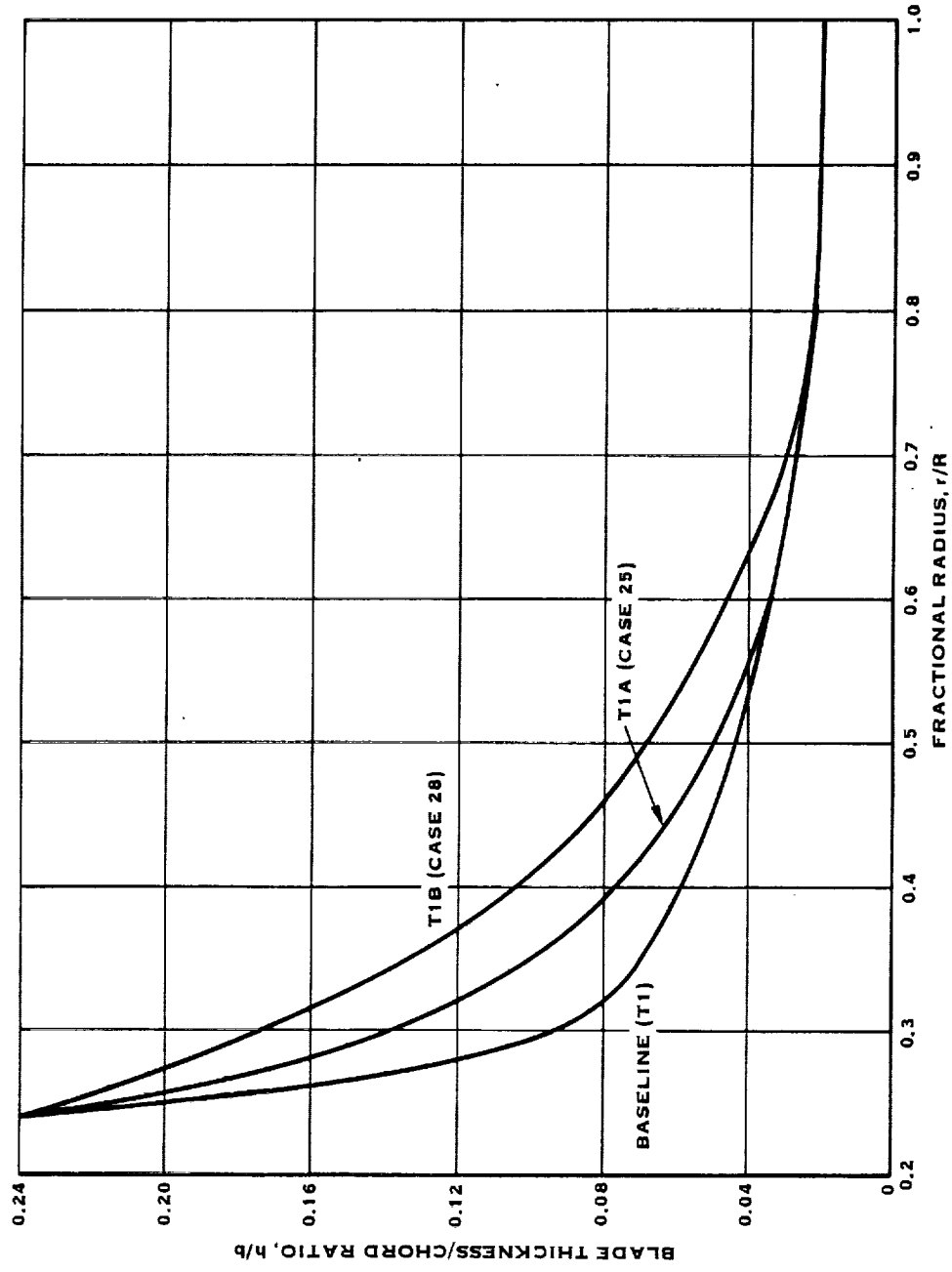

FIGURE 8.3 THICKNESS RATIO DISTRIBUTION

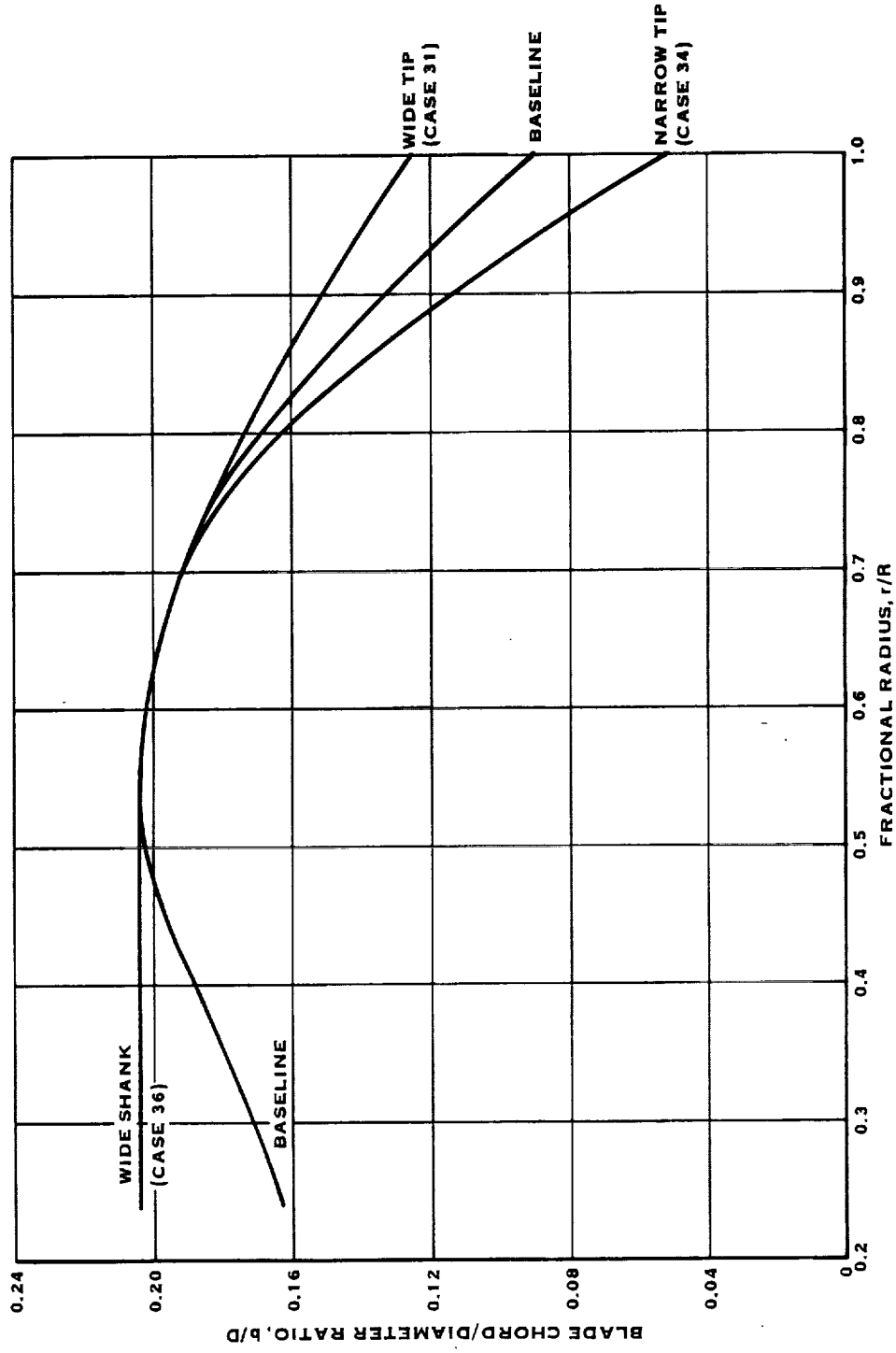

FIGURE 8.4 PLANFORM DISTRIBUTION

Figure 8.5 presents the four design lift coefficients, C_{LD}, distributions used in the trade-off study. The baseline C_{LD} is identical to that used for the SR-3 design. The lower camber distribution shown was used for the SR-1M design. The higher camber variation shown completes the curve family. In addition, the distribution shown as a dashed line in Figure 8.5 was selected to assess the effect of shifting the peak C_{LD} toward the mid portion of the blade.

Various blade twist distributions are given in Figure 8.6. Three tip twists, including the baseline were assessed in the trade-off study. A higher inboard blade shank twist was also selected because of possible acoustic and blade choke margin advantages.

The final geometric blade parameter studied was the blade stacking, defined as the fifty percent chord location in three dimensional space. The nondimensional, X, Y, Z coordinates of the half chord are shown in Figure 8.7 for three blade stackings all having the same sweep. The baseline blade is located on a helical surface (defined by the local resultant velocity direction) including nacelle velocity perturbations, which are discussed below.

The reason for the two restacks was to reduce the in-plane lean (the Y coordinate) to improve the blade structural integrity. Note in Figure 8.7 as the Y/R is reduced the axial blade coordinate, Z/R, increases to maintain constant sweep.

The spinner-nacelle body, retards the flow over the inner portion of the blade and can accelerate the flow near the blade tip. Figure 8.8 shows the nacelle generated flow field perturbation in the vicinity of the baseline blade. Figure 8.9 shows the radial distribution of the velocity defined at the blade leading edge. The narrow tip chord blade, and the 25° tip sweep blade are used as representative blades to show how redefining the sweep or planform redefines the nacelle retardation.

8.4.7 Discussion of Results

8.4.7.1 Baseline Blade Study - The baseline eight bladed Prop-Fan with shape characteristics defined in the previous section, was evaluated over a range of tip speeds and power loadings to determine the performance and noise levels. The tip speed was varied in four steps, 259.1 M/S (850 FT/S), 243.8 M/S (800FT/S), 213.4 M/S (700 FT/S), 182.9 M/S (600 FT/S) and the power loading in three steps, between 301.0 KW/M^2 (37.5 HP/FT^2) and 160.5 KW/M^2 (20.0 HP/FT^2) to form a matrix of twelve points, shown in Table 8.5.

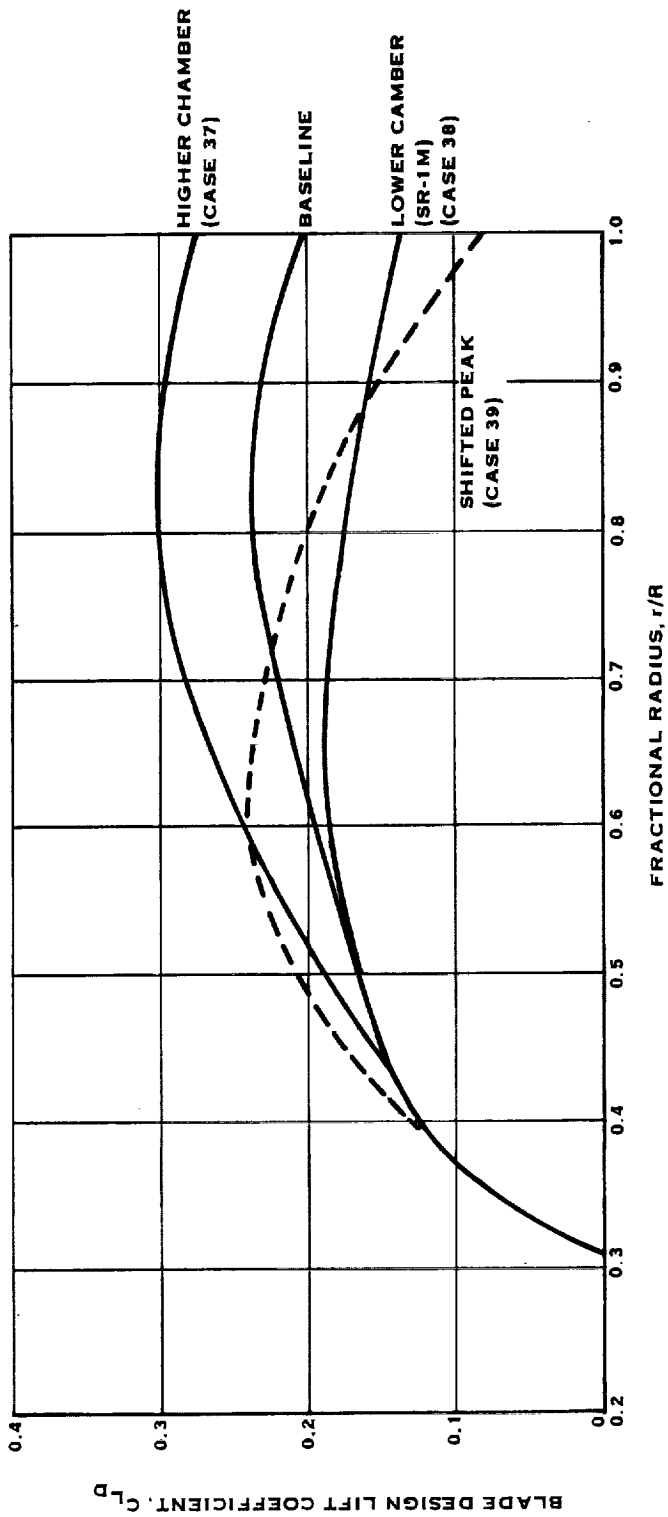

FIGURE 8.5 INTEGRATED DESIGN LIFT COEFFICIENT DISTRIBUTION

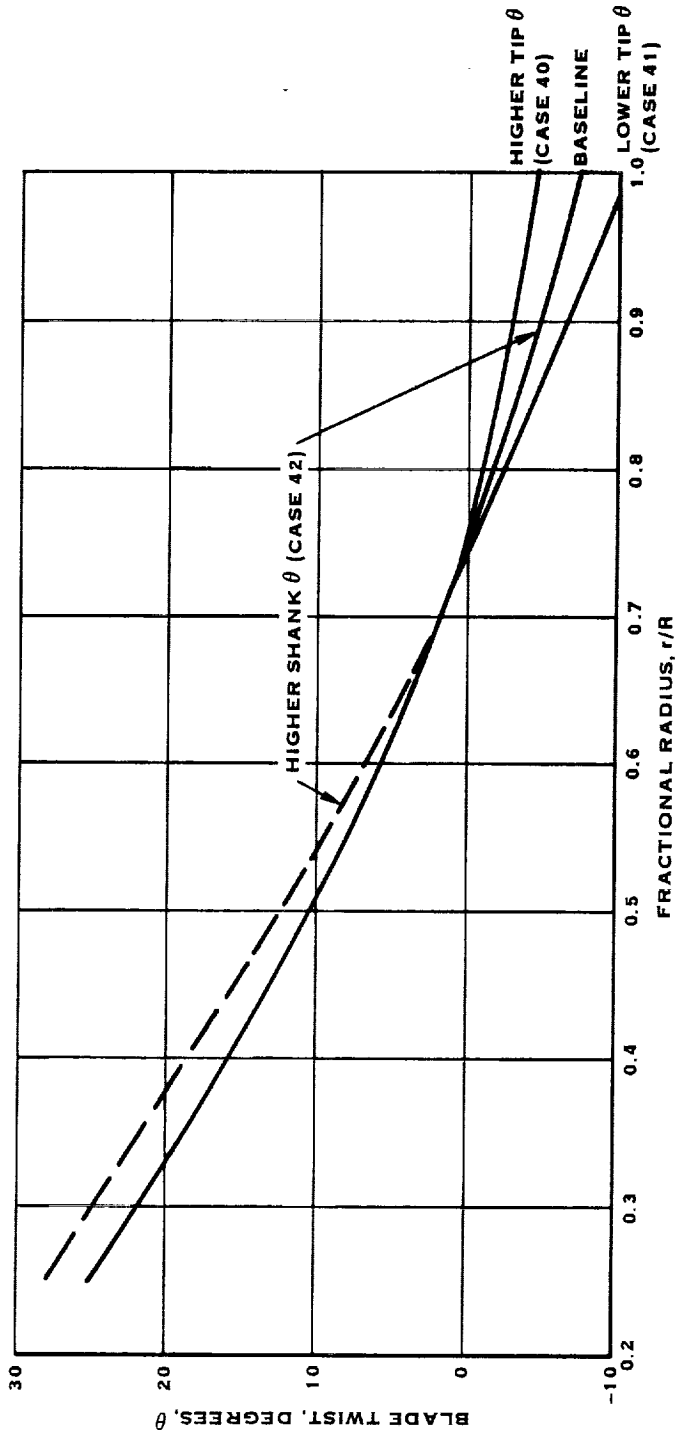

FIGURE 8.6 TWIST DISTRIBUTION

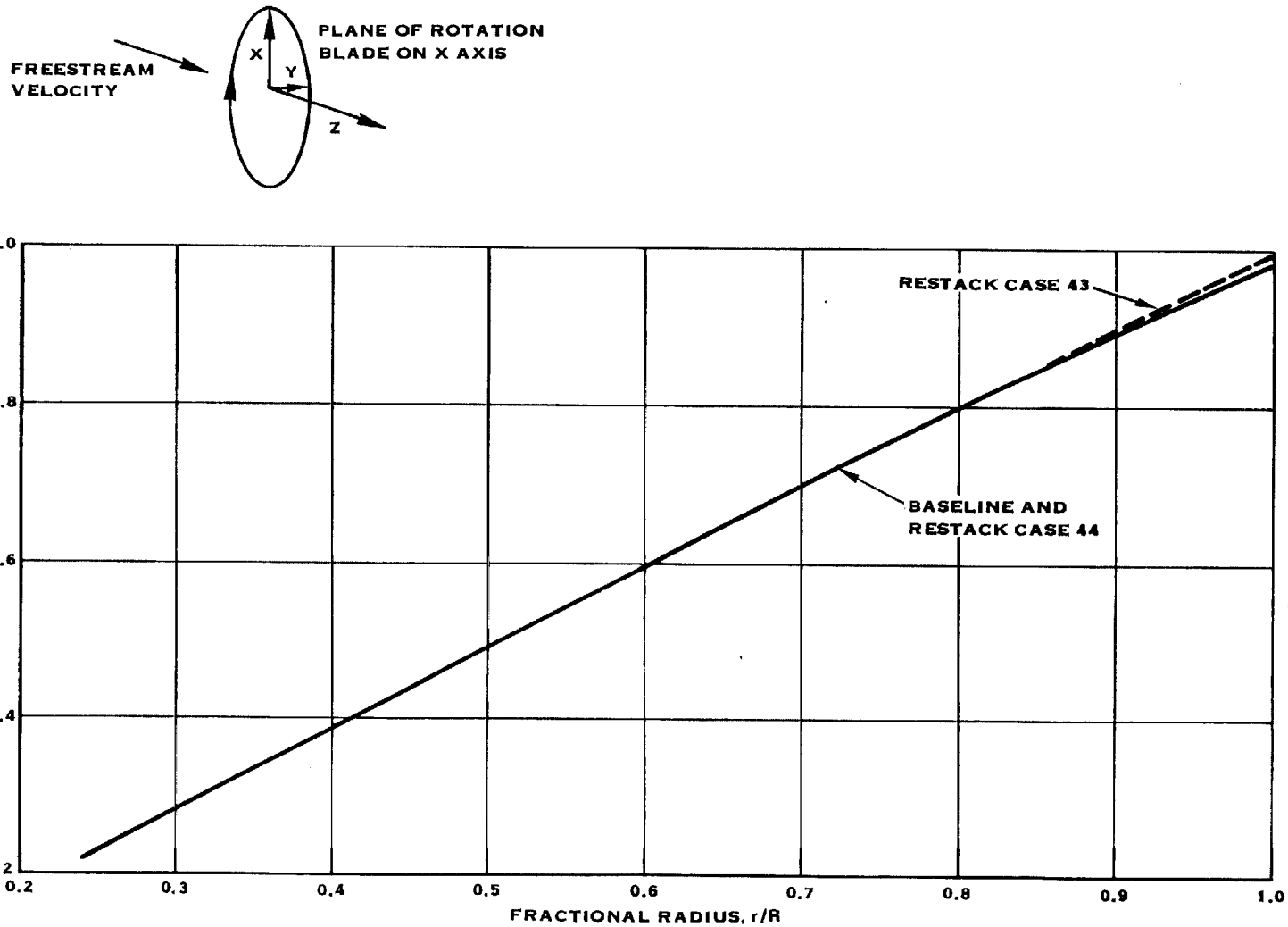

FIGURE 8.7 STACKING DISTRIBUTION

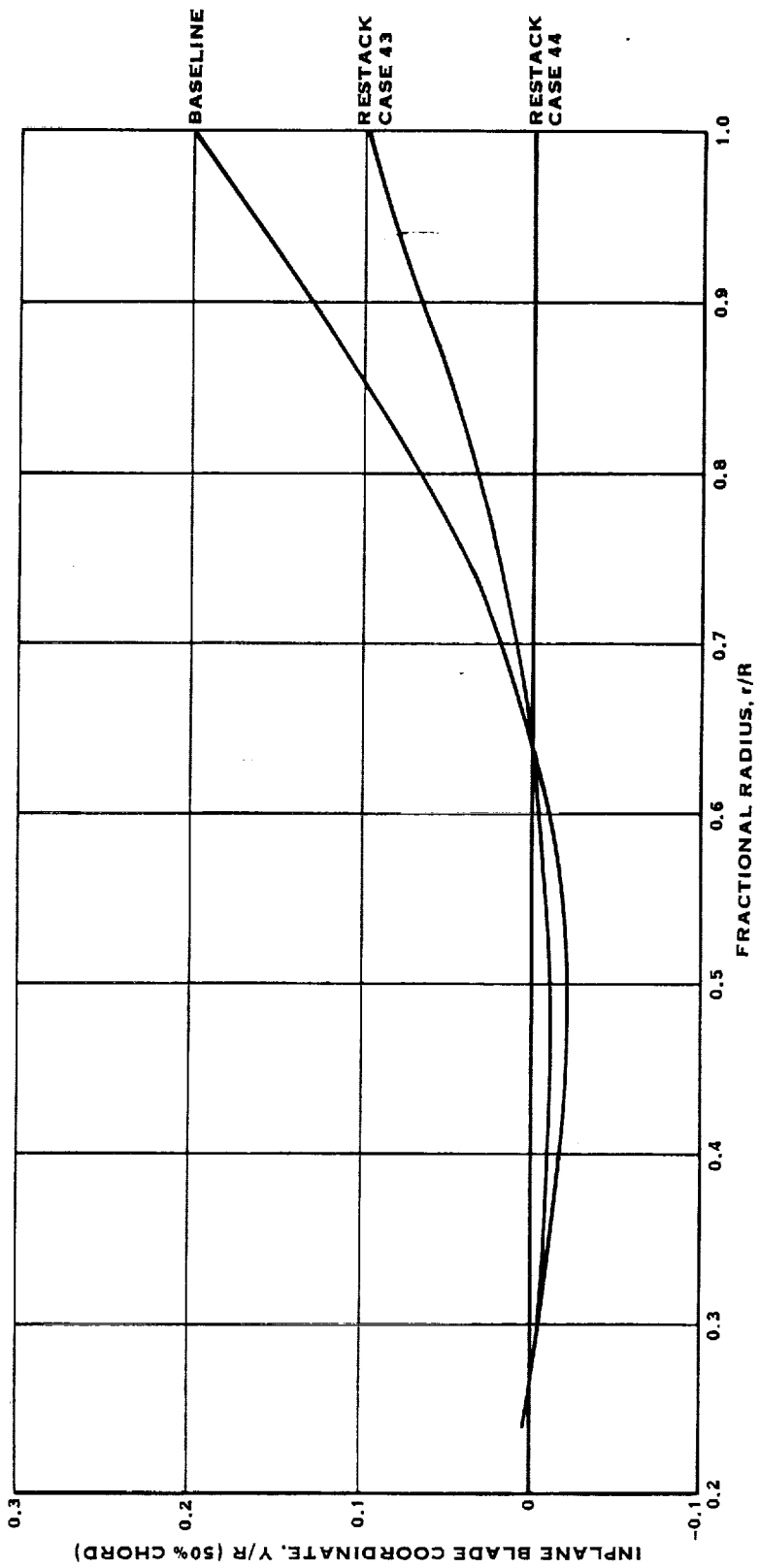

FIGURE 8.7 STACKING DISTRIBUTION (CONT'D)

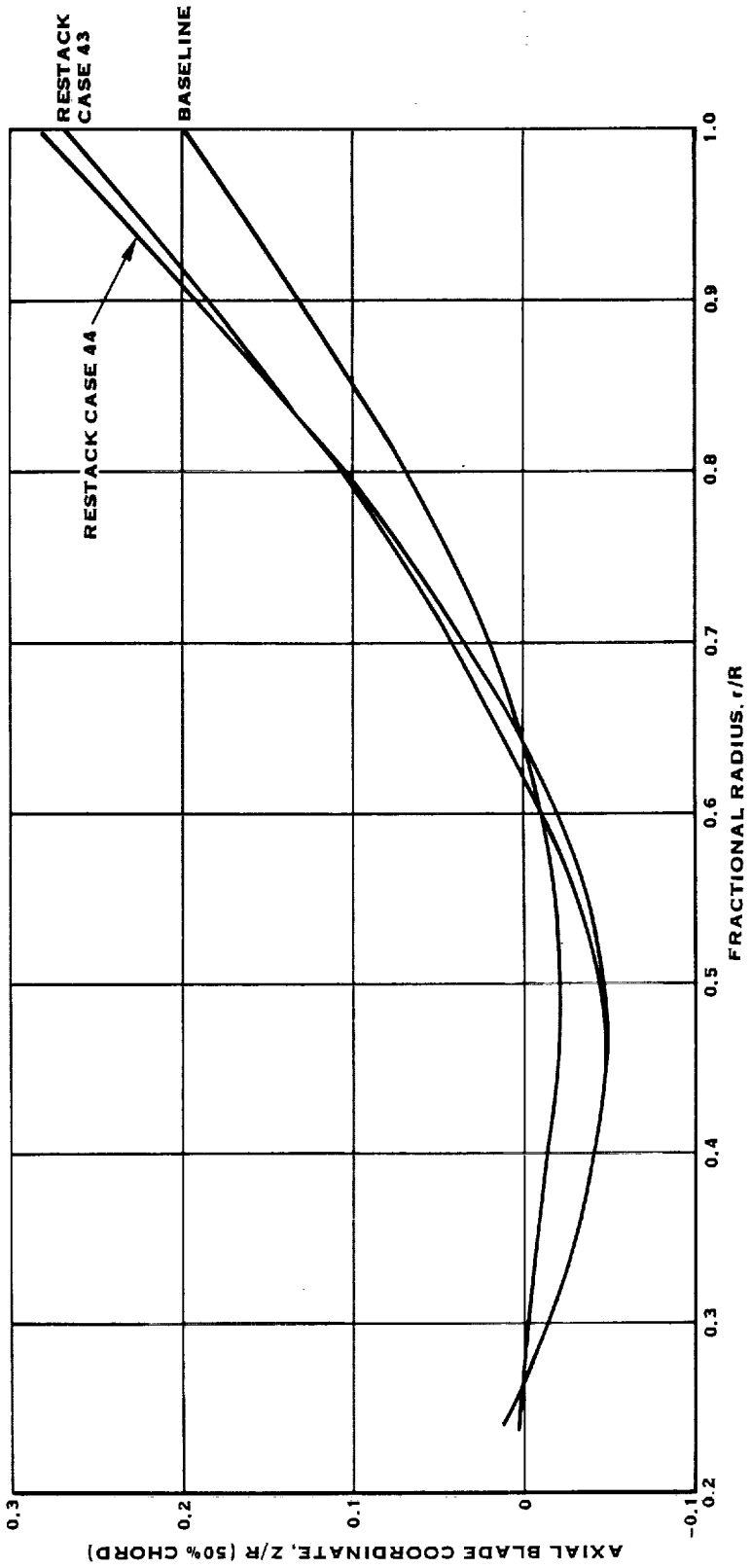

FIGURE 8.7 STACKING DISTRIBUTION (CONT'D)

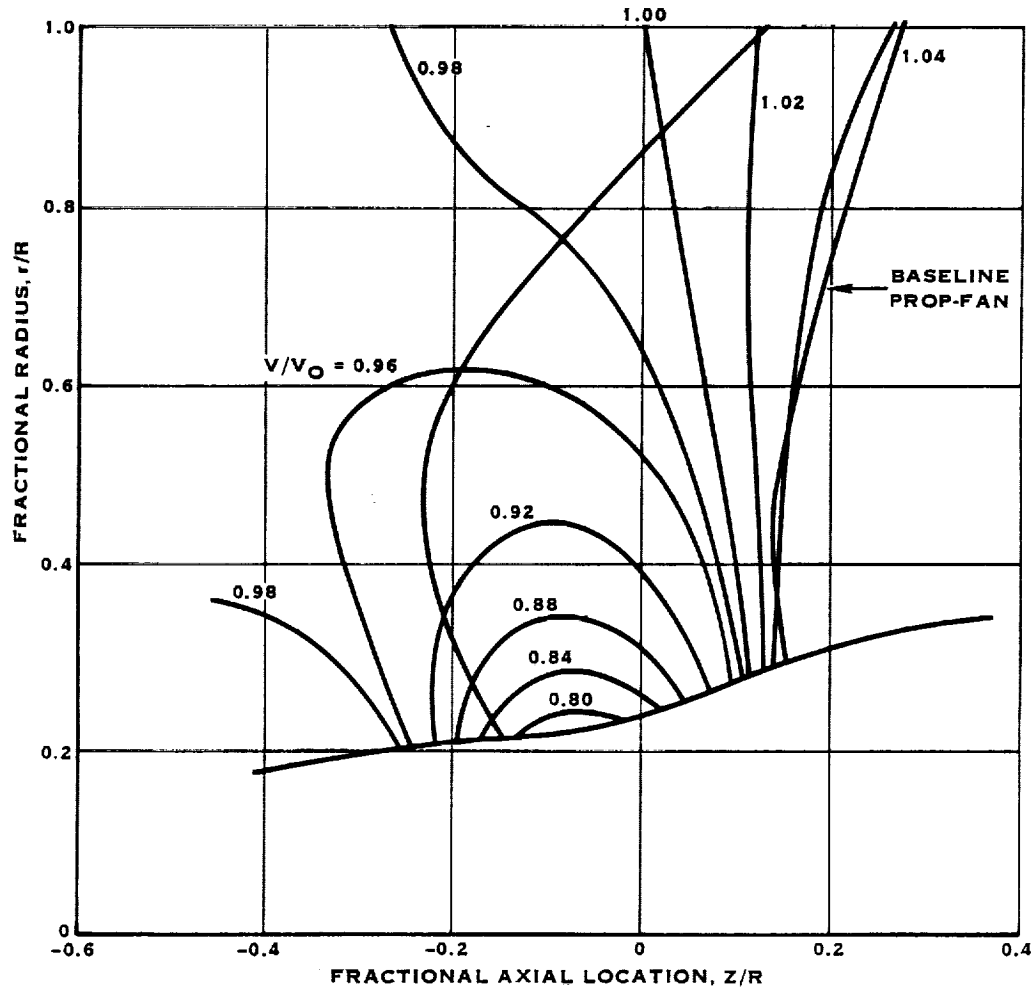

FIGURE 8.8 CENTERBODY BLOCKAGE

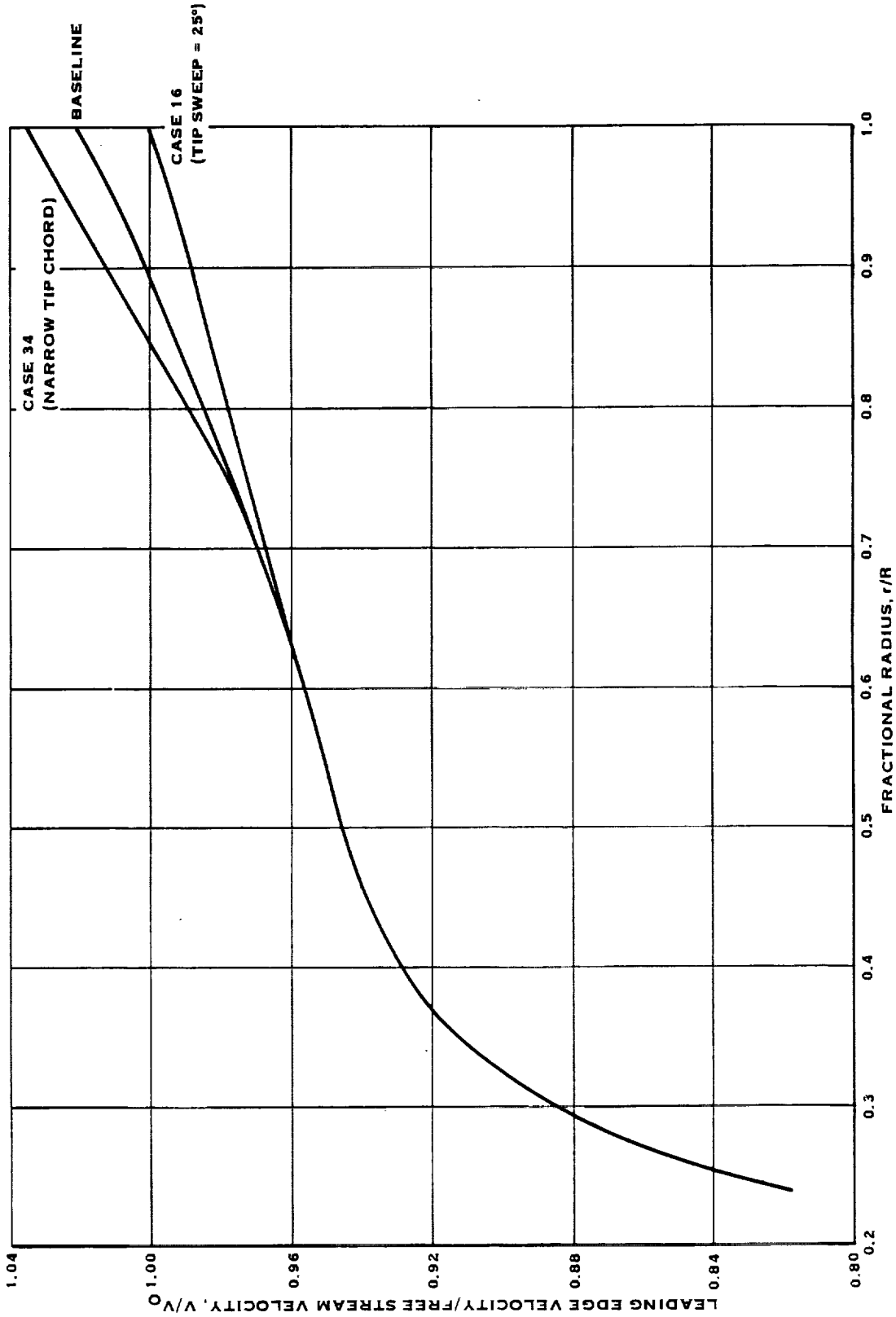

FIGURE 8.9 VELOCITY DISTRIBUTION

TABLE 8.5 BASELINE BLADE STUDY RESULTS

#	CASE	TIP SPEED M/S	POWER LOADING kW/M^2	TIP SPEED FT/SEC	POWER LOADING HP/FT^2	NO. BLADES	BLADE TIP SWEEP, DEG.	THICKNESS RATIO	PLANFORM	DESIGN CL	TWIST	STACKING LINE RELATED TO HELIX	NET EFFICIENCY	PEAK NOISE dB-BPF	Δ FUEL BURNED IMPROVEMENT, %	Δ DIRECT OPERATING COST IMPROVEMENT, %
1	TIP SPEED ↑	259.1	301.0	850	37.5	8	39.6	T1	BASELINE	BASELINE	BASELINE	ON	0.789	143.9	−0.01	0.29
2		259.1	240.8	850	30.0	↓	↓	↓	↓	↓	↓	↓	0.798	143.6	−0.07	−0.04
3		259.1	208.7	850	26.0								0.793	144.2	−2.15	−1.47
4		243.8	301.0	800	37.5								0.783	143.2	−0.95	−0.17
5		243.8	240.8	800	30.0								0.798	143.3	−0.08	−0.18
6		243.8	208.7	800	26.0								0.800	144.2	−1.45	−1.25
7		213.4	301.0	700	37.5								0.752	143.8	−6.97	−3.32
8		213.4	240.8	700	30.0								0.783	140.3	−1.97	−0.93
9		213.4	184.6	700	23.0								0.802	141.6	−1.83	−1.60
10		182.9	240.8	600	30.0								0.744	137.3	−7.89	−3.67
11		182.9	208.7	600	26.0								0.760	138.0	−6.94	−3.59
12	↓	182.9	160.5	600	20.0	↓	↓	↓	↓	↓	↓	↓	0.773	136.4	−6.09	−4.05

The aerodynamic performance for the baseline Prop-Fan was calculated using Hamilton Standard program H409, and is shown in Table 8.5 and Figure 8.10 through 8.14 for the matrix of operating points. Also shown in Figure 8.10 is measured performance for the SR-3 Prop-Fan, as reported in Reference 20. The SR-3 blade is very similar to the baseline blade which has a slightly wider tip chord and slightly higher tip sweep angle. Performance and noise level prediction (using Hamilton Standard program F091) differences between the SR-3 and baseline Prop-Fans are insignificant. Comparing test data and prediction, the major differences occur at the 259.1 M/S (850 FT/S) tip speed and at the power loading extremes at 213.4 M/S (700 FT/S). The comparison was made to develop corrections to the predicted net efficiency to improve the trade-off analysis accuracy. In general, the predicted net efficiency increases with increasing tip speed levels for the baseline Prop-Fan. In Figure 8.11, it is noted that the peak near-field blade passage frequency noise level increases with increasing tip speed.

Using the aircraft trade sensitivity factors discussed in Section 8.4.1, the percentage improvement in fuel burned with respect to the baseline prop-Fan at a reference cruise condition, can be assessed for the performance and noise levels given in Figure 8.12. The reference cruise condition has been defined as a mid-range tip speed of 243.8 M/S (800 FT/S).

From Figure 8.11, it can be seen that at this tip speed, minimum fuel burned occurs at a power loading of 256.9 KW/M^2 (32 HP/FT^2). This combination of tip speed and power loading was thus selected as the reference condition.

A locus of selected power loadings for various tip speeds is shown in the figure as a dashed curve. This curve was obtained by selecting the power loadings at each tip speed both as a function of minimum fuel burned and operating costs depicted in Figures 8.12 and 8.13 and then selecting close to the minimum fuel burned power loading weighted slightly toward minimum Direct Operating Cost (DOC). On these figures, the lowest fuel burned and DOC occurs at the highest tip speed. As tip speed falls off, the fuel burned and DOC increase optimizing at progressively lower power loadings.

A component breakdown of the various factors that affect the percent change in fuel burned, at a selected tip speed of 243.8 M/S (800 FT/S) are shown in Figure 8.14. It can be seen that changes in fuel burned caused by changes in Prop-Fan net efficiency increase the fuel burned as the power loading increases. From Figure 8.15, it can be seen that aircraft and Prop-Fan weight components tend to be reduced with increased power loading causing an improvement in fuel burned with power loading. The opposing effects of net efficiency and component weights, thus cause a peaking of the improvement in fuel burned including all components, at some power loading.

In order to limit the trade-off study to a manageable matrix of operating conditions, three combinations of tip speed and power loading were selected for the study. These combinations were chosen by using the locus of selected power loadings of Figure 8.12 and are listed in Table 8.6. The Prop-Fan diameters and rotational speeds are indicated in the Table for an average cruise power of 4312 KW (5782 HP).

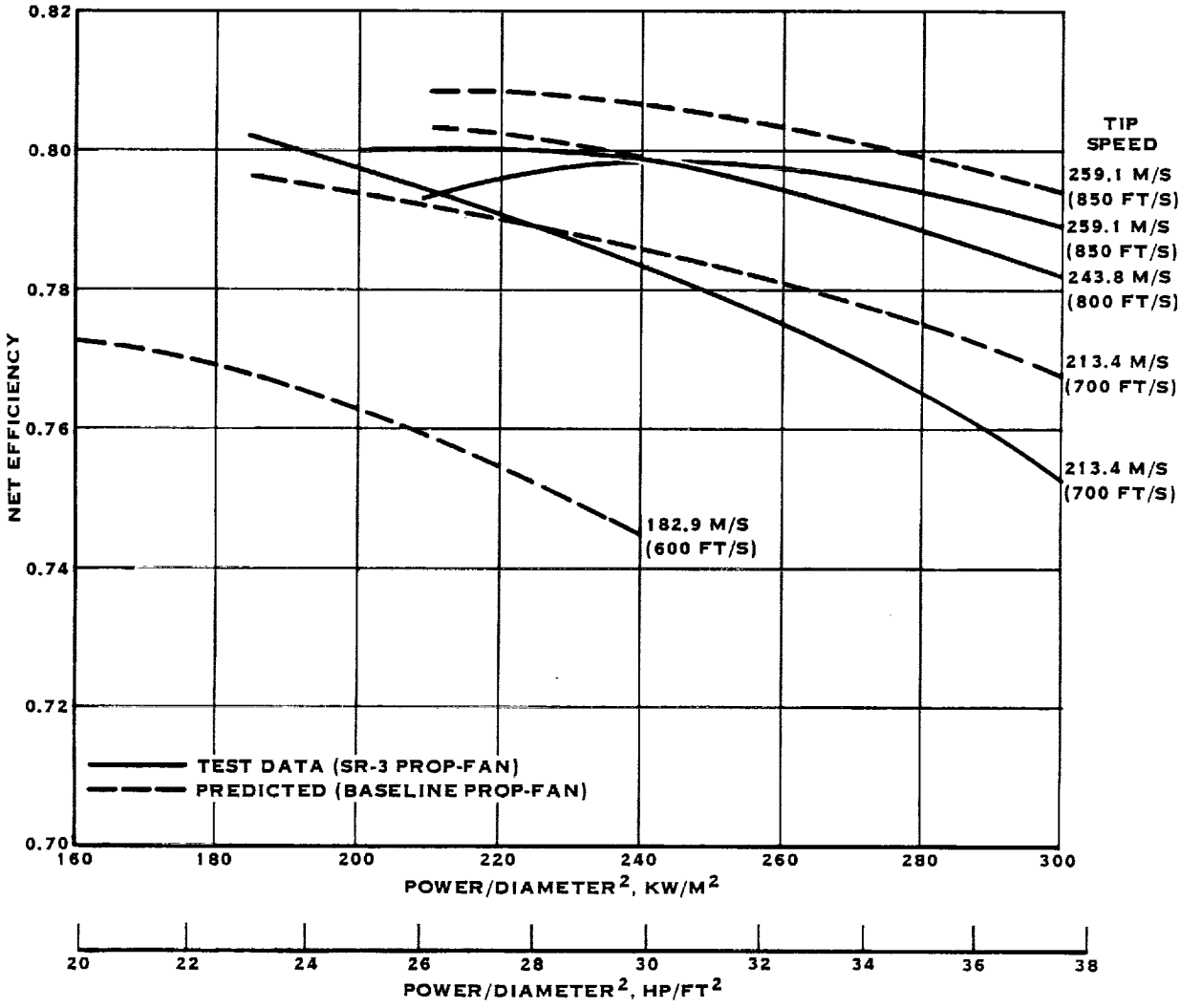

FIGURE 8.10 NET EFFICIENCY VS. POWER LOADING

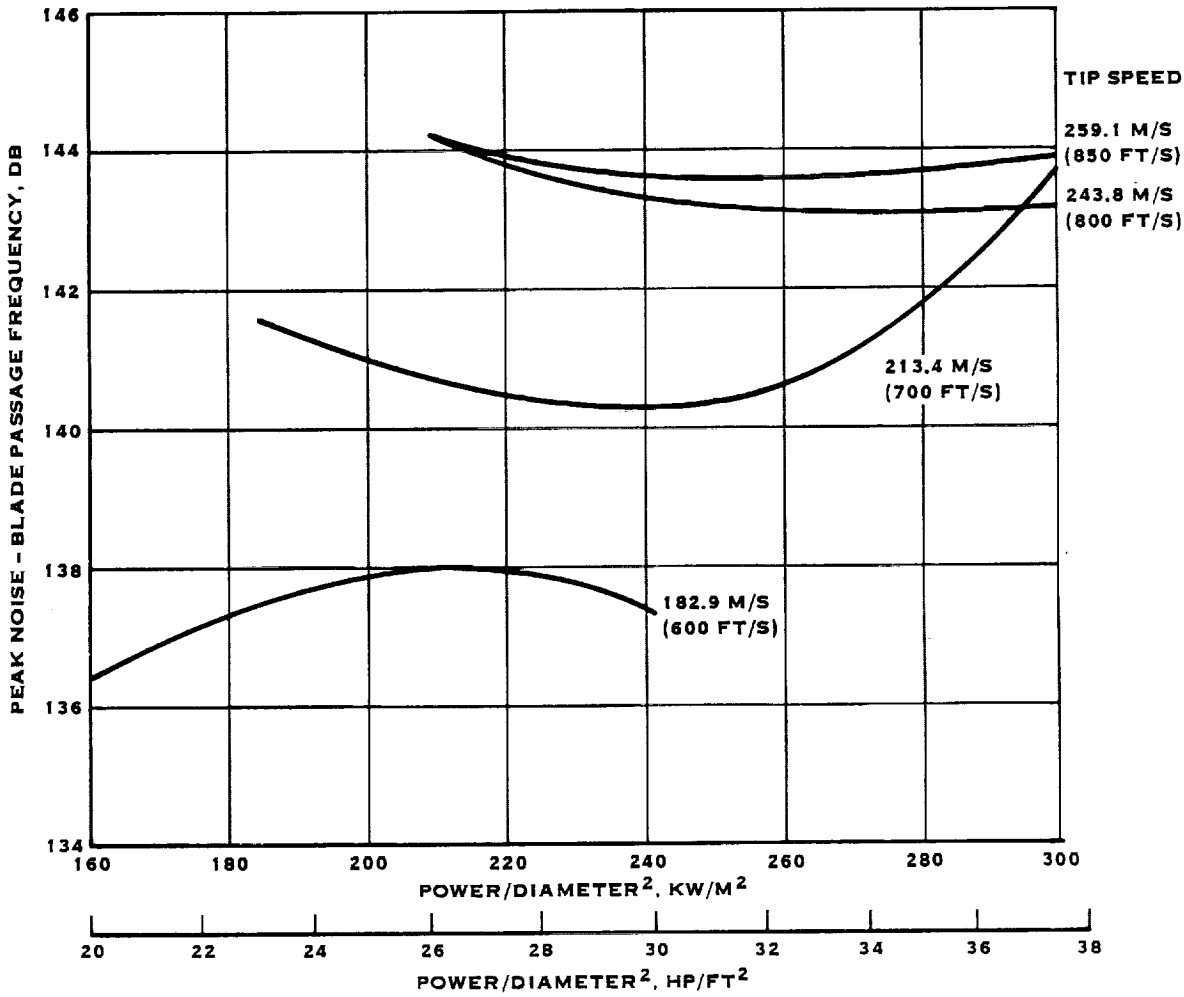

FIGURE 8.11 PEAK NOISE VS. POWER LOADING

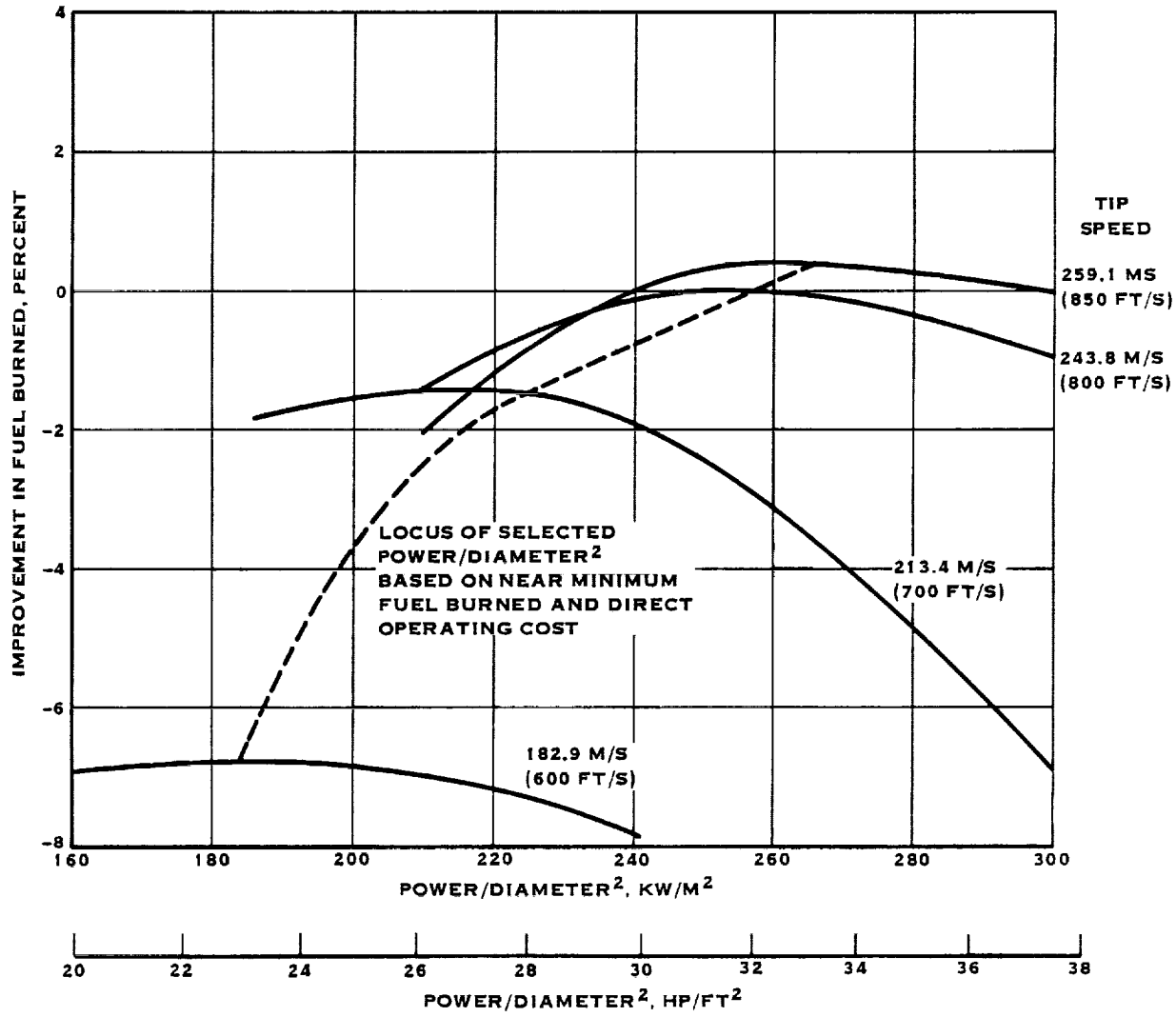

FIGURE 8.12 IMPROVEMENT IN FUEL BURN VS. POWER LOADING

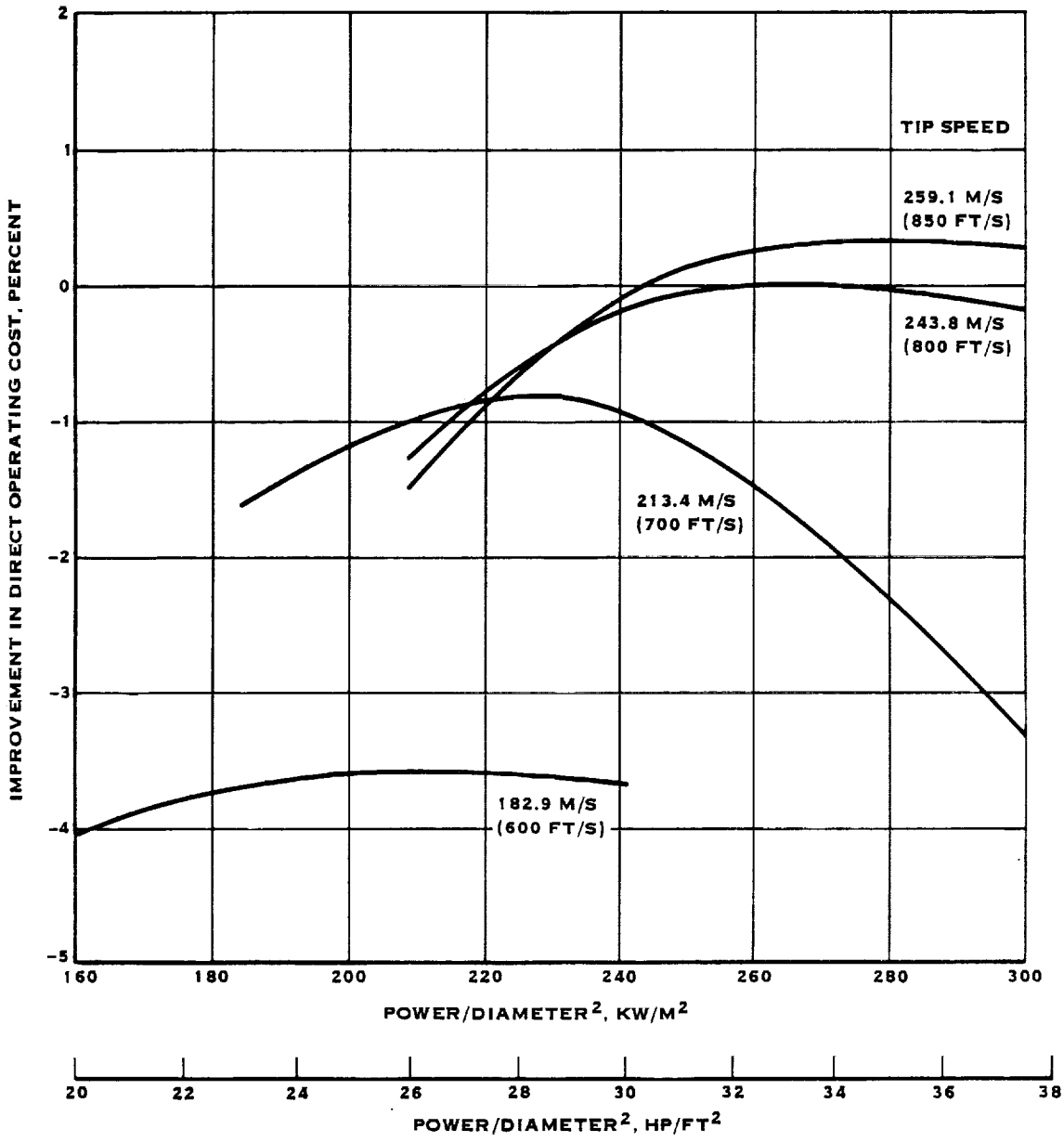

FIGURE 8.13 IMPROVEMENT IN DIRECT OPERATING COST VS. POWER LOADING

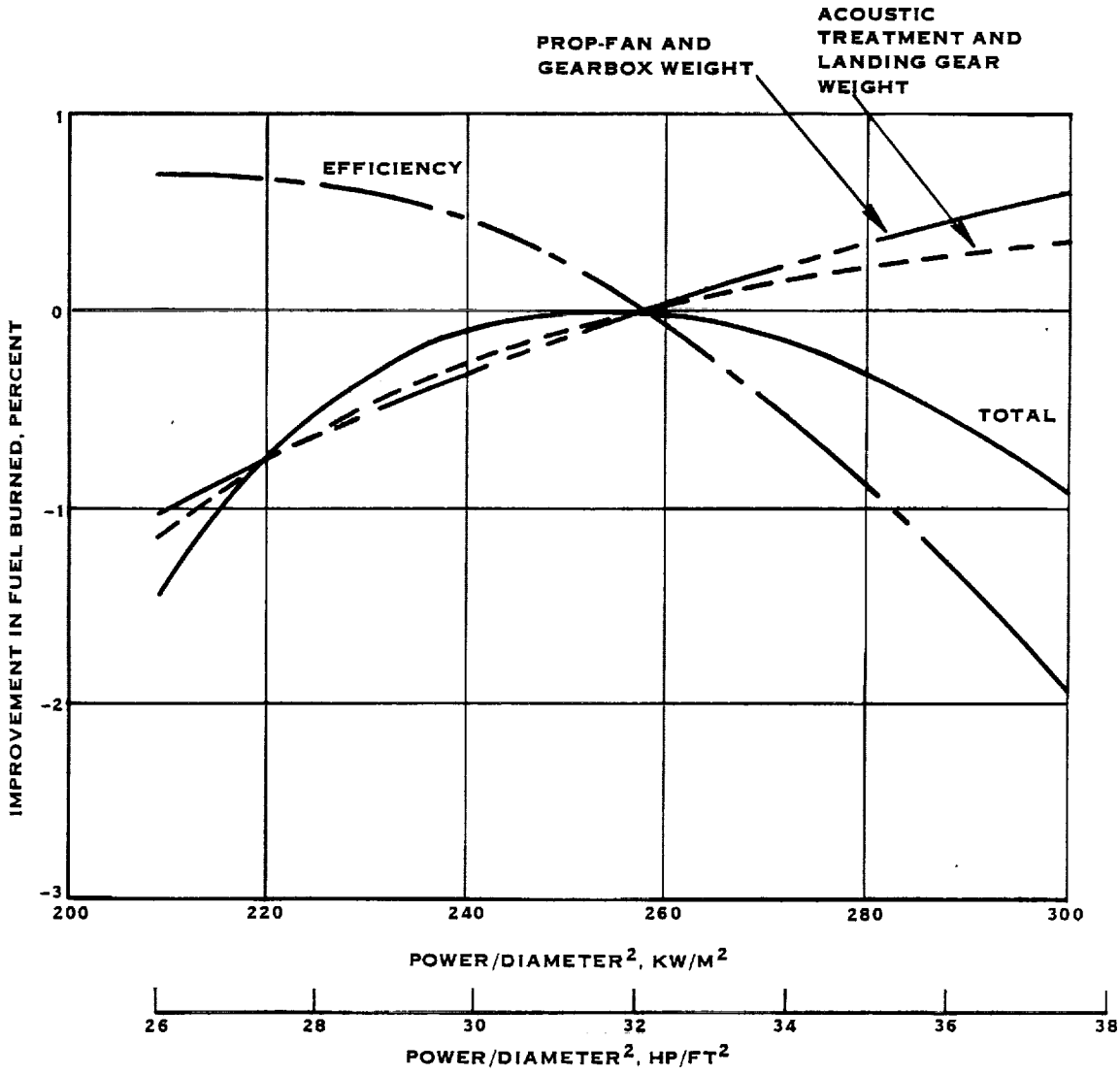

FIGURE 8.14 IMPROVEMENT IN FUEL BURNED VS. POWER LOADING

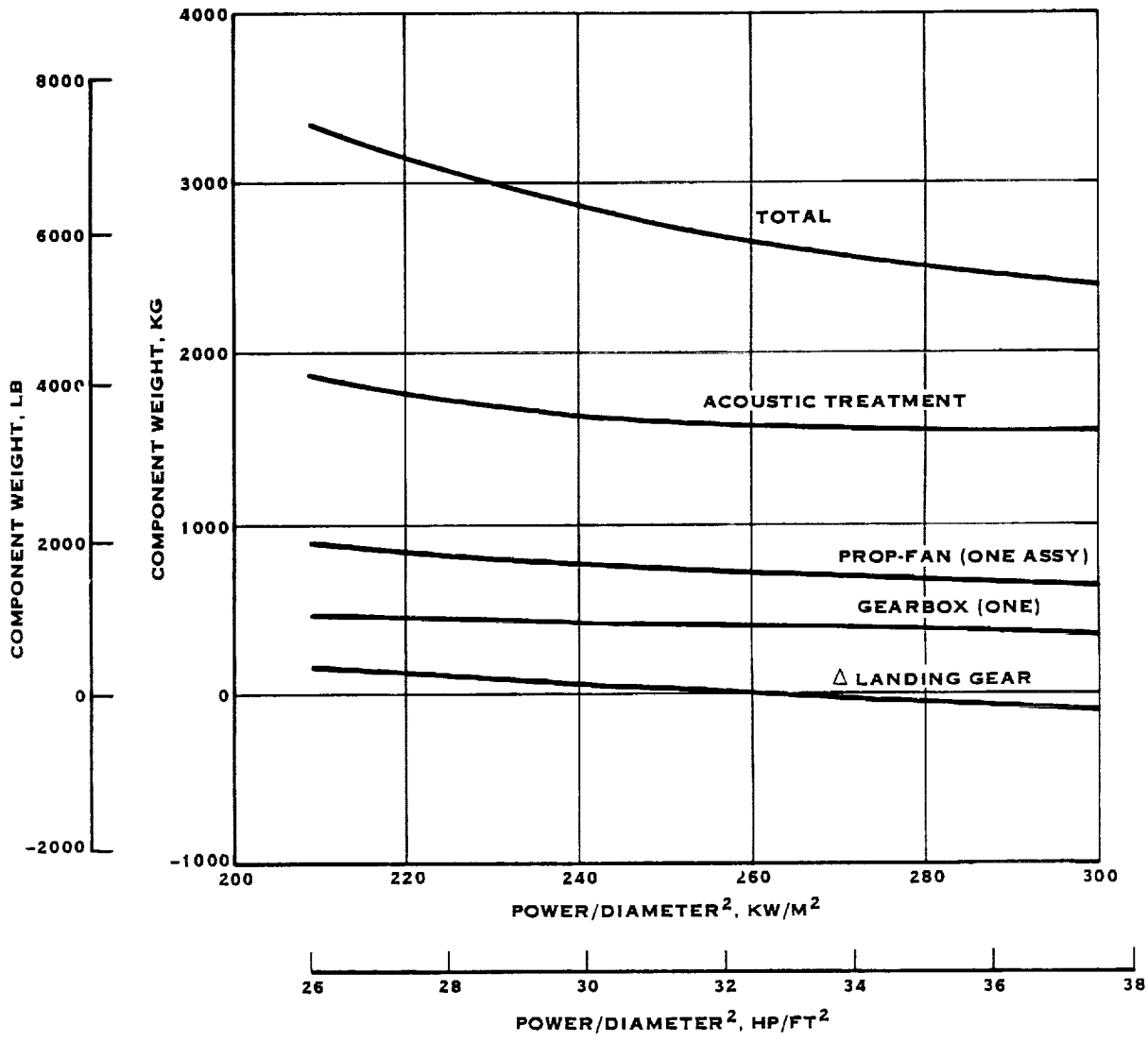

FIGURE 8.15 COMPONENT WEIGHTS VS. POWER LOADING

TABLE 8.6
SELECTED OPERATING CONDITIONS FOR TRADE-OFF STUDY

Power Loading		Tip Speed		Ave Cruise Power		Blade Diameter		
KW/M2	HP/Ft2	M/S	Ft/S	KW	HP	M	Ft	RPM
264.9	33.0	259.1	850	4312	5782	4.03	13.24	1226.4
256.9	32.0	243.8	800	4312	5782	4.10	13.44	1136.7
224.7	28.0	213.4	700	4312	5782	4.38	14.37	930.3

8.4.7.2 Blade Parametric Trade-Off Study - The blade parameters evaluated in the trade-off study were discussed in detail in Section 8.4.5. They are shown in tabular form in Table 8.7 along with the corresponding case number. A total of 51 cases were run. Cases 1-12 are the baseline Prop-Fan cases discussed previously. Cases 13 through 44 were obtained by varying one geometric parameter at a time. The next seven cases (45 - 51) were evaluated less systematically in that more than one parameter was varied. This was done to check the superposition characteristics of blade geometry changes, in an effort to obtain the initial SR-7 configuration to be selected for further structural feasibility study (Case 51). The results of the above cases are summarized in Table 8.7. Figures 8.16 through 8.23 are graphical representations of the data of Table 8.7 and indicate the effects of varying blade geometry on net efficiency, peak blade passage frequency noise, fuel burned and direct operating cost.

8.4.7.2.1 Blade Number - The effect of changing blade number, for a constant solidity, is presented in Figures 8.16 for Cases 13 and 14. It is shown that increasing blade number increases net efficiency and reduces noise, thus lowering the fuel burned and direct operating cost (DOC).

8.4.7.2.2 Tip Sweep - The effect of varying tip sweep (defined in Figure 8.2), is shown in Figures 8.17 and 8.18 for Cases 15 -23, 45, 46 and 49. In general, increasing sweep improves performance until about 40 degrees of tip sweep is reached. As shown in Figure 8.17, the net efficiency peaks and then starts to fall off at sweep angles up to 39.6. However, for a blade sweep of 48.0°, efficiency continued to increase with increasing tip speed. Prop-Fan noise is reduced with increasing sweep. Improvements in fuel burned and DOC are also obtained with increasing sweep.

TABLE 8-7 TRADE-OFF STUDY RESULTS

#	CASE	TIP SPEED M/S	POWER LOADING kW/M^2	TIP SPEED FT/SEC	POWER LOADING HP/FT^2	NO. BLADES	BLADE TIP SWEEP, DEG.	THICKNESS RATIO	PLANFORM	DESIGN LIFT COEFFICIENT	TWIST	STACKING LINE RELATED TO HELIX	NET EFFICIENCY	PEAK NOISE dB-BPF	Δ FUEL BURNED IMPROVEMENT, %	Δ DIRECT OPERATING COST IMPROVEMENT, %
—	BASELINE	243.8	256.9	800	32	8	39.6	T1	BASELINE (AF = 238)	BASELINE (CLI = 0.214)	BASELINE	ON (Y/R_{TIP} = 200)	0.796	143.2	0.00	0.00
—		259.1	264.9	850	33	↓	↓	↓	↓	↓	↓	↓	0.796	143.8	0.43	0.31
—		213.4	224.7	700	28								0.790	140.2	− 1.43	−0.88
13	BLADE NUMBER	243.8	256.9	800	32	10							0.804	141.8	2.92	1.80
14		↓	↓	↓	↓	12							0.811	139.2	4.81	2.92
15	●	259.1	264.9	850	33	8	25.0						0.776	147.8	− 5.16	−2.99
16		243.8	256.9	800	32		↓						0.785	147.7	− 4.32	−2.78
17		213.4	224.7	700	28								0.786	146.8	− 5.90	−3.94
18		259.1	264.9	850	33		32.5						0.785	146.2	− 2.75	−1.57
19	SWEEP	243.8	256.9	800	32		↓						0.790	145.8	− 2.25	−1.44
20		213.4	224.7	700	28								0.786	144.3	− 3.90	−2.55
21		259.1	264.9	850	33		46.0						0.803	138.7	3.17	2.06
22		243.8	256.9	800	32		↓						0.796	138.5	1.76	1.28
23	●	213.4	224.7	700	28			T1A					0.787	139.3	− 1.53	−0.77
24	●	259.1	264.9	850	33		39.6	↓					0.775	143.8	− 2.97	−1.33
25		243.8	256.9	800	32		↓	T1B					0.774	143.2	− 3.44	−1.62
26	THICKNESS RATIO	213.4	224.7	700	28			↓					0.768	142.8	− 5.68	−3.82
27		259.1	264.9	850	33			T1					0.736	143.7	− 8.99	−4.15
28		243.8	256.9	800	32			↓					0.736	143.2	− 9.42	−4.44
29	●	213.4	224.7	700	28								0.729	141.7	−11.68	−5.77
30	●	259.1	264.9	850	33				WIDE TIP (AF = 258)				0.791	144.1	− 0.81	−0.37
31		243.8	256.9	800	32				NARROW TIP (AF = 217)				0.795	143.3	− 0.38	−0.18
32		213.4	224.7	700	28				WIDE SHANK (AF = 240)				0.794	141.3	− 1.47	−0.98
33	PLANFORM	259.1	264.9	850	33				BASELINE				0.799	144.4	0.66	0.34
34		243.8	256.9	800	32				↓				0.799	142.7	1.02	0.58
35		213.4	224.7	700	28								0.784	140.4	− 2.15	−1.12
36	●	243.8	256.9	800	32					HIGHER CLI = 0.273			0.788	143.2	− 1.22	−0.58
37	DESIGN LIFT COEFFICIENT	243.8	256.9	800	32					LOWER CLI = 0.163			0.788	143.2	− 1.22	−0.58
38										SHIFTED PEAK CLI = 0.171			0.794	142.2	0.14	0.19
39										BASELINE			0.792	143.4	− 0.66	−0.34
40	●									↓	HIGHER TIP		0.784	145.5	− 3.05	−1.78
41	TWIST										LOWER TIP		0.776	142.3	− 2.72	−1.17
42	●										HIGHER SHANK		0.783	142.8	− 1.76	−0.78
43	STACKING LINE										BASELINE	OFF (Y/R_{TIP} = 0.097)	0.795	144.3	− 0.61	−0.44
44											↓	OFF (Y/R_{TIP} = 0)	0.800	145.9	− 0.75	−0.76
45						10	46.0					ON	0.804	139.4	3.37	2.13
46						↓	25.0					↓	0.794	147.5	− 1.46	−1.02
47							39.6	T1A					0.784	140.7	− 0.20	0.36
48			224.7		28		32.5	T1					0.803	145.4	0.00	−0.25
49			256.9		32		0.0	↓					0.784	150.4	− 5.84	−3.26
50			↓		↓	8	36.0	T1 MOD	NARROW TIP	LOWER BASELINE		OFF (Y/R_{TIP} = 0.096)	0.791	143.9	− 0.75	−0.41
51						↓	36.0	↓	↓	↓	↓	↓	0.794	144.2	− 0.52	−0.35

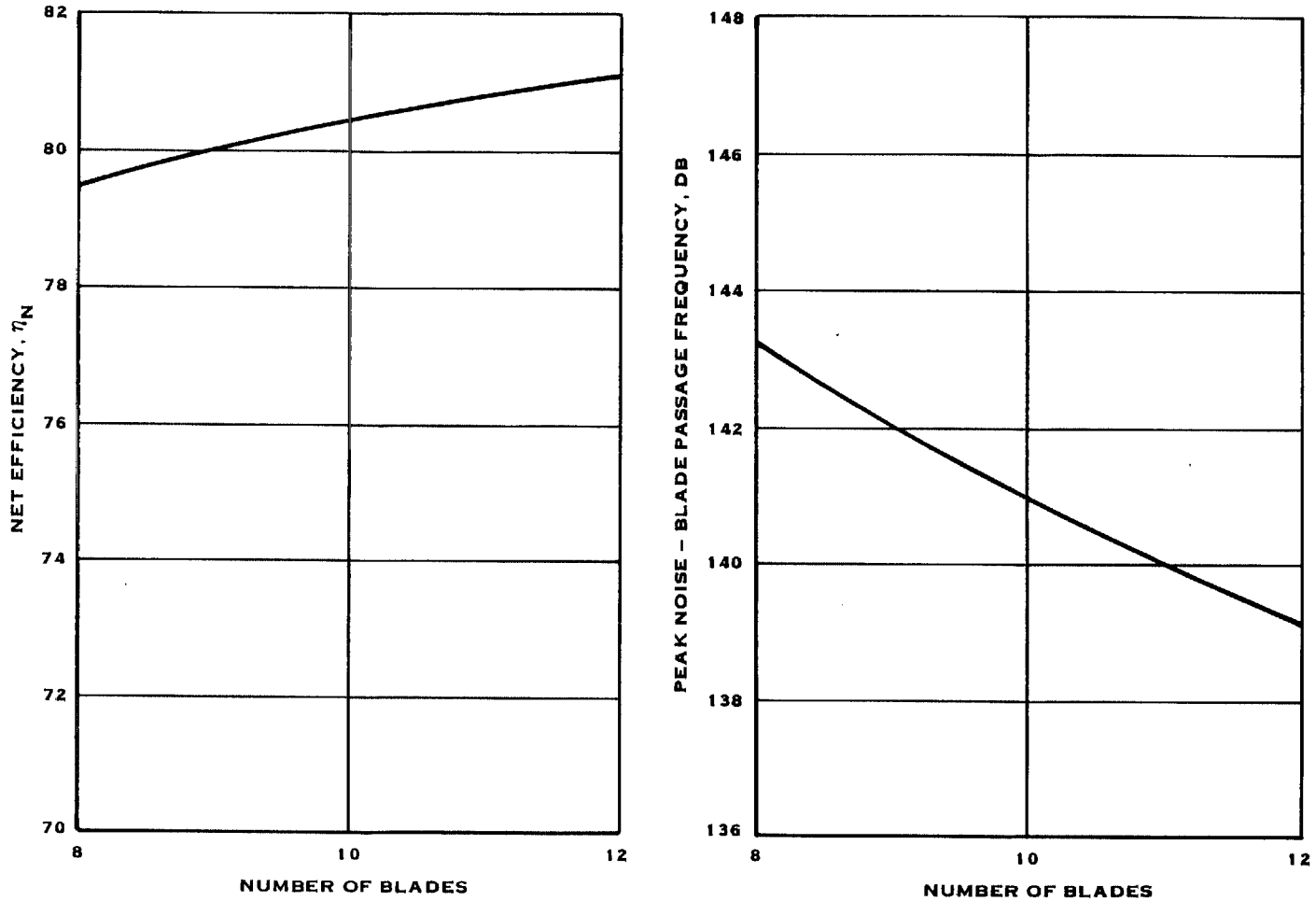

FIGURE 8.16 NET EFFICIENCY, PEAK NOISE AND IMPROVEMENT IN FUEL BURNED AND DIRECT OPERATING COST VS. NUMBER OF BLADES

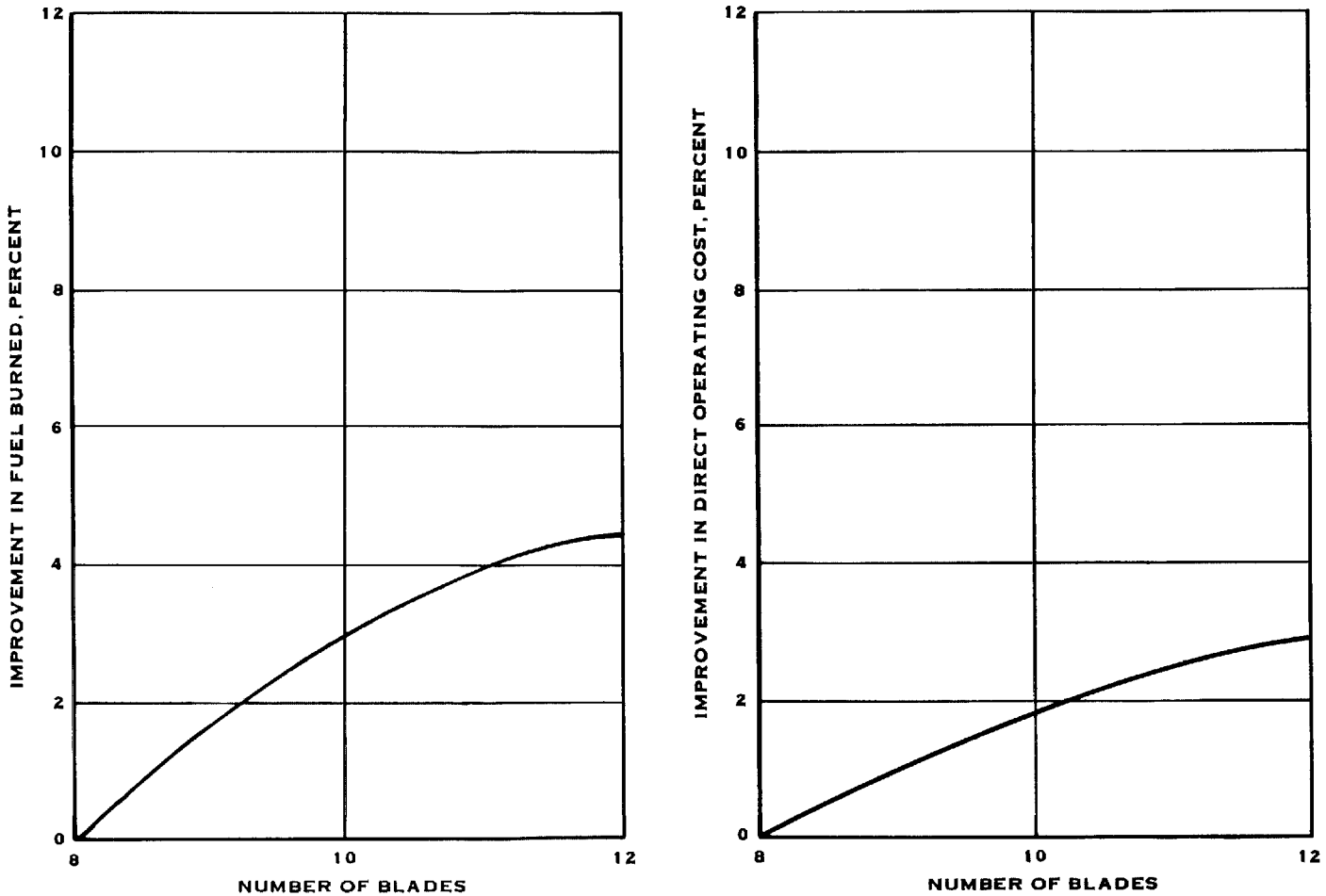

FIGURE 8.16 NET EFFICIENCY, PEAK NOISE AND IMPROVEMENT IN FUEL BURNED AND DIRECT OPERATING COST VS. NUMBER OF BLADES (CONT'D)

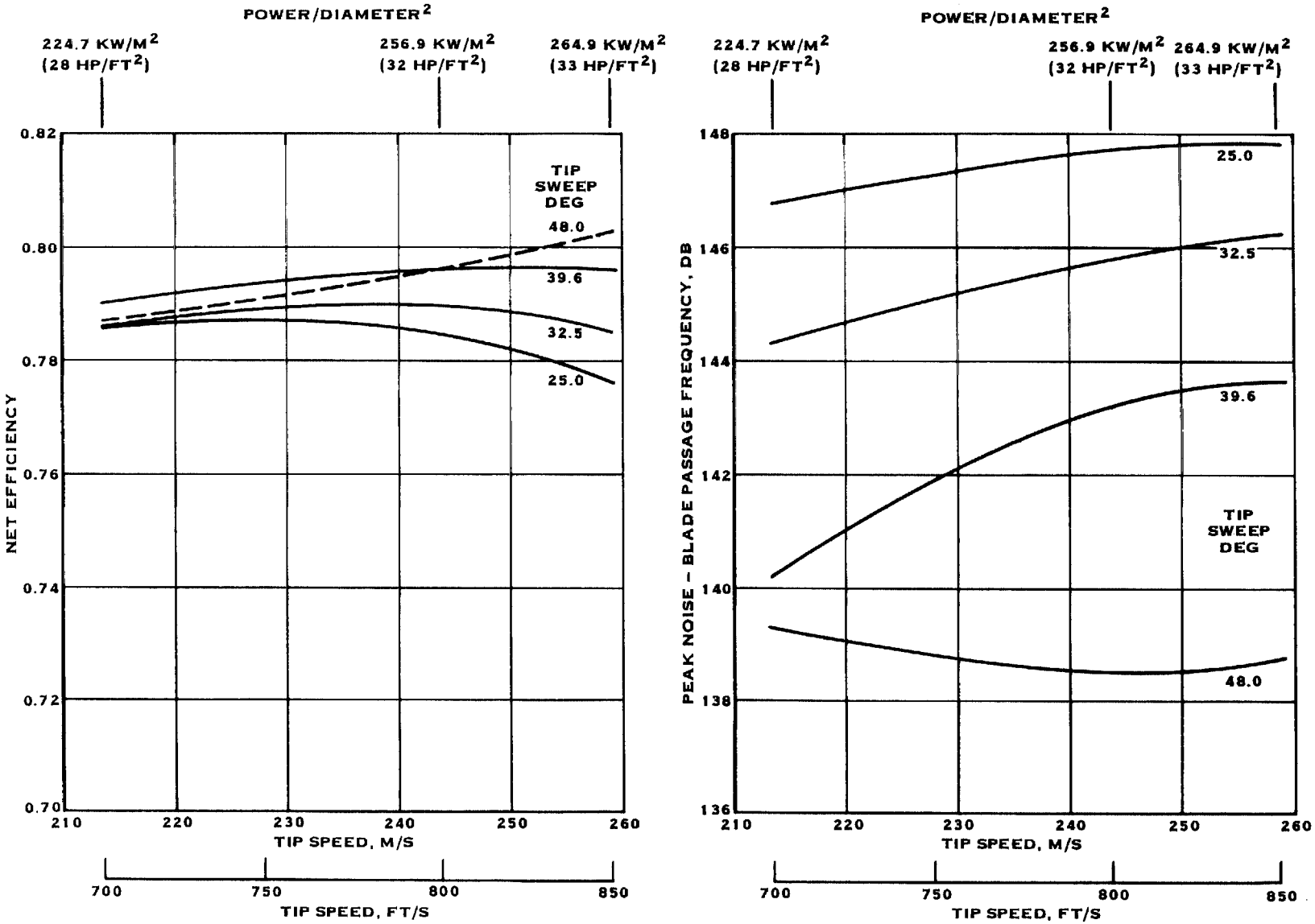

FIGURE 8.17 NET EFFICIENCY, PEAK NOISE AND IMPROVEMENT IN FUEL BURNED AND DIRECT OPERATING COST VS. TIP SPEED AND POWER LOADING FOR VARYING TIP SWEEP

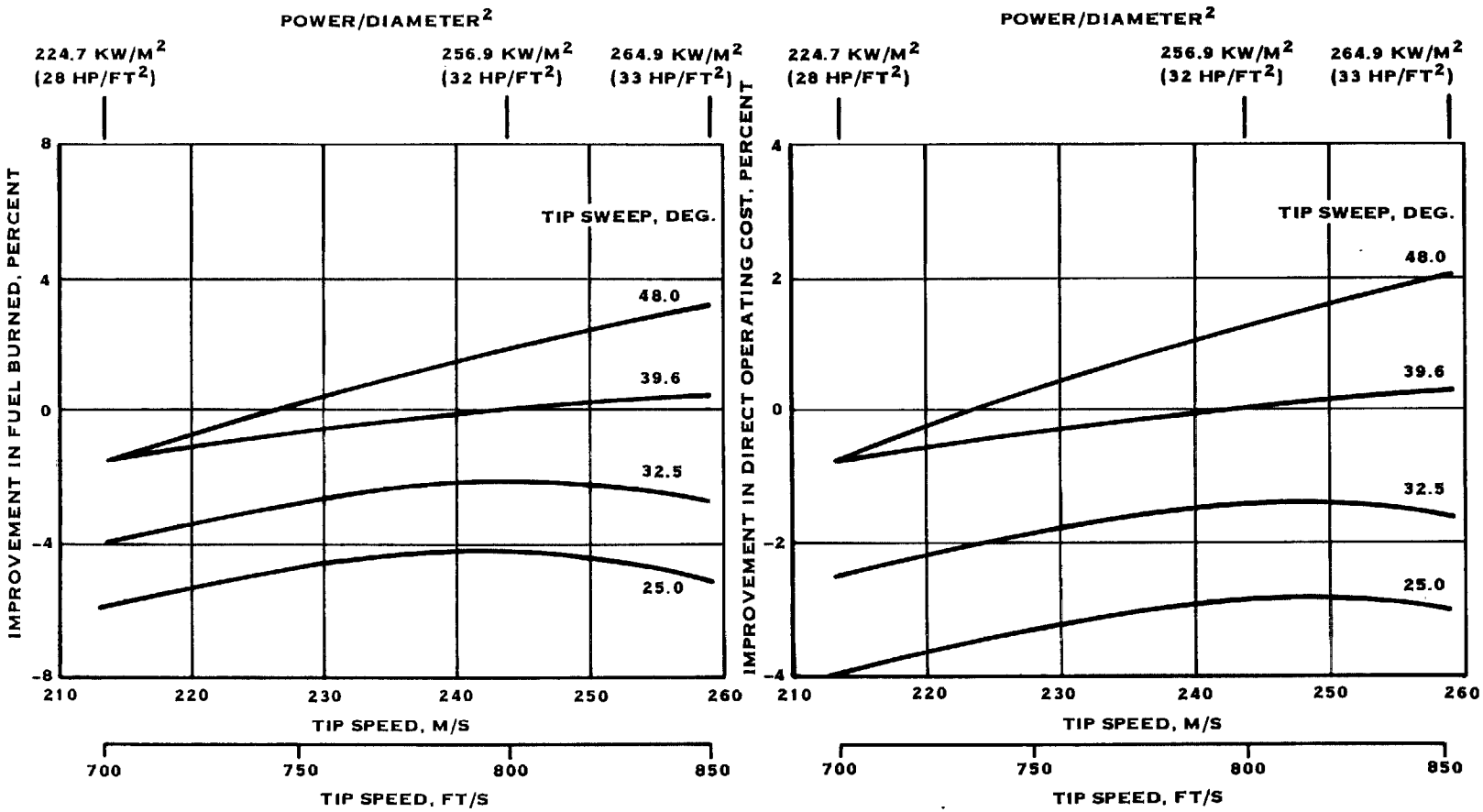

FIGURE 8.17 NET EFFICIENCY, PEAK NOISE AND IMPROVEMENT IN FUEL BURNED AND DIRECT OPERATING COST VS. TIP SPEED AND POWER LOADING FOR VARYING TIP SWEEP (CONT'D)

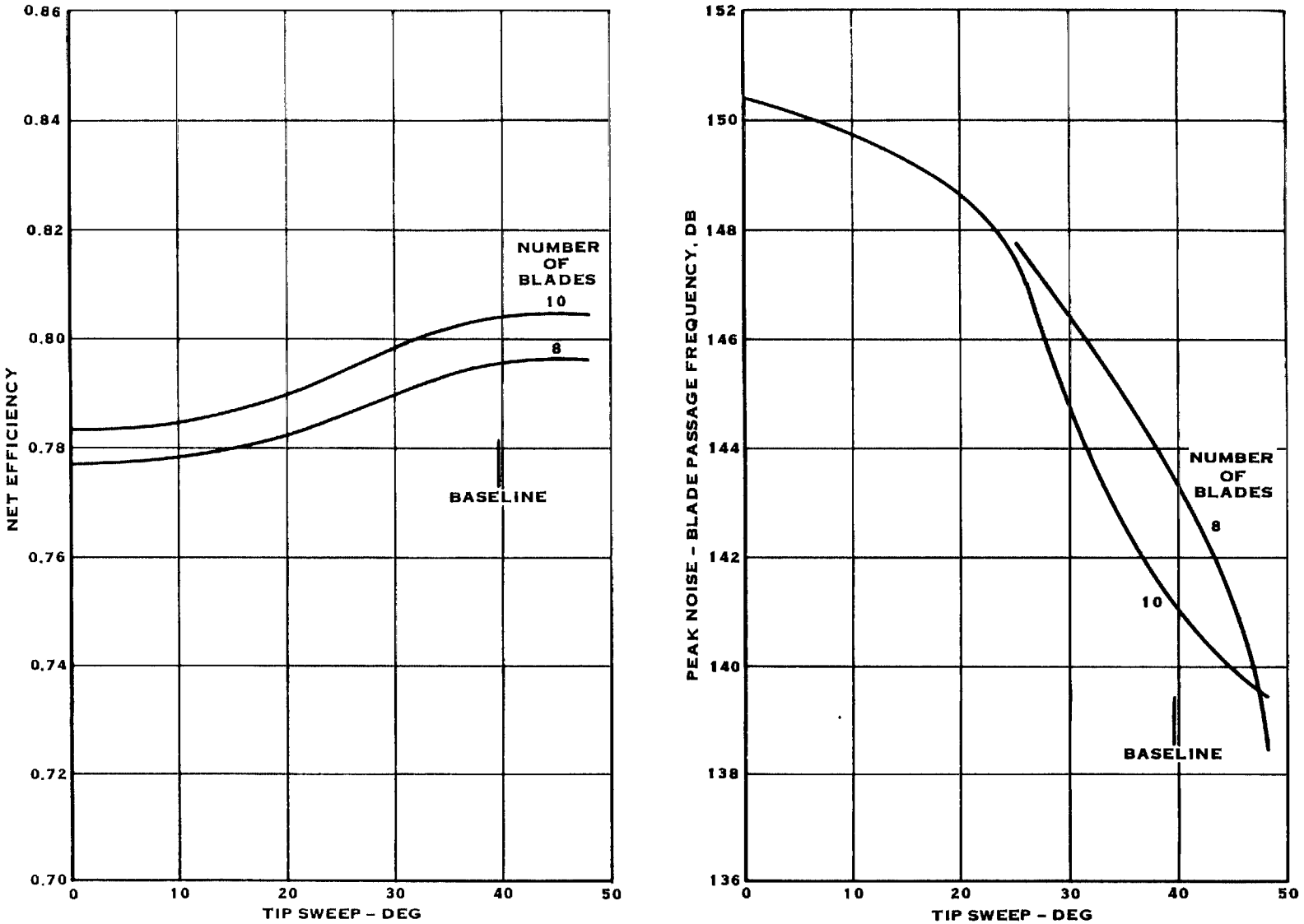

FIGURE 8.18 NET EFFICIENCY, PEAK NOISE AND IMPROVEMENT IN FUEL BURNED AND DIRECT OPERATING COST VS. TIP SWEEP FOR VARYING NUMBER OF BLADES

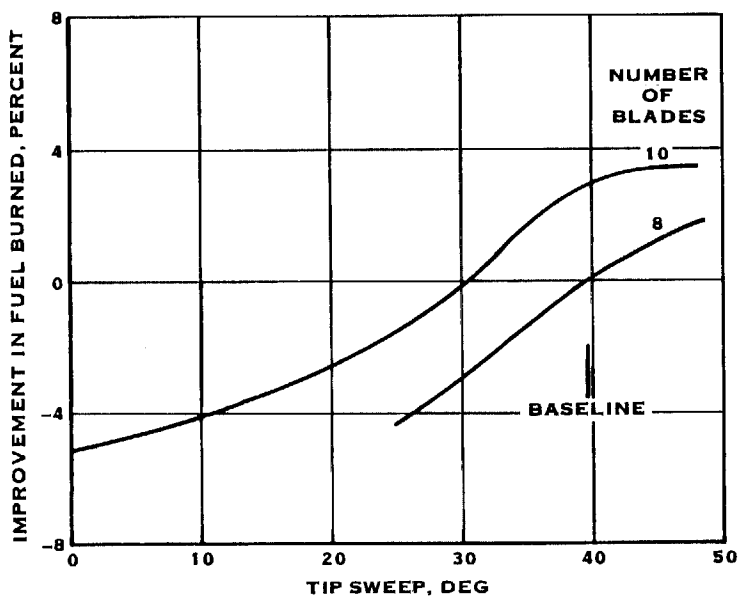

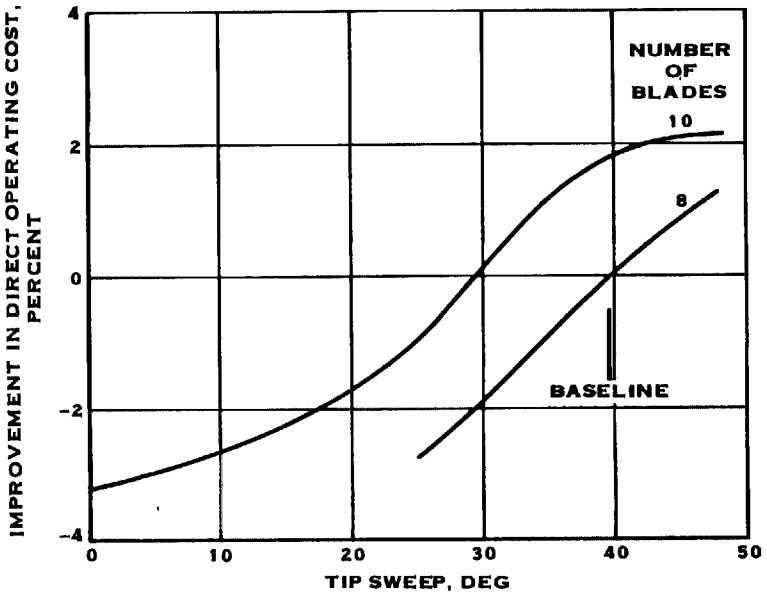

FIGURE 8.18 NET EFFICIENCY, PEAK NOISE AND IMPROVEMENT IN FUEL BURNED AND DIRECT OPERATING COST VS. TIP SWEEP FOR VARYING NUMBER OF BLADES (CONT'D)

Figure 8.18 presents net efficiency, noise, fuel burned and DOC, as a function of tip sweep, at a power loading of 256.9 KW/M^2 (32 HP/FT^2) and a tip speed of 243.8 M/S (800 FT/S) for both an 8 and 10 bladed Prop-Fan. As shown in the figure, an improvement in both net efficiency and noise level is evidenced as sweep increases. Efficiency begins to peak beyond 40° and noise level continues to be suppressed. The figure indicates the fuel burned and DOC peaking at 48° of sweep for the 10 bladed Prop-Fan, but not for 8 blades.

8.4.7.2.3 Thickness Ratio - The next geometry parameter varied, Cases 24 - 29, involved blade thickness ratio distribution, defined in Figure 8.3. Figure 8.19 shows the effect of thickness ratio on net efficiency and noise. The major effect is on performance, and is caused by a combination of higher profile losses and reduced choke margin with increased thickness ratio. Noise is affected only at the lower tip speeds. The figure shows the increase in fuel burned and DOC at increased thickness ratios to be quite severe.

8.4.7.2.4 Planform - Blade planform variations, defined in Figure 8.4, include Cases 31 - 36 of Table 8.7. Figure 8.20 shows that the effect of blade planform on net efficiency and noise is highly dependent on tip speed and power loading. The narrow tip blade shows an improvement in performance at the higher tip speeds, and the wide tip blade is better at lower tip speeds. The wide shank blade shows an appreciable performance loss. The narrow tip blade results in lower noise over most of the tip speed range. The figure shows the narrow tip planform to be the best planform for most tip speeds in terms of reduced fuel burned and DOC.

8.4.7.2.5 Design Life Coefficient - The blade design lift coefficient distributions studies are shown in Figure 8.5 and include Cases 37 - 39 of Table 8.7. In Figure 8.21 the net efficiency and noise are plotted as a function of integrated design lift coefficient, CLi.

The curve shows that the baseline C_{L_D} distribution is best for performance; whereas noise improves as CLi decreases. Shifting the peak design C_L inboard (Case 39) lowers efficiency and raises noise. The figure shows that very little improvement in fuel burned or direct operating cost is attainable by reducing the CLi below that of the baseline blade. However, raising the integrated design CL, results in progressively increased losses.

8.4.7.2.6 Twist - The blade twist distributions studies are shown in Figure 8.6 and include three twist changes in the outer 25% of the blade and one inboard retwist. The twist change plotted in Figure 8.22 includes Cases 40 - 42. The twist change between the .75 radius and the tip is shown as the abscissa of the figure. It is noted in the figure that the baseline twist yields peak efficiency. The higher shank twist (Case 42) unloads the blade tip similar to the high twist (Case 41), which has a lower tip blade angle. Both cases show a large reduction in net efficiency. In contrast, unloading the blade tip is beneficial in lowering the noise level. In the figure, it is seen that efficiency and not noise is the driver, since improvement in fuel burned and DOC peak at the baseline blade twist.

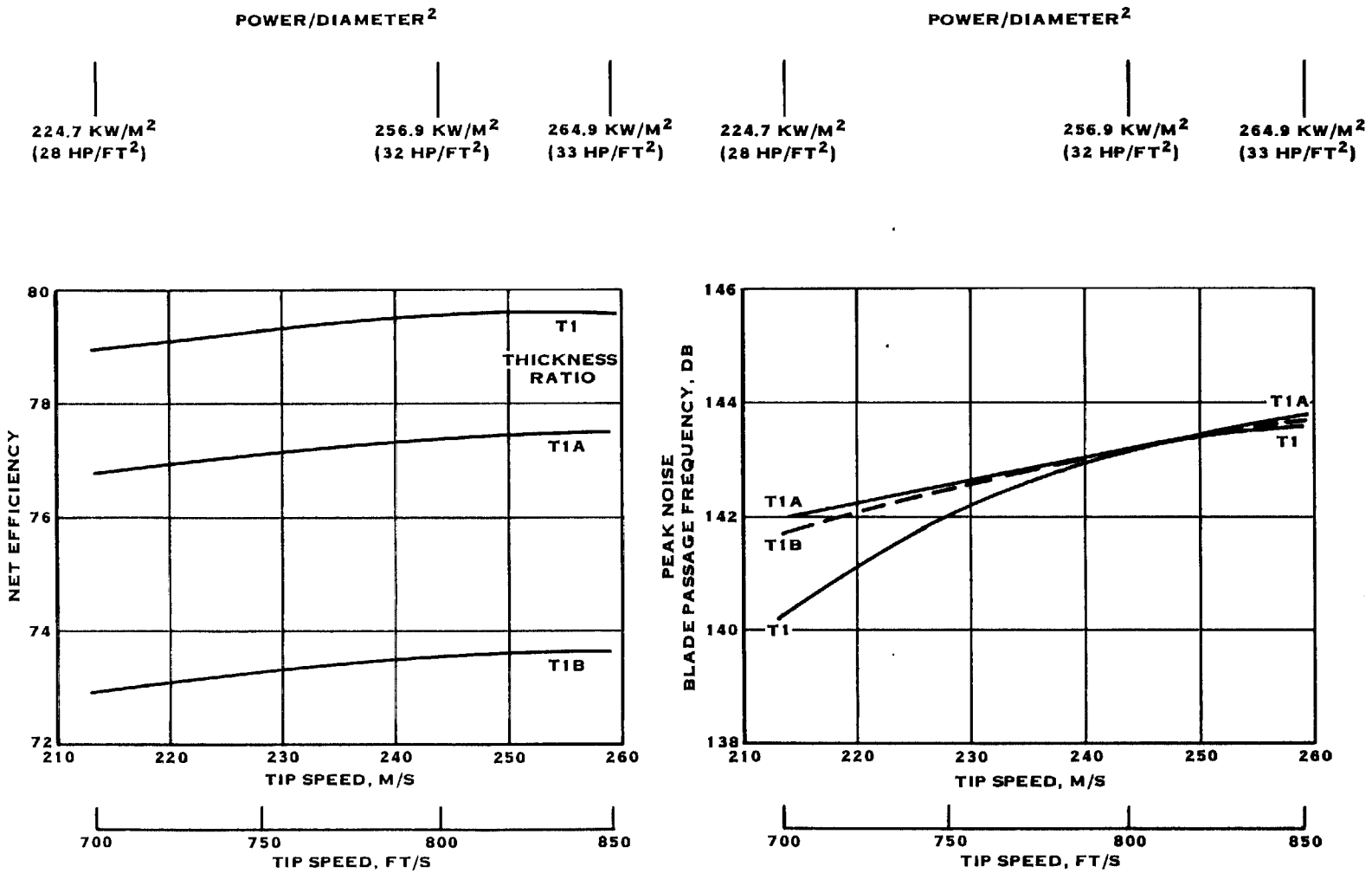

FIGURE 8.19 NET EFFICIENCY, PEAK NOISE AND IMPROVEMENT IN FUEL BURNED AND DIRECT OPERATING COST VS. TIP SPEED AND POWER LOADING FOR VARYING THICKNESS RATIO

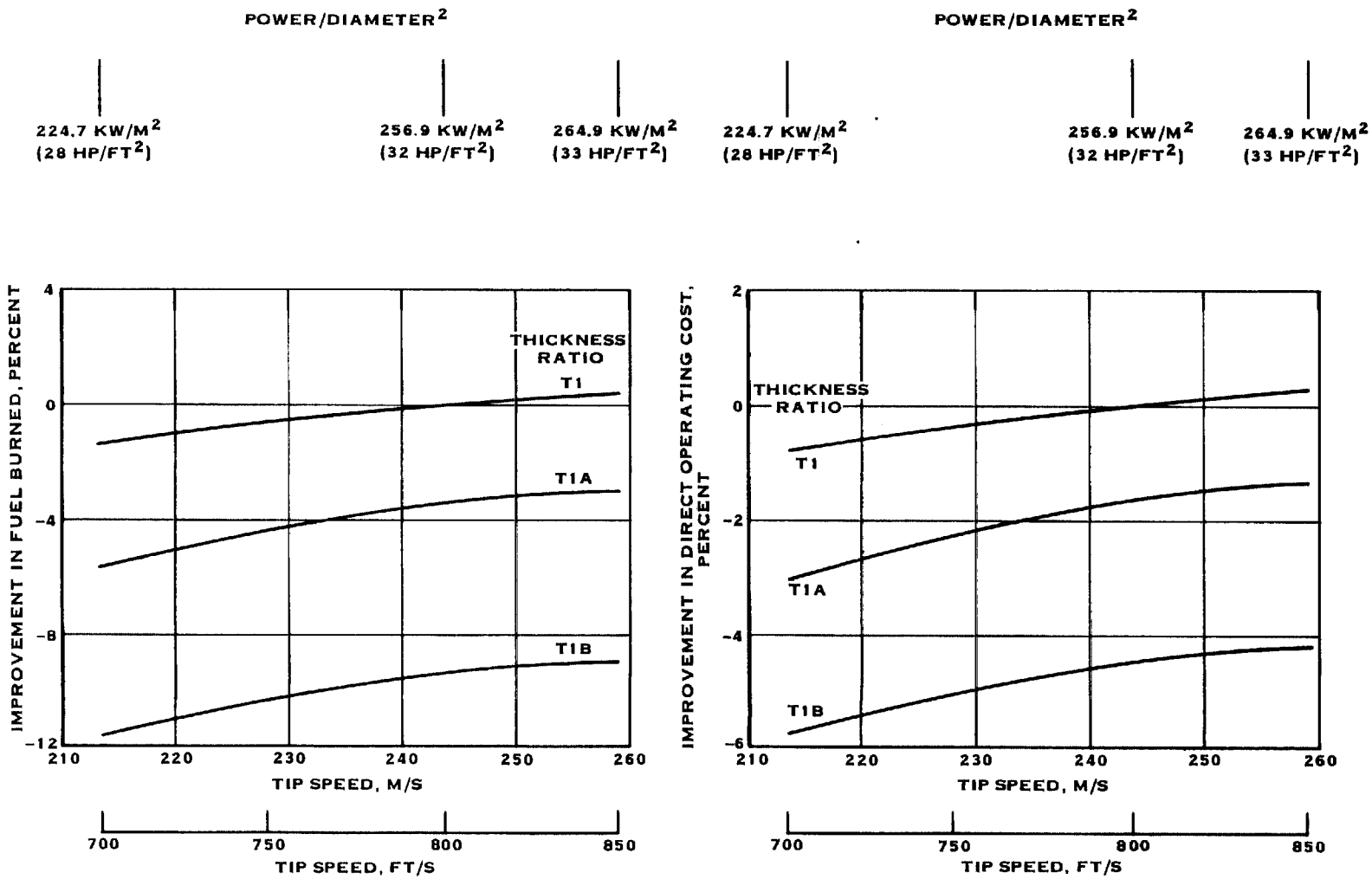

FIGURE 8.19 NET EFFICIENCY, PEAK NOISE AND IMPROVEMENT IN FUEL BURNED AND DIRECT OPERATING COST VS. TIP SPEED AND POWER LOADING FOR VARYING THICKNESS RATIO (CONT'D)

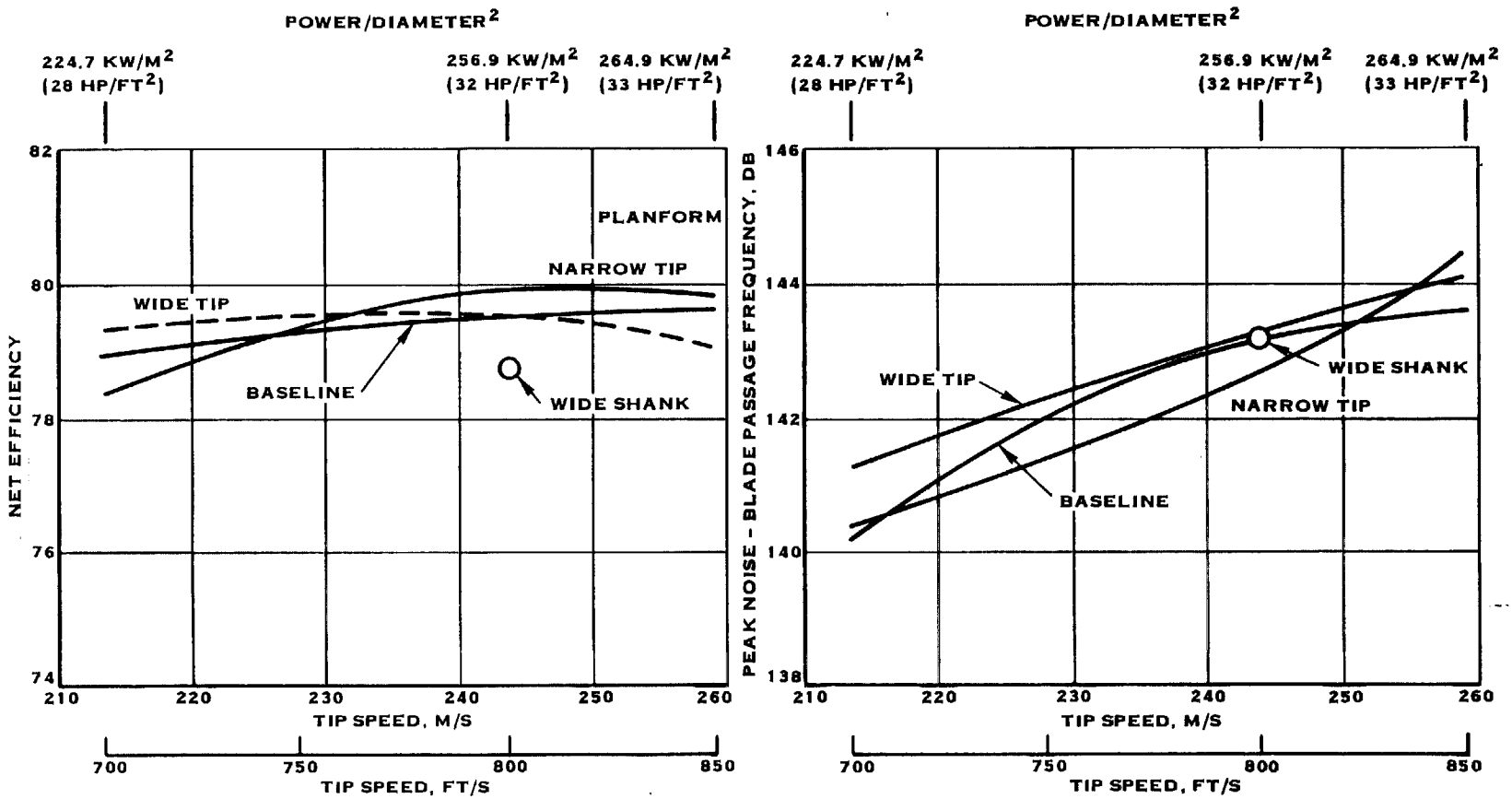

FIGURE 8.20 NET EFFICIENCY, PEAK NOISE AND IMPROVEMENT IN FUEL BURNED AND DIRECT OPERATING COST VS. TIP SPEED AND POWER LOADING FOR VARYING PLANFORM

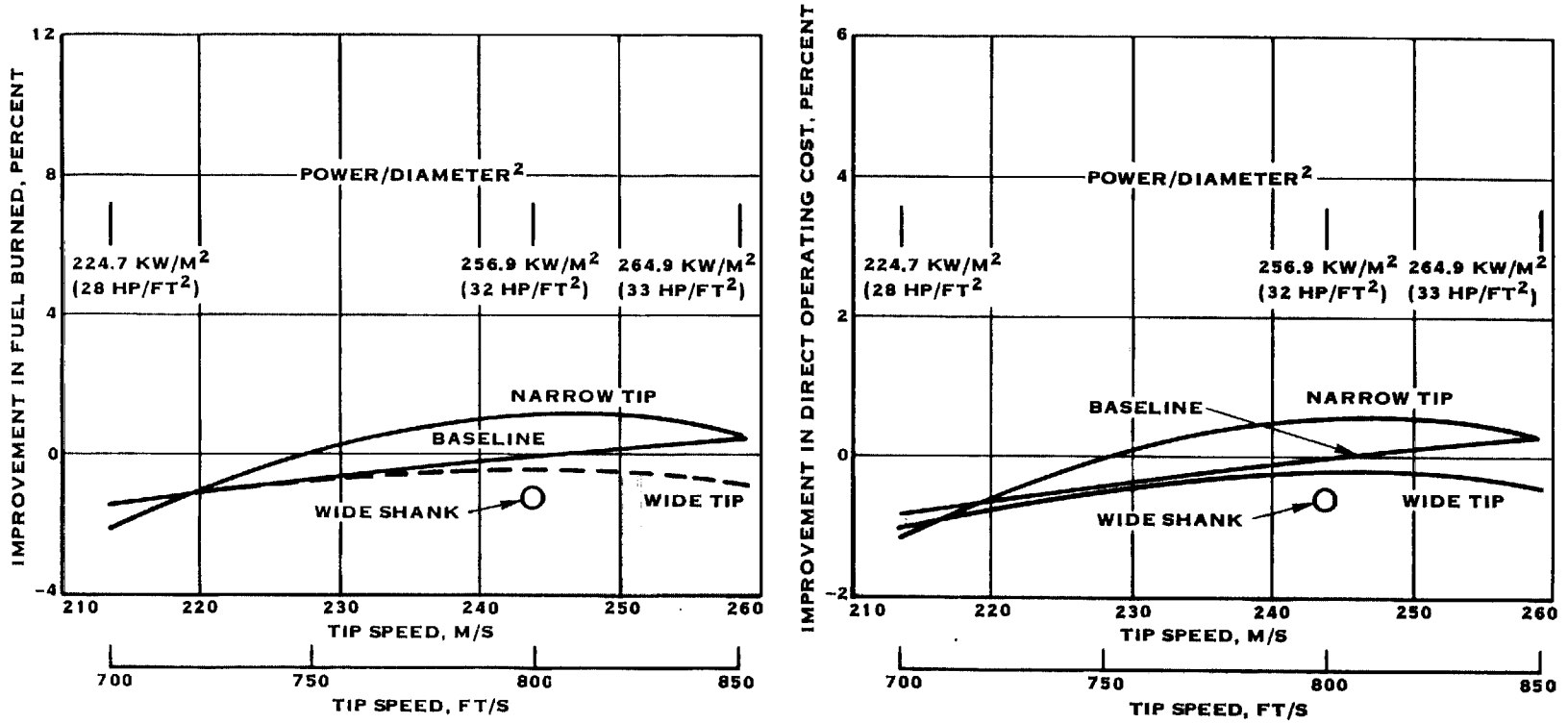

FIGURE 8.20 NET EFFICIENCY, PEAK NOISE AND IMPROVEMENT IN FUEL BURNED AND DIRECT OPERATING COST VS. TIP SPEED AND POWER LOADING FOR VARYING PLANFORM (CONT'D)

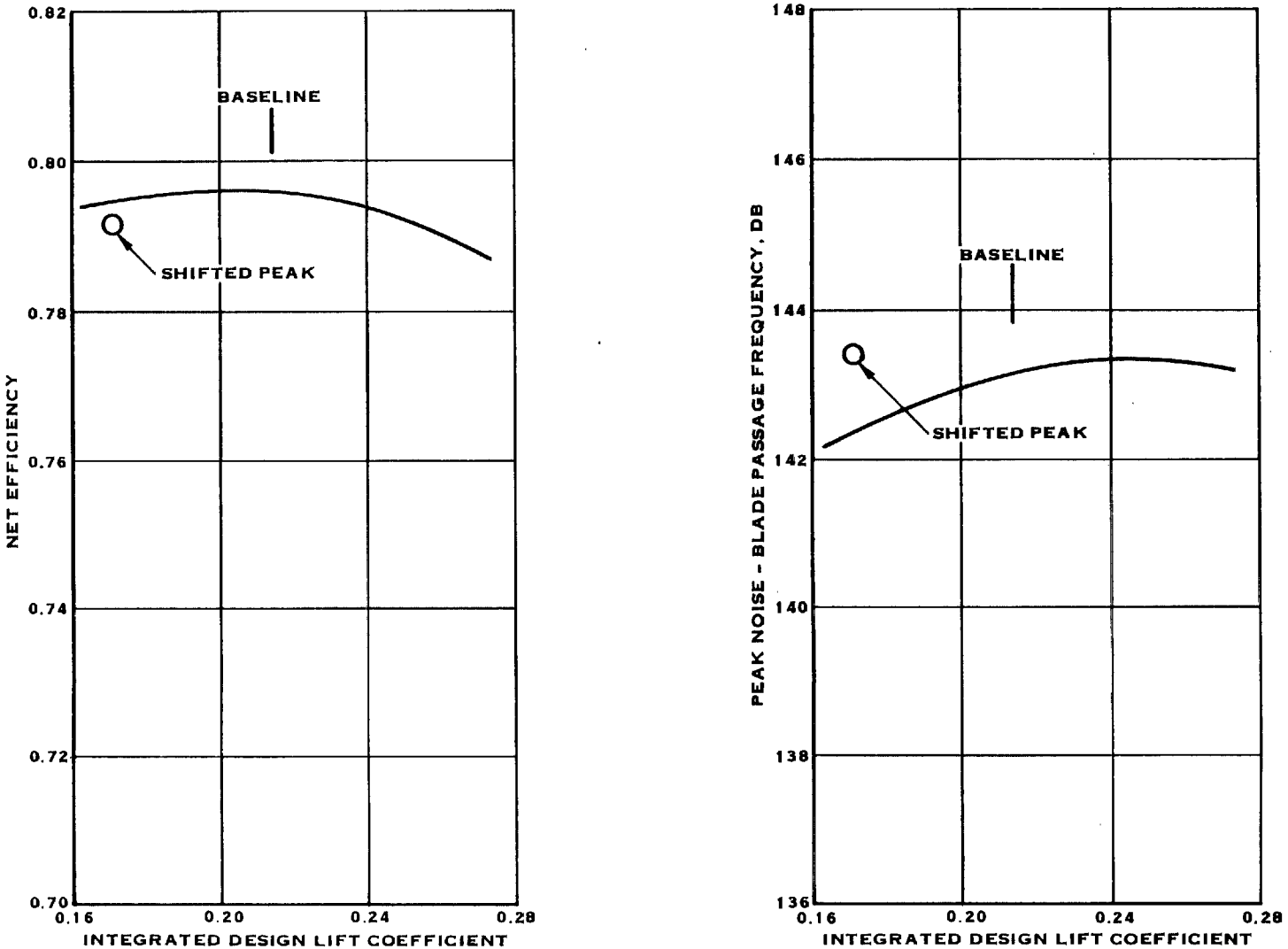

FIGURE 8.21 NET EFFICIENCY, PEAK NOISE AND IMPROVEMENT IN FUEL BURNED AND DIRECT OPERATING COST VS. INTEGRATED DESIGN LIFT COEFFICIENT

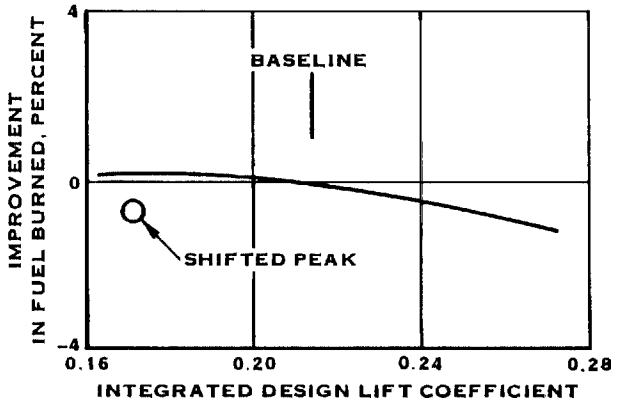

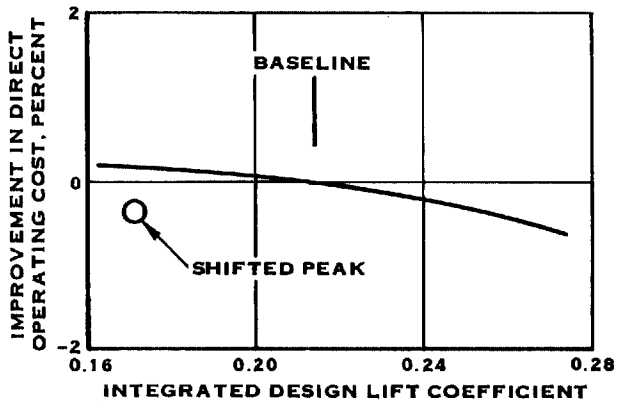

FIGURE 8.21 NET EFFICIENCY, PEAK NOISE AND IMPROVEMENT IN FUEL BURNED AND DIRECT OPERATING COST VS. INTEGRATED DESIGN LIFT COEFFICIENT (CONT'D)

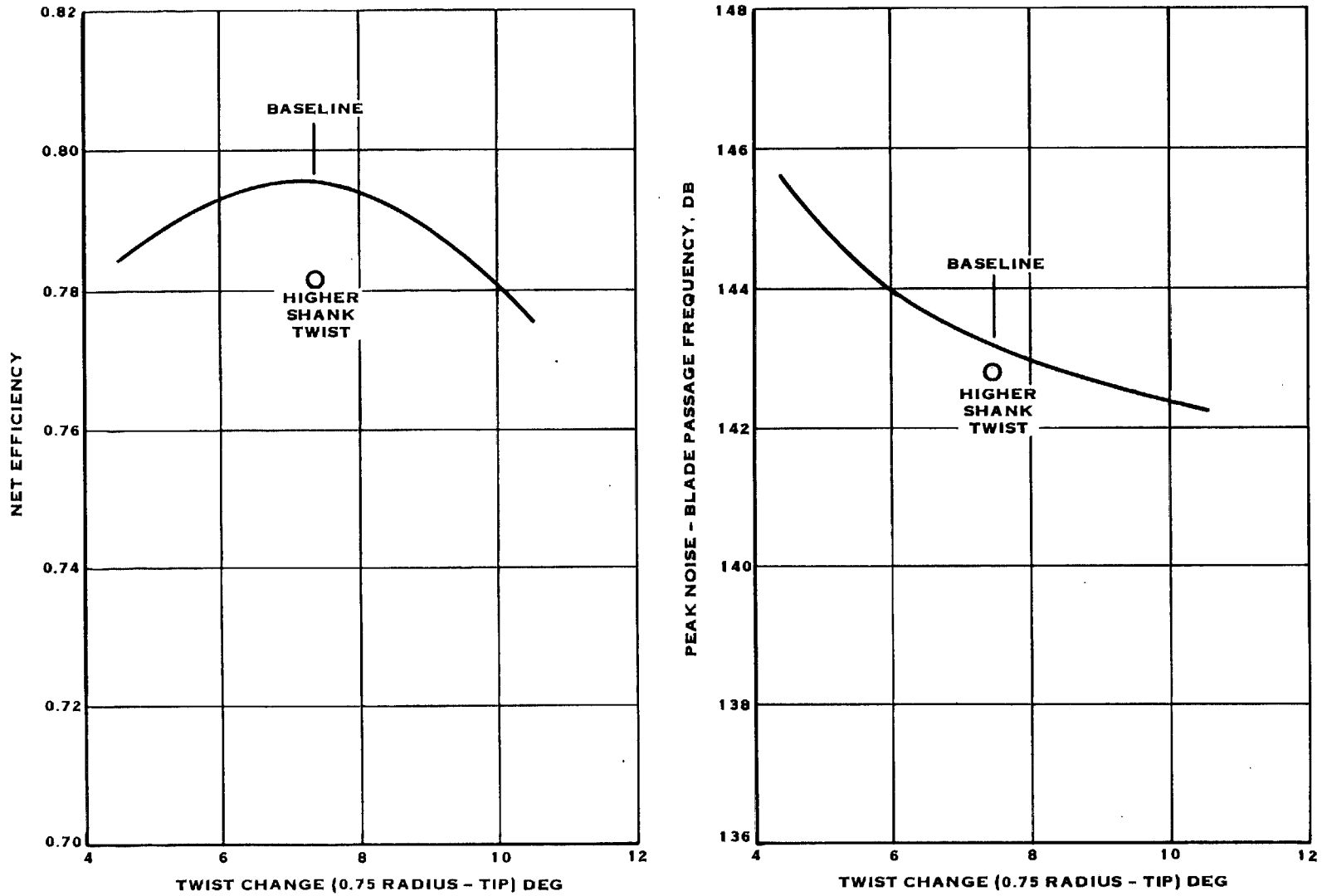

FIGURE 8.22 NET EFFICIENCY, PEAK NOISE AND IMPROVEMENT IN FUEL BURNED AND DIRECT OPERATING COST VS. TWIST CHANGE

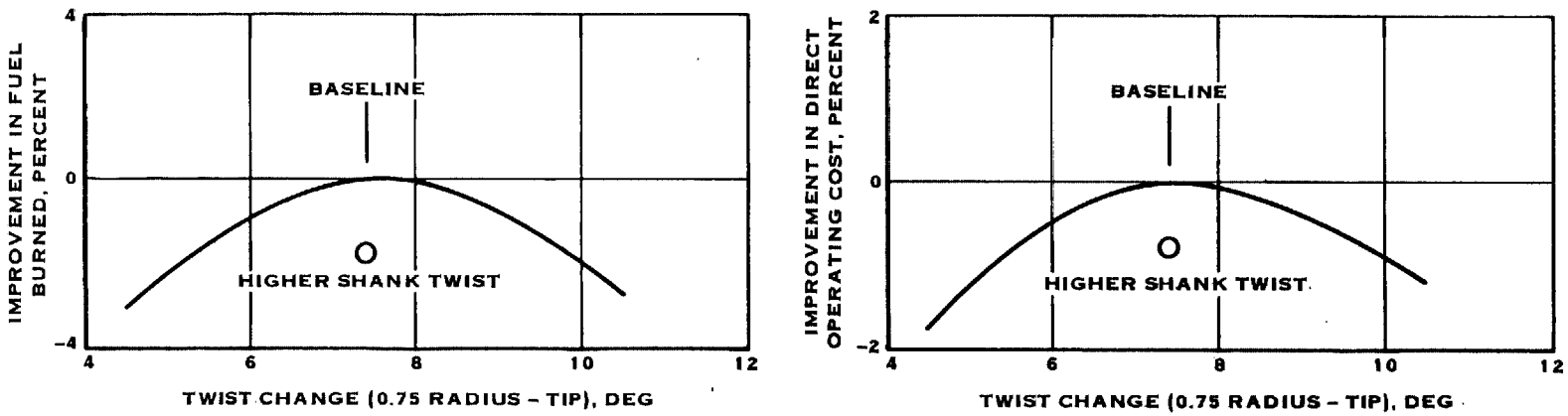

FIGURE 8.22 NET EFFICIENCY, PEAK NOISE AND IMPROVEMENT IN FUEL BURNED AND DIRECT OPERATING COST VS. TWIST CHANGE (CONT'D)

8.4.7.2.7 Stacking - The final blade parameter studied was blade stacking (reference Figure 8.7). The variations and the definition of the X, Y, Z coordinates of the 50% chordline are shown in Figure 8.7. Cases 43 and 44 were studied, and the performance and noise results are given in Figure 8.23.

It is noted that restacking has essentially no effect on performance with an increasingly adverse effect on noise as the blade stacking moves away from the helix.

The results are plotted versus the tip inplane coordinate Y/R, for convenience, and it should be noted that a decrease in Y/R requires an increase in the axial coordinate, Z/R to maintain constant sweep angle.

Thus, the baseline Prop-Fan stacked on the helix has the lowest fuel burned and direct operating cost as shown in Figure 8.23. However, the effect of restacking on fuel burned is quite small, and there appears to be good structural reasons for desiring less in-plane lean, Y/R.

8.4.8 Sensitivity Factor Check - The sensitivity factor for Prop-Fan net efficiency (1 point efficiency = 1.57% fuel burned as shown in Table 8.4) used in this study is an average value for the entire mission. The question can be raised whether the best Prop-Fan configuration at the 0.8 Mach number average cruise of this study will also be the best at the other flight conditions of the mission. Since a 0.6 Mach number on route climb condition is the other major fuel consumption portion of the mission, a check of the net efficiency at this MN was made for three configurations. It is maintained that if it can be shown that the efficiency trend with geometric variations is similar at both 0.6 and 0.8 Mach number, then a single overall mission efficiency sensitivity factor can legitimately be used. The three blade configurations studied included the baseline, the 10 bladed design (Case 13) and the 48° of tip sweep blade (Case 22). The tip speed was held constant at 243.0 M/S (800 FT/S). The power loading at the .6 Mach number, on-route climb case, was selected to be maximum continuous power at the Mach number. The altitude selected was 3048M (10,000 FT).

Table 8.8 shows the results of this sensitivity check. The last column shows the change in net efficiency for the three configurations with respect to the baseline Prop-Fan. It is immediately noted that the efficiency change is very similar at both 0.6 and 0.8 Mach number, representing the on-route climb and average cruise conditions, respectively. Thus, running the trade-off study at only 0.8 Mach number and using a mission sensitivity factor for propulsive efficiency is justified.

8.4.9 0.7 Mach Number Results - Since there is interest in cruising at Mach numbers lower than 0.8 MN, calculations were made at a 0.7 Mach number, 243.8 M/S tip speed (800 FT/S) condition for the three blade configurations studied in the previous section (the baseline, Case 13 and Case 22). These configurations are defined in Table 8.9. It was assumed that the power loading varied directly with Mach number to the third power. Consequently, a power loading of 172.6 KW/M^2 (21.5 HP/FT^2) was obtained at 0.7 MN. The

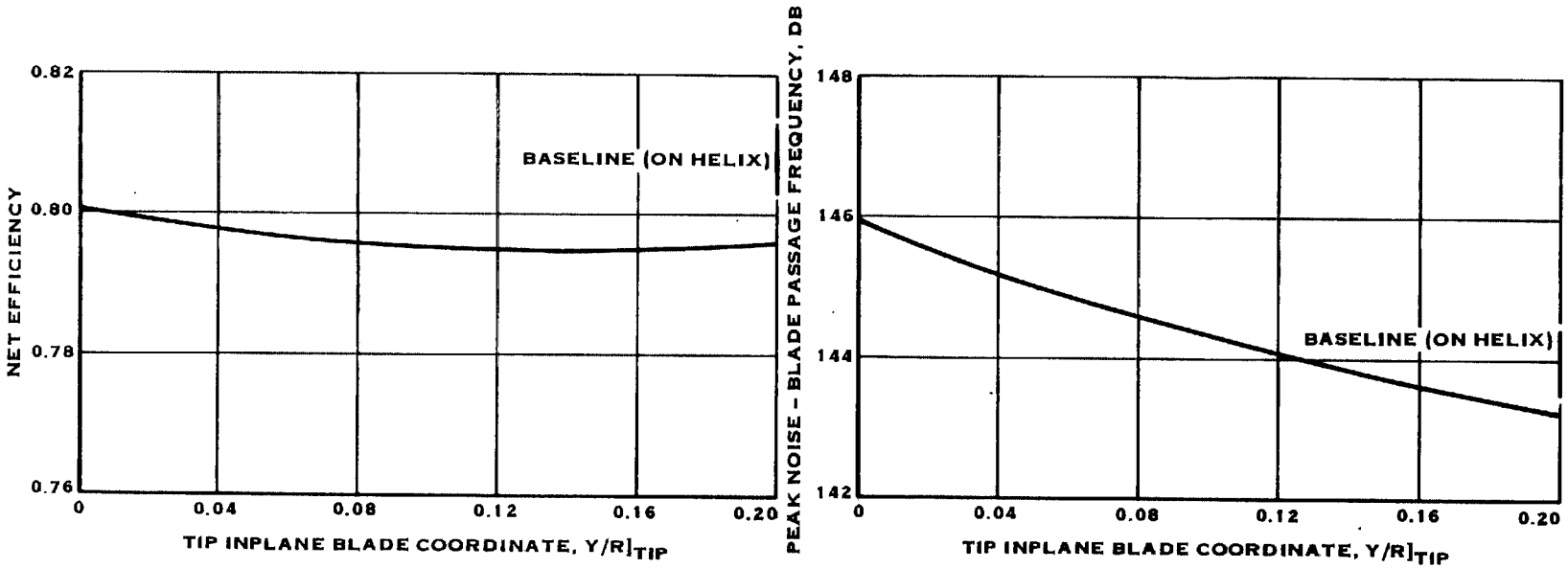

FIGURE 8.23 NET EFFICIENCY, PEAK NOISE AND IMPROVEMENT IN FUEL BURNED AND DIRECT OPERATING COST VS. STACKING LINE CHANGE

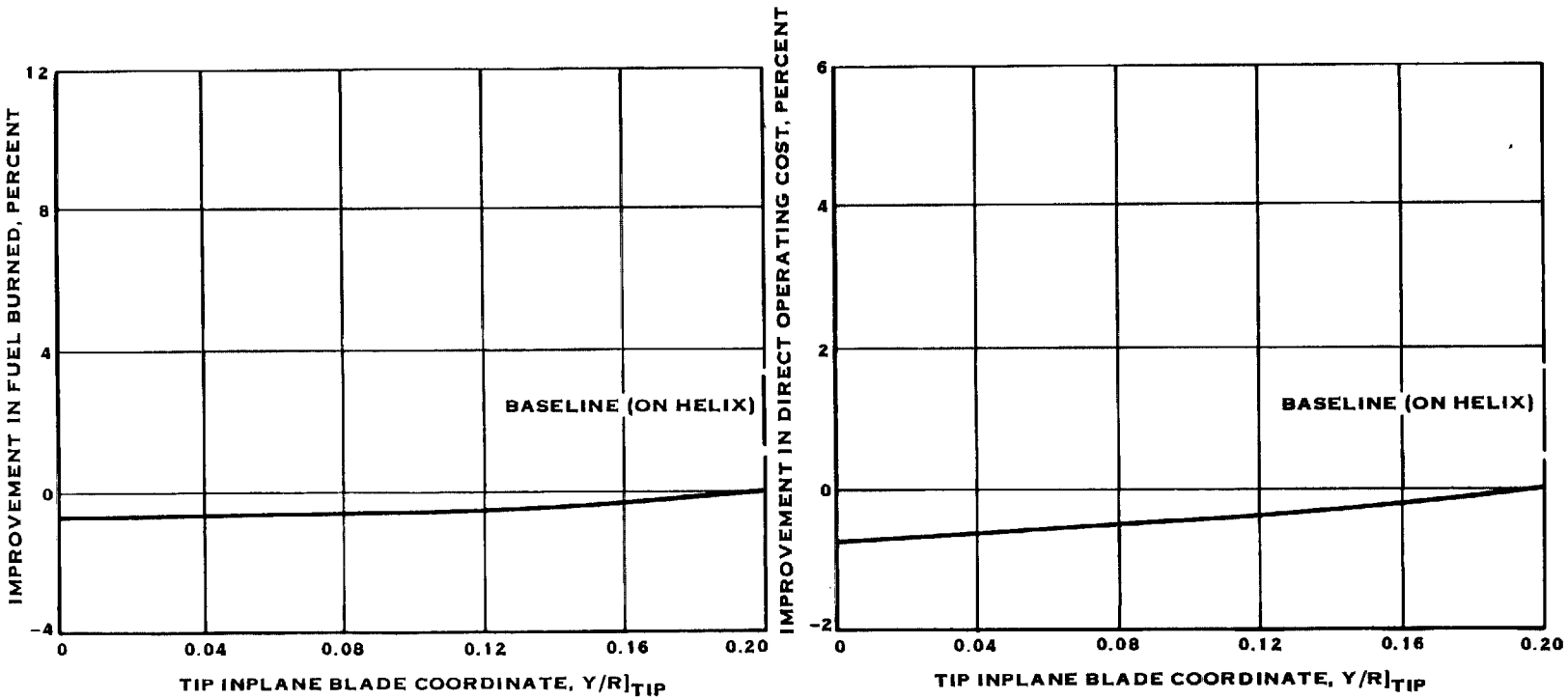

FIGURE 8.23 NET EFFICIENCY, PEAK NOISE AND IMPROVEMENT IN FUEL BURNED AND DIRECT OPERATING COST VS. STACKING LINE CHANGE (CONT'D)

TABLE 8-8 MISSION SENSITIVITY FACTOR CHECK RESULTS

#	CASE	MACH NUMBER	TIP SPEED M/S	POWER LOADING, kW/M^2	TIP SPEED FT/SEC	POWER LOADING, HP/FT^2	NO. BLADES	BLADE TIP SWEEP, DEG.	THICKNESS RATIO	PLANFORM	DESIGN LIFT COEFFICIENT	TWIST	STACKING LINE RELATED TO HELIX	NET EFFICIENCY	ΔNET EFFICIENCY
—	BASELINE	0.8	243.8	243.8	800	32.0	8	39.6	BASELINE	BASELINE	BASELINE	BASELINE	ON	0.796	0
—	↓	0.6	↓	475.4	↓	59.2	↓	↓	↓	↓	↓	↓	↓	0.806	0
13	BLADE NUMBER	0.8	↓	243.8	↓	32.0	10	↓	↓	↓	↓	↓	↓	0.804	0.008
—	↓	0.6	↓	475.4	↓	59.2	↓	↓	↓	↓	↓	↓	↓	0.813	0.007
22	SWEEP	0.8	↓	243.8	↓	32.0	8	48.0	↓	↓	↓	↓	↓	0.796	0
—	↓	0.6	↓	475.4	↓	59.2	↓	↓	↓	↓	↓	↓	↓	0.807	0.001

TABLE 8-9 0.7 MACH NUMBER RESULTS

#	CASE	MACH NUMBER	TIP SPEED M/S	POWER LOADING kW/M^2	TIP SPEED FT/SEC	POWER LOADING HP/D^2	NO. BLADES	BLADE TIP SWEEP, DEG.	THICKNESS RATIO	PLANFORM	DESIGN LIFT COEFFICIENT	TWIST	STACKING LINE RELATED TO HELIX	NET EFFICIENCY	PEAK NOISE dB-BPF	Δ FUEL BURNED IMPROVEMENT, %	Δ DIRECT OPERATING COST IMPROVEMENT, %
—	BASELINE	0.8	243.8	256.9	800	32.0	8	39.6	BASELINE	BASELINE	BASELINE	BASELINE	ON	0.796	143.2	0.00	0.00
—	↓	0.7	↓	172.6	↓	21.5	↓	↓	↓	↓	↓	↓	↓	0.812	137.0	2.57	1.21
13	BLADE NUMBER	0.8	↓	256.9	↓	32.0	10	↓	↓	↓	↓	↓	↓	0.804	141.0	2.92	1.80
—	↓	0.7	↓	172.6	↓	21.5	↓	↓	↓	↓	↓	↓	↓	0.819	135.9	5.29	2.92
22	SWEEP	0.8	↓	256.9	↓	32.0	8	48.0	↓	↓	↓	↓	↓	0.796	138.5	1.76	1.28
—	↓	0.7	↓	172.6	↓	21.5	↓	↓	↓	↓	↓	↓	↓	0.817	133.6	5.04	2.83

0.7 Mach number efficiencies and noise levels are shown in the table. At 0.7 Mach number, the net efficiency is higher and the noise levels are lower for all three blade configurations. In computing the change in fuel burned and DOC, it was assumed that the aircraft sensitivity factors at M = 0.8 were applicable at 0.7. It was also assumed that the acoustic treatment was sized at 0.8 Mach number. Thus, the fuel burned and DOC are only effected by Prop-Fan net efficiency. Based on these assumptions, it is noted that a 0.7 Mach number cruise reduces the fuel burned by 2.4 to 3.3%, depending on the configuration.

8.5 DESIGN REQUIREMENTS

8.5.1 Introduction

In Task I of this study (reference Section 3.0, Volume I), the design requirements for the structural design analysis to be conducted under Task III (reference Section 5.0, Volume I) were established.

8.5.2 Object

The object of this task is to reassess the design requirements established in Task I and change them as necessary to cover the SR-7 Prop-Fan for use in proposed wind tunnel and flight tests and reflect any new knowledge gained since the first requirements were defined.

8.5.3 Method

The studies being conducted under NASA contracts NAS3-22346 and NAS3-22347 by Lockheed and McDonnell Douglas, and the effort conducted under Task III of this contract were reviewed. Based on these reviews, a new Design Requirements Document was prepared and is included in Appendix D. A description of the design methods used is also included.

The major differences between the old and new documents is the incorporation of the latest flutter calculation method, and the design requirements and goals for the SR-7.

8.6 DESIGN SELECTION

In general, the results of the trade-off study show that a high number of very thin highly swept blades gives the optimum design from a fuel burn/DOC standpoint. However, the results of Task III and other studies have shown that it is not possible to structurally design this type of blade using state-of-the-art materials and manufacturing processes.

Therefore, the Prop-Fan selected for the initial structural analysis has eight blades and is moderately swept. The selected Prop-Fan is defined in Table 8.10. When compared to the baseline blade, this configuration yields a fuel burn loss of 1/2 percent (reference Table 8.7, configuration 51).

8.7 DESIGN SELECTION DOCUMENT

A design selection document was prepared and is included in Appendix E.

TABLE 8.10
PARAMETERS OF SELECTED PROP-FAN

	Testbed	Production
Mach Number (at 35,000 feet)	0.8	0.8
Number of Blades	8	8
Tip Speed (feet/second)	800	800
Power Loading (SHP/D^2)	32	32
Tip Diameter (feet)	9.0	14.0
Chord Ratio	See Figure 8.24	
Thickness Ratio	See Figure 8.24	
Twist Angle	See Figure 8.24	
Camber Angle	See Figure 8.24	
Cone Angle	See Figure 8.24	
Design Lift Coefficient	See Figure 8.24	
Sweep Angle	See Figure 8.24	
Sweep Coordinates	See Figure 8.24	
Fabrication Concept	•Solid Aluminum Spar •Fiberglass Shell •Nickel Sheath •Foam Fill	•Hollow Steel Spar •Fiberglass Shell •Titanium Sheath •Honeycomb Fill and •Solid Aluminum Spar •Fiberglass Shell •Nickel Sheath •Foam Fill

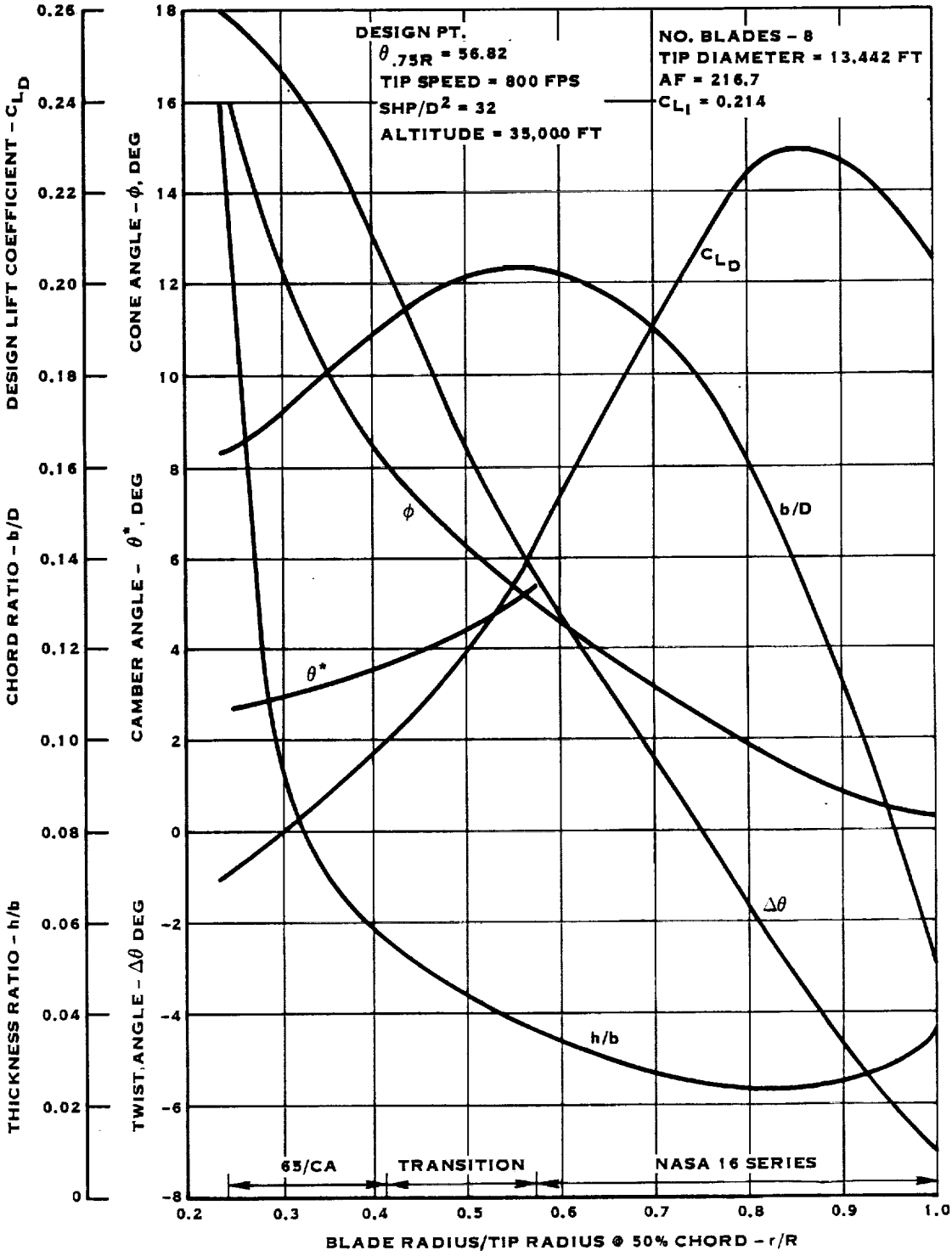

FIGURE 8.24 SELECTED BLADE CHARACTERISTICS

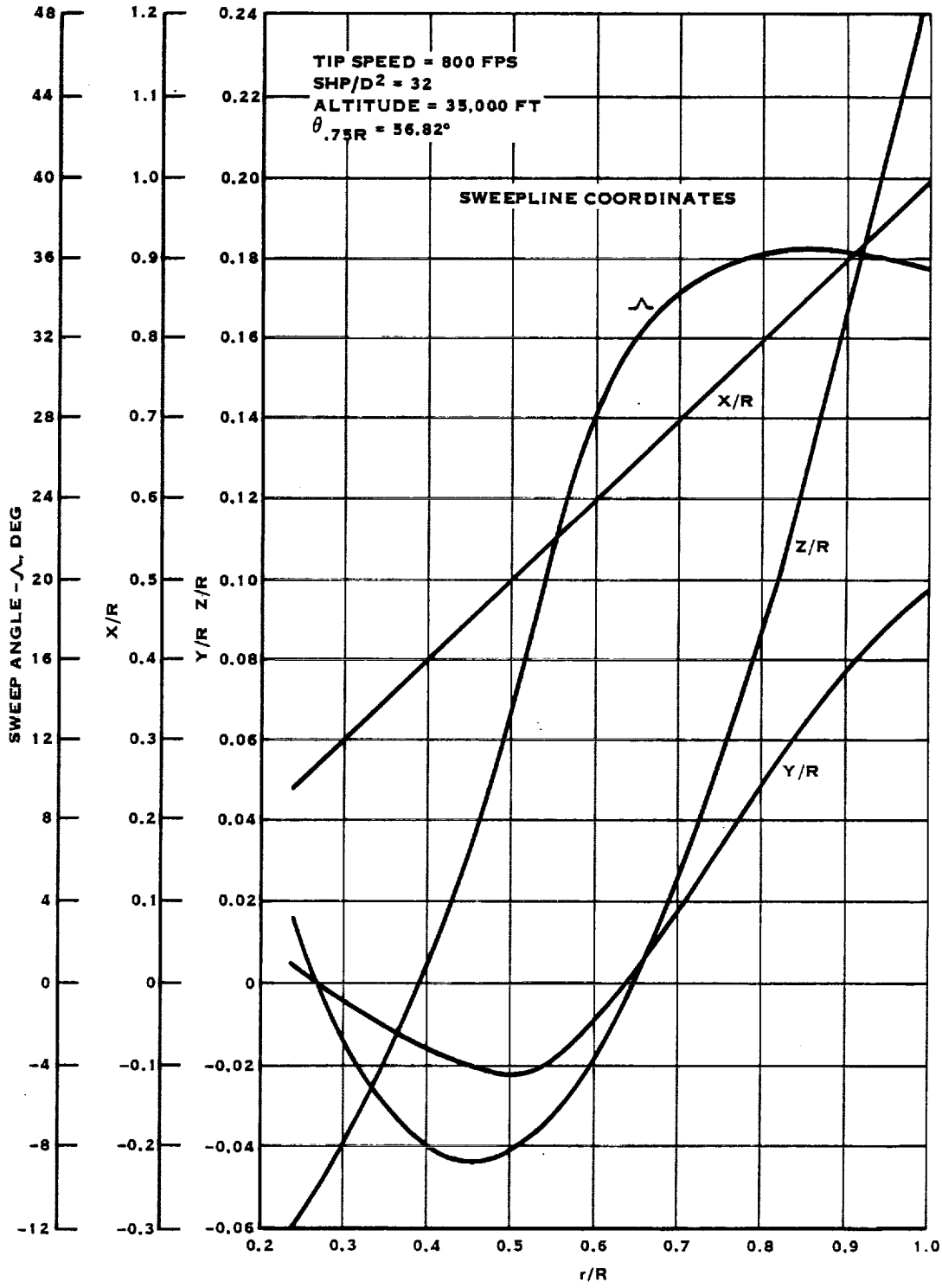

FIGURE 8.24 SELECTED BLADE CHARACTERISTICS (CONT'D)

9.0 TASK VII - DESIGN ANALYSIS

9.1 AERODYNAMIC EXCITATION ANALYSIS

9.1.1 Introduction

A propeller aerodynamic excitation sensitivity study was performed on five candidate Prop-Fan test bed aircraft. These aircraft were the Gulfstream II, KC-135A, C-141, DC-9, and the B-52B. Aerodynamic excitations were also calculated for a representative Prop-Fan aircraft. The representative Prop-Fan aircraft was specifically designed with a Prop-Fan propulsion system based on the requirements set forth in Table 9.1.

In performing the sensitivity study, effects on aerodynamic excitations for variations of the following parameters were considered: Prop-Fan axis angular orientation with aircraft (nacelle downtilt, and toe-in), Prop-Fan position relative to the wing, wing sweep, direction of Prop-Fan rotation, and Prop-Fan diameter. The effects of fuselage size, and nacelle size were not investigated. The aerodynamic excitation results from this study will be used to assess how similar the aerodynamic excitations on a testbed aircraft installation would be to an aircraft designed for Prop-Fan propulsion.

Theory shows that the aerodynamic excitation of propeller blades due to the aircraft characteristics and operating conditions are related to the angularity of the flow into the propeller, A or Ψ, and the aircraft operation dynamic pressure, $q = 1/2(\rho V^2)$. A list of symbols is provided in Table 9.2. Because of this, it is common practice to define the aircraft flow field vibratory loading on the propeller either in terms of aerodynamic excitation Aq or in terms of excitation factor, EF, which is related to Aq by the relationship $Aq = 409EF$. In this study, the aerodynamic excitation of the Prop-Fan is being defined in terms of Excitation Factor, EF.

9.1.2 Summary of Results

The total contribution of the higher orders for all the candidate aircraft other than the Prop-Fan Aircraft defined in Table 9.1, varied from 11 to 23% of the total EFQ. This is compared to a 37.5% contribution of the higher orders for the Prop-Fan aircraft. There are representative Prop-Fan installations that have lower nP's, as have been reported in previous NASA studies. Specifically, EF evaluations in support of NASA, contract NAS2-10178, performed for Douglas Aircraft indicated small nP contributions for overwing nacelle type installations, similar to the testbeds reported on here.

The five candidate aircraft exhibited similar sensitivity trends for each of the geometric parameters evaluated.

Of all the parameters evaluated, EFQ is sensitive to nacelle downtilt (high and low speeds), axial position (high and low speeds), and nacelle vertical displacement (only high speeds).

TABLE 9.1 PROP-FAN AIRCRAFT PARAMETERS USED IN EXCITATION STUDY

BASELINE VALUES

Airplane:	Seats	120
	Design Range	2222 KM (1200 NM)
	Design Cruise Speed	Mach 0.8
	Typical Mission	926 KM (500 NM) @ 60% load factor
	Design Takeoff Gross Wt	54840 Kg (120900 lb)
	Design Operating Wt Empty	36696 kg (80900 lb)
	Acoustic Treatment Wt	839 Kg (1860 lb)
	Typical Mission Block Fuel	2041 Kg (4500 lb)
Engine:	Type	Scaled PWA STS589-4
	Sizing Condition	35000' ICAO @ Mach 0.8 on Design Mission
	Size	0.893 Thrust Scale
Propeller:	Type	10 Blade (HSD D.P. #SP 04A82)
	Diameter	4.24m (13.9 ft.)
	SHP/D^2	34.4 HP/ft^2
	Vtip	244m/s (800 FPS)
	Weight	680 kg (1500 lb)
Mounting:	Nacelle Location	Underwing

TABLE 9.2. LIST OF SYMBOLS

A	Vertical location of Prop-Fan centerline with respect to wing zero lift line, positive when Prop-Fan above wing, m.
D	Prop-Fan Diameter, m.
EF_D	Excitation Factor $(V_{EAS}/179)^2$, degrees
N	Direction of Propeller Rotation, positive when blades nearest fuselage are going up.
n-P	nth order response of blade
P1	1st order Fourier Coefficients of blade shank bending
P2	2nd order Fourier Coefficients of blade shank bending
P3	3rd order Fourier Coefficients of blade shank bending
P4	4th order Fourier Coefficients of blade shank bending
P5	5th order Fourier Coefficients of blade shank bending
V_{EAS}	Velocity, equivalent airspeed, m/s.
WLE	Distance from Prop-Fan plane of rotation to wing leading edge
WM	In direction of fuselage centerline, position Prop-Fan ahead of wing leading edge, m.
ψ	Average inflow angle with respect to Prop-Fan centerline, positive when flow is coming from below, degrees
ψ_A	Inflow angle of advancing blade at 75% radius, deg.
ψ_D	Nacelle downtilt angle from wing zero lift line, positive nose down, deg.
ψ_R	Inflow angle of retreating blade at 75% radius, deg.
ψ_T	Nacelle toein angle from fuselage centerline, deg.
ΔEFQ	Change in Equivalent Excitation Factor from Baseline Aircraft Value of EFQ. Positive value implies increase in EFQ. [EFQ - EFQ (Baseline)].

9.1.3 Analytical Methods

9.1.3.1 Excitation Factor - The term Aerodynamic Design Excitation Factor, EF_D, is used to represent the magnitude and sense of the flow field at the Prop-Fan and is defined by the following expression:

$$EF_D = \psi_{deg} \, (V_{EAS}/179m/s)^2 \quad (1)$$

where:

$$\psi = [(\psi_A + \psi_R)/2](degrees)$$

and ψ_A and ψ_R are the inflow angles, measured from the Prop-Fan axis of rotation of the advancing and retreating blades, respectively, as sketched below.

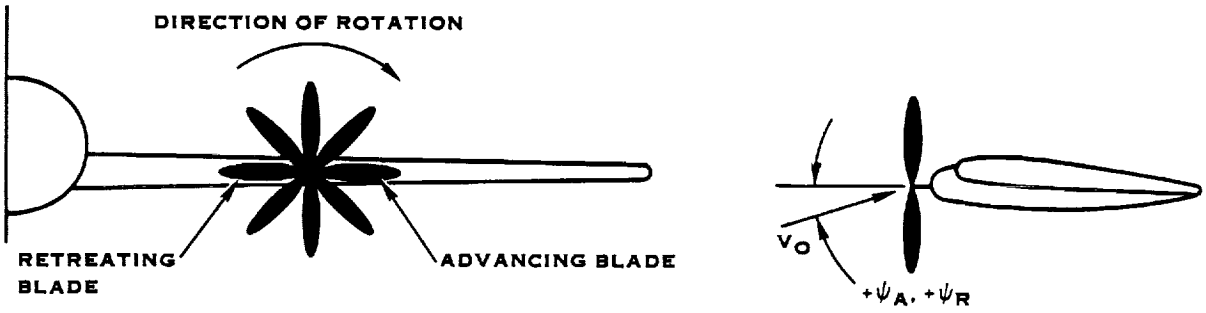

(ψ_A and ψ_R are positive below the axis of rotation.)

The inflow angle ψ, in Equation 1 defines the direction of the average flow into the Prop-Fan. If the Prop-Fan is aligned at an angle to the uniform flow field, a sinusoidal (1-P) loading results, with some n-P loading due to blade sweep and nonlinear blade loading effects. However, because of the non-uniform flow field about the aircraft additional n-P loading will be generated and the 1P loading will be modified from that given by equation 1. For preliminary design purposes, in order to account for the additional n-P loadings, an Equivalent Excitation Factor, EFQ, is approximated, and is defined as

$$EFQ = EF_D \left(1 + \frac{(3xP2/P1)^2}{3xP2/P1 + .3} + \frac{3xP3}{P1} + \frac{3xP4}{P1} + \frac{3xP5}{P1} \right) \quad (2)$$

where P1, P2, P3, P4, and P5 are the 1st, 2nd, 3rd, 4th and 5th order Fourier coefficients of the excitation load defined by the blade shank resultant bending moments.

Normally, the increase in EF due to higher η-P loadings is between 10 and 25%; however, for cases where the 1P level approaches zero resulting in lower EFQ values, the higher order excitations contribute a larger percentage of the total EFQ.

For normal aircraft operation, the maximum Excitation Factor occurs at one or both of the following aircraft operating conditions:

a. Maximum aircraft gross weight, and minimum aircraft speed without flaps.

b. Minimum aircraft gross weight, and maximum aircraft speed.

9.1.3.2 Flow-Field Calculation - The flow-field at the plane of the Prop-Fan due to the presence of the aircraft for a given altitude is calculated using an incompressible - inviscid potential flow computer program developed at Hamilton Standard. This program computes the flow-field about individual aircraft components separately and uses the superposition principle to combine these flow-fields to obtain the total flow-field. The fuselage and nacelle are treated as axisymmetric Rankine bodies, while the wing is analyzed as a swept lifting line. The velocity perturbations due to axial flow and cross flow are considered on all aircraft components, (wing, nacelle and fuselage). The program also accounts for the effects of the propeller slipstream and swirl on the aircraft and, therefore, flow-field. The influence of the tail surfaces has been found to be negligible. Consequently, these surfaces were not considered in the calculations for wing mounted Prop-Fans. This flow-field calculation requires significantly less information about the aircraft geometry than do other more elaborate methods, such as the well known Hess Code. Computer costs are also significantly less for this procedure than for the more elaborate panel methods. An extensive comparison of this aircraft flow field program with the Hess code method revealed reasonable agreement; see reference 25. This flow field program has been used for several decades at Hamilton Standard for accurately predicting propeller design loads.

9.1.3.3 Aerodynamic Loads - The Prop-Fan aerodynamic loads are calculated in the presence of the aircraft flow field. These loads are Fourier analyzed to obtain the harmonic components of the loads, which are used to calculate the Equivalent Excitation Factor, (EFQ; equation 2). The 1P loads are based on the difference between those for the advancing and retreating blades.

The aerodynamic spanwise loadings of the Prop-Fan blades are calculated at a series of azimuthal positions as the Prop-Fan makes one revolution. These calculations are made using a form of the Goldstein-Locke propeller vortex analysis of reference 26, with the assumption of quasi-steady aerodynamics.

9.1.4 Model Descriptions

All aircraft examined were configured with a 2.74 meter (9 ft.) diameter Prop-Fan, except for the representative Prop-Fan aircraft which had a 4.24 meter (13.9 ft) diameter Prop-Fan. Figures 9.1 - 9.6 are schematic representations of the Prop-Fan Aircraft, B-52B, C-141, DC-9, GS-II, and KC-135A aircraft respectively, with a Prop-Fan installation. The figures were drawn to the same scale so that the differences between them are readily apparent.

As shown in Figure 9.1, the Prop-Fan aircraft installation is a low wing design with about 34° of leading edge wing sweep. The nacelle is located slightly below the wing, about 1 wing chord ahead of the wing, and about 1.8 Prop-Fan diameters from the fuselage centerline (.8 diameter clearance). The B-52B configuration in Figure 9.2 has the nacelle below the high wing at 1/2 of a wing chord upstream of the wing leading edge and 2 Prop-Fan diameters from the fuselage centerline. The C-141 aircraft installation, see Figure 9.3, is an over-the-wing design, with the Prop-Fan less than half a wing chord ahead of the wing leading edge, and 1-1/2 Prop-Fan diameters from the fuselage centerline. Figure 9.4 shows the DC-9 aircraft installation with the Prop-Fan slightly above the wing at about a wing chord ahead of it's leading edge, and 2 Prop-Fan diameters from the fuselage centerline. The DC-9 installation is very similar to that of the Prop-Fan aircraft, except that the nacelle is above the wing. Figure 9.5 shows the Gulfstream II aircraft with the Prop-Fan slightly above the wing at about 2/3 of a wing chord ahead of its leading edge and 1 1/2 Prop-Fan diameters from the fuselage centerline. Like the B-52 and the C141, the KC-135A has a large wing chord, and as shown in Figure 9.6, the Prop-Fan is mounted at less than 1/2 of a wing chord ahead of its leading edge, and 2 diameters from the fuselage centerline.

For the baseline version of each aircraft, the nacelle toe-in was assumed to be zero and the nacelle downtilt was selected to obtain reasonable excitation factors.

Table 9.3 gives the pertinent baseline geometric parameters, as defined in Figure 9.7, for the six aircraft studied.

9.1.5 Analysis Procedure

The Equivalent Excitation Factor (EFQ) was calculated, and an EFQ diagram was generated, for the baseline configuration of each of the five candidate testbed aircraft and the Prop-Fan aircraft at the four aircraft operating conditions listed in Table 9.4. With these diagrams, EFQ can now be determined for any velocity and gross weight by a simple cross plot. The sensitivity of the EFQ to changes in selected aircraft/Prop-Fan geometric parameters were calculated for the more critical operating conditions 1 and 4 in Table 9.4. The eight aircraft/Prop-Fan geometric parameters for which the EFQ sensitivities were calculated are defined in Figure 9.7. The sensitivity for any one of these parameters was calculated, by holding the other seven constant. Thus, for example, when the spanwise location of the Prop-Fan axis, WM (Figure 9.7) was varied, the distance of the Prop-Fan plane ahead of the wing leading edge, WLE in Figure 9.7, was held constant.

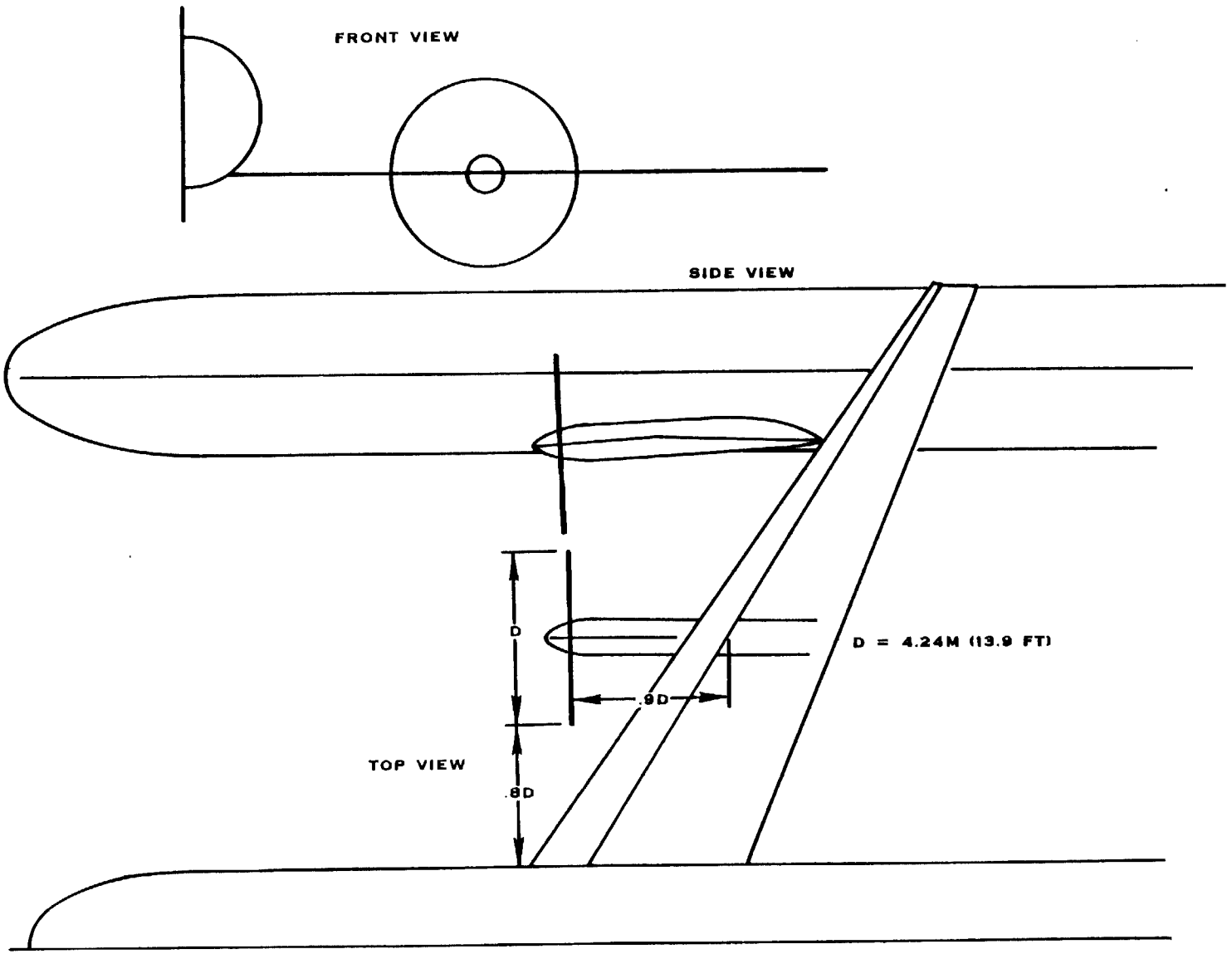

FIGURE 9.1. SCHEMATIC OF PROP-FAN AIRCRAFT

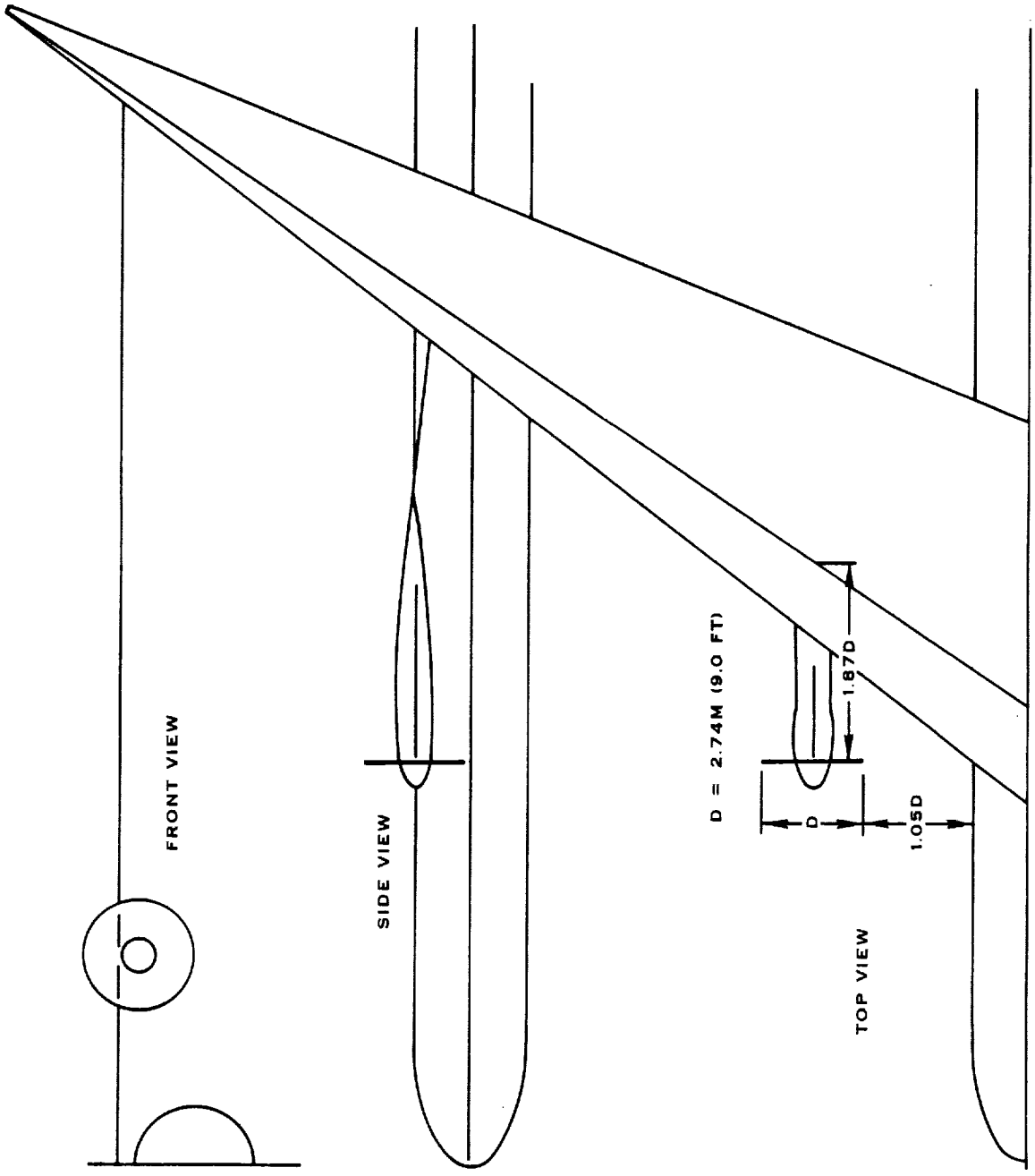

FIGURE 9.2. SCHEMATIC OF B-52B AIRCRAFT

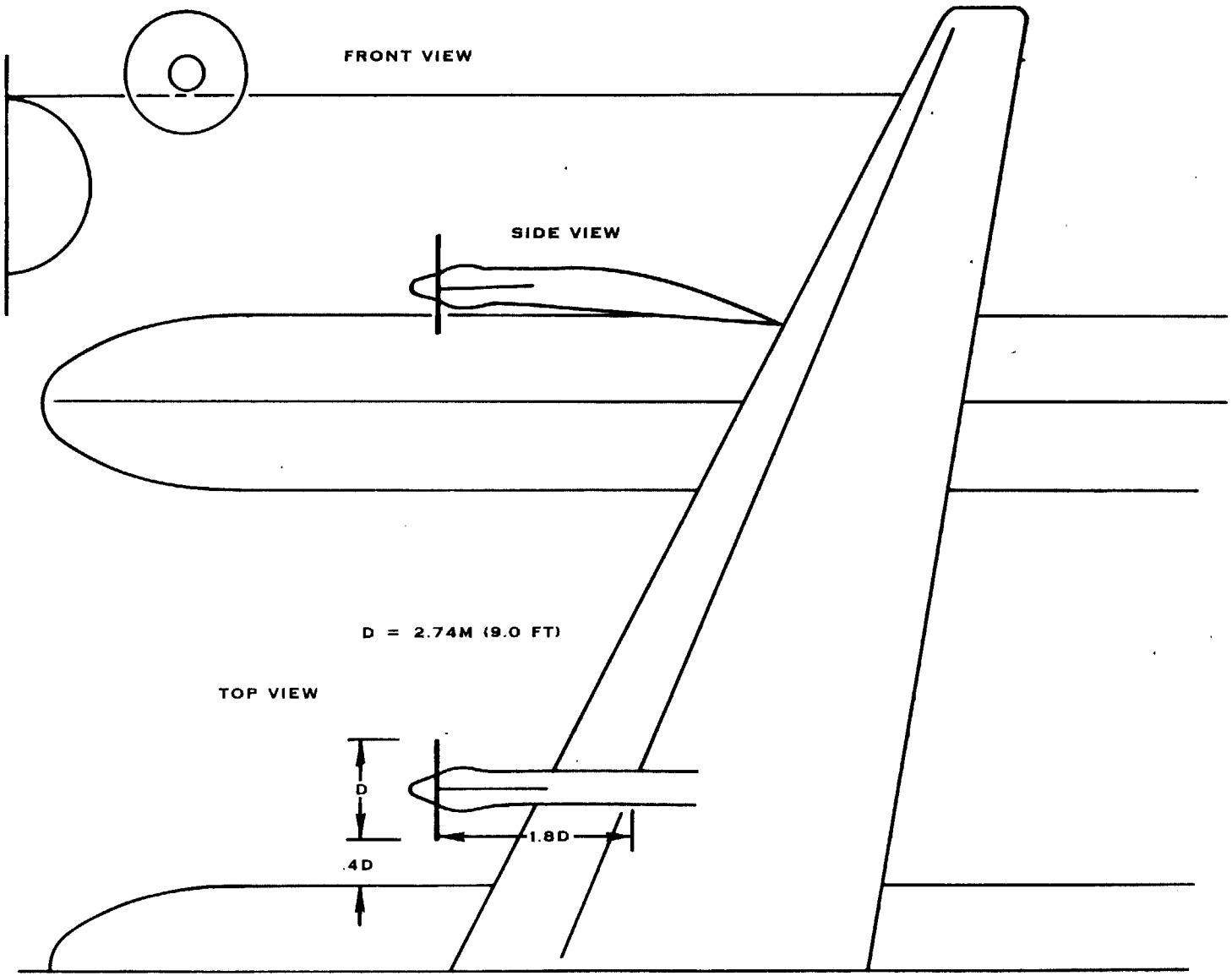

FIGURE 9.3. SCHEMATIC OF C-141 AIRCRAFT

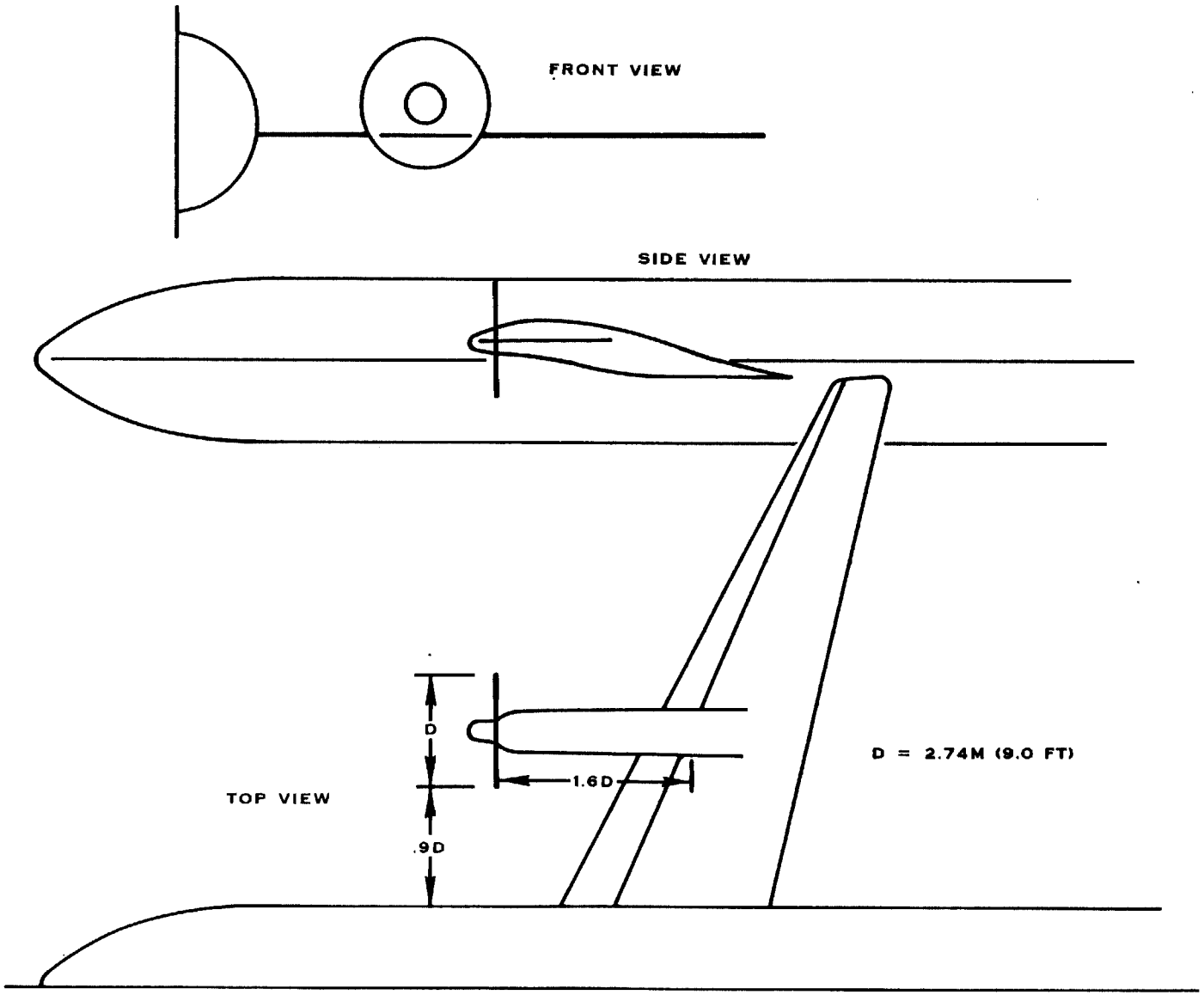

FIGURE 9.4. SCHEMATIC OF DC-9 AIRCRAFT

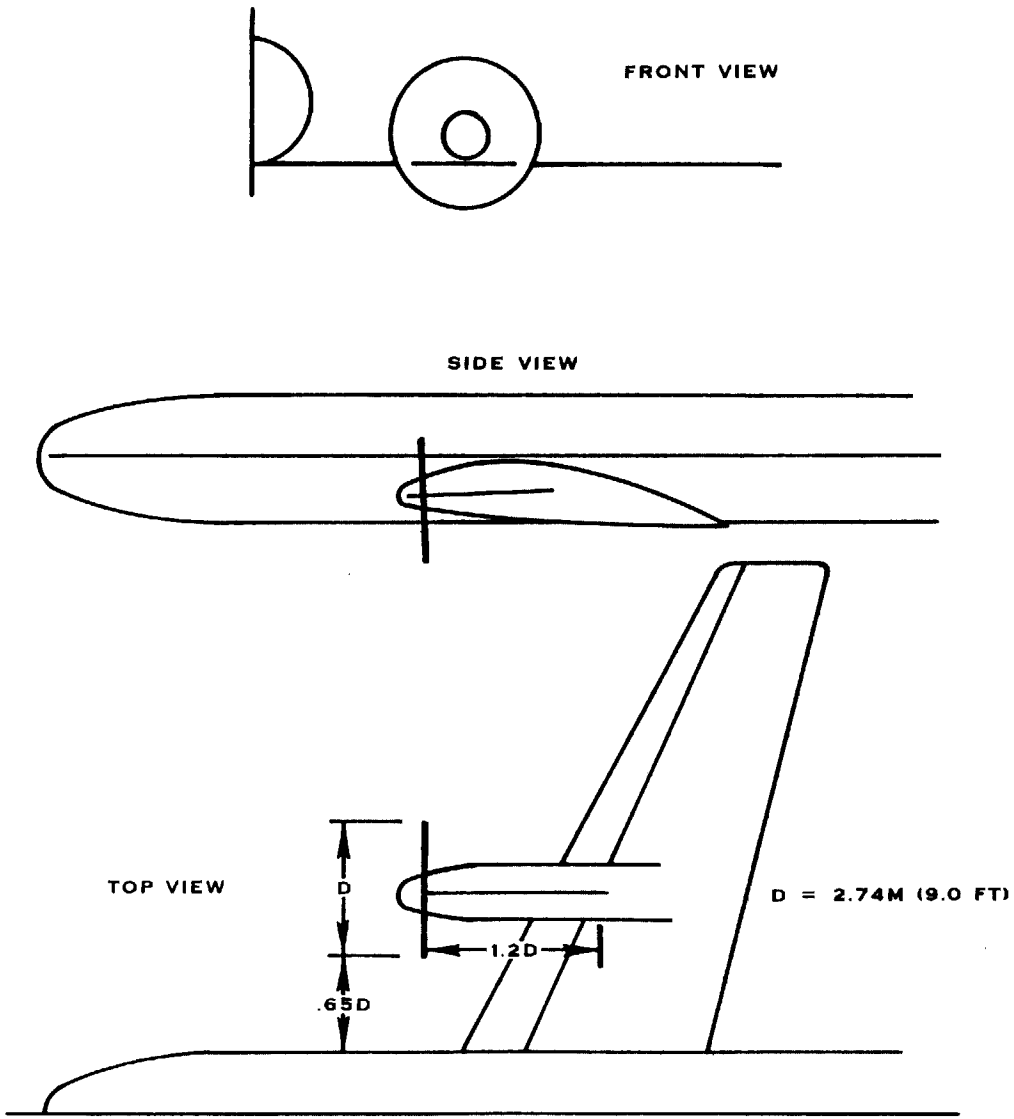

FIGURE 9.5. SCHEMATIC OF GULF STREAM II AIRCRAFT

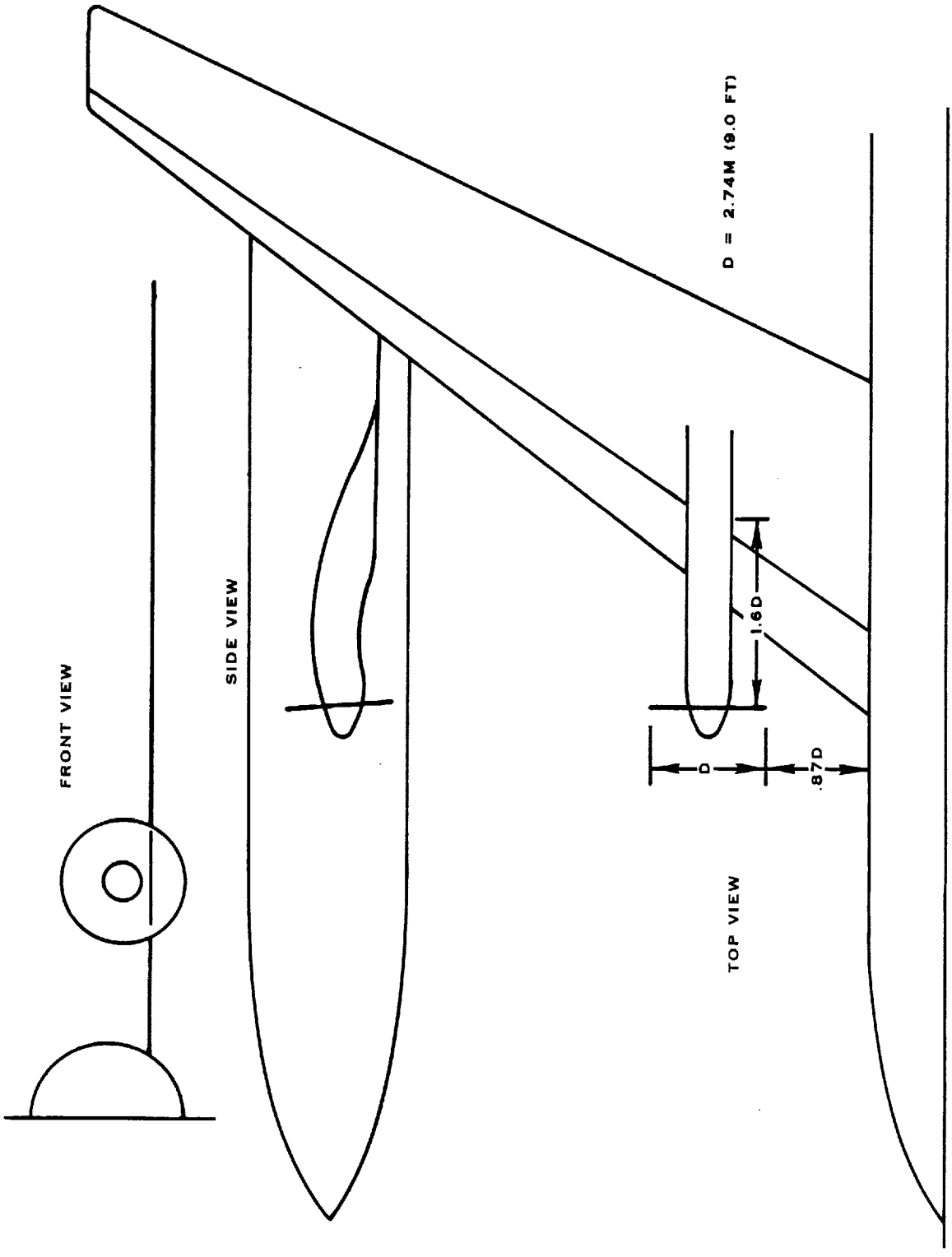

FIGURE 9.6. SCHEMATIC OF KC-135A AIRCRAFT

TABLE 9.3. VALUES OF GEOMETRIC PARAMETERS FOR BASELINE AIRCRAFT

Parameter[1]	Aircraft PF	B-52	C-141	DC-9	GS-II	KC-135A
Nacelle Downtilt, ψ_D, (Deg.)	7.0	8.0	6.0	4.5	5.0	6.0
Quarter Chord Sweep, $\Lambda c/4$, (Deg.)	32.0	35.0	23.0	24.0	25.0	35.0
Axial Position, WLE, (m)	3.05	3.23	2.74	3.47	2.36	2.84
Vertical Position, A, (m)	0.192	0.55	-0.57	-0.66	-0.53	-0.61
Spanwise Position, WM, (m)	7.41	5.51	4.62	5.63	4.19	5.59
Toein, ψ_T, (Deg.)	0	0	0	0	0	0
Prop-Fan Diameter, D, (m)	4.24	2.74	2.74	2.74	2.74	2.74
Direction of Rotation, N[2]	↑	↑	↑	↑	↑	↑
Wing Loading, N/m^2(lb/ft^2)	5027(105)	4549(95)	4692(98)	4644(97)	3926(82)	3591(75)

[1] A/C geometry and operating conditions supplied by airframer industry

[2] Blades closest to fuselage going "up"

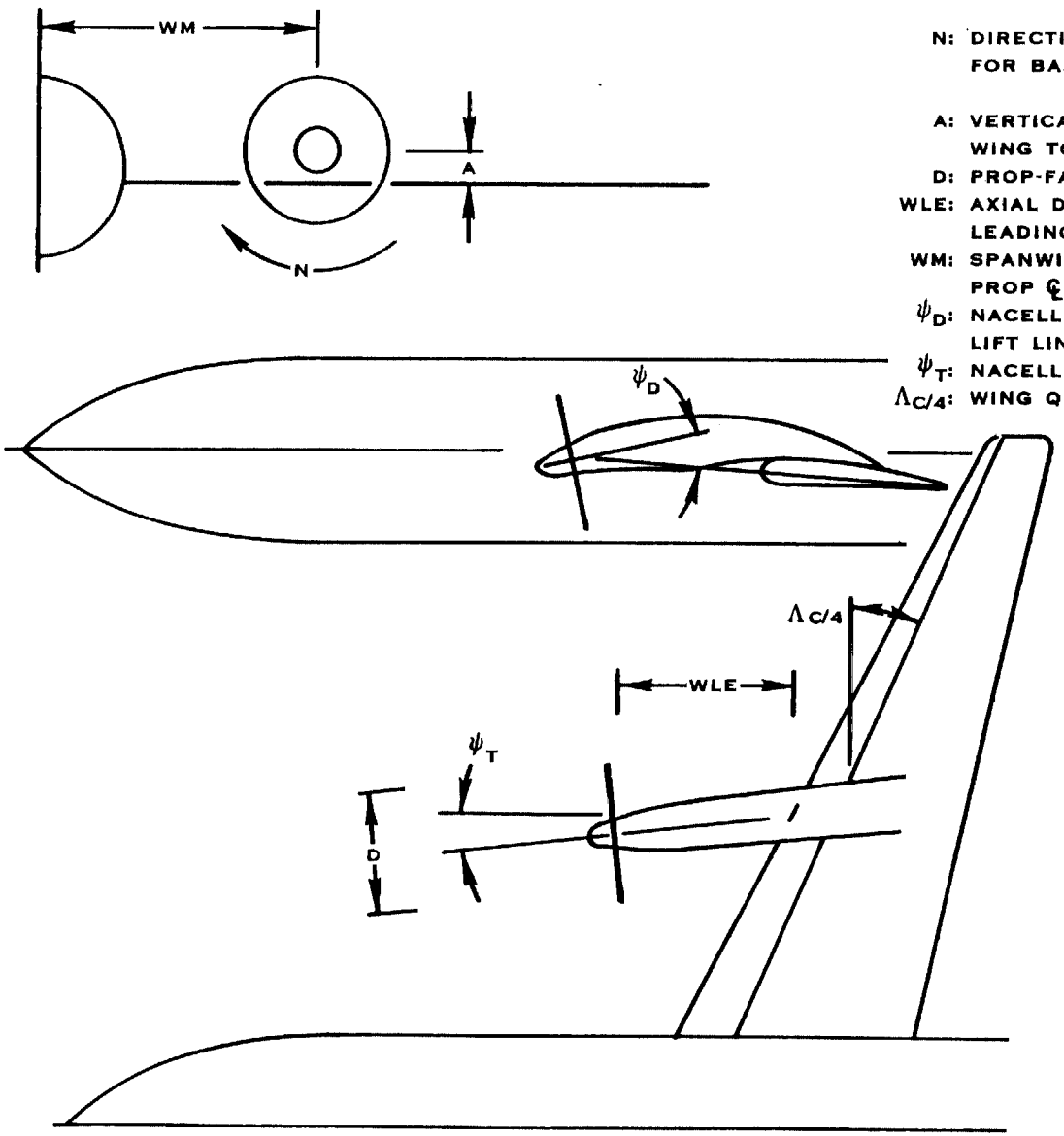

N: DIRECTION OF PROPELLER ROTATION FOR BASELINE CONFIGURATION.

A: VERTICAL DISTANCE OF PROP ℄ ABOVE WING TO LIFTING LINE (+ PROP ABOVE WING)

D: PROP-FAN DIAMETER

WLE: AXIAL DISTANCE OF PROP AHEAD OF WING LEADING EDGE. (+ PROP AHEAD OF WING)

WM: SPANWISE DISTANCE FROM FUSELAGE ℄ TO PROP ℄

ψ_D: NACELLE DOWN TILT ANGLE FROM WING ZERO LIFT LINE. (+ AS SHOWN).

ψ_T: NACELLE TOEIN ANGLE (+ AS SHOWN).

$\Lambda_{C/4}$: WING QUARTER AHEAD SWEEP.

FIGURE 9.7. GEOMETRIC PARAMETERS FOR WHICH EFQ SENSITIVITIES WERE CALCULATED

TABLE 9.4 AIRCRAFT OPERATING CONDITIONS FOR CALCULATED EQUIVALENT EXCITATION FACTORS

Operating Conditions	Aircraft					
	PF	B-52B	C-141	DC-9	GS-II	KC-135A
1. Maximum Gross Weight (Kg)	54900	171800	143600	41140	29600	83000
Minimum Airspeed(1) (m/s EAS)	93	88	139	73	93	93
2. Minimum Gross Weight (Kg)	38600	84900	62600	27940	15380	48600
Minimum Airspeed(1) (m/s EAS)	93	88	139	73	93	93
3. Maximum Gross Weight (Kg)	54900	171800	143600	41140	29600	83000
Maximum Airspeed (m/s EAS)	136	141	153	171	141	147
4. Minimum Gross Weight (Kg)	38600	89900	62600	27940	15380	48600
Maximum Airspeed (m/s EAS)	136	141	153	171	141	147

(1) W/o flaps and with gear up.

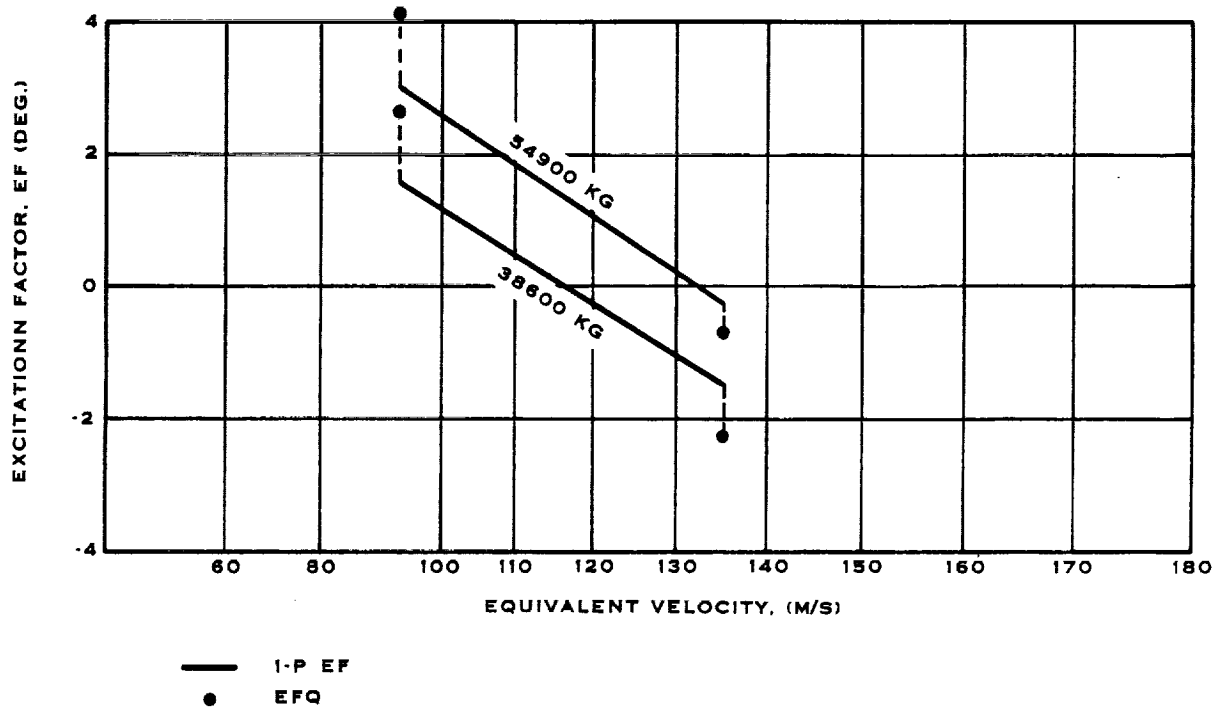

FIGURE 9.8. BASELINE EF DIAGRAM FOR PROP FAN AIRCRAFT

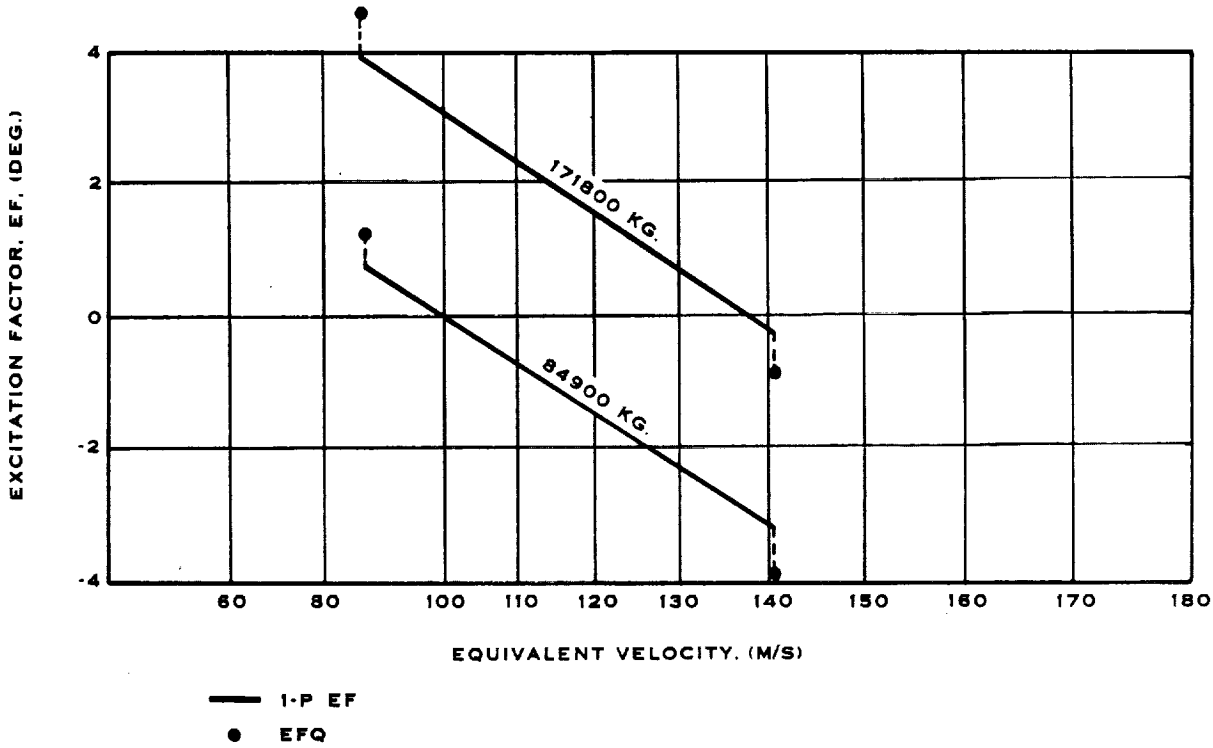

FIGURE 9.9. BASELINE EF DIAGRAM FOR B-52 AIRCRAFT

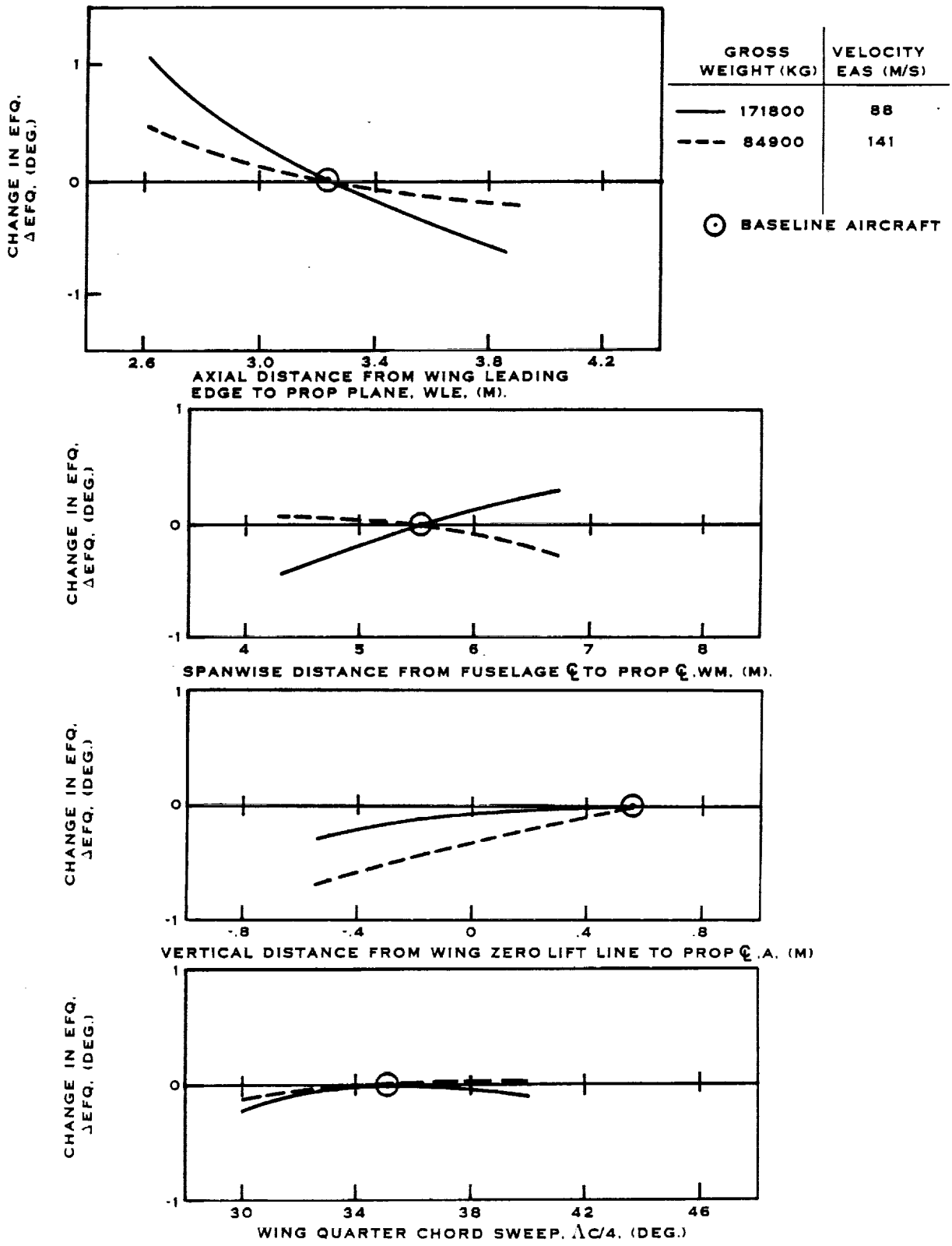

FIGURE 9.10. B-52 EFQ SENSITIVITY TO CHANGES IN PROP-FAN ORIENTATION

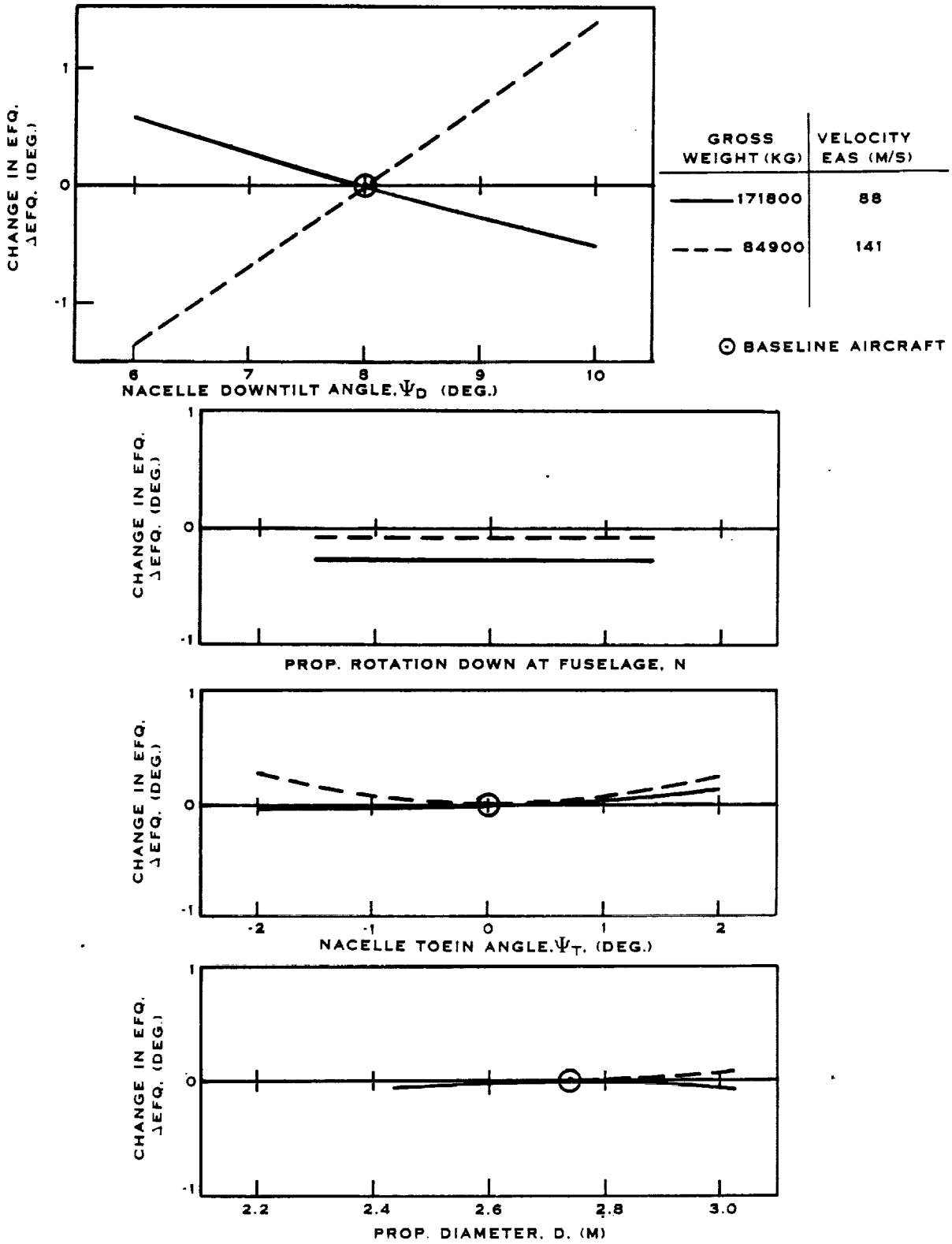

FIGURE 9.10. (CONCLUDED)

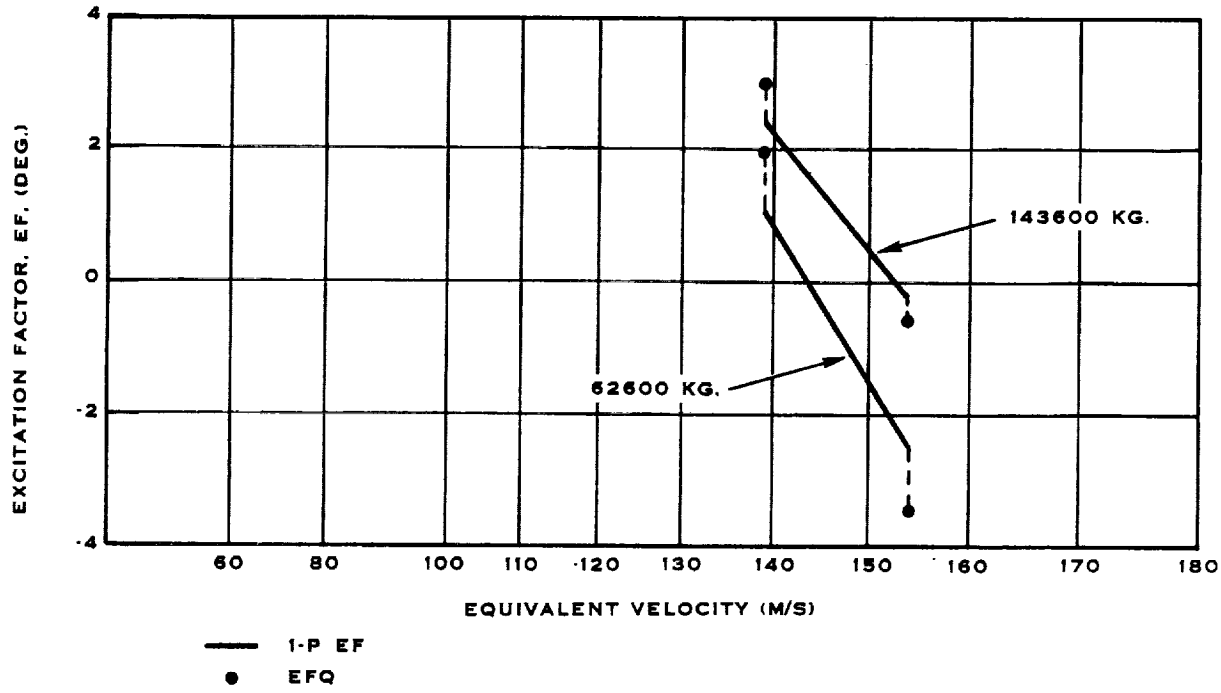

FIGURE 9.11. BASELINE EF DIAGRAM FOR C-141 AIRCRAFT

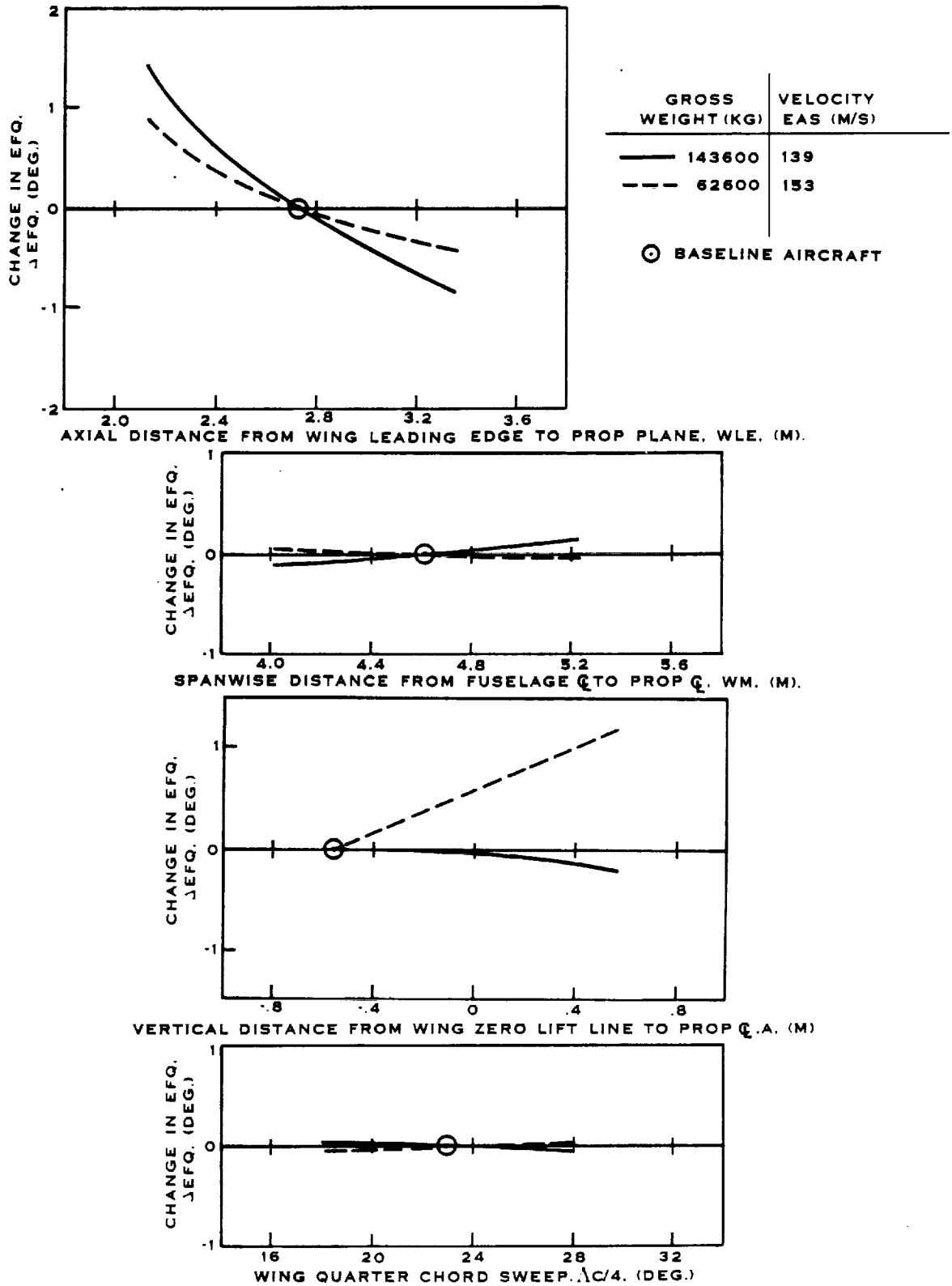

FIGURE 9.12. C-141 EFQ SENSITIVITY TO CHANGES IN PROP-FAN ORIENTATION

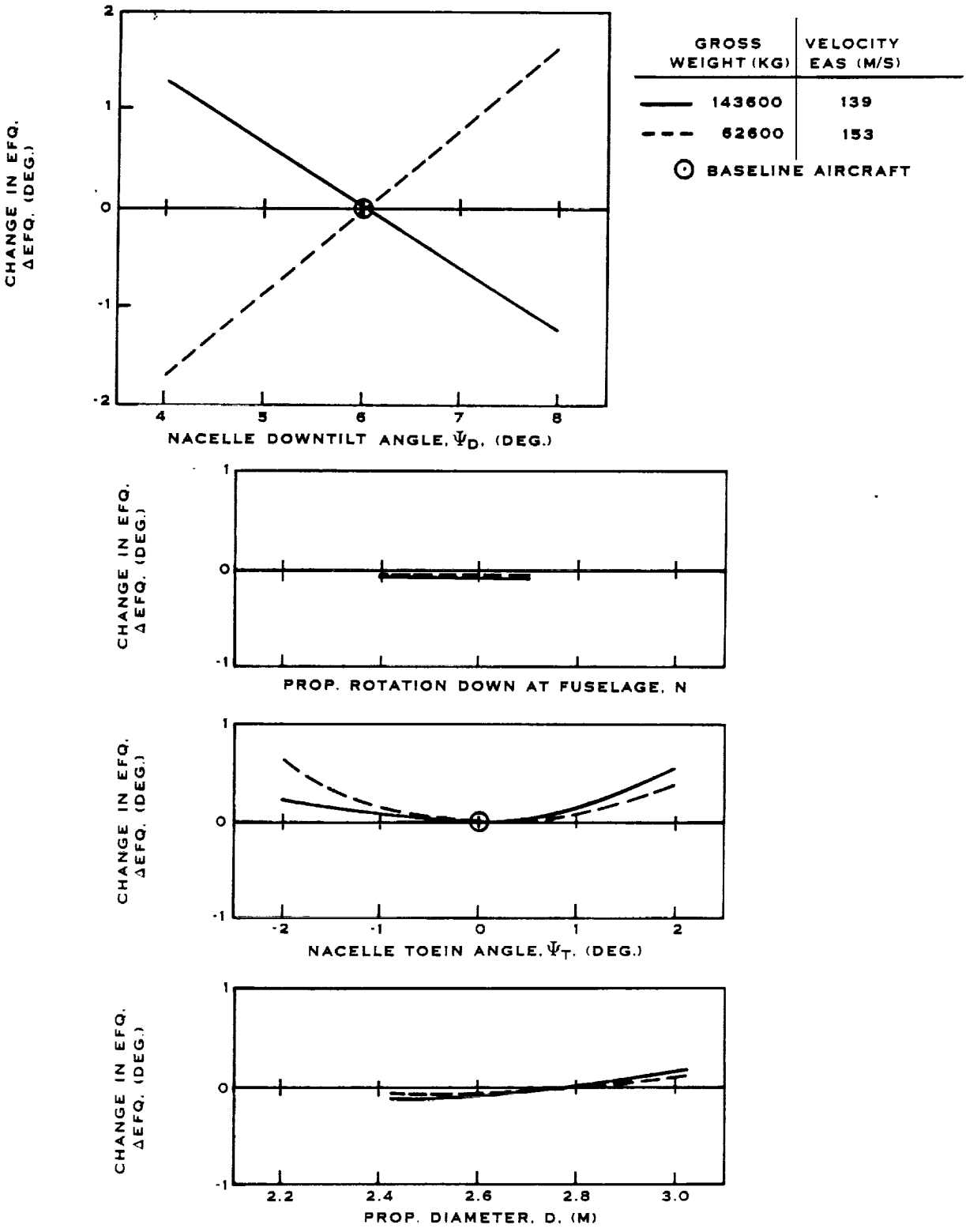

FIGURE 9.12. (CONCLUDED)

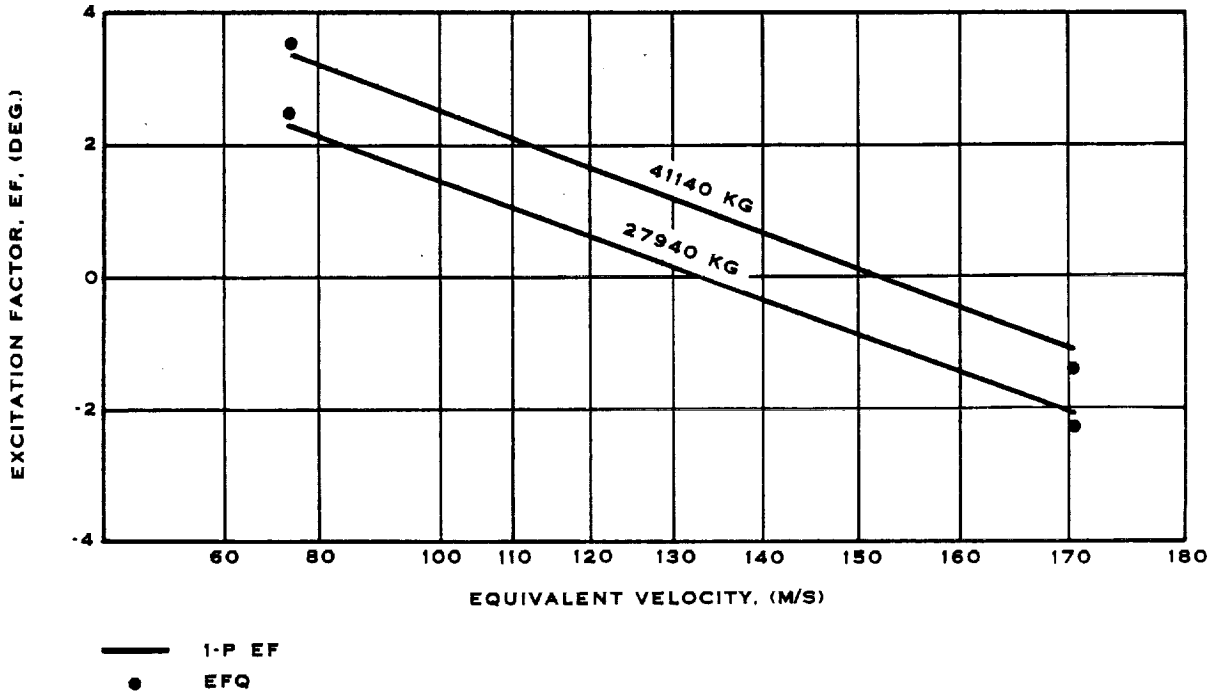

FIGURE 9.13. BASELINE EF DIAGRAM FOR DC-9 AIRCRAFT

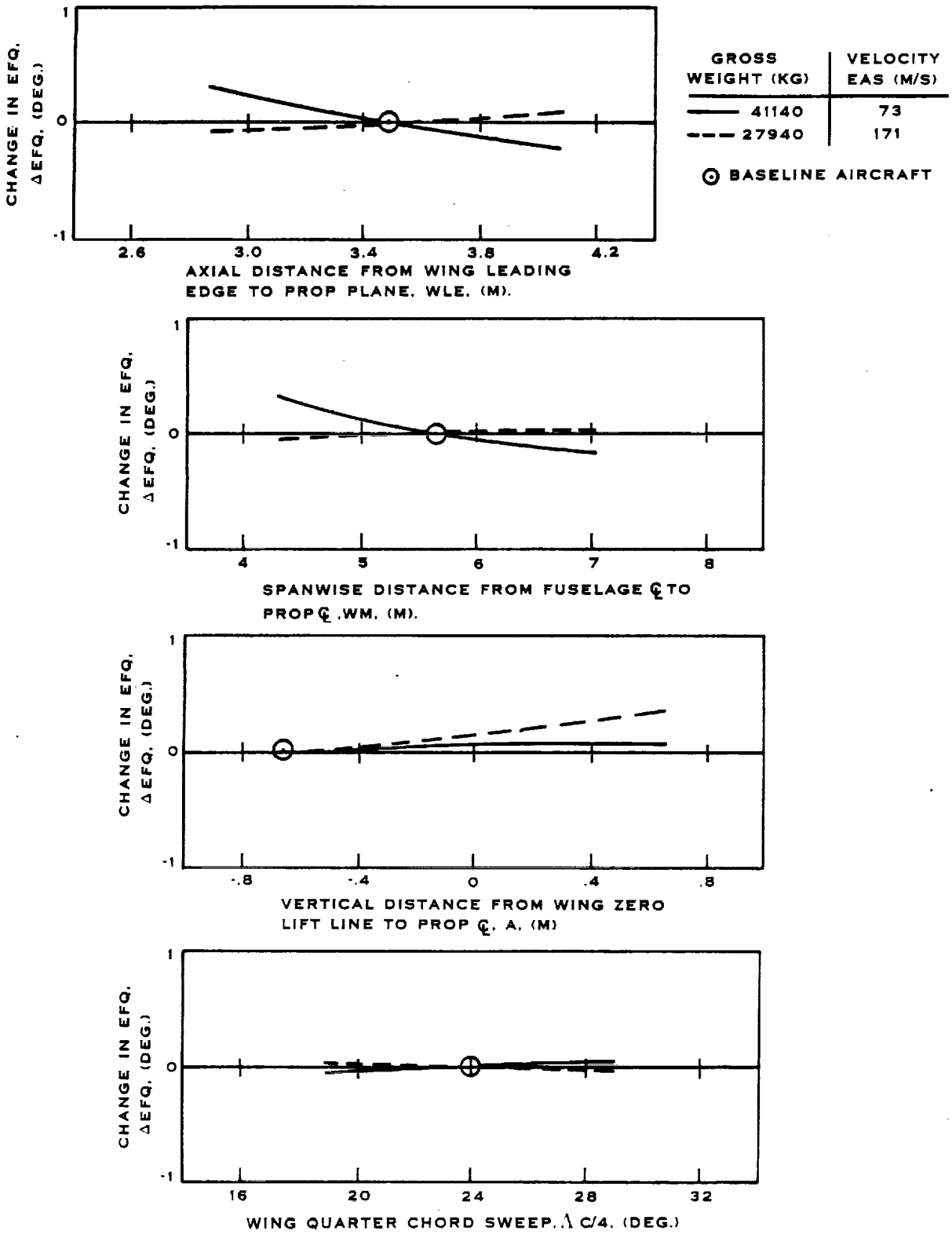

FIGURE 9.14. DC-9 EFQ SENSITIVITY TO CHANGES IN PROP-FAN ORIENTATION

C-2

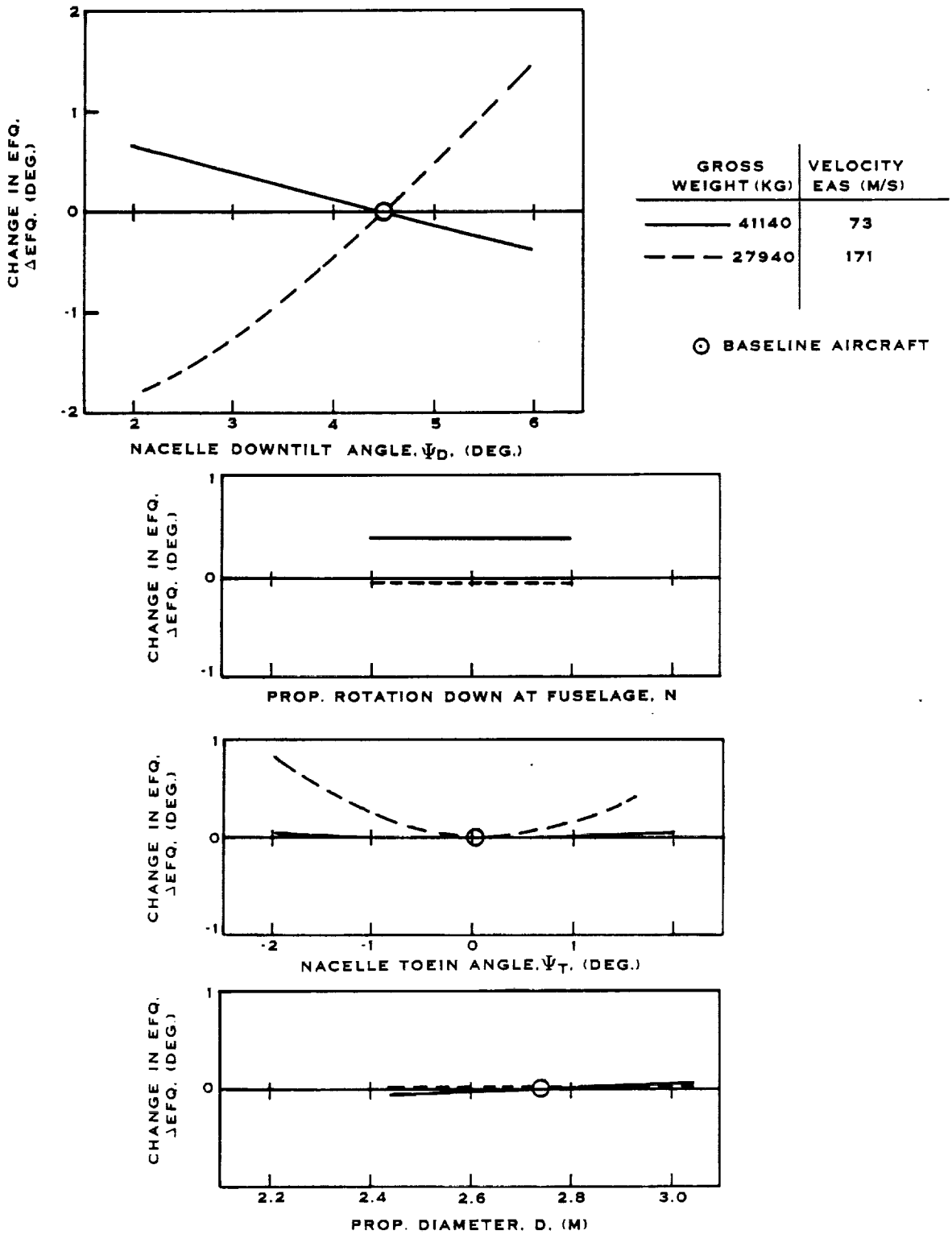

FIGURE 9.14. (CONCLUDED)

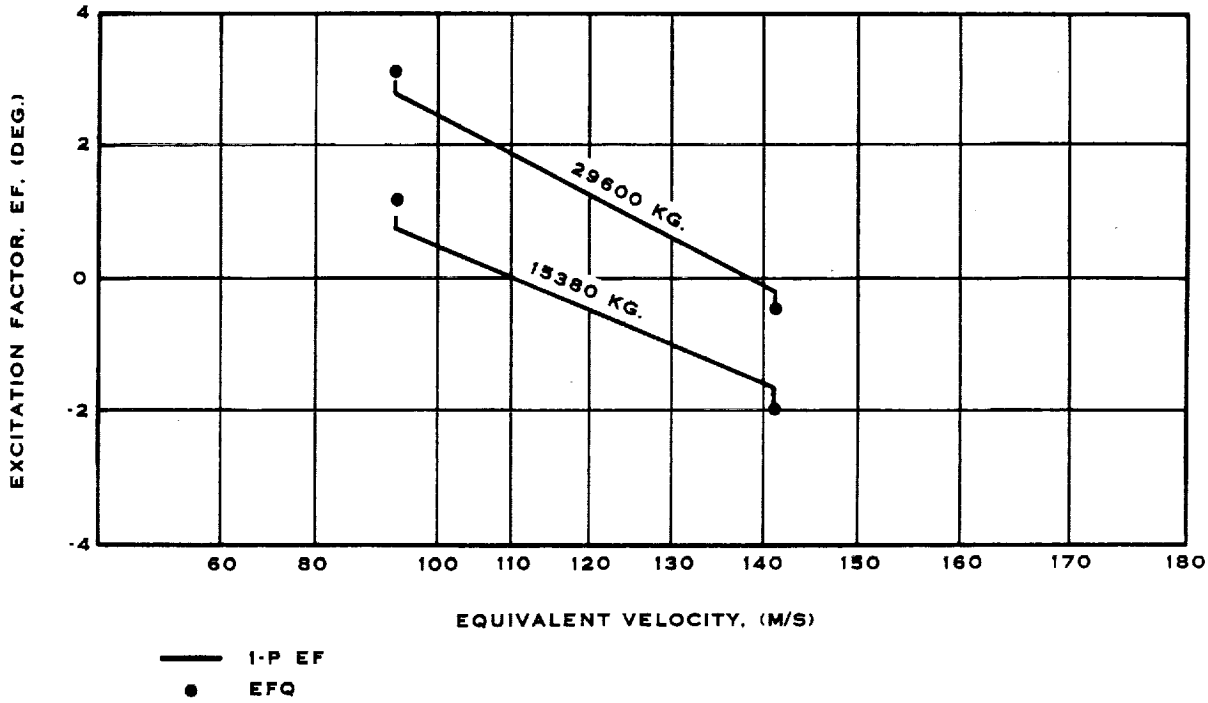

FIGURE 9.15. BASELINE EF DIAGRAM FOR GS-II AIRCRAFT

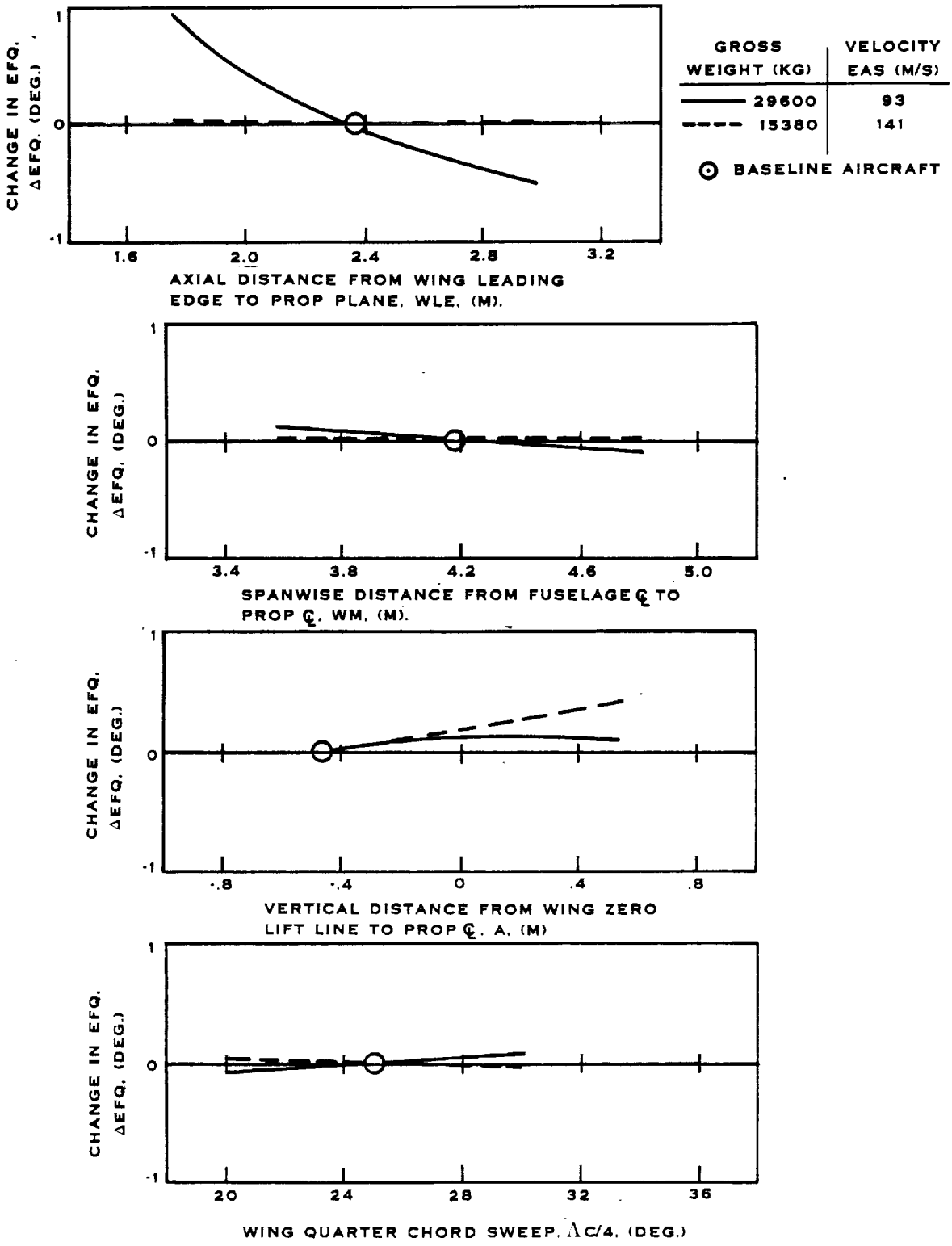

FIGURE 9.16. GS-II EFQ SENSITIVITY TO CHANGES IN PROP-FAN ORIENTATION

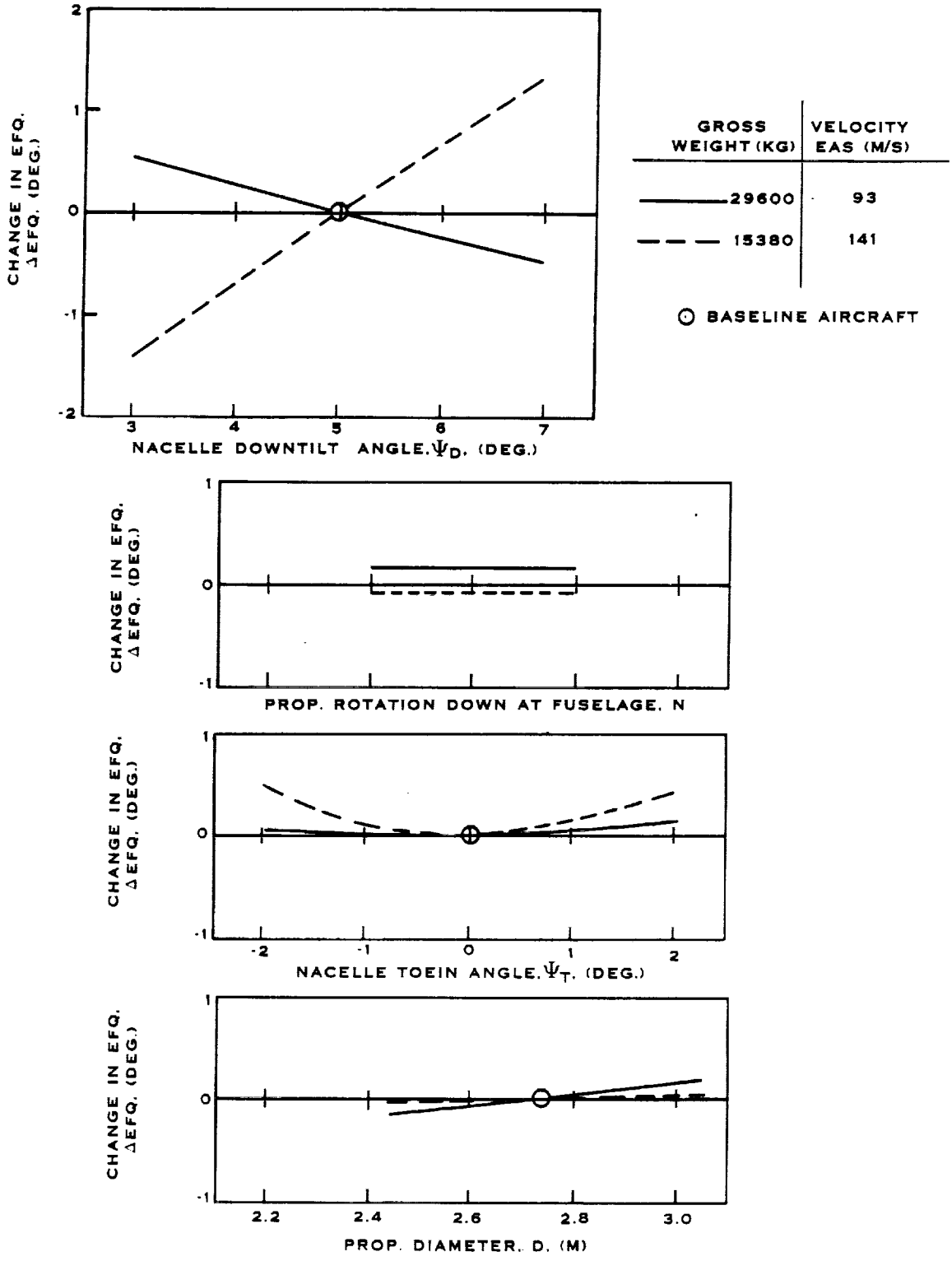

FIGURE 9.16. (CONCLUDED)

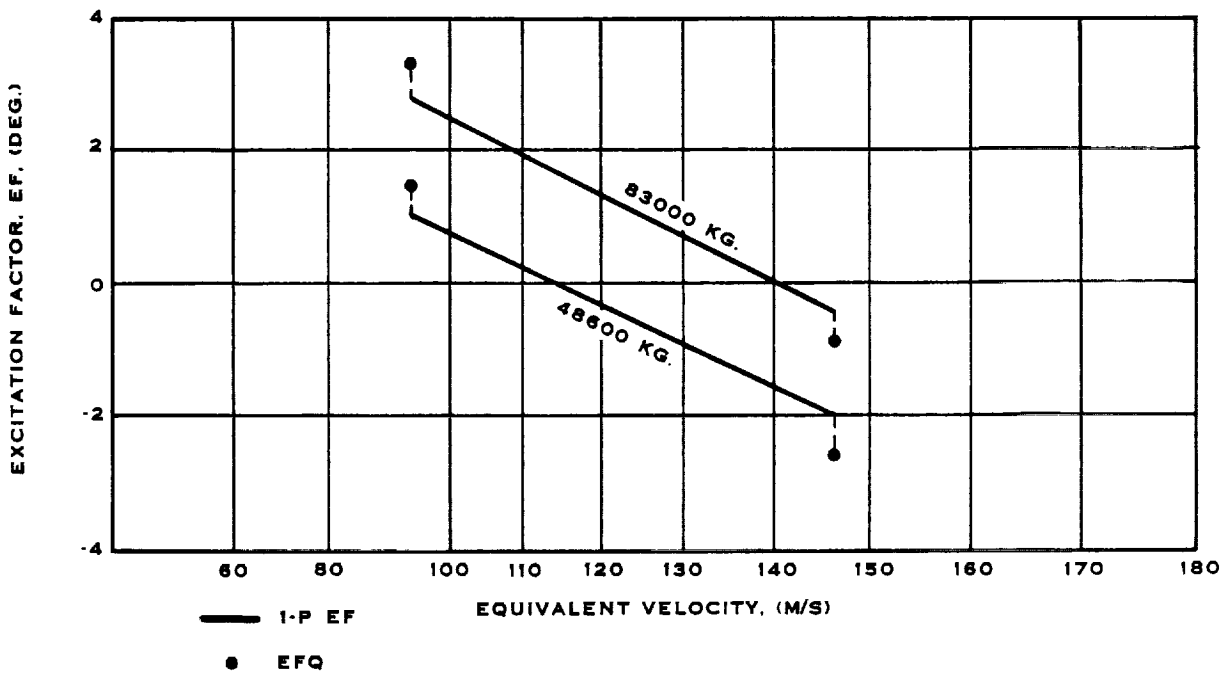

FIGURE 9.17. BASELINE EF DIAGRAM FOR KC-135 AIRCRAFT

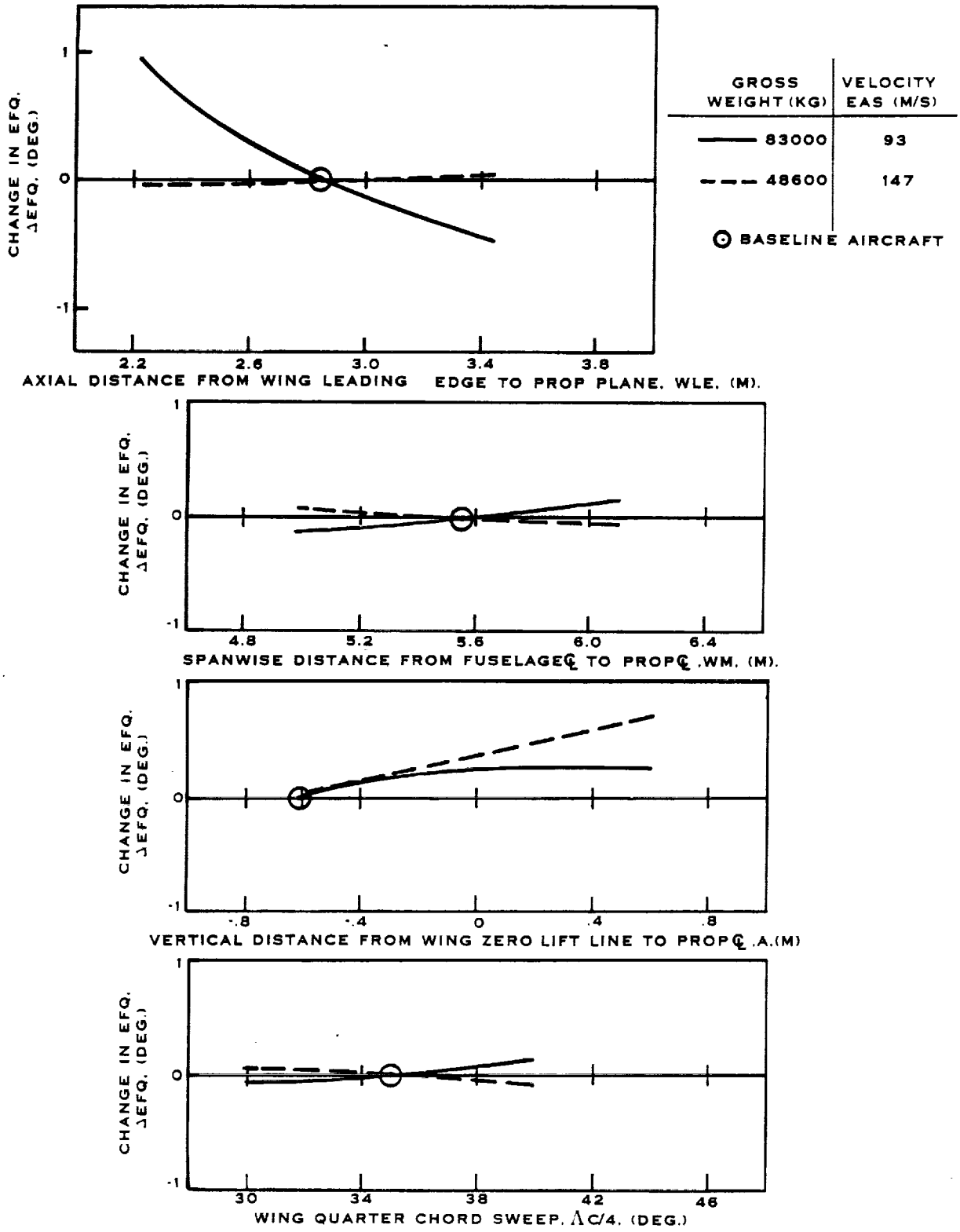

FIGURE 9.18. KC-135 SENSITIVITY TO CHANGES IN PROP-FAN ORIENTATION

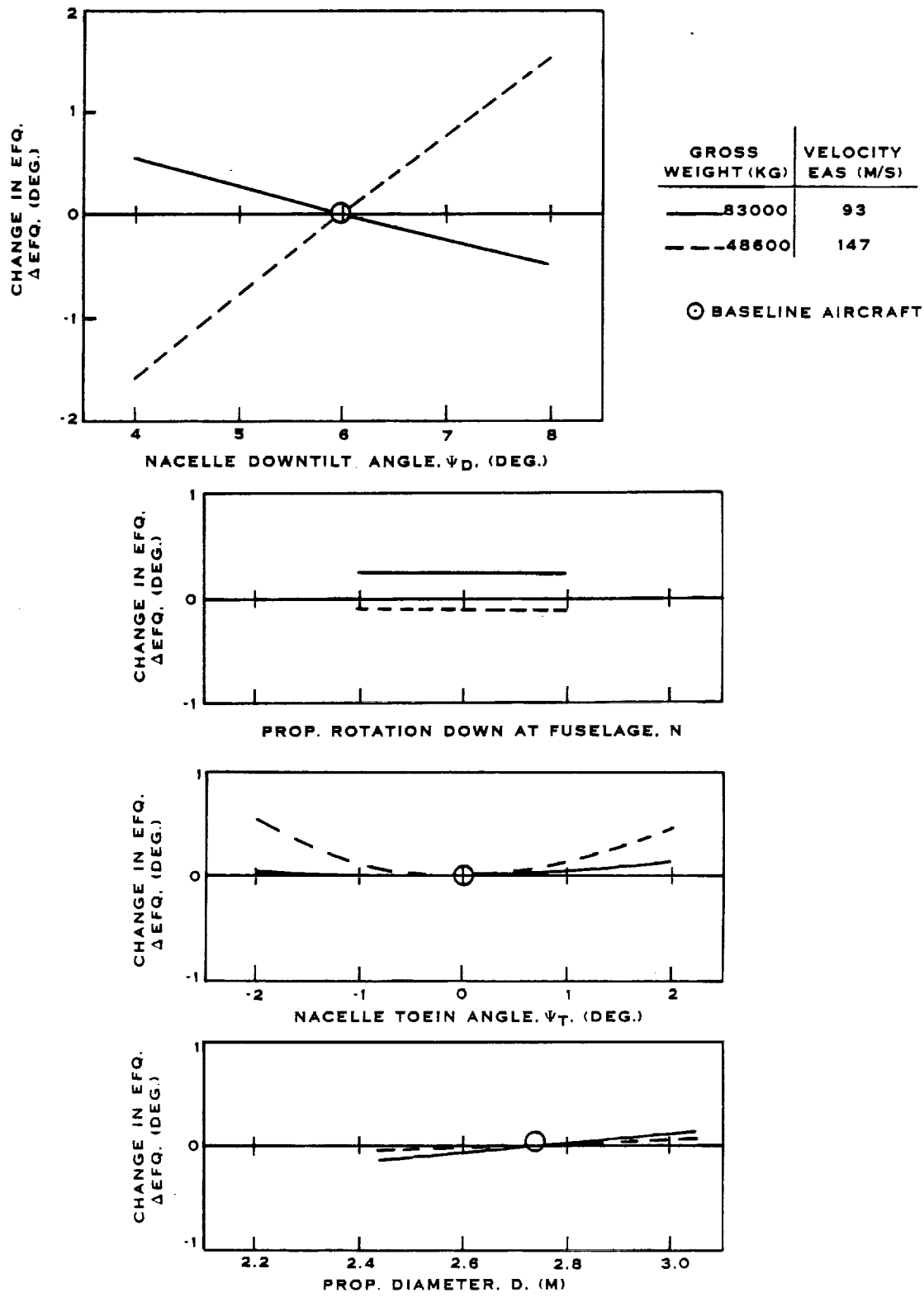

FIGURE 9.18. (CONCLUDED)

9.1.6 Results

The EFQ diagram for the Prop-Fan aircraft with a 4.24 m (13.9 ft.) diameter Prop-Fan is shown in Figure 9.8. The square of the equivalent airspeed is plotted on the abscissa by utilizing the appropriate graph paper with a linear scale. The Equivalent Excitation Factor EFQ is thus assumed to follow the EFD, which is a linear function of the equivalent airspeed squared. The lowest airspeed for which the Equivalent Excitation Factor is shown represents the minimum aircraft airspeed without flaps (aircraft operating points 1 and 2 in Table 9.4), and the maximum airspeed to which the curve is drawn represents the maximum aircraft cruise airspeed (aircraft operating points 3 and 4 in Table 9.4).

The EFQ diagram for the baseline candidate aircraft and the results of the sensitivity study are presented respectively in Figures 9.9 - 9.18; Figures 9.9 and 9.10 being for the B-52, Figures 9.11 and 9.12 for the C-141, Figures 9.13 and 9.14 for the DC-9, Figures 9.15 and 9.16 for the Gulfstream II and Figures 9.17 and 9.18 for the KC-135A.

In general, the five candidate aircraft exhibit similar trends, with the following observations:

a. The EFQ is very sensitive to the nacelle downtilt, with increased sensitivity at the higher airspeed because of the high dynamic pressure.

b. The distance ahead of the wing (axial position) has a pronounced effect on the EFQ primarily due to the wing circulation. The sensitivity of EFQ to axial position decreases with increased airspeed, e.g., has a greater effect during low speed climb than high speed cruise (due to increased wing circulation at low speed).

c. The vertical placement of the nacelle with respect to the wing chord has a significant, consistent affect on EFQ at high speeds. At low speed, all aircraft show little affect of vertical nacelle placement because of the large angle of attack of the wing.

d. The effect of spanwise location of the nacelle on the wing is minor, except for the B-52B, which shows a somewhat higher sensitivity at low speed. Because of the nonlinearity affects of this parameter, the sensitivity is influenced by the initial baseline spanwise position.

e. Wing sweep has a negligible effect on EFQ for all the candidate aircraft. This is probably because the nacelle locations on the baseline aircraft are sufficiently ahead of the wing to minimize the changes in wing circulation with blade radius due to wing sweep.

f. Nacelle toe out effects primarily the EFQ at maximum velocity and has virtually no effect on the EFQ at low speeds, except for the C-141. This is because the pitch inflow angles are low at high speeds and high at low speeds. The C-141 is more sensitive to toe in or toe out because of the relatively close proximity of the Prop-Fan axis to the fuselage.

g. Only the DC-9 and KC-135A show any sensitivity to direction of rotation of the Prop-Fan. For these aircraft, downward rotation at the fuselage increases the low speed EFQ.

h. EFQ is basically insensitive to Prop-Fan diameter over the range of diameters studied for all the candidate aircraft.

9.1.7 Discussion

Most of the aircraft showed similar and meaningful sensitivity trends, in spite of the significant differences in the aircraft geometry and nacelle placement. The EFQ showed the most sensitivity to the axial location of the Prop-Fan ahead of the wing, the nacelle downtilt and the toe in.

Table 9.5 is a summary of the resulting equivalent design 1P, basic 1P, and relative higher order excitations for the maximum gross weight - minimum air speed, and minimum gross weight - maximum air speed conditions for the Prop-Fan and all the candidate aircraft in their baseline configurations. Also included for reference is the DC-9-80 study estimates for a nonoptimized installation. With the exception of the Prop-Fan Aircraft, the changes in the excitations were due mainly to changes in the 1P component. As indicated in Table 9.5, the total contribution of the higher orders for all the candidate aircraft was relatively small (i.e., 11-23% vs. 37.5% for the Prop-Fan Aircraft). Since the baseline aircraft are all so different, it is difficult to determine why there are significant differences in the higher order excitations between the candidate aircraft.

Using the sensitivities developed in this study, it should be possible to position a Prop-Fan nacelle on any of the candidate testbed aircraft to achieve a reasonable EFQ of approximately 3.5 - 4.5.

9.1.8 Recommendations

It is recommended that a more detailed EF analysis be performed on the final testbed aircraft as part of future NASA efforts. This detailed analysis should include a more accurate flow-field distribution, as well as a more accurate definition of the aircraft and its operating conditions. This kind of detailed analysis will lead us to an installation design which more accurately achieves the desired excitation factor levels.

TABLE 9.5. RATIO OF n-P LOADS TO 1-P LOADS FOR BASELINE AIRCRAFT

Maximum Gross Weight - Minimum Airspeed

	Prop-Fan	B-52	C-141	DC-9	GS-II	KC-135A	DC9-80
EF(1-P)	3.06	3.95	2.42	3.54	2.75	2.89	2.55
P2/P1	0.319	0.277	0.266	0.095	0.127	0.125	0.036
P3/P1	0.133	0.008	0.079	0.065	0.090	0.060	0.005
P4/P1	0.055	0.006	0.021	0.006	0.022	0.014	-
P5/P1	0.022	0.002	0.006	0.002	0.007	0.004	-
EFQ/EF(1-P)	1.375	1.149	1.230	1.107	1.157	1.115	1.02
EFQ	4.20	4.54	2.98	3.92	3.18	3.22	2.60

Minimum Gross Weight - Maximum Airspeed

	Prop-Fan	B-52	C-141	DC-9	GS-II	KC-135A	DC9-80
EF(1-P)	1.44	3.27	2.55	2.16	1.65	2.09	3.68
P2/P1	0.437	0.255	0.413	0.130	0.218	0.278	0.025
P3/P1	0.161	0.045	0.083	0.034	0.074	0.078	0.016
P4/P1	0.076	0.012	0.022	0.008	0.023	0.025	0.005
P5/P1	0.033	0.003	0.006	0.002	0.008	0.008	-
EFQ/EF(1-P)	1.529	1.178	1.350	1.083	1.196	1.244	1.065
EFQ	2.20	3.85	3.44	2.34	1.97	2.60	.392

9.2 AERODYNAMIC ANALYSIS

9.2.1 Introduction

The influence of the aircraft flow-field on the aerodynamic efficiency of the Prop-Fan was evaluated at seven aircraft operating conditions. The aerodynamic twisting moments, side loads and shaft moments were also evaluated for these operating conditions.

9.2.2 Analytical Methods

9.2.2.1 Flow-Field Calculation - The flow field at the plane of the Prop-Fan, due to the presence of the aircraft, for a given altitude is calculated using an incompressible-inviscid potential flow computer program developed at Hamilton Standard. This program computes the flow-field about individual aircraft components separately and uses the superposition principle to combine these flow-fields to obtain the total flow-field. The fuselage and nacelle are treated as axisymmetric Rankine bodies, while the wing is analyzed as a swept lifting line. The velocity perturbations due to axial flow and cross flow are considered on all aircraft components (wing, nacelle and fuselage). The program also accounts for the effects of the propeller slipstream and swirl on the aircraft flow-field. The influence of the tail surfaces has been found to be negligible. Consequently, these surfaces were not considered in the calculations for wing mounted Prop-Fans. This flow-field calculation requires significantly less information about the aircraft geometry than do other more elaborate methods, such as the Hess code. An extensive comparison of this aircraft flow field program with the Hess code method revealed reasonable agreement; see Reference 25. This flow field program has been used for several decades at Hamilton Standard for accurately predicting propeller design loads.

9.2.2.2 Aerodynamic Loads - The Prop-Fan aerodynamic loads are calculated in the presence of the aircraft flow field using the Goldstein-Locke propeller vortex strip analyses of reference 26, with the assumption of quasi-steady aerody- namics. The spanwise aerodynamic loads on the Prop-Fan blades are calculated at a series of azimuthal positions as the Prop-Fan makes one revolution. These loads are radially integrated and Fourier analyzed to obtain the harmonic components of the blade airloads. The aerodynamic twisting moments about the blade pitch change axis are calculated for an isolated Prop-Fan operating in an azimuthally uniform flow field.

9.2.3 Model Description

The aircraft used in this study is a scaled version of the "Prop-Fan Aircraft" used in the reference 27 study. Figure 9.19 shows a schematic of this aircraft, and Table 9.6 lists some of the geometric parameters of this aircraft. The Prop-Fan geometry used in this study is that of the SR-7 as defined in Section 8.6.

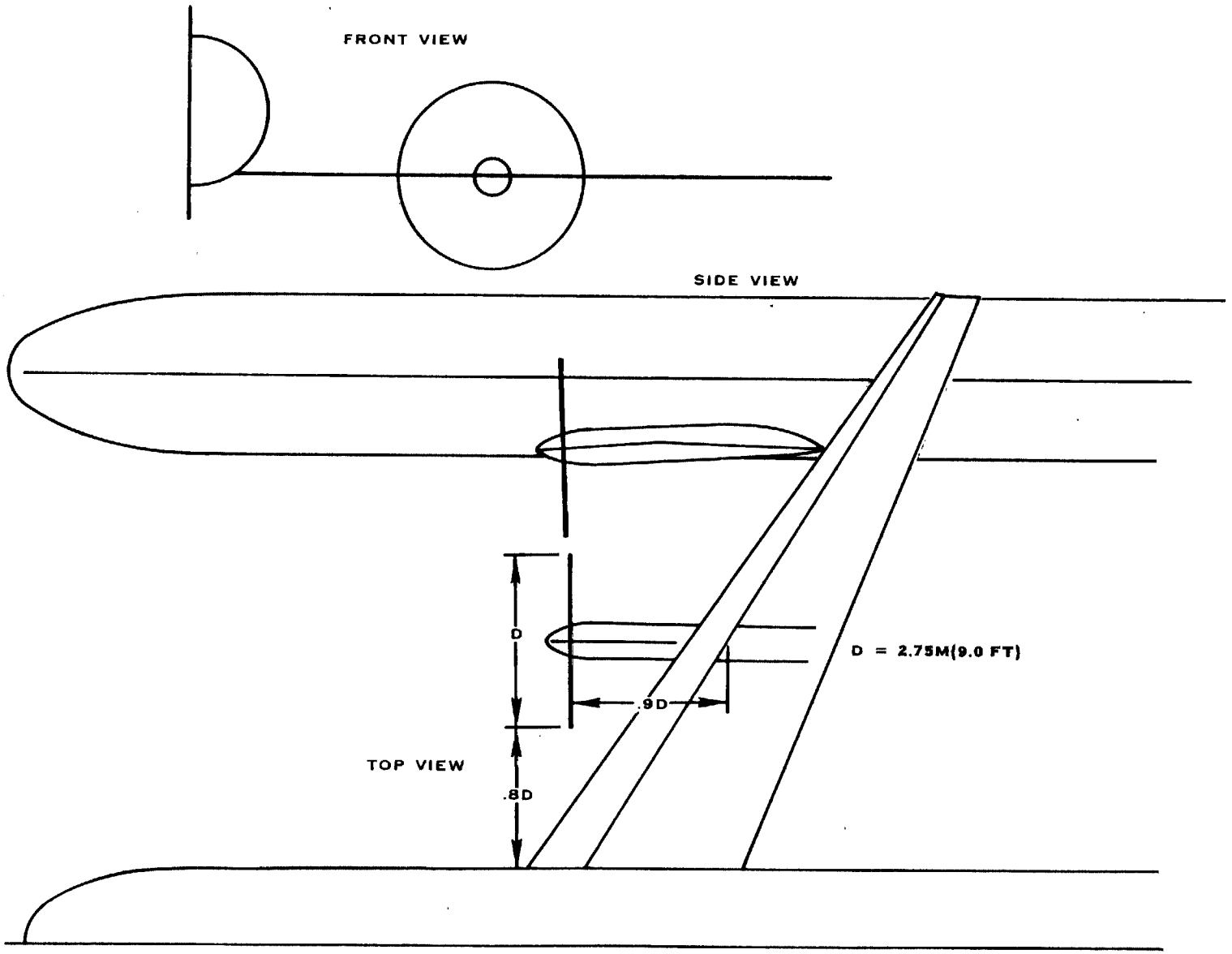

FIGURE 9.19 SCHEMATIC OF PROP-FAN AIRCRAFT

TABLE 9.6. VALUES OF GEOMETRIC PARAMETERS FOR PROP-FAN AIRCRAFT

Parameter	Value
Nacelle Downtilt	7.0 deg.
Quarter Chord Sweep	32.0 deg.
Prop-Fan Diameter	2.75 m (9.0 ft)
Toein Angle	0.0 deg.
Maximum Gross Weight(1)	22993 kg (50700 lbs)
Minimum Gross Weight (1)	16145 kg (35600 lbs)
Wing Area (1)	44.9 m^2 (483 ft^2)
Maximum Wing Loading	512 kg/m^2 (105 lb/ft^2)
Direction of Rotation	Blades moving vertically upward @ fuselage.

(1) A/C geometry scaled from airframes industry supplied A/C for 4.24 m (13.9 ft) Prop-Fan.

TABLE 9.7. SR-7L ESTIMATED INSTALLED EFFICIENCY

Operation	Gross Weight (Kg)	Mach No.	Altitude (M)	SHP/D^2 (Kw/M^2)	Tip Speed (M/Sec)	αNAC (Deg)	η_{ISO} %	η_{SHAFT} %	η_{FLIGHT} %
Takeoff-Climb (15° Flaps)	16145	.20	S.L.	594.8	244	- 3.8	51.6	51.1	50.9
Climb	16145	.50	3048	535.4	244	- 4.3	76.2	76.1	74.9
Cruise	16145	.80	10667	256.9	244	- 4.0	79.4	79.4	77.3
Approach (35° Flaps)	16145	.20	S.L.	134.9	198	-13.0	75.0	75.5	71.8
Hold	16145	.45	4572	167.8	213	- 3.0	82.8	82.5	82.0
70% Cruise	16145	.80	10667	224.0	244	- 4.0	79.6	79.7	77.2
Max. Cruise	16145	.80	10667	306.3	244	- 4.0	78.1	78.0	76.3
Cut Back (15° Flaps)	16145	.20	S.L.	334.3	213	- 3.8	60.2	59.5	59.3
Takeoff-Climb (15° Flaps)	22993	.20	S.L.	594.8	244	1.1	51.6	50.9	50.8
Climb	22993	.50	3048	535.4	244	-3.2	76.2	75.8	75.4
Cruise	22993	.80	10667	256.9	244	-2.7	79.4	78.9	78.6
Approach (35° Flaps)	22993	.20	S.L.	134.9	198	-8.1	75.0	74.1	73.3
Hold	22993	.45	4572	167.8	213	-1.3	82.8	82.1	81.8
70% Cruise	22993	.80	10667	224.0	244	-2.7	79.6	79.2	77.9
Max. Cruise	22993	.80	10667	306.3	244	-2.7	78.1	77.5	77.4
Cut Back (15° Flaps)	22993	.20	S.L.	334.3	213	1.1	60.2	59.3	59.2

η_{ISO} = Isolated Efficiency
η_{SHAFT} = (Thrust Along Prop-Fan Shaft) x Velocity/Power
η_{FLIGHT} = (Thrust In Flight Direction) x Velocity/Power

The aircraft performance and loads shown in Tables 9.7 and 9.8 were evaluated at both the minimum and maximum aircraft gross weights. In order to isolate the effects of the installed flow-field from the effects of changes in Prop-Fan loading, the airloads at each gross weight were calculated at the same Prop-Fan operating condition, e.g., power, tipspeed, altitude and velocity. However, the flow-field at the Prop-Fan was recalculated for each gross weight, and thus, Tables 9.7 and 9.8 show the result of extremes in aircraft attitude on Prop-Fan airloads.

TABLE 9.8. SR-7L ESTIMATED INSTALLED AIRLOADS

Operation Gross Weight (KG)	NF (KG)	SF (KG)	PM (M-KG)	VM (M-KG)	ATM (M-KG/BLADE)
Takeoff-Climb (16145)	66	51	- 82	91	30.2
Climb	-310	40	232	33	18.4
Cruise	-231	49	119	31	6.9
Approach	-118	40	157	73	4.9
Hold	-577	46	44	46	- 0.5
70% Cruise	-229	51	120	32	4.1
Max. Cruise	-237	49	119	30	19.4
Cut Back	- 54	47	- 68	83	6.9
Takeoff-Climb (22993)	282	78	-347	142	30.2
Climb	-128	62	95	57	18.4
Cruise	- 41	73	22	50	6.9
Approach	- 6	64	- 11	118	4.9
Hold	- 99	68	- 78	71	- 0.5
70% Cruise	- 42	74	23	51	4.1
Max. Cruise	- 43	72	22	48	19.4
Cut Back	236	72	-288	128	6.9

9.2.4 Analysis and Results

The flow-field around the aircraft was calculated for each operating condition with the aircraft angle of attack chosen such that the wing lift equaled the aircraft gross weight.

Figure 9.20 shows the sign convention used in presenting the efficiency levels and air loads determined in this study. Table 9.9 is a list of the symbols used. Table 9.7 presents the calculated efficiency levels for each operating condition. Three efficiencies are shown in the table. η_{ISO} is the net efficiency of the Prop-Fan at zero angle of attack in the presence of the nacelle, i.e., isolated efficiency. Obviously, these values will be the same at both aircraft gross weights. η_{SHAFT} is the efficiency of the Prop-Fan in the presence of the aircraft flow-field based on the thrust developed on the Prop-Fan drive shaft (η_{SHAFT}). Because the Prop-Fan shaft may not be aligned with the direction of flight, a third efficiency, η_{FLIGHT} is shown in Table 9.7 and is based on the net thrust in the flight direction, as determined from the following equation:

$$T_{FLIGHT} = T_{SHAFT} \times \cos(\alpha_{NAC}) + N_F \times \sin(\alpha_{NAC})$$

N_F is the "normal force" which is shown in Figure 9.20; N_F is usually positive for $\alpha_{NAC} > 0$, and negative for $\alpha_{NAC} < 0$. The nacelle angle of attack, α_{NAC}, is dependent upon the aircraft angle of attack and the downtilt angle of the nacelle. The downtilt angle of the nacelle is very dependent upon the axial distance between the wing and the nacelle, that distance has not been optimized for this aircraft, and therefore, the downtilt angle may not be optimized.

Table 9.7 shows a loss in cruise flight efficiency ($\eta_{ISO} - \eta_{FLIGHT}$) of 2.1% at minimum aircraft gross weight, and 0.8% at maximum aircraft gross weight due to installation effects. Shaft efficiency, η_{SHAFT}, for this operating condition was not changed at minimum gross weight, but was reduced by 0.5% at maximum gross weight from the isolated Prop-Fan efficiency level. In order to assess the influence of downtilt angle on flight efficiency the downtilt angle was reduced by 1° and the cruise case rerun at minimum gross weight. The flight efficiency loss dropped from 2.1% to 1.1%.

Shaft efficiency losses of less than 0.9% due to the effect of the aircraft flow-field on the Prop-Fan blade loading can be seen in Table 9.7. A slight gain in shaft efficiency is shown in Table 9.7 for several cases where the gain in efficiency, when the Prop-Fan is operating at an axial velocity lower than free stream due to nacelle angle of attack, over comes the losses encountered due to the non-uniformity of the flow field. The normal force, side force, pitching moment and yawing moments calculated from the once per revolution loading on the blades is shown in Table 9.8.

Table 9.8 also lists the aerodynamic twisting moment about the pitch change axis. This was calculated for an azimuthally uniform flow-field.

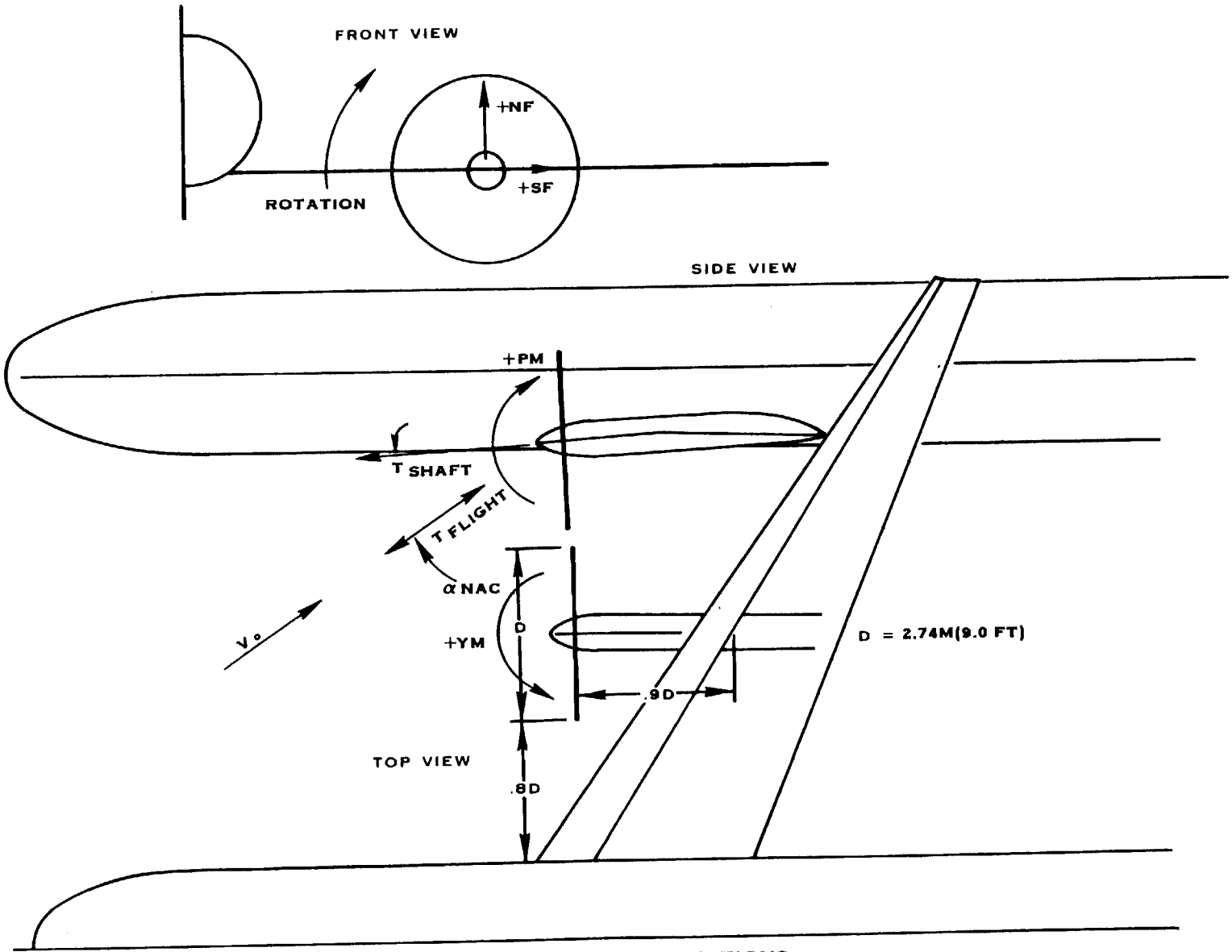

FIGURE 9.20 SIGN CONVENTIONS

TABLE 9.9
LIST OF SYMBOLS

ATM	Aerodynamic twisting moment about blade pitch change axis, + nose up, (m-kg/blade)
N_F	Normal force in plane of propeller centerline of rotation, m-kg.
SHP	Shaft Power, KW
S_F	Side force in plane of propeller, kg
T_{FLIGHT}	Thrust along propeller flight direction, in presence of an aircraft, kg.
T_{ISO}	Thrust along propeller centerline of rotation of an isolated propeller, kg.
T_{SHAFT}	Thrust along propeller centerline of rotation in the presence of an aircraft, kg.
V_o	Flight velocity, m/s
YM	Yawing moment, normal to propeller centerline of rotation, m-kg
α_{NAC}	Nacelle angle of attack, deg.
η_{FLIGHT}	$T_{FLIGHT}\ V_o/(102\ SHP)$
η_{ISO}	$T_{ISO}\ V_o/(102\ SHP)$
η_{SHAFT}	$T_{SHAFT}\ V_o/(102\ SHP)$

9.2.5 Summary

Shaft efficiency losses of less than 1/2% may be expected due to the aircraft flow-field.

Cruise flight efficiency losses up to 2.1% were calculated, due primarily to the nacelle angle of attack. A reduction in the cruise efficiency loss from 2.1% to 1.1% was calculated by reducing the downtilt angle 1.0 degree.

9.3 ACOUSTIC ANALYSIS

9.3.1 Introduction

Noise levels have been calculated for the SR-7 Prop-Fan configuration (defined in Section 8.6) in two versions; 9-foot diameter and 13.9-foot diameter. The 13.9 foot diameter was chosen as it corresponds to the size required for the aircraft defined in Section 8.3. Near-field noise was calculated for the design cruise and take-off operating conditions. Far-field noise levels was calculated for three conditions representative of FAR-36 certification. This section also includes a description of the methods used to calculate the noise, the operating conditions selected, the calculation results in tabular form and a brief discussion of the calculation results.

9.3.2 Noise Prediction Method

Noise predictions were made using the Hamilton Standard Prop-Fan noise Prediction Computer Program based on the frequency domain propeller noise theory developed by Hanson (Reference 28). Near and far-field calculations of monopole (thickness), dipole (loading), and quadrupole noise sources are included in this program. For far-field predictions, the noise due to the interaction of non-uniform inflow with the Prop-Fan are also included. Sources of non-uniform inflow include distortion due to the airplane geometry (wing circulation, fuselage and nacelle blockage, etc.) and geometric inflow due to aircraft angle-of-attack.

The noise prediction program is coupled to the Hamilton Standard aerodynamic performance programs, which provide the Prop-Fan geometry (thickness, chord, twist and sweep distributions of the blade) and aerodynamic loads necessary for a noise calculation.

9.3.3 Operating Conditions

The airplane used is the same as the one used in the design trade-off study. This airplane was used to establish the flow-field at the propeller for far-field noise calculations. The operating conditions selected for analysis were the full-power take-off, cut-back power take-off (far-field only), approach and design cruise (near-field only) conditions. The cut-back power condition is representative of SR-7 operation during noise certification. The cut-back power condition was defined as "the thrust level required to maintain level flight with one engine out or a minimum of 4% climb gradient". This meets the requirements of FAR Part 36 for power cut-back conditions. This resulted in a requirement of 65% of the thrust available at full power and some reduction in tip speed. A complete description of the operating conditions used is included in Table 9.10. All calculations were done for acoustic standard day conditions (77°F and 70% relative humidity at sea level) assuming twin-engine airplanes.

TABLE 9.10. OPERATING CONDITIONS USED FOR NOISE CALCULATIONS

Condition	Altitude (feet)	Flight Mach No.	Disk Loading SHP/D^2	Tip Rotational Speed (ft/sec)	Types of Noise Calculations
Full-Power Takeoff	SL	.2	74.1	800	Near and Far Field
Cut-Back Power Takeoff	SL	.2	41.6	700	Far Field
Approach	SL	.2	16.8	650	Far Field
Cruise	35,000	.8	32.0	800	Near Field

9.3.4 Calculation Results

9.3.4.1 Near-Field - Tables 9.11 and 9.12 summarize the free field noise calculated for three tip clearances and seven fore and aft locations for the full power take-off and design cruise conditions. The fore and aft locations (axial positions) represent measurement stations on the fuselage, with 0. being the plane of rotation. Positive values denote axial positions forward, and negative values denote positions aft of the plane of rotation. The tip clearance and axial positions were normalized by the Prop-Fan diameter for these caiculations, so the noise levels presented are valid for the 9-foot or the 13.9-foot diameter SR-7.

It should be noted that the directivity patterns are different for the take-off and cruise flight speeds due to changes in the source characteristics and propagation with changing flight Mach number. Therefore, different directivity points were selected for the two operating conditions so that the data presented includes the maximum noise at the fuselage.

The joint levels at Blade Passage Frequency (BPF) and its harmonics for the design cruise condition are much higher than those for the take-off condition due to the higher tip relative Mach number at cruise (1.147 vs. 0.744).

TABLE 9.11. NEAR FIELD NOISE FOR THREE TIP CLEARANCES AT FULL POWER TAKEOFF, FREE-FIELD CONDITIONS

	BPF Harmonic	Axial Position Along Fuselage, X/D, from Plane of Rotation						
		Aft -1.0	-.7	-.4	-.1	.2	.5	Forward .8
0.5D Clearance	1	108.0	118.1	126.2	129.2	125.6	117.2	106.4
	2	72.1	91.0	106.4	112.8	106.9	92.9	72.8
	3	40.3	67.2	87.9	96.4	89.3	69.5	44.4
	4	6.9	42.5	70.0	82.1	74.5	50.5	17.5
	5	-26.3	18.0	52.3	67.8	59.6	31.1	-9.8
	OASPL	108.0	118.1	126.2	129.3	125.7	117.2	106.4
0.8D Clearance	1	114.0	120.7	125.1	126.0	122.9	117.1	109.8
	2	85.5	98.2	107.1	109.7	105.2	95.6	82.7
	3	59.1	77.2	89.8	94.2	89.1	75.8	58.0
	4	32.5	56.6	73.4	79.9	74.6	58.9	36.3
	5	6.1	36.0	57.2	65.8	60.1	41.7	14.1
	OASPL	114.0	120.7	125.2	126.1	123.0	117.1	109.8
1.0D Clearance	1	116.0	121.1	124.2	124.4	121.6	116.8	110.7
	2	90.4	100.3	106.7	108.1	104.3	96.5	86.1
	3	66.4	80.6	90.0	92.9	88.7	78.1	63.4
	4	42.6	61.5	74.2	78.7	74.3	61.9	43.6
	5	18.9	42.5	58.4	64.6	59.9	45.5	23.5
	OASPL	116.0	121.1	124.3	124.5	121.7	116.8	110.7

TABLE 9.12. NEAR FIELD NOISE FOR THREE TIP CLEARANCES AT DESIGN CRUISE, FREE-FIELD CONDITIONS

	BPF Harmonic	Axial Position Along Fuselage, X/D, from Plane of Rotation						
		Aft -.6	-.4	-.2	-.1	0	.3	Forward .6
0.5D Clearance	1	129.1	138.0	146.1	146.8	144.6	141.7	127.1
	2	123.4	138.3	143.9	142.6	141.1	136.8	115.1
	3	124.0	135.8	138.1	134.0	132.6	135.8	123.0
	4	119.9	131.8	134.0	127.7	127.2	131.6	118.8
	5	115.8	128.3	124.8	125.2	118.7	127.6	116.1
	OASPL	131.5	142.8	148.7	148.4	146.4	144.0	129.4
0.8D Clearance	1	133.5	140.4	143.8	143.3	141.6	141.7	133.2
	2	131.6	140.0	141.0	139.4	138.6	137.2	126.5
	3	130.7	135.7	134.6	130.4	130.4	133.2	130.3
	4	127.5	129.8	130.3	124.3	125.0	127.8	127.6
	5	124.5	125.0	115.0	122.1	116.4	124.1	127.0
	OASPL	137.6	144.1	146.1	145.0	143.6	143.6	136.7
1.0D Clearance	1	135.4	140.5	142.3	141.5	140.1	140.9	135.2
	2	134.3	139.4	139.3	137.8	137.3	136.3	130.1
	3	132.3	134.8	132.3	128.8	129.1	131.7	131.4
	4	128.3	129.4	127.4	122.8	123.7	126.2	128.5
	5	124.7	126.8	118.4	120.3	115.1	122.2	127.0
	OASPL	139.5	143.9	144.4	143.3	142.2	142.7	138.4

9.3.4.2 Far-Field - Noise calculations for noise certification conditions are summarized in Table 9.13. The noise was calculated at 1/2-second intervals and integrated to give the Effective Perceived Noise Level (EPNL) as required in Federal Aircraft Regulations Part 36. The EPNL values are presented in Table 9.13 for two types of calculations; 1) assuming free-field conditions (no ground reflections) and 2) assuming the measuring microphone is 4 feet above a grass-covered earth surface, as required for FAR-36 certification.

TABLE 9.13. FAR-FIELD NOISE LEVELS FOR THE 9-FOOT AND 13.9-FOOT DIAMETER PROP-FANS (2-ENGINE AIRCRAFT)

Condition	Aircraft Height Above ground, ft	Free Field	EPNL Microphone 4 Feet Above Ground	FAR-36 Stage 3 Limit
9-Foot Diameter				
Full-Power Takeoff	2900	88.4	86.7	89.0
Cut-Back Power Takeoff	2750	78.2	78.2	89.0
Approach	394	78.8	81.7	98.0
13.9-Foot Diameter				
Full-Power Takeoff	2900	89.6	95.0	89.8
Cut-Back Power Takeoff	2750	79.5	84.4	89.8
Approach	394	81.1	83.0	99.5

Based on previous studies the aircraft height above the ground plane was estimated to be 2900 feet for the full-power condition and 2750 feet for the cut-back power condition at the measurement location 21,327 ft. (6500 meters) down range from the start of take-off roll. For the approach noise predictions the height above ground was assumed to be 394 feet at the measurement location 6562 ft. (2000 meters) from the runway threshold.

Because of its smaller diameter, the source noise levels of the 9 foot SR-7 are about 4dB lower and the BPF is about 1.5 times higher than the values for the 13.9 foot SR-7. These differences account for the differences in noise levels seen in Table 9.13.

For example, the free-field EPNL values for the 9-foot SR-7 are about 1.3 EPNdB lower than those of the 13.9 foot SR-7, although the source level is 4dB lower. This is explained by the fact that the EPNL is frequency weighted, and the higher BPF of the smaller Prop-Fan is weighted more heavily than that of the larger.

The EPNL values are also dependent on the presence of the ground plane, because the sound reflected from the ground plane can reinforce or interfere with the direct sound at the measurement microphone. The frequency of the incident sound determines whether reinforcement or interference occurs for a given microphone position. As an example, consider the full power take-off flyover case. At 800 ft/sec tip speed the BPF is 146.6 Hz for the 13.9 foot diameter Prop-Fan and 226.4 Hz for the 9 foot diameter Prop-Fan. For a four-foot microphone height the sound reflected from the ground will cause maximum reinforcement of the incident sound at 135 Hz and will cause maximum interference (cancellation) at 210 Hz. Since the BPF of the 13.9 foot Prop-Fan is close to the reinforcement peak, the EPNL with ground reflection is increased 5.4 dB relative to the free-field level, while the EPNL with ground reflection for the 9 foot diameter Prop-Fan is reduced 1.7 dB relative to the free field level by the cancellation. Thus, for a microphone located 4 ft. above a ground plane, the reduction in EPNL for the reduction in diameter is 1.2 EPNdB due to source noise reduction and an additional 7.1 EPNdB due to different ground reflection effects.

At the power cut-back condition (tip speed reduced to 700 ft/sec) the BPF is reduced for both diameters resulting in different ground reflection effects. The reduction in source level (free-field EPNL) due to power cut-back is about 10 dB for both diameters. The BPF of the 13.9 ft. SR-7 is reduced from the maximum reinforcement frequency and that of the 9-foot SR-7 is reduced from the maximum interference frequency. Thus, the change in noise caused by reducing the diameter from 13.9 to 9 ft. is 4.9 EPNdB due to the effects of ground reflection. These examples illustrate the dependence of the far-field noise on flyover geometry, showing that there is a complex interaction of diameter, blade passage frequency, and measurement microphone height above the ground plane.

Finally, FAR-36 noise requirements are shown in Table 9.13 for the two diameters at the take-off, cut-back take-off, and approach conditions. These limits are based on aircraft gross weight and number of engines. From Hamilton Standard studies, the aircraft weight with the 9-foot SR-7 was estimated to be 50,200 lb. while that for the 13.9-foot SR-7 was estimated to be 121,000 lb.

It is apparent from Table 9.13 that both the 9-foot diameter and 13-foot diameter SR-7's will meet the FAR Part 36 requirements with power cutback.

9.4 TESTBED-SIZE BLADE STRUCTURAL ANALYSIS

9.4.1 Introduction

A program to study the structural feasibility of full-size, high speed, advanced Prop-Fan blades was previously completed under Task 3 of this contract and reported in Volume I. As a continuation of that effort, this task establishes the preliminary design of a 2.74 meter (9 ft) diameter blade of this type. Results of the previous study were incorporated in the initial configuration selection process, along with preliminary parametric variations of tip speed, number of blades, disk loading, thickness, chord width, and blade stacking parameters of sweep and offset. The aero-acoustic parametric study is reported in Section 8.0. Many design iterations were required to define an acceptable preliminary design which was also optimized (within cost and schedule constraints) for structural integrity, aerodynamic efficiency, low noise, aero-elastic stability, high reliability, and ease of fabrication.

9.4.2 Selection of Initial Design Configuration

As mentioned in the introduction, results of a previous full-size blade feasibility study, along with preliminary aero-acoustic optimization studies, were reviewed prior to the selection of an initial design configuration for the SR-7 blade. Unfortunately, the former study showed that the recommended, aero-acoustically optimum design, would not be structurally feasible. That is, a large number of thin, highly swept blades, built of conventional materials, most likely would not meet the stress, resonant frequency, and/or aero-elastic stability requirements of a high-speed Prop-Fan installation. In fact, without some sort of structural modification, all blades of the earlier full-size study were found deficient, relative to high-speed aero-elastic stability. Variations in external/internal geometry were not permitted within the scope of the earlier full size study. Therefore, additional parametric structural studies were performed at the start of this program on two moderately swept blades from that earlier study, prior to the selection of an initial configuration. Also, stacking variations were explored as a means of improving the stability of a small, highly swept, solid titanium, model blade (SR-5) found to be unstable during wind tunnel tests.

The two blades selected from the full-size study, for additional evaluation, were the eightand ten-bladed SR-3 configurations which had moderate sweep, and conventional solid aluminum spars, covered with glass-fabric-reinforced, epoxy resin shells. The individual effects on stability of changing tip chord width, center of gravity location, and resonant frequency level were explored. Analysis showed that individual changes in these parameters for the narrower, ten-bladed, SR-3 configuration produced only minor improvements not capable of meeting high-speed stability requirements. On the other hand, significant stability improvements were predicted for the wider, eight-bladed, SR-3 design. These were attained by moving the center-of-gravity forward toward the blade leading edge, narrowing the blade tip width, and increasing both the resonant frequencies and the degree of separation between them.

An aerodynamic optimization study was also conducted, and reported in Section 8.4. This study examined the influence of tip speed, number of blades, disk loading, as well as thickness, chordwidth, and sweep distributions on efficiency, noise, fuel consumption, and direct operating cost. The baseline blade design in this study was an eight-bladed design similar to the SR-3 design. From a fuel consumption viewpoint, this study showed the following modifications to be beneficial; increasing the number of blades, increasing sweep, narrowing the blade tip chord, and maintaining the blade thickness-to-chord ratio.

Since each of the above studies recommended different blade characteristics, compromises were required to yield a successful design. The blade chosen resembled the SR-3 eight-bladed design. This configuration is compared to the baseline design in Table 9.14. It was chosen for many reasons. Its aerodynamic performance is nearly the same as the performance of the baseline blade. Stress results from the 3.35 m (11 ft) diameter SR-3 design study and from the structural optimum study show that this SR-7 blade configuration can be designed to satisfy the stress criteria. Frequency results from the same two studies indicate that this configuration can also satisfy frequency criteria. The stability study also recommended a modified SR-3 eight-bladed design. Foreign object impact results for the SR-3 eight-bladed design, in the large-scale blade feasibility study, satisfied the design requirements; implying that the SR-7 design should also satisfy the requirements.

TABLE 9.14. SR-7 DESIGN CONFIGURATION

	Baseline	Initial Configuration
Number of Blades	8	8
Tip Diameter, m (ft)	2.74 (9.00)	2.74 (9.00)
Tip Speed, m/sec (ft/sec)	244 (800)	244 (800)
Forward Speed, Mn	0.8	0.8
Tip Sweep Angle, deg.	39.8	36
Power Loading, KW/M^2 (HP/ft^2)	256.8 (32.0)	256.8 (32.0)
Efficiency	0.795	0.791
Noise (BPF)	143.2	144.5
(Fuel Burned)	Base	+1.16 (greater)
(Direct Operating Cost)	Base	+0.69 (higher)

The fabrication concept chosen for the initial SR-7 design configuration was the same as that assumed for the large-scale SR-3 eight-blade study. This concept has a forged, solid aluminum spar; woven, fiberglass cloth reinforced, epoxy resin shell; and lightweight foam fill in the shell cavities. This is a current, service-proven fabrication method, and hence eliminates the need for developing new fabrication technology. The sheath material was changed from titanium to nickel. Its higher density aids in moving the center of gravity forward which was shown to be beneficial to blade stability. Using nickel for the sheath material is also a current, service-proven fabrication process. Additionally, the spar was moved toward the leading edge of the blade, again to move the center of gravity forward for stability purposes.

9.4.3 Operating Conditions

The SR-7 preliminary blade design was analyzed to satisfy the design requirements at two specific flight conditions. Design cruise and take-off climb. These are summarized in Table 9.15. The cruise condition was used to evaluate high speed stability, frequencies, and elastic deflections of the blade while the take-off/climb condition was used to evaluate combined steady and cyclic stress levels as well as deflections. In addition to the above operating conditions, two overspeed cases were also analyzed to evaluate the blades ability to withstand high centrifugal forces due to inadvertent overspeeds. The first is a 25% overspeed which produces, roughly, a 50% increase in load; while the second is a 40% overspeed, resulting in roughly twice the centrifugal load. These latter two cases were analyzed only after a blade was found which satisfied the requirements of the two flight conditions.

TABLE 9.15. FLIGHT CONDITIONS

	Cruise	Take-off/Climb
Velocity, Mn	0.8	0.2
Altitude, m (Ft)	10,668 (35,000)	Sea Level
Propeller Speed, rpm	1698	1698
Power Loading, Kw/M^2 (HP/Ft^2)*	256.8 (32)	570.7 (71.1)
Excitation Factor	-	4.5

*Based on 2.74 m (9 ft) diameter.

9.4.4 Design Evaluation Criteria

The SR-7 blade design criteria is specified in the design requirements document, "Design Requirements for Advanced Turboprop Blades, SR-7" (reference Appendix D).

The stress requirements are reproduced in Figure 9.21. Combined steady and cyclic stresses are plotted on a modified Goodman diagram for comparison to material allowables for each blade component. Design stress allowables are based on conservative assessments of each material's strength, environment, size factors as well as full-scale fatigue tests. Stresses for the take-off/climb conditions condition were evaluated against the fatigue requirements in Table 9.16.

TABLE 9.16. CRITERIA FOR STRESS EVALUATION

(1) High-cycle fatigue - designed for infinite life, i.e., 10^8 cycles.

(2) Low-cycle fatigue - designed for 50,000 start/stop cycles, from no stress to peak stress.

(3) 25% overspeed - the steady stress shall be below the 0.2% offset yield strength for homogenous metal materials, or below the 5% change in elastic modulus limit for fiber reinforced resin materials.

(4) 40% overspeed - the steady stress shall be below the utlimate tensile strength for homogenous metal materials, or below the fracture limit for fiber reinforced resin materials.

In order to avoid dynamic magnification from operating too near a resonant frequency, resonance avoidance zones are specified at integer orders (1P, 2P, 3P, etc) of design RPM as shown in Figure 9.22. These zones are defined both as a percentage of the rotational speed and the corresponding integer frequency. The avoidance band is 10% for 2-P during flight operating and increases to 20% for ground operation due to potential exposure to rear-quartering cross-winds flowing over the wing and/or fuselage. This ground operation percentage decreases with P-order, down to 2.5% for the 5-P intersection.

The foreign object impact design criteria is summarized in Table 9.17, which specifies the size of the object and the damage limit for each impact size classification. In terms of evaluating the blade designs, the moderate impact criteria can be satisfied if the spar stress remains below the 0.2% offset yield stress, for homogenous metal materials, or below the 5% change in elastic modulus limit for fiber reinforced resin materials. The major impact criteria can be satisfied if the spar stress remains below the ultimate tensile strength, for homogeneous metal materials, and below the fracture limit, for fiber reinforced resin material.

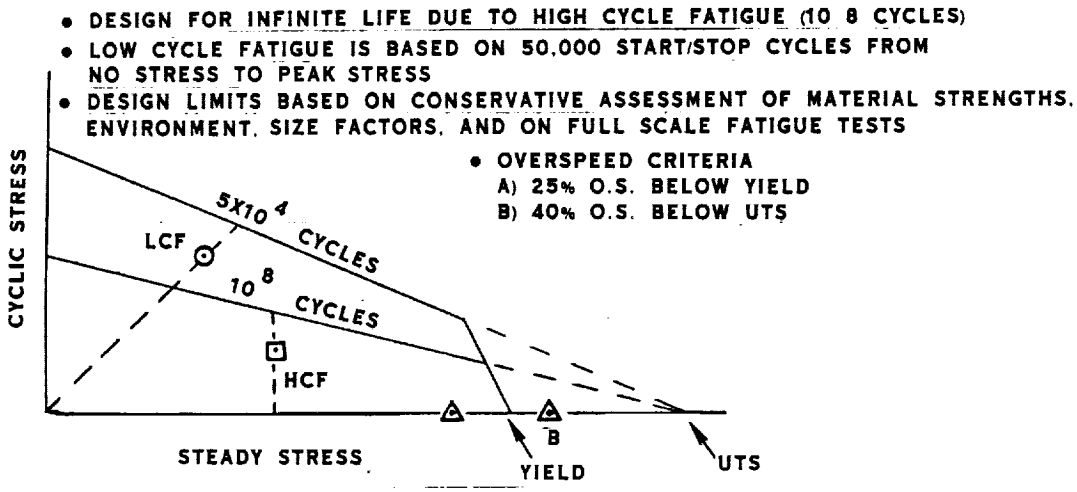

FIGURE 9.21 DESIGN STRESS CRITERIA

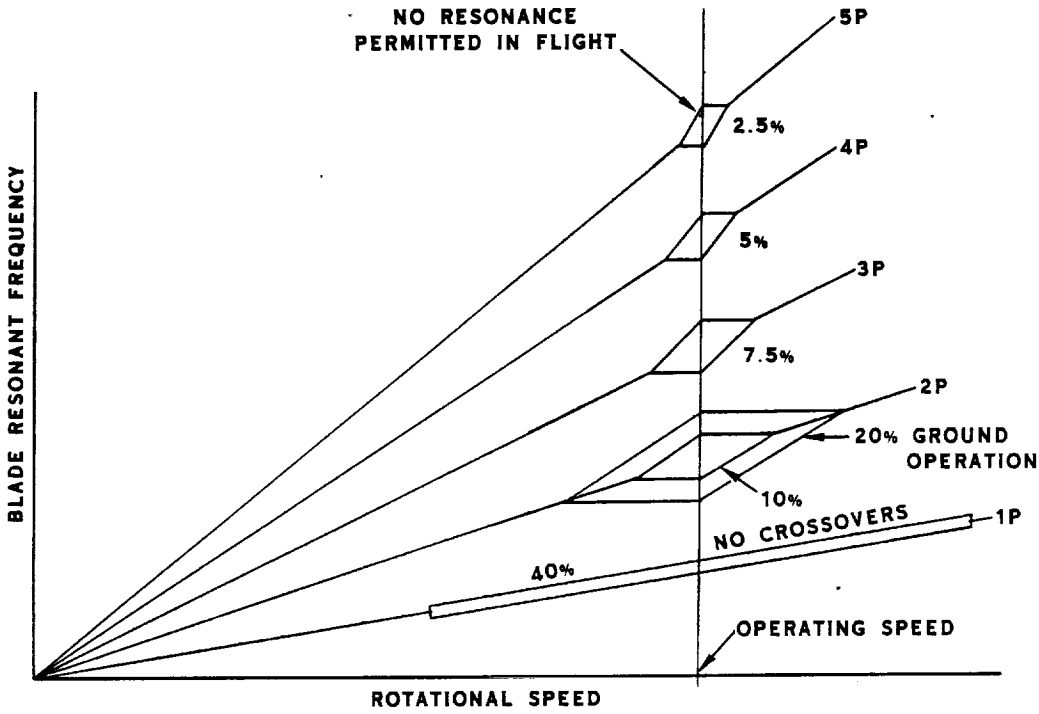

FIGURE 9.22 DESIGN FREQUENCY CRITERIA AVOIDANCE ZONES

TABLE 9.17. FOREIGN OBJECT IMPACT CRITERIA

Minor Impact	- Sand, small stones, up to 4 oz. birds - No damage to basic blade structure - Continued operation
Moderate Impact	- 2 inch hailstones, up to 2 pound birds - Loss of material or airfoil distortion acceptable - operation at 75% power for 5 minutes - No metal fragments will penetrate fuselage - Rotor unbalance force <5000#'s
Major Impact	- Up to 4 pound bird - Loss of material or airfoil distortion acceptable - Ability to feather - No metal fragments will penetrate fuselage - Rotor unbalance force <25,000#'s

The design criteria for blade stability includes requirements for high speed (unstalled flutter) as well as low speed (stall flutter). The onset of the unstalled flutter is not permitted to occur below the Mach number/flutter boundary offset from flight profile as shown in Figure 9.23. In addition the predicted onset of unstalled flutter at 4267 m. (14,000 ft) must be greater than 0.8 m to allow testing in the Modane wind tunnel. These unstalled flutter requirements are to be met with blade frequencies degraded by 15% at all operating speeds, up to 105% of the normal maximum. The propeller must also be free of stall flutter up to 120% maximum (baseline) power at 100% rpm.

9.4.5 Calculation Technique

Finite element analysis was used to calculate the deflections, stresses, resonant frequencies and mode shapes of the SR-7 blade design. The finite element model is illustrated in Figure 9.24. An in-house three-dimensional finite element analysis program, BESTRAN, was used as the primary analysis program. BESTRAN is very similar to NASTRAN. In fact, comparative analyses of an intermediate blade design, conducted part way through this design iteration process, showed the two programs yielded identical results. Results of the comparative analyses are presented at the end of this section. In the past, the BESTRAN method has also been confirmed through correlation of predicted versus measured deflections, stresses, and frequencies of spar/shell blades. Also, a variety of pre- and post-processors, available only for BESTRAN, at the time, gave it a clear advantage for use as an iterative tool.

For each operating condition, a spanwise distribution of in-plane and out-of-plane airload was obtained. These airload distributions were integrated and converted to resultant forces acting at each of the specific finite element model stations. This force was then distributed equally among the nodes across the model station, except at the leading and trailing edge nodes where no force was applied. This procedure was performed at the take-off/climb condition for both the steady-state and cyclic airloads, since blade combined stresses were evaluated at this condition. The forces for the steady-state cruise condition, on the other hand were not distributed across the chord since this condition was used only as an indicator of cruise deflections and steady-state stress in the blade.

The steady-state operating conditions were analyzed using the steady-state airloads as well as the centrifugal loads and differential stiffening effects caused by rotation. The cyclic operating conditions were analyzed using the differential stiffening effects from the steady state case, and applying the cyclic airloads due to an equivalent excitation factor (EF), adjusted to account for flow distortion through the plane of the propeller. As specified in the design requirements, the basic EF attributed to 1P (once-per-revolution) excitation is 3.30. However, an additional amount of excitation was lumped into the 1P cyclic analysis to account for potential higher-order (nP) harmonics. This raises the total equivalent EF to 4.5. The assumed magnification factor is 1.0 for the 1P excitation and 3.0 for the nP excitations.

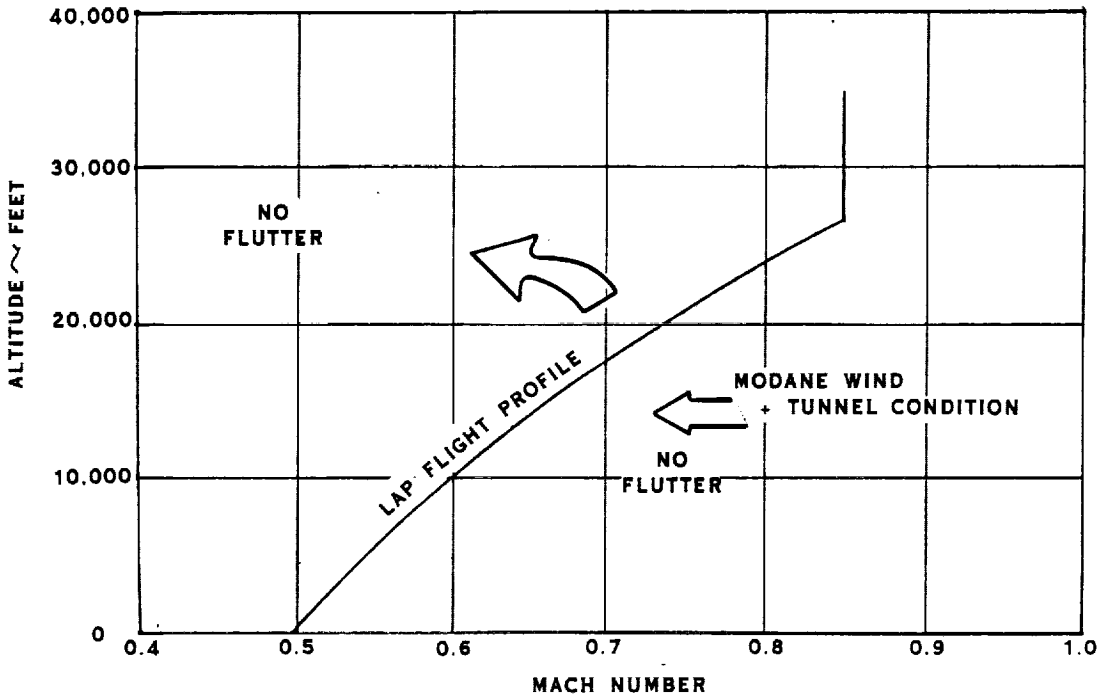

FIGURE 9.23 HIGH SPEED STABILITY CRITERIA

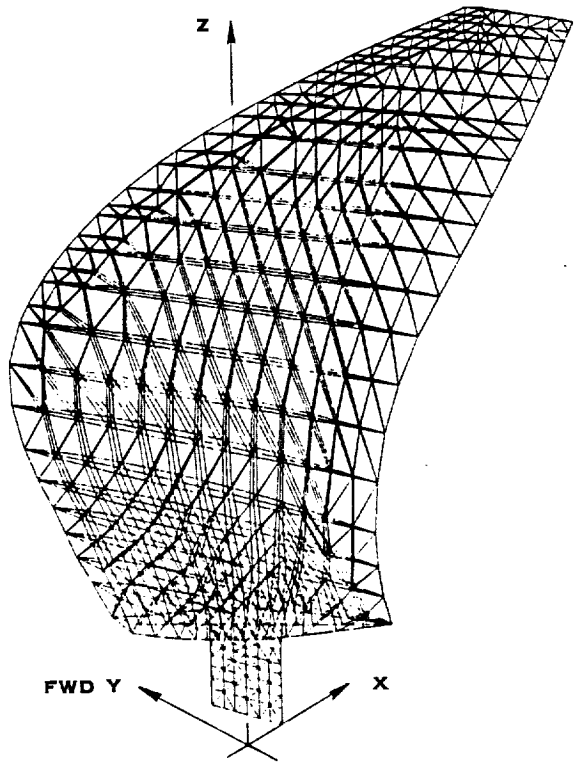

FIGURE 9.24 FINITE ELEMENT MODEL

An empirically derived correction factor was applied to the cyclic stresses because measured 1P response stresses for small, solid metal, swept blades were higher than the calculated stresses. This correction factor varied with radius as is shown in Figure 9.25. The factor was applied only to the calculated cyclic stresses for the blade.

Resonant frequencies and mode shapes were calculated using a hybrid finite element technique requiring both BESTRAN and NASTRAN solution codes. The mass, stiffness, and differential stiffening matrices were calculated using BESTRAN. These matrices were then modified to represent appropriate input for the NASTRAN eigenvalue solver. This technique yielded the primary frequencies and mode shapes very quickly. Experience has shown these results to be in excellent agreement with those obtained from lengthy BESTRAN determinant search methods.

The second BESTRAN method employed the same solution process except that it was repeated in a stepwise manner, increasing the load between each step, and correcting the model for deflection and cumulative differential stiffness, based on cumulative stress. This latter method provides a better approximation of blade non-linear behavior. (Reference 29).

The final two methods employed the NSC NASTRAN code. The NASTRAN FEA model was generated by converting the multi-layered BESTRAN model to an equivalent single-layered NASTRAN composite element model. The first NASTRAN method is an iterated solution capable of accounting for large displacements. The loads are first applied/generated in the static position to determine an approximate deflected position.

Subsequent solutions utilize the last deflected position to recalculate the loads for application once again to the static model. Relative strains/displacements are compared after each calculation until they fall within acceptable tolerance bands, which is indicative of achieving equilibrium. The second NASTRAN method involved a piecewise linear technique, based on the similar BESTRAN procedure of small, linear, load steps described above.

During blade design iterations on the SR-7 blade, one intermediate design was selected to evaluate differences between various finite element solution techniques. Excellent agreement was found among the various methods. Results are presented below for comparison purposes.

The first two techniques involve solutions with the BESTRAN code. In the first method, centrifugal loads and airloads are applied to the static geometry in a single load step. Differential stiffening is employed to account for restoring centrifugal effects.

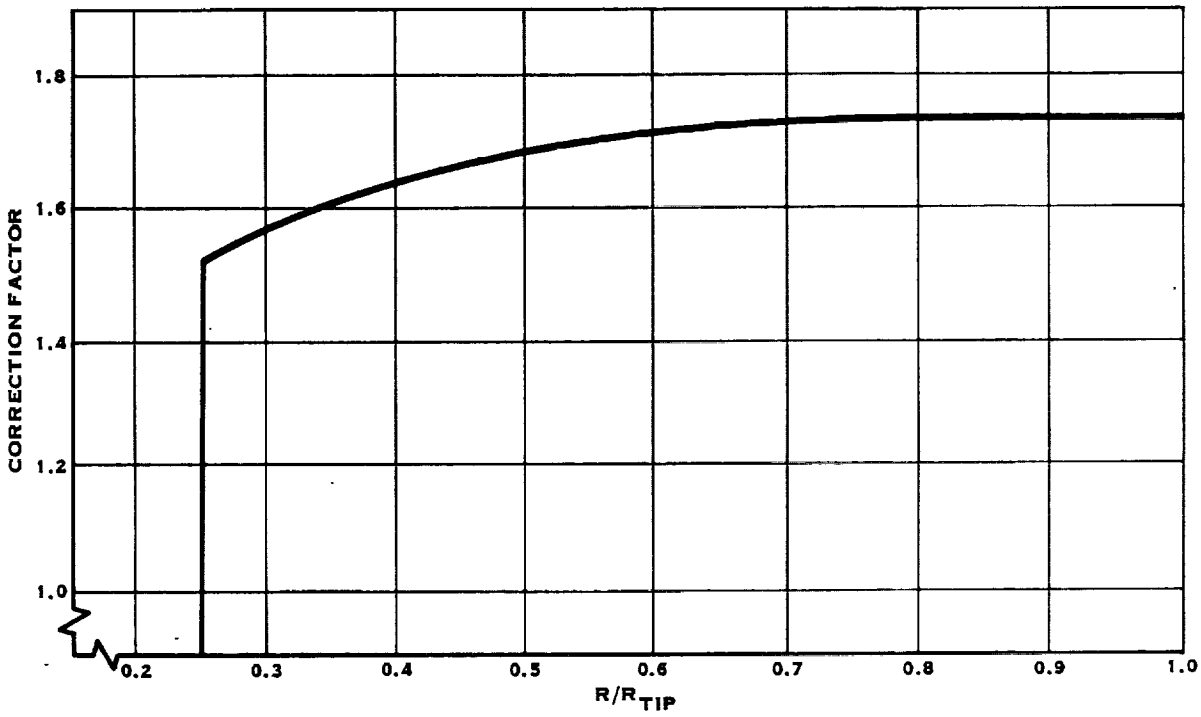

FIGURE 9.25 CYCLIC STRESS CORRECTION FACTOR VS. R/R_{TIP}

Deflection results from the different analytical techniques are compared in Figures 9.26 and 9.27, while frequencies and stabilities are compared in Table 9.18. Steady-state deflection contours for both methods are shown in Figure 9.26. The cumulative piecewise linear deflections of the blade tip, using BESTRAN and NASTRAN, are compared in Figure 9.27. Table 9.18 lists the resonant frequencies and the stabilities based on the corresponding mode shapes. The latter results were not calculated using the NASTRAN piecewise linear method. Stress comparisons are not possible because stresses for the MSC NASTRAN element were not available and/or valid at the time of calculation. In all cases, the methods show excellent agreement.

TABLE 9.18. COMPARISON OF ANALYSIS METHODS
(STEADY-STATE CRUISE CONDITION)

ITEM	BESTRAN		NASTRAN	
	One Load Step	P.W.L.	Iterated @ Full Load	P.W.L.
Tip Defl. @ Mid Chord	0.861	0.842	0.846	0.849
Resonant Frequencies				
1	42.5	42.6	41.1	
2	73.8	73.9	74.0	
3	103.8	103.9	102.7	Not
4	145.3	144.7	136.3	Calc'd
5	177.4	177.8	173.4	
6	226.4	225.1	211.8	
Stability Isolated Blade At Sea Level	1.01 Mn	1.01 Mn	0.98 Mn	Not Calc'd

9.4.6 Design Procedures

Two computerized procedures were developed to aid in the finite element design iteration process. The first was a code which provided quick conversions between aerodynamic 3-D stacking (global x, y, z coordinates of mid-chord) and structural stacking (sweep and offset, measured parallel and normal to chord). See Figure 9.28. The second procedure provided rapid capability to modify geometric distributions of an existing finite element model: stacking, blade chord and/or spar widths, as well as blade thickness, with or without accompanying shell thickness variations. See Figure 9.29.

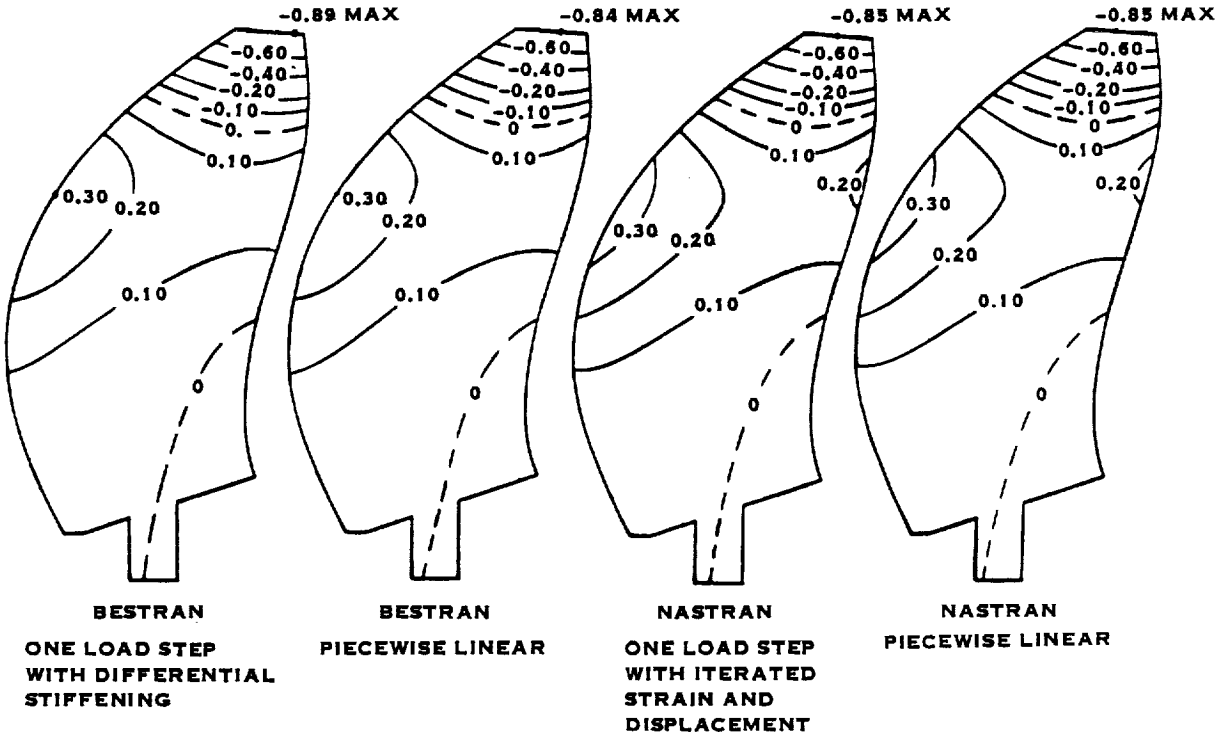

FIGURE 9.26 DEFLECTION RESULT COMPARISON FOR DIFFERENT ANALYSIS METHODS (STEADY-STATE CRUISE, DEFL. NORMAL TO 3/4 RADIUS STATION)

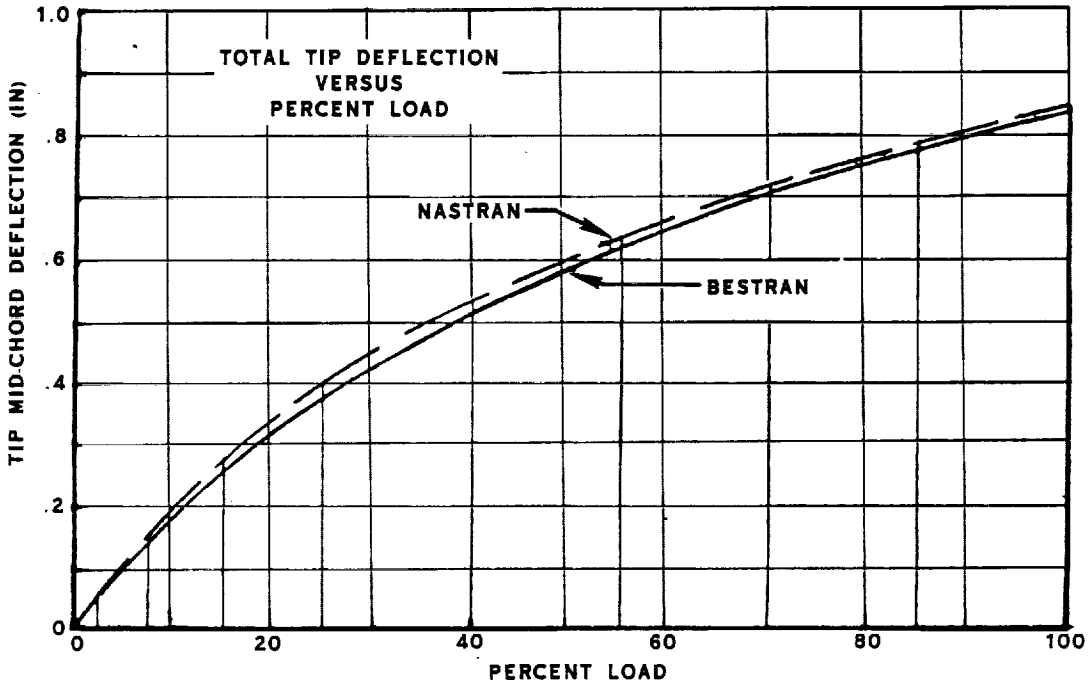

FIGURE 9.27 PIECEWISE LINEAR RESULT COMPARISON FOR DIFFERENT ANALYSIS METHODS (STEADY-STATE CRUISE)

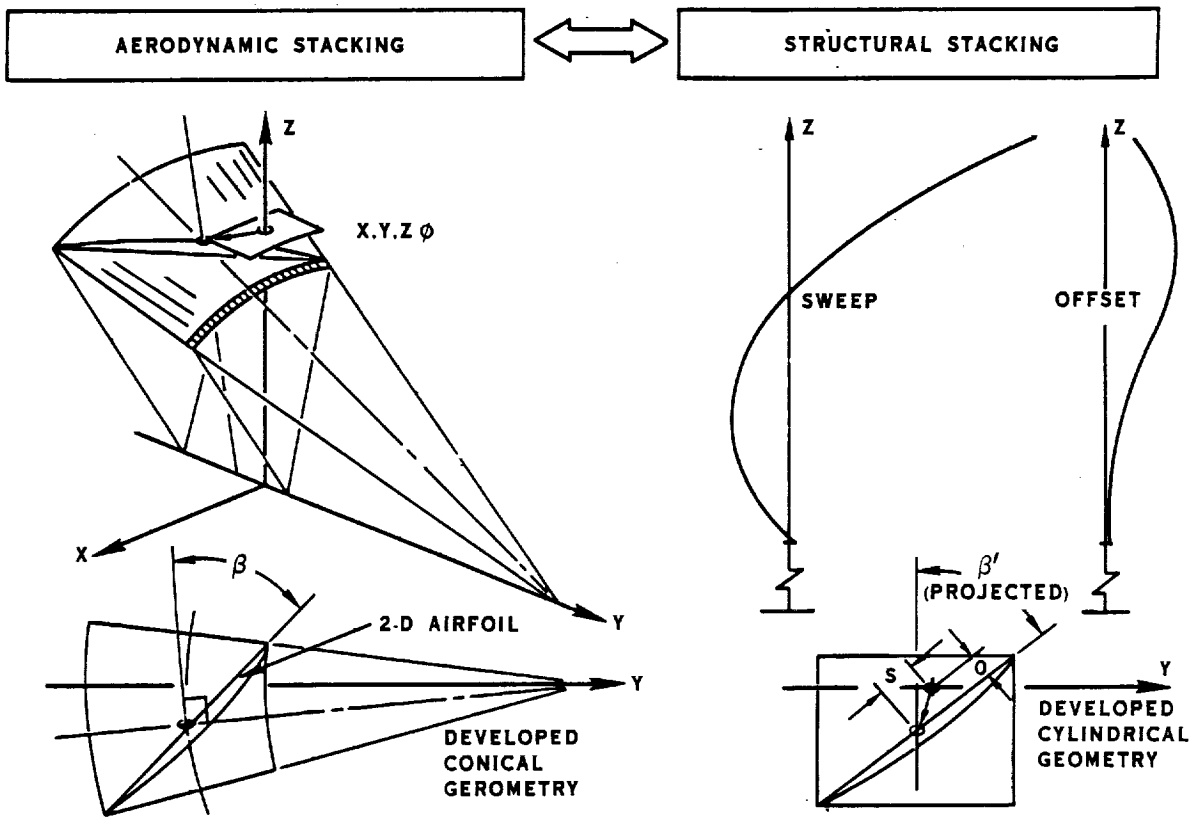

FIGURE 9.28 GEOMETRY CONVERTER

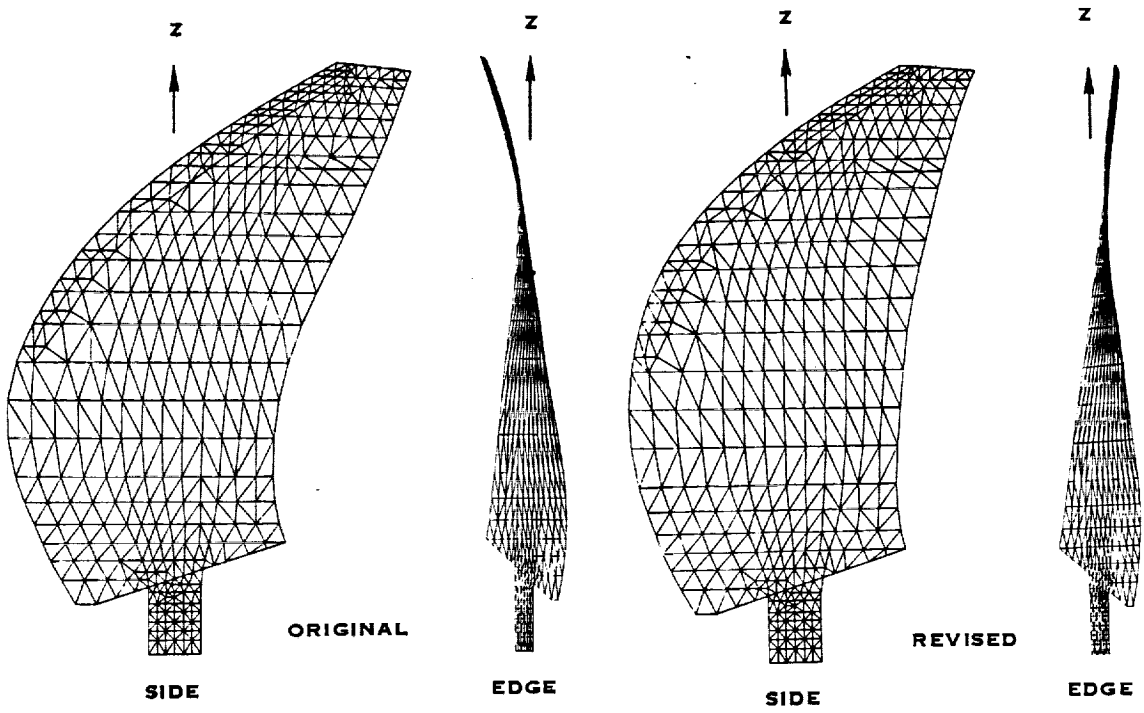

FIGURE 9.29 FINITE ELEMENT GEOMETRY MODIFIER

For expediency, early finite element models, and analyses of those models were conducted with the blade already in the desired aerodynamic position. It was assumed that deflections would be nearly linear and the the blade could be "pre-deflected" an amount equal and opposite to that predicted using the desired aerodynamic position, thereby defining the static position for manufacturing. This assumption was later studied as described below. Finite element differential stiffening terms were utilized for both the steady state and resonant frequency analyses, again, using the model geometry corresponding to the desired aerodynamic position. Many iterations were performed using the stacking geometry converter and finite element model modifier program described earlier.

Criteria evaluated in most iterations for the design included aero/acoustic performance (in terms of fuel burn and Direct Operating Cost (DOC)), steady-state deflection and stress, resonant frequency placement, mode shapes, and aero-elastic stability. Steady state and cyclic stress were also combined to evaluate blade life at the take-off climb condition. Finally, preliminary configurations were established which met the design criteria.

9.4.7 Pre-deflection Study

The objective of this study was to identify a blade design that not only satisfied the design criteria, but also attained the desired aerodynamic shape when deflected under load at the Design Cruise condition. The process of determining the static geometry that deflects to the desired aerodynamic shape has been termed pre-deflecting the blade. The resulting static shape is called the pre-deflected geometry. In the iterative blade design process, the BESTRAN single load step analysis was used as the primary analytical tool. The designs were not pre-deflected, since it was assumed that the blade would behave almost linearly. That is, the analysis results from applying the loads to the blade geometry in the desired aerodynamic position would be nearly the same as the analysis results from applying the loads to the blade in the pre-deflected position. This process was continued until the design satisfied the stress, frequency, and stability criteria before pre-deflecting.

At this point, a pre-deflection analysis was performed on the blade geometry. The pre-deflected static geometry was iterated using the BESTRAN single load step analysis until the operating geometry was sufficiently close to the desired aerodynamic shape. The analysis results of this pre-deflected geometry were then compared to the design criteria. This design was also studied using a BESTRAN piecewise linear analysis. It was anticipated that the results from the single load step analysis and the piecewise linear analysis would be similar.

In practice, the results from the single load step analysis of the initial pre-deflected geometry exhibited significantly higher deflections, higher stresses, and lower stability, as compared to the results before pre-deflecting. At this point, a NASTRAN single load step iterated solution was performed on the blade design, and it confirmed the high deflections.

Iterations were continued on the blade design that existed before pre-deflecting until the deflections were reduced. This design was pre-deflected and analyzed, but its deflections were very similar to the deflections of the previous pre-deflected blade design. Pre-deflecting the blade was then dropped as a design procedure since the beneficial characteristics of the initial geometry were being changed by pre-deflection. Instead, the pre-deflected geometry was modified and analyzed, and these iterations resulted in a blade design that satisfied the design requirements.

9.4.8 Design Iteration Sequence

The iteration process to find an acceptable design turned out to be very lengthy. Nearly sixty configurations were considered; forty of those were fully analyzed. As the iterations progressed, parametric trends were deduced; and these trends were used in the determination of the next configuration to be analyzed. This section will review this iteration sequence and will highlight important designs during that sequence.

The initial SR-7 configuration analyzed structurally (#1) had excellent stability (unstalled flutter), but had unacceptable combined stress in the shell, had poor frequency placement and had high steady-state deflections. Seven iterations were then performed as an attempt to reduce the steady stress. The resulting design (#5C) had a wider spar in the high stress area, and had a greatly different offset distribution. This design had lower steady-state deflections and lower steady-state stress than design #1. However, the design was still overstressed (from combined steady and cyclic stress results), had unacceptable frequency placement, and had extremely low stability. The first mode shape deflection isocontour plot showed increased coupling between the torsional and bending mode of the blade, as compared to design #1. Design #5C also had lower values for fuel burn and DOC, both of which are related to aerodynamic efficiency and noise calculations.

Since the most significant difference between designs #1 and #5C was in the offset distribution, an intermediate offset curve was chosen for the next design to determine why the stability decreased drastically from #1 to #5C. Two iterations yielded design #6A. This design had reduced tip thickness, and an offset curve midway between #1 and #5C. Analysis of #6A showed steady-state deflections that were slightly higher than #5C but still lower than #1. Steady-state stresses were comparable to the stress of #5C. Combined steady and cyclic stressing was not calculated for #6A, but was expected to be similar to those of #5C, since the steady stress was similar. Hence, since #5C was overstressed, the stresses in #6A will probably need to be reduced in order to be acceptable. Design #6A had unacceptable frequency placement, but significantly higher stability, although the stability was still not acceptable. The dramatic increase in stability was due to the change in mode shapes. The increase in edgewise stiffness due to reducing the amount of tip offset reduced the amount of bending and torsional coupling in the first few modes. (These modes are the most influential in stability calculations.) In addition, design #6A showed significant reduction in fuel burn and DOC.

Two techniques were then used to increase the thickness of the blade in the high stress region in order to reduce this stress. In the first, design #6C, the thickness-to-chord (t/b) ratio was increased in the region of high stress. The resulting deflections were slightly lower than design #6A. The steady stress in the spar increased slightly, but the shell steady stress decreased slightly. Most importantly, the combined stress showed a great improvement over design #5C. The shell combined stress was now marginally acceptable, although the spar stress was unacceptable. In addition, the stability was also not acceptable, but the frequency placement was good. The performance was similar to #5C, which was worse than #6A. Hence, increasing the t/b ratio helped the structural design, but hurt the aerodynamic performance.

The second technique increased the chord-to-diameter (b/D) ratio in the area of high steady stress, while maintaining the t/b ratio of #6A. In this design, #7, maintaining the t/b ratio kept the performance similar to #6A. The steady-state deflections and stress was similar to #6A, while the stability showed a slight increase. Based on the results of these two designs, an increase in the overall thickness of the blade should be done by changing the b/D ratio and not by changing the t/b ratio, in order to maintain aerodynamic performance.

Since design #6A had shown an improvement in stability compared to #5C, additional modification of the offset curve was pursued in attempts to raise the stability to an acceptable level. These iterations resulted in design #13.

In this design, the sweep was reduced slightly and the offset was also reduced. This combination of sweep and offset curves produced a static geometry with a "straight leading edge", that is, the leading edge region of the outboard half of the blade was visually aligned nearly in a plane. This should increase the edgewise stiffness of the blade in the same manner that a flat plate has a higher edgewise stiffness than a curved plate.

Analysis results of design #13 showed excellent stability, higher than that of #6A and #1. The change in mode shapes was again responsible for the stability increase. The mode shapes for #13 showed even less coupling in the bending and torsional behavior than in #6A. Frequency placement and steady-state deflections were satisfactory. The performance of #13 was the lowest of all designs studied thus far, primarily due to the decrease in sweep. Combined stress results were similar to #6C with marginally acceptable shell stress and unacceptable spar stress. This design demonstrated that the stability is very sensitive to the amount of bending and torsional coupling in the mode shapes, and that this coupling can be controlled by the blade stacking (i.e., sweep and offset).

To regain some of the performance that was lost in design #13, design #14 had a sweep midway between #13 and #6A, which had very good performance. The offset had less curve than the average of #13 and #6A. Most importantly, the stability was less than both #13 and #6A. Hence the amount of curvature in the offset distribution in the outboard region of the blade also has a significant influence on blade stability.

Blade #14 had performance results that were nearly the same as the initial design #1. The steady-state stresses were the lowest of all the designs studied thus far, apparently due to the reduced sweep. Since designs #13 and #14 showed that stability can be improved by changes in the offset distribution, the objective of the next set of iterations was to reduce the combined stresses to an acceptable level, while maintaining stability.

The result of these iterations was design #18A. This design had the sweep distribution from design #14 and all other characteristics from design #7. The analysis results showed this design had satisfactory combined stress levels and frequency placement. However, the stability and performance values were slightly less than desired, and the steady-state deflections were slightly more than desired.

The offset curve was then modified to produce the straight leading edge effect used in design #13. These iterations produced design #18E. The stability increased to an acceptable value, and the frequency placement remained acceptable. The combined stress levels improved above the satisfactory values from design #18A. Steady-state deflections were slightly higher and performance was slightly lower than desired. However, the values for blade #18E were accepted.

The second phase of the blade design iteration sequence was then initiated: pre-deflecting the blade design. Design #18E was pre-deflected from its desired position, and this new static geometry, #18E(PRE), was analyzed. The results showed that this pre-deflected design had unsatisfactory steady-state deflections and stresses, and unsatisfactory combined stress levels. Stability dropped to slightly below the acceptable level. Only the frequency placement and performance were satisfactory. A NASTRAN single load step iterated solution (ref. Para 9.3.7) was performed on #18E(PRE) and predicted similar steady-state deflections.

After several iterations to reduce sweep and modify chordwidth and thickness in the high stress area, design #20A was reached. In its initial geometry (not pre-deflected geometry), this design satisfied all criteria, except its performance was very poor. The steady-state deflections, at the tip, were one-third less than the deflections of #18E. As a confirmation of the steady-state deflections of #20A predicted by the BESTRAN single load step analysis, three other methods of analysis were also used on #20A. (The results presented in Figure 9.26 are based on these four analyses.) A

BESTRAN piecewise linear analysis was performed to verify the linear behavior of the blade design. Since the results of the single load step analysis and piecewise linear analysis demonstrated excellent agreement, the use of the linear, single load step analysis is justified as an analysis method. A NASTRAN single load step, iterated solution was the second method that was used to check results. The predicted deflections were in excellent agreement with the two BESTRAN analysis results. NASTRAN frequency results showed slight variations in certain modes, due to differences in the element formulation between the two programs, but nonetheless, the results are in very good agreement. A NASTRAN piecewise linear analysis also showed excellent deflection agreement. The stability predictions based on the mode shapes from the first three methods showed excellent correlation.

Because blade #20A satisfied all preliminary design criteria (although it had very low performance), and since the deflections of #20A were significantly less than those of #18E, a pre-deflection analysis was performed on design #20A. Once a pre-deflected blade design is found that satisfies the design criteria, further iterations on the pre-deflected geometry would be performed to increase the performance level, if necessary. The pre-deflected blade #20A(PRE) was expected to have lower stress and deflections than #18E(PRE) because the deflections of #20A were much less than those of #18E. However, analysis results of blade #20A(PRE) showed deflections nearly as high as the deflections of #18E(PRE). The steady-state stresses were similar to #18E, and the combined stress results showed #20A(PRE) to be overstressed.

Since analysis of both pre-deflected blade designs #18E(PRE) and #20A(PRE) yielded results that were drastically different from the analysis results of their initial geometries, some beneficial characteristic of the initial geometries was apparently being eliminated by pre-deflecting. Since the deflection patterns showed that the offset increases toward the tip on designs #18E and #20A, the straight leading edge concept that was developed in design #13 is being eliminated by pre-deflecting the geometry. The straight leading edge concept was shown to be responsible for increasing the edgewise stiffness and uncoupling the bending and torsional behavior of the blade. These effects increased the stability and tended to reduce the steady-state deflections. Therefore, the decision was made to incorporate the straight leading edge concept in the static blade shape and not to pre-deflect the blade geometry to obtain the running shape. The blade performance would be evaluated for the resulting operating geometry of the blade.

For design #21, the sweep was increased over the sweep of design #20A to raise the performance. The results of the analysis showed satisfactory combined stress levels, frequency placement and stability. The performance was slightly less than desired, but was acceptable. Blade design #21 was thus accepted as the final blade iteration in this study.

9.4.9 SR-7-21 Blade Geometry

The modifications that were made to the SR-7 initial geometry in order to achieve a satisfactory design are illustrated in Figures 9.29 and 9.30. Figure 9.30 shows the reduction in tip sweep, the change in offset distribution, and the increase in thickness that were required. The SR-7-21 planform is compared to the SR-7 initial design planform in Figure 9.31.

The SR-7-21 fabrication is illustrated in Figure 9.32. The spar is solid forged aluminum. Woven fiberglass cloth with epoxy resin will be used for the shell. The sheath will be made of nickel. The entire SR-7-21 fabrication uses current state-of-the-art technology, and does not require any technology development.

The aerodynamic characteristics are shown in Figures 9.33. Figure 9.34 gives the sweep line coordinates and sweep angle.

The aerodynamic performance of the SR-7-21 design is compared to the baseline design in Table 9.19. The baseline values have changes from those in Table 9.14 due to a change in calculation procedure.

TABLE 9.19. SR-7-21 AERODYNAMIC PERFORMANCE

	Baseline*	Initial Configuration	SR-7-21
Tip Sweep, Deg.	39.6	36	34.9
Efficiency	0.796	0.791	0.791
Noise (BPF)	141.2	144.5	143.3
(Fuel Burned)	0.0	+ 1.16	+ 1.55
(Direct Operating Cost)	0.0	+ 0.69	+ 0.96

* Baseline values reflect changes in calculation procedure, as compared to values in Table 9.14.

9.4.10 SR-7-21 Analysis Results

Deflection contour for the steady-state cruise, steady-state take-off, and 1-P cyclic take-off operating conditions are plotted in Figure 9.35. The deflections are resolved normal to the chord of the 3/4 radial station. Figure 9.36 shows contour plots of the local rotations for the same three operating conditions. The local rotations are the rotations about an axis parallel to the pitch change axis, at each finite element node point.

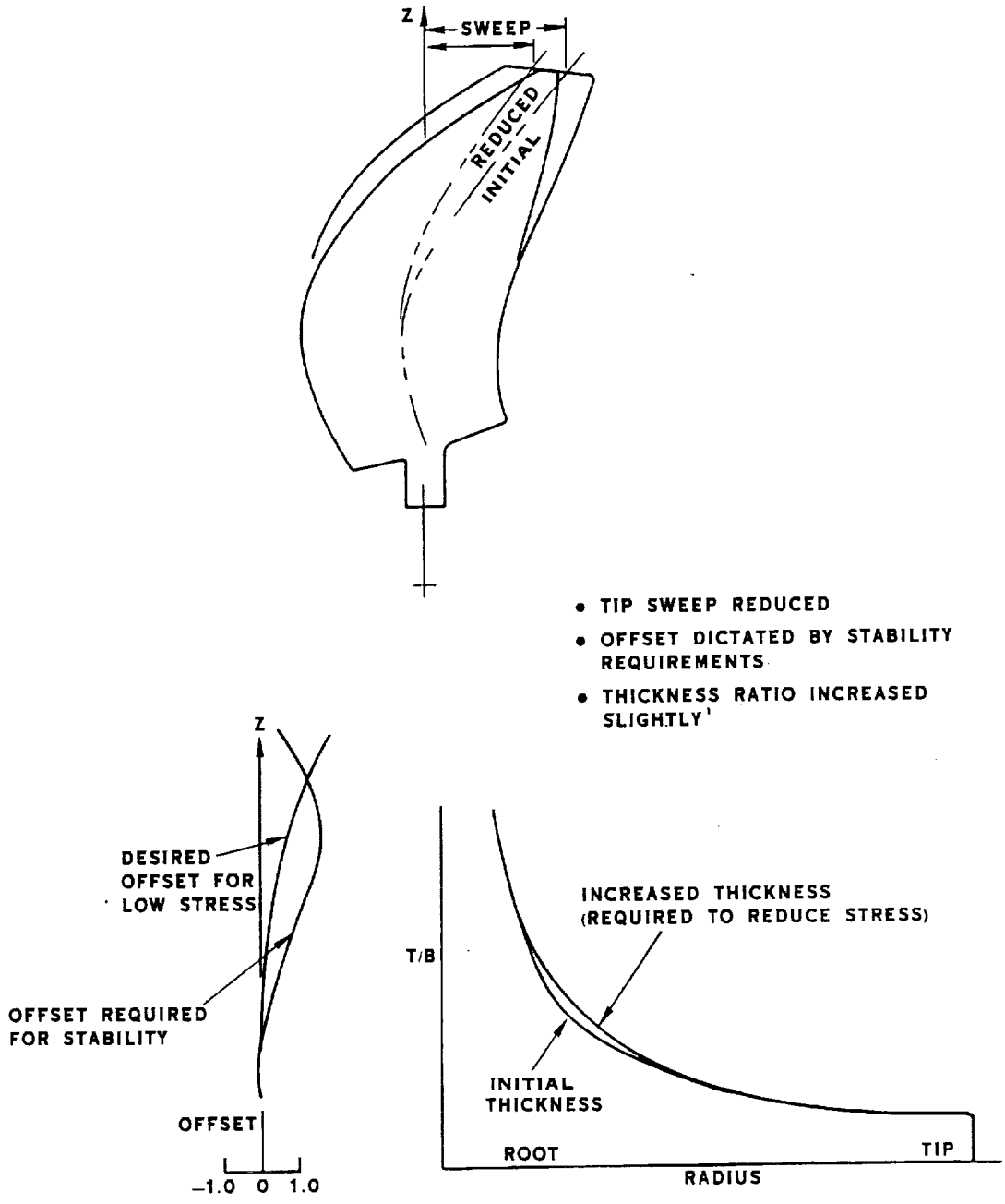

FIGURE 9.30 DESIGN MODIFICATIONS NECESSARY TO ACHIEVE SATISFACTORY DESIGN

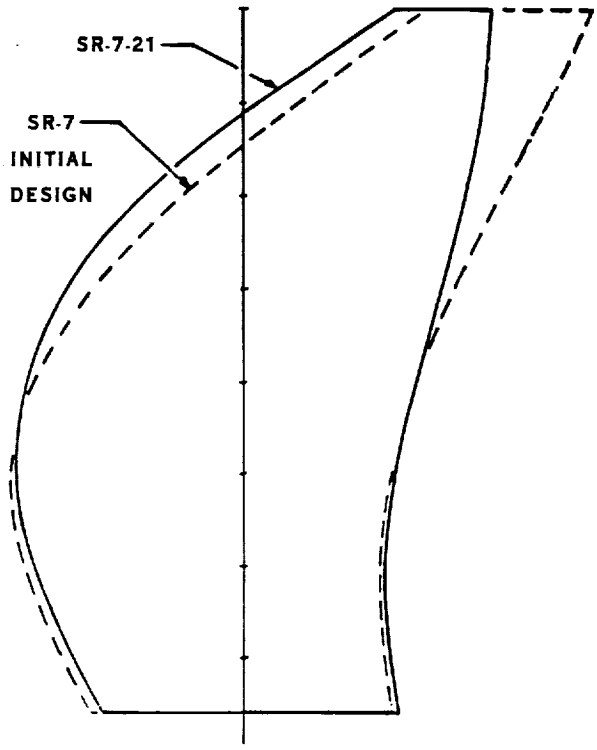

FIGURE 9.31 PLANFORM MODIFICATION TO ACHIEVE SUCCESSFUL DESIGN

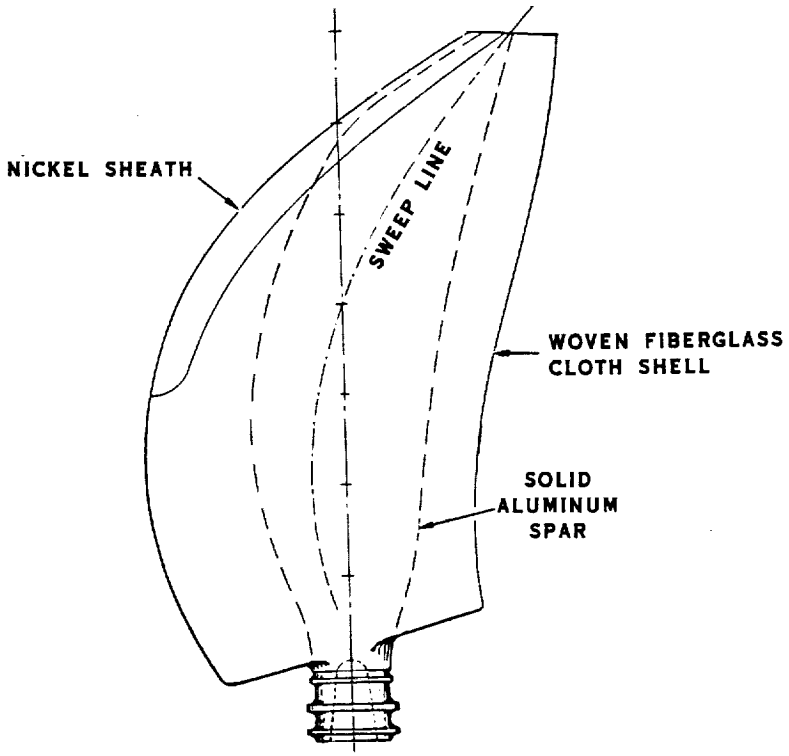

FIGURE 9.32 SR-7-21 MATERIALS

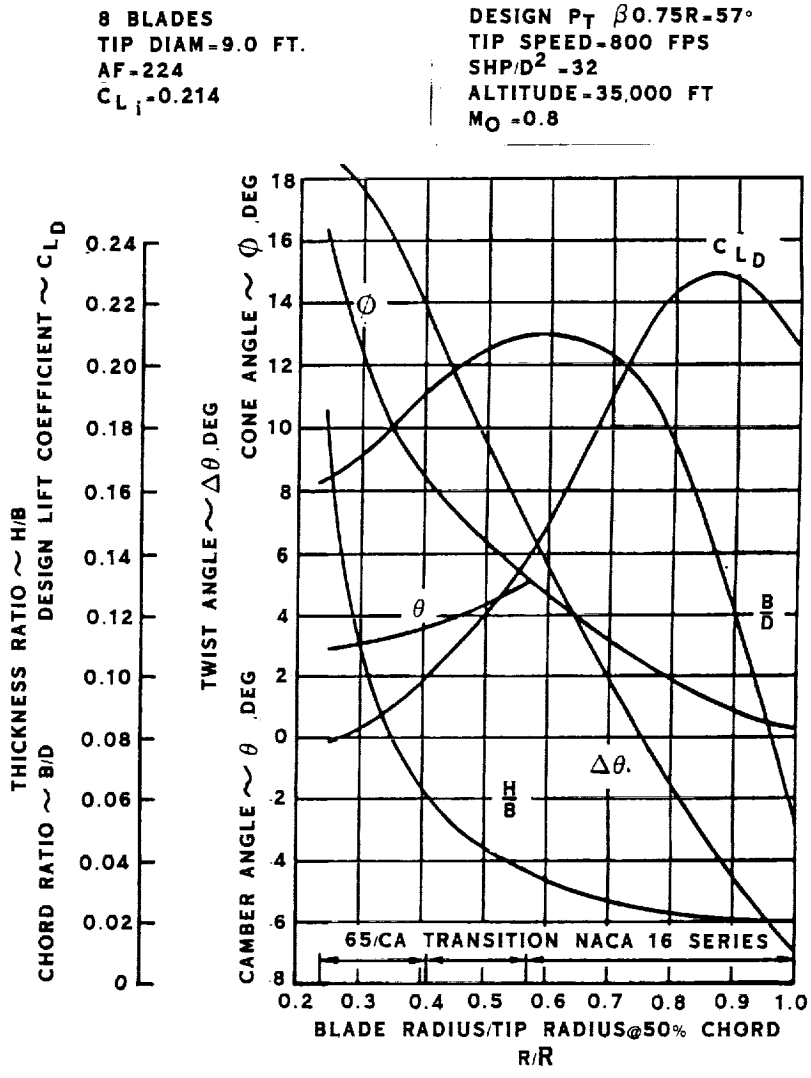

FIGURE 9.33 SR-7-21 AERODYNAMIC DESCRIPTION

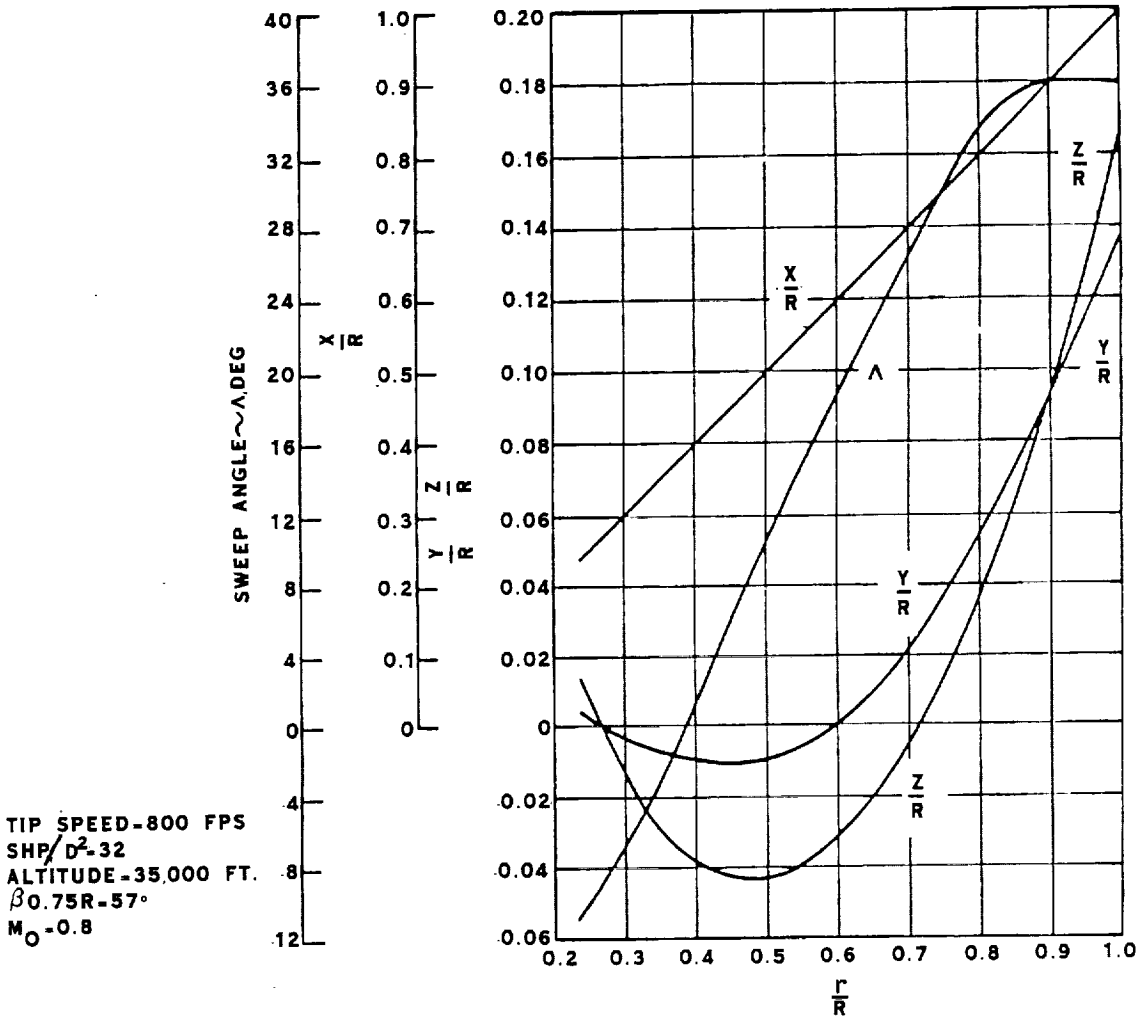

FIGURE 9.34 SR-7-21 SWEEP LINE COORDINATES

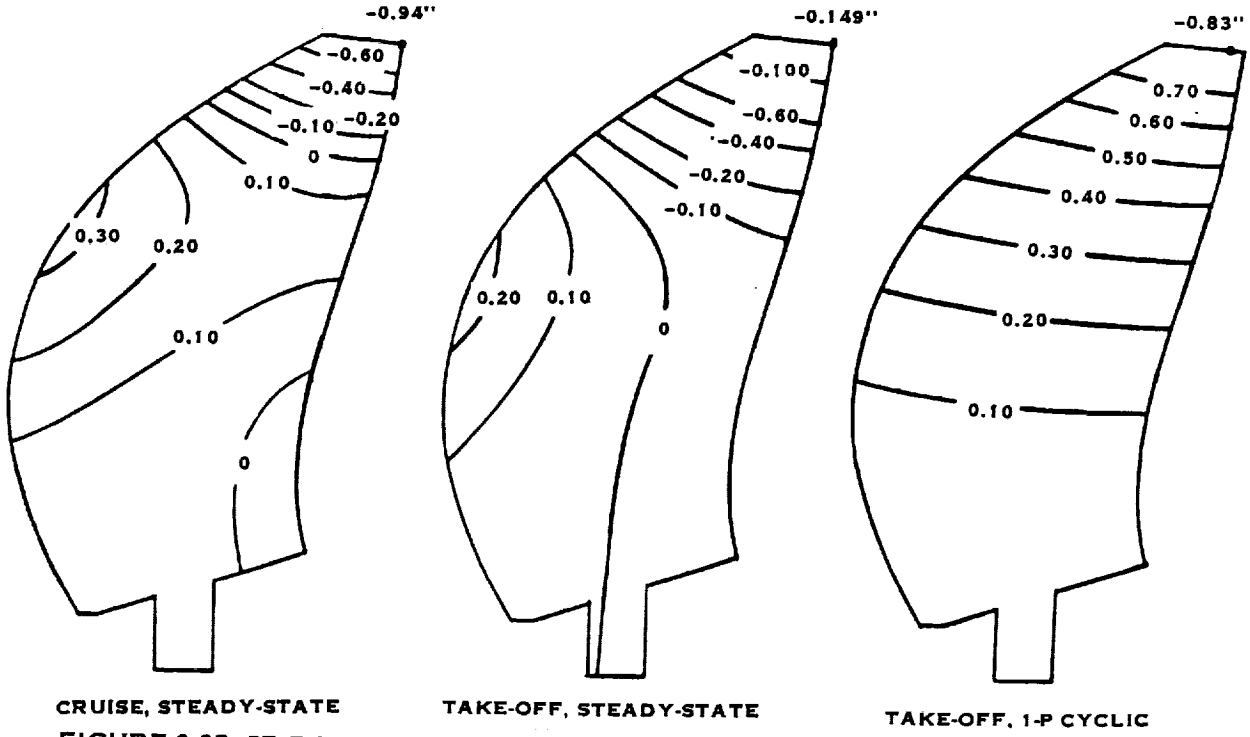

CRUISE, STEADY-STATE TAKE-OFF, STEADY-STATE TAKE-OFF, 1-P CYCLIC

FIGURE 9.35 SR-7-21 DEFLECTIONS MEASURED NORMAL TO 3/4 STATION CHORD (INCHES, POSITIVE TOWARD FACE)

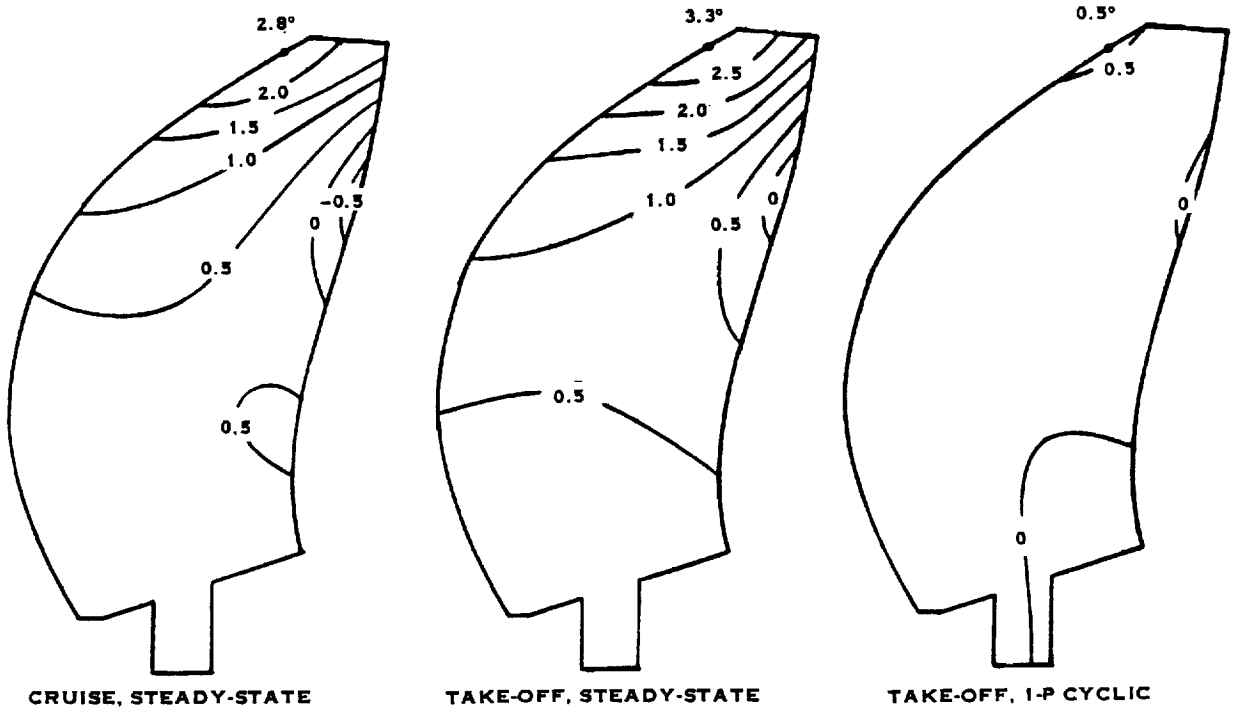

FIGURE 9.36 SR-7-21 ROTATIONS - LOCAL ROTATIONS ABOUT PITCH CHANGE AXIS (DEGREES, POSITIVE TOWARD DECREASING BLADE ANGLE)

The steady-state and cyclic operating condition stresses were combined and plotted on Goodman diagrams. The cyclic stress was multiplied by the correction factor as discussed in Section 9.3.5 and plotted in Figure 9.25. The resulting combined stress was then compared to the material allowable stress limit for the specific blade component. Figures 9.37 and 9.38 show the high cycle fatigue, 25% overspeed, and 40% overspeed spanwise stress data points for the spar and shell, respectively.

The high cycle fatigue stress state that is plotted is the point that has the highest percent of material allowable stress limit in that blade component. The material allowable stress is the allowable cyclic stress at the specific steady stress for a given data point. The ratio, expressed as a percent, of the actual cyclic stress to the allowable cyclic stress is the percent of allowable limit for that stress state. This percent is calculated for each element in the finite element model, and the data point with the maximum percent of allowable limit is determined and plotted on the goodman diagram. Contour plots of the percent of allowable limit for the face and camber sides of the spar and shell are shown in Figures 9.39 and 9.40, respectively.

For the 25% overspeed and 40% overspeed conditions, only the steady-state stress was considered since the steady loads dominate the cyclic loads. The maximum steady-state stress point was determined and multipled by 1.5 and 2.0 to account for the increased rotational speeds of the 25% overspeed and 40% overspeed conditions, respectively.

The results in Figures 9.37 thru 9.40 show that the SR-7-21 blade design satisfied the high cycle fatigue, 25% overspeed and 40% overspeed stress requirements.

The maximum low cycle fatigue stress point for the spar and shell for the SR-7-21 design are plotted on Goodman diagrams in Figures 9.41 and 9.42, respectively. This stress point represents the highest stress variation due to start/stop cycling, from no stress to peak stress. The spar meets the low cycle fatigue design criteria, but the shell is overstressed.

The first five resonant frequencies of the SR-7-21 blade are plotted as a function of propeller speed in Figure 9.43. As described in Paragraph 9.3.4, the resonance avoidance zones are also shown. The mode shapes for the first five modes at cruise operating speed are illustrated in Figure 9.44.

During the iteration sequence, a classical flutter Mach number of 0.9 was used to screen blade designs. This analysis was based on an isolated blade at sea level. For the SR-7-21, the classical flutter Mach number is 0.92, and is illustrated in Figure 9.45. The stability boundary for this design was then calculated for altitudes from sea level up to 10,668 m. (35,000 ft) for three conditions: (1) cascade with a gap/chord ratio cut-off of 2.0 at 100% frequency, (2) cascade with a gap/chord ratio of 2.0 at 85% frequency (15% degradation), and (3) full cascade from root to tip at 100% frequency.

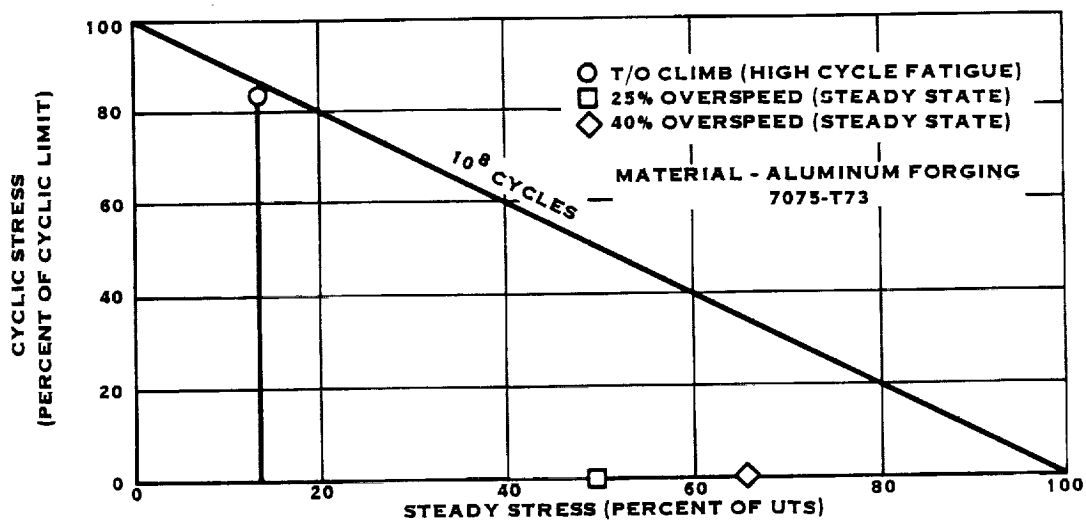

FIGURE 9.37 SR-7-21 SPAR - MAXIMUM SPANWISE STRESS RESULTS

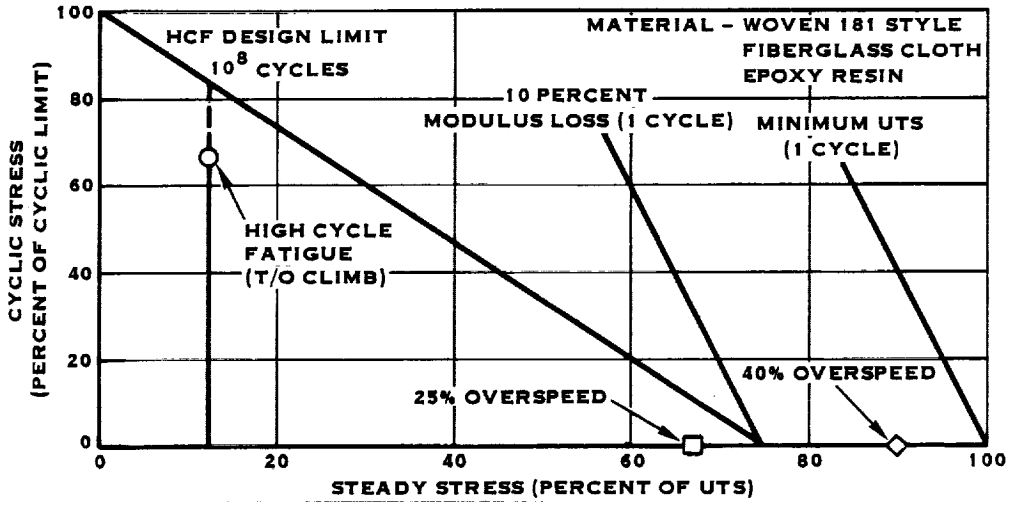

FIGURE 9.38 SR-7-21 SHELL - MAXIMUM SPANWISE STRESS RESULTS

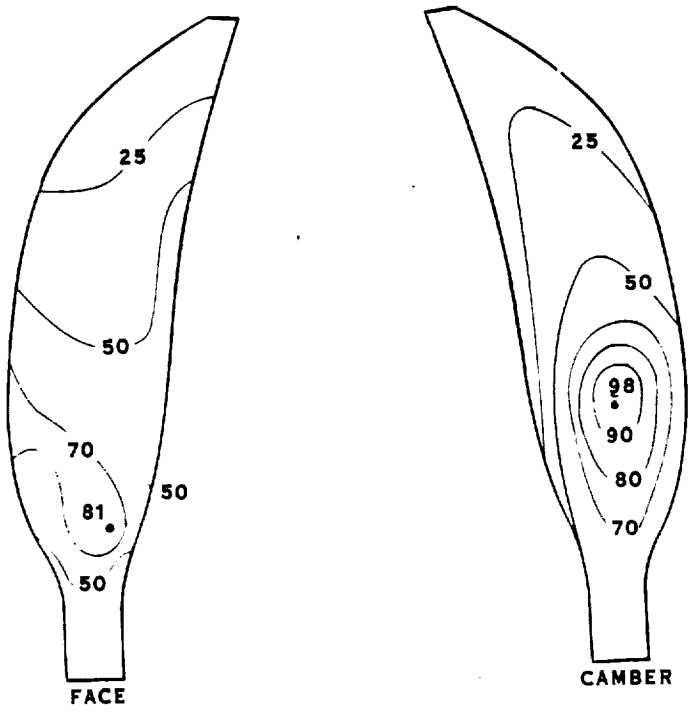

PERCENT OF ALLOWABLE
STRESS LIMIT-HIGH CYCLE FATIQUE

FIGURE 9.39 SR-7-21 SPAR STRESS

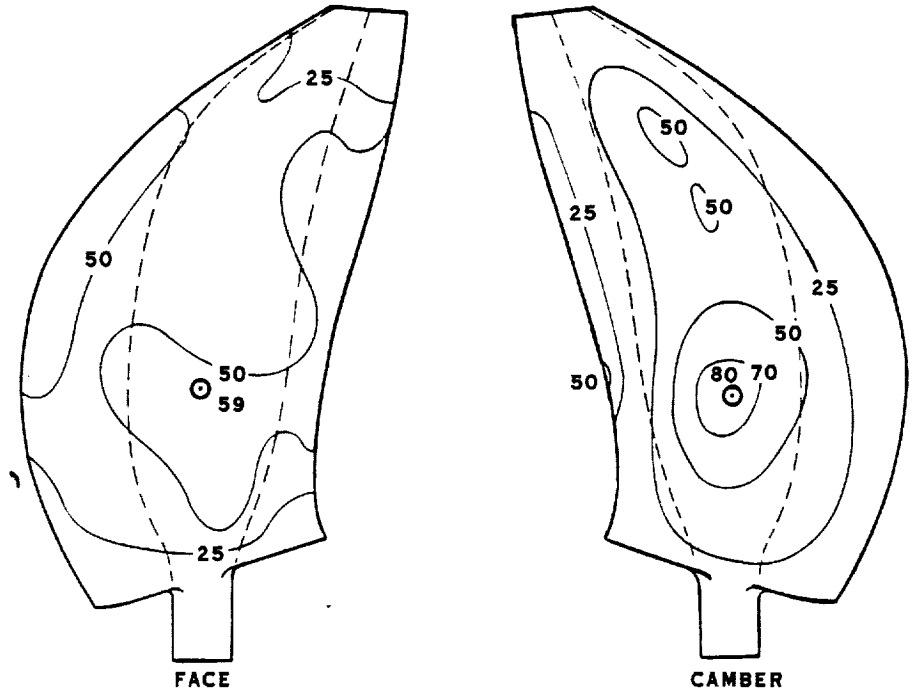

PERCENT OF ALLOWABLE

STRESS LIMIT - HIGH CYCLE FATIQUE

FIGURE 9.40 SR-7-21 SHELL STRESS, PERCENT OF ALLOWABLE STRESS-LIMIT-HIGH CYCLE FATIGUE. TAKE-OFF CLIMB CONDITION (INCLUDING 1-P STRESS FACTORS)

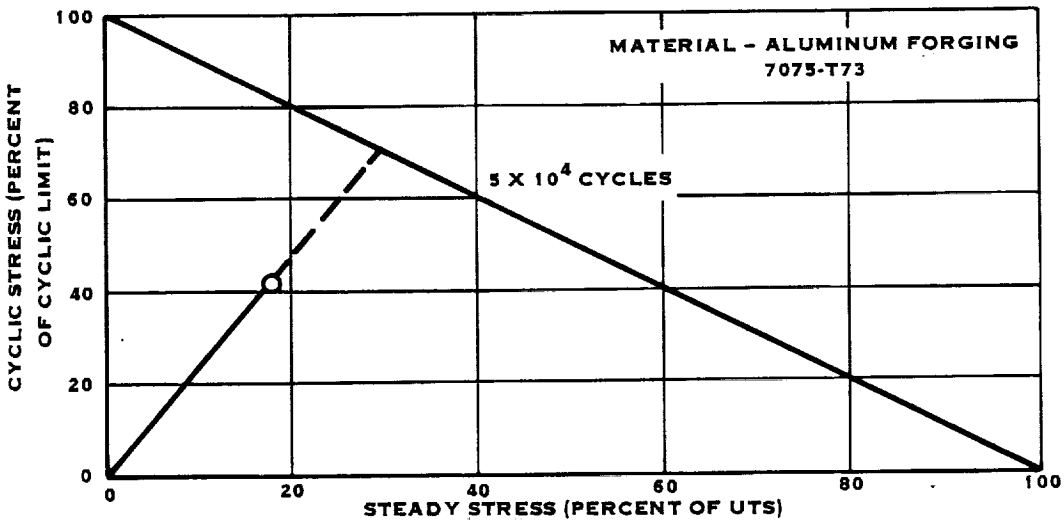

FIGURE 9.41 SR-7-21 SPAR - SPANWISE STRESS - LOW CYCLE FATIGUE

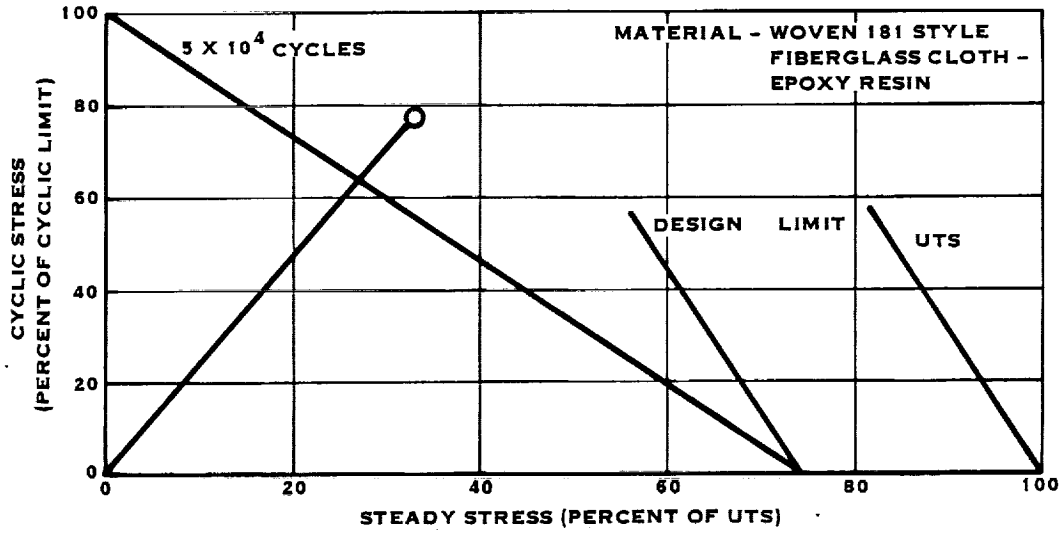

FIGURE 9.42 SR-7-21 SHELL SPANWISE STRESS - LOW CYCLE FATIGUE

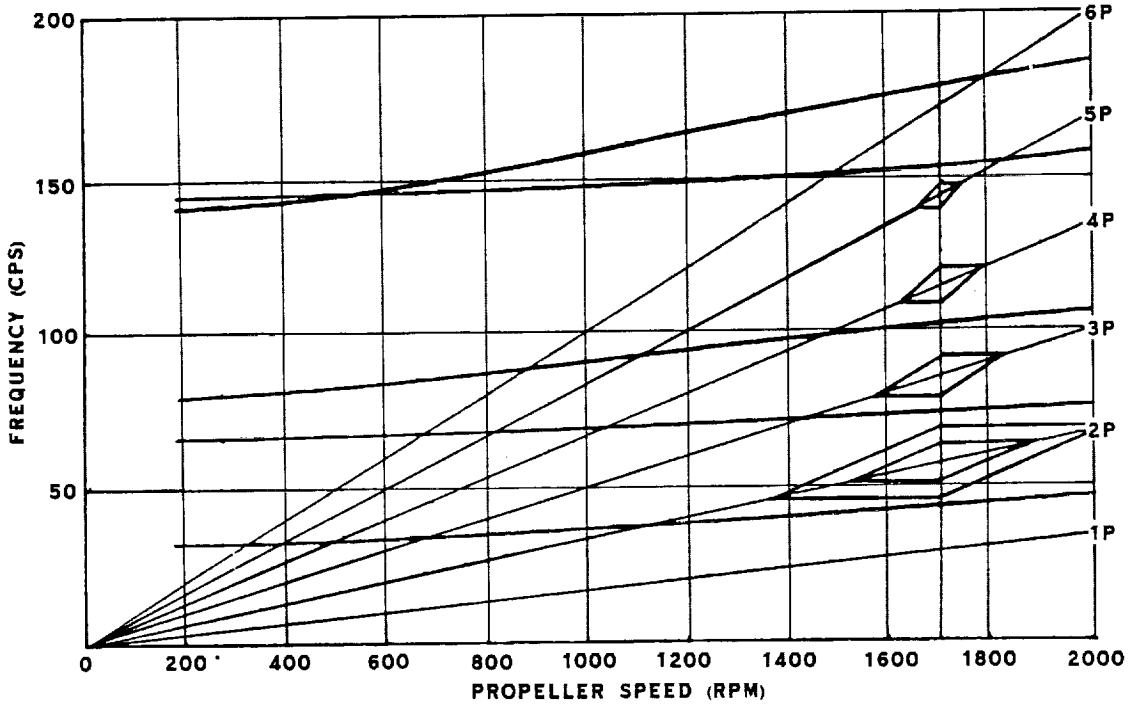

FIGURE 9.43 SR-7-21 CRITICAL SPEED DIAGRAM

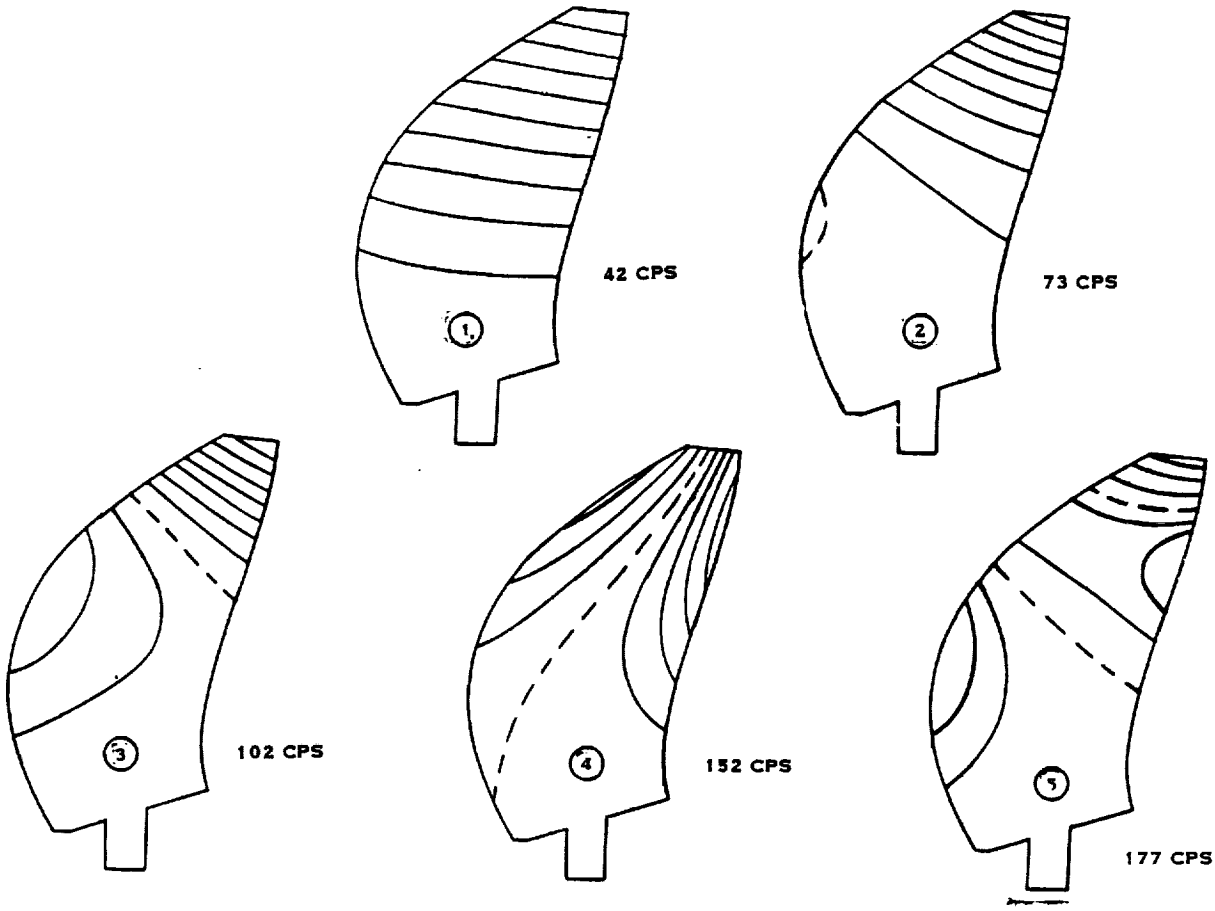

FIGURE 9.44 SR-7-21 MODE SHAPES (CRUISE CONDITION)

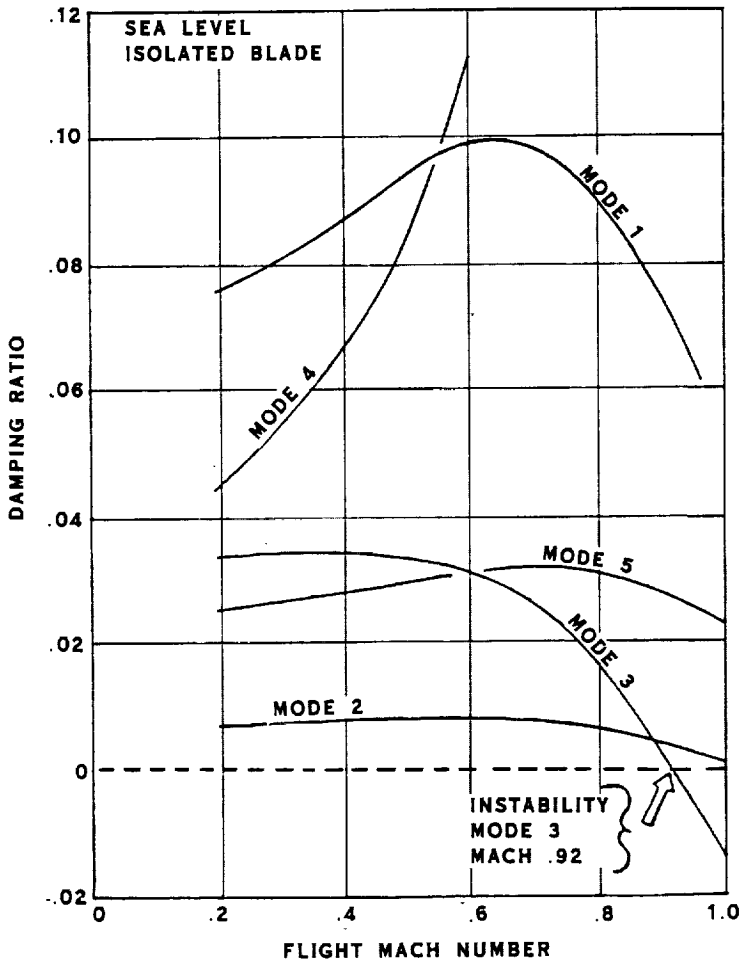

FIGURE 9.45 SR-7-21 BLADE DAMPING

The stability boundaries predicted by these three methods are plotted versus the SR-7-21 flight profile and the Modane tunnel test condition in Figure 9.46. During the iteration sequence, conditions 2 and 3 were relaxed from design requirements to design goals. Failure to satisfy a design goal would not make the design unsatisfactory. However, the stability analysis results indicate the SR-7-21 design will meet conditions 1 and 2. Hence the SR-7-21 blade design does satisfy the stability requirements.

A foreign object impact analysis was not performed on the SR-7-21. As reported in the large-scale, high speed advanced propeller blade feasibility study (Section 5.0, Volume I), an SR-3 (8) style spar and shell blade design satisfied all foreign object impact criteria. Since the SR-7-21 (and all the designs in the iteration sequence) is similar to the SR-3 (8) large-scale design, the SR-7-21 design is expected to have a sufficient foreign object impact capacity.

9.4.11 Results

The blade design iteration sequence yielded a great deal of parametric information about the designing of full-size, high speed advanced propeller blades. The following parametric effects were observed:

a. Sweep

- Causes complex bending/torsional coupling of vibratory modes.
- Increase causes increased aerodynamic performance.
- Increase causes decreased classical flutter limit.
- Increase causes increase in steady-state stress.

b. Offset

- Increase in curvature of offset distribution causes increased steady-state stress.
- Straightening leading edge decreases bending/torsional coupling of vibratory modes.
- Straightening leading edge increases classical flutter limit.

c. Thickness-to-chord Ratio

- Increase will generally cause decreased local stress and decreased aerodynamic performance.
- Modifications will change the blade frequency placement.

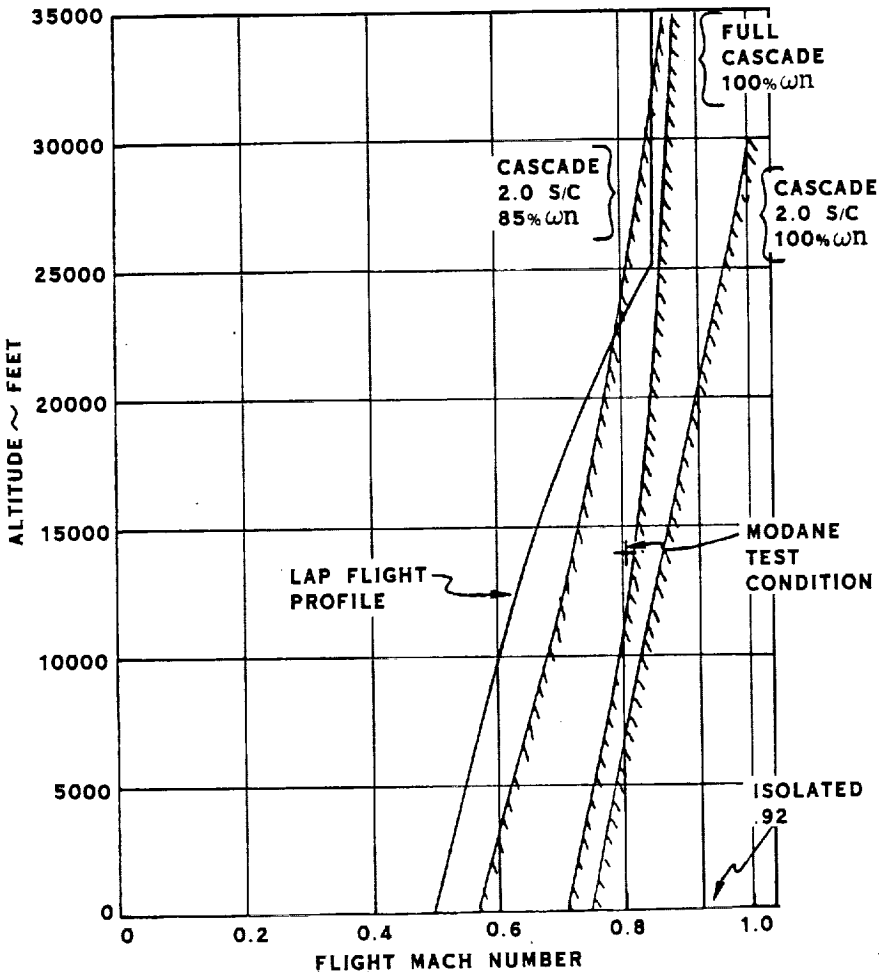

FIGURE 9.46 SR-7-21 STABILITY BOUNDARY

d. Chord Width

- Increase causes increase in actual thickness with minimum performance loss.

e. Advanced Composites in Shell

- Can decrease deflections and spar stress.
- Can improve stability.
- Requires advances in materials and manufacturing technology.

The SR-7-21 blade design satisfies the necessary design requirements to be acceptable as the preliminary blade design. For the detailed blade design, the twist and camber distributions should be optimized for aero-acoustic performance. A foreign object impact analysis should be performed on the detailed blade design to verify that the impact capacity is sufficient.

9.5 FULL SIZE BLADE STRUCTURAL ANALYSIS

9.5.1 Introduction

A program to structurally evaluate a full size blade with (14 foot diameter) the external configuration of the SR-7 blade was conductedt to determine how similar the 9 foot diameter testbed size blade design is to a full-size design.

In accordance with the contract requirements, a blade fabrication concept was submitted to the NASA Project Manager for approval prior to conducting the evaluation. A hollow steel spar, composite shell concept was suggested for two reasons. First, a lower weight Prop-Fan system would result from the lower blade weight, retention and pitch change loads; and second, the technology for manufacture of a hollow steel spar was judged near term.

As the study progressed, the hollow steep spar blade did not appear to offer a weight savings over a solid aluminum spar of this size, and some deficiences were indicated by the analysis of the first model. The hollow steel spar blade was locally overstressed in two regions and the unstalled flutter margin was low. In view of these developments, the solid aluminum spar, composite shell construction concept was adopted, and a structural evaluation conducted on this concept.

Presented in this section are the preparation, methods, and results of the structural evaluation of a 14.0 foot (4.27 meter) diameter SR-7 blade. Combined stress, frequency placement, stability, stress margins and deflections, calculated by a finite element analysis for two load conditions, Cruise and Climb, were used to evaluate the acceptability of the design concept.

9.5.2 Blade Concept Model Description

The aerodynamic geometry for the full size Prop-Fan blade was generated by scaling the existing 9.0 foot (2.74 meter) blade data to 14.0 feet (4.27 meters). Using this scaled data, finite element models for the two construction concepts were generated. Both concepts were similar except for the spar. Concept #1 had a hollow steel spar, while concept #2 had a solid aluminum spar.

Concept #1	Concept #2
Hollow steel spar	Solid aluminum spar
Fiberglass shell	Fiberglass shell
Titanium leading edge sheath	Nickel leading edge sheath
Honeycomb filler	Foam filler
8.0" (20.32 cm) pitch diameter, 2-row, ball bearing retention	9.40" (23.88 cm) pitch diameter, 1-row, ball bearing retention
Adhesive bond	Adhesive bond

The spar geometry for concept #1 was established by keeping the same percentage of airfoil chord and location within the airfoil as the 9.0 foot (2.74 meter) blade until the wall thickness to internal radius ratio became less than unity. The spar was then shifted toward the trailing edge of the blade to keep this ratio at unity or above and faired back into the inboard spar geometry. An illustration of the spar reposition and the comparison to the solid and hollow spar geometry concepts are shown in Figures 9.47 and 9.48.

A node pattern generated for the spar, shell, sheath, and filler components defining the quadrilateral, QUAD4, and triangular, TRIA3 elements in the MSC Version 61b, NASTRAN bulk data deck is shown on Figures 9.49 and 9.50.

The QUAD4 elements were chosen because they are generally used by the industry to model hollow cylinders and give good results. The TRIA3 elements were used to transition between regions having an unequal number of quadrilateral elements. Both elements have variable node thickness inputs and six degrees of freedom at each node. Rigid link, RBE2's were used to connect the spar, shell and filler nodes.

Concept #2 utilized the node pattern and element connectivity shown on Figure 9.51 previously established for the 9.0 foot (2.74 meter) model and is a 14/9 scale version of that model set up for an in-house finite element code, BESTRAN.

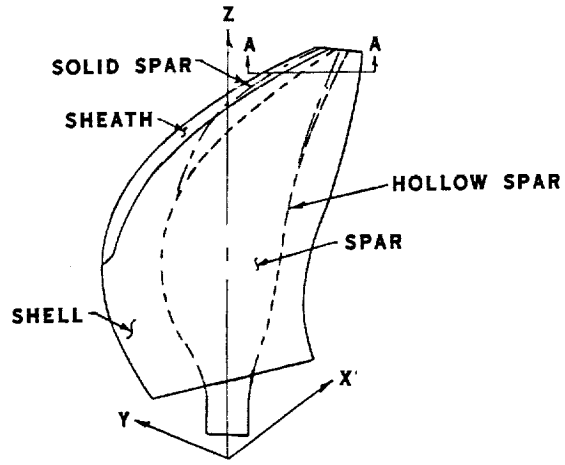

FIGURE 9.47 FULL SCALE PROP-FAN SPAR & SHELL CONCEPTS #1 & #2

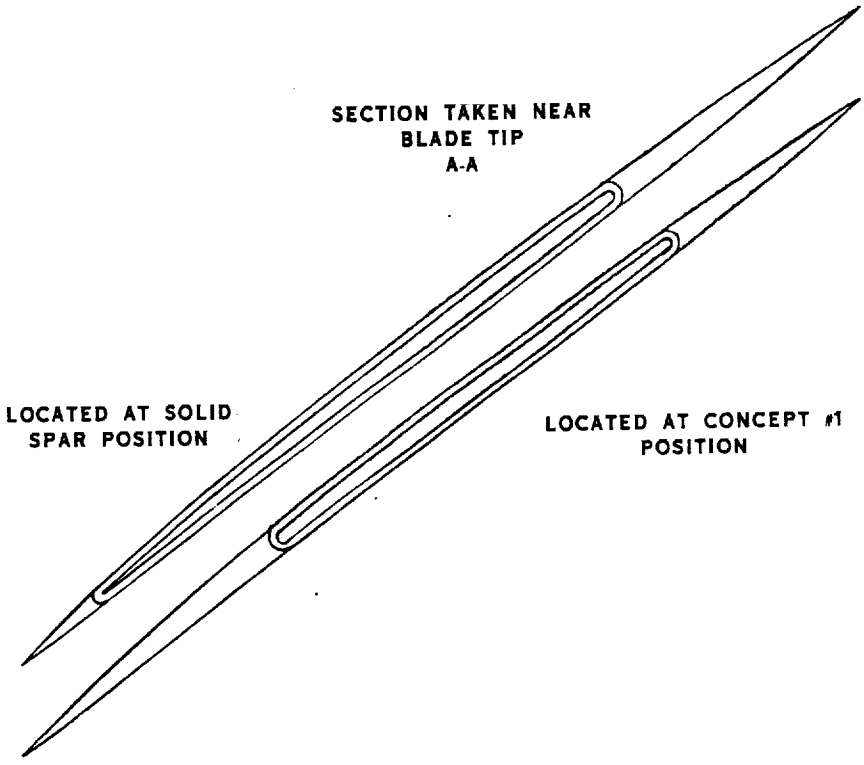

FIGURE 9.48 HOLLOW STEEL CROSS SECTION

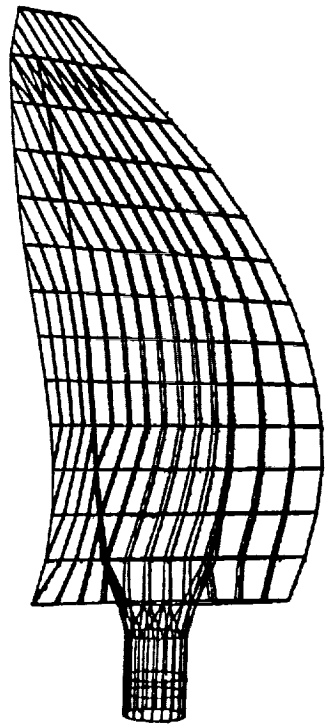

FIGURE 9.49 FINITE ELEMENT MODEL - CONCEPT #1

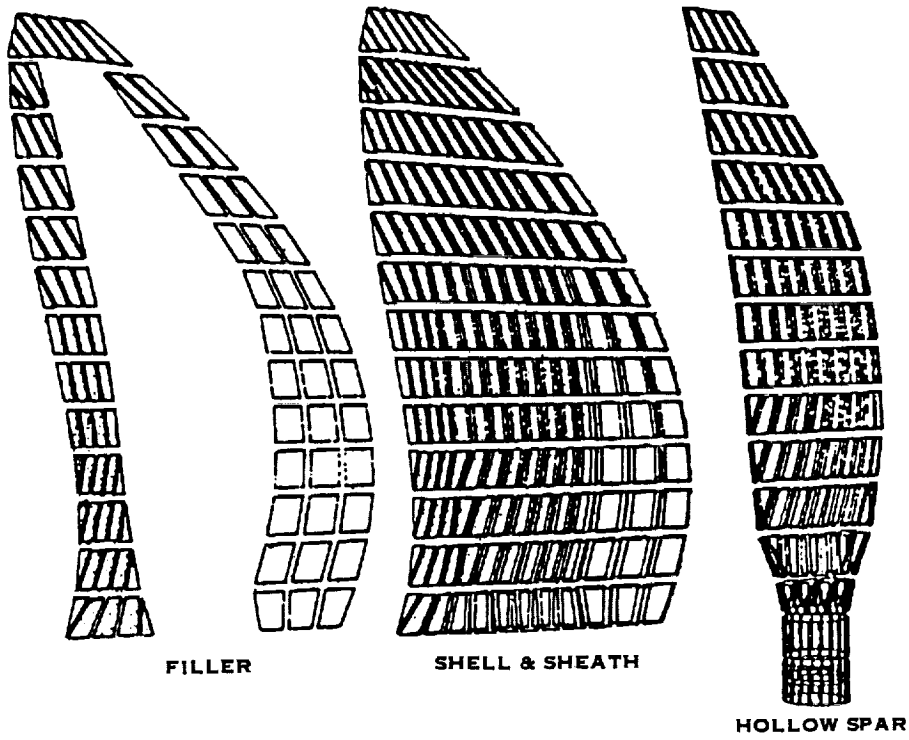

FIGURE 9.50 FINITE ELEMENT MODEL - CONCEPT #1

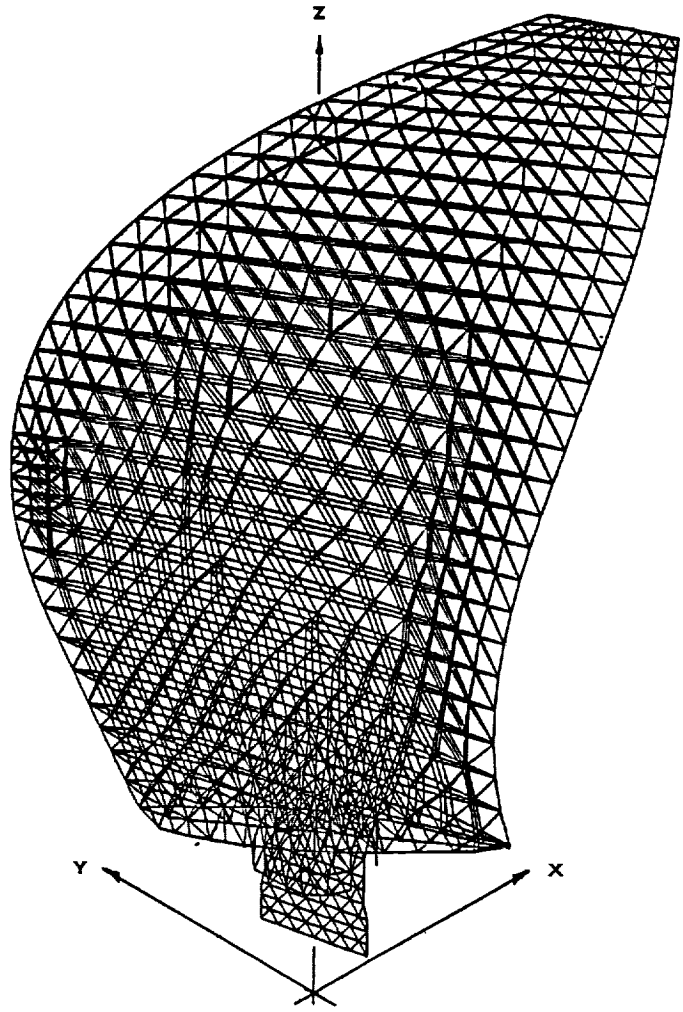

FIGURE 9.51 FINITE ELEMENT MODEL - CONCEPT #2

9.5.3 Retention Model Description

The 2-row blade root retention for concept #1 was modeled as an infinitely rigid attachment. Since the stiffness of this retention configuration had not yet been analyzed, the nodes in this region were constrained to zero motion for the first series of calculations.

The retention model for concept #2, illustrated in Figure 9.52, was modeled by springs scaled up from the 9.0 foot (2.74 meter) model. The moment spring rates are simulated force couple springs attached at the pitch diameter node locations, and axial and torsional spring rates are attached to a central node location.

9.5.4 Analysis

The structural evaluation for the 14.0 foot (4.27 meter) SR-7 blade was conducted in accordance with the requirements set forth in the design requirements document (reference Appendix D) for stress, natural frequency, and stability for the Cruise and Climb conditions imposed on the 9.0 foot (2.74 meter) blade design (reference Table 9.20). Finite element models of the blades (reference Figures 9.49 thru 9.51) were generated for both concepts #1 and #2 using scaled data from the 9.0 foot (2.74 meter) design. Concept #1 was modeled using the variable thickness node, isoparametric plate elements QUAD4 and TRIA3, keeping element aspect ratios of 10 or less wherever possible, for MSC NASTRAN Version 61b. Concept #2 was modeled using triangular plate elements, Type 1 and Type 5, for the in-house finite element code, BESTRAN, by scaling the global coordinates of the SR-7 analytical model by 14/9. Although two different finite element codes were used for the evaluation, the basic solution sequence, shown on Figure 9.53 for the NASTRAN approach, was similar. A two-step method to include the differential stiffening effects of the centrifugal and air loads on the elements was employed by both sequences. The one difference that occurred between the two sequences was that concept #2 was placed in its deflected position after step 1, and concept #1 geometry remained the same. This was because concept #2 had been generated from the pre-deflected geometry of the SR-7 blade and concept #1 had never been iterated on to establish a pre-deflected geometry.

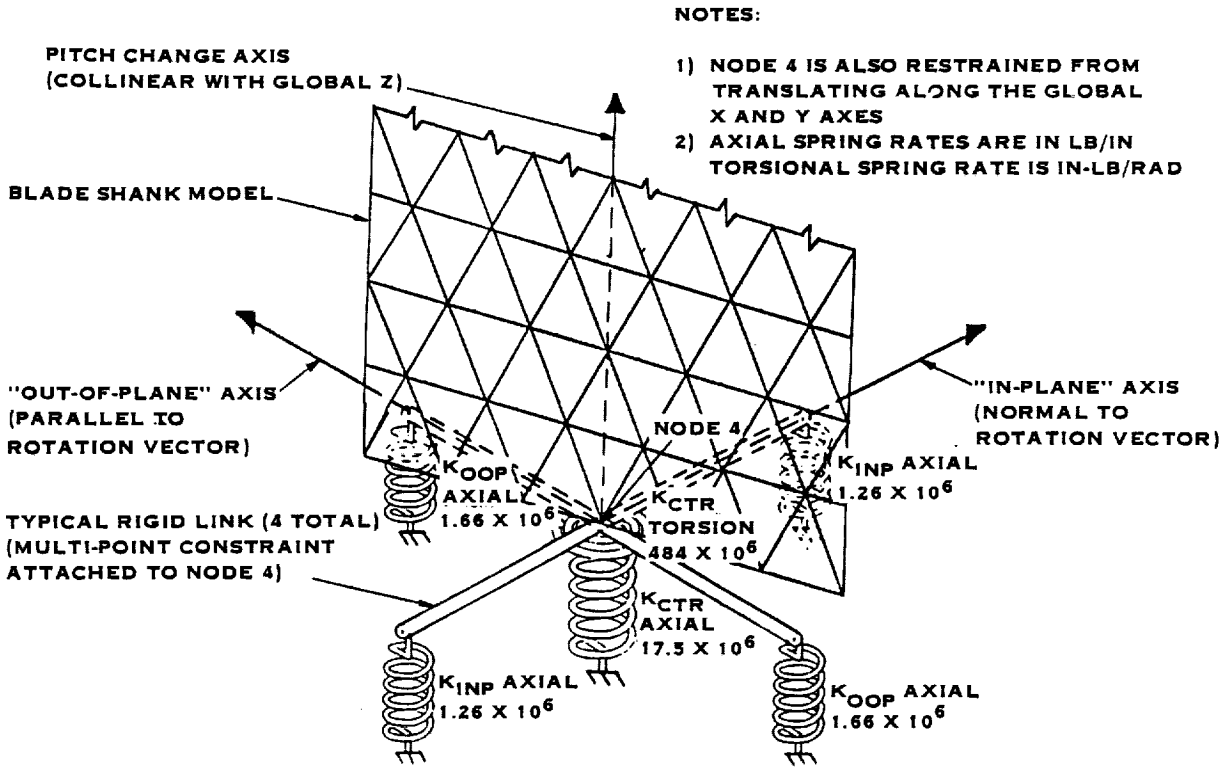

FIGURE 9.52 CONCEPT #2 RETENTION SIMULATION

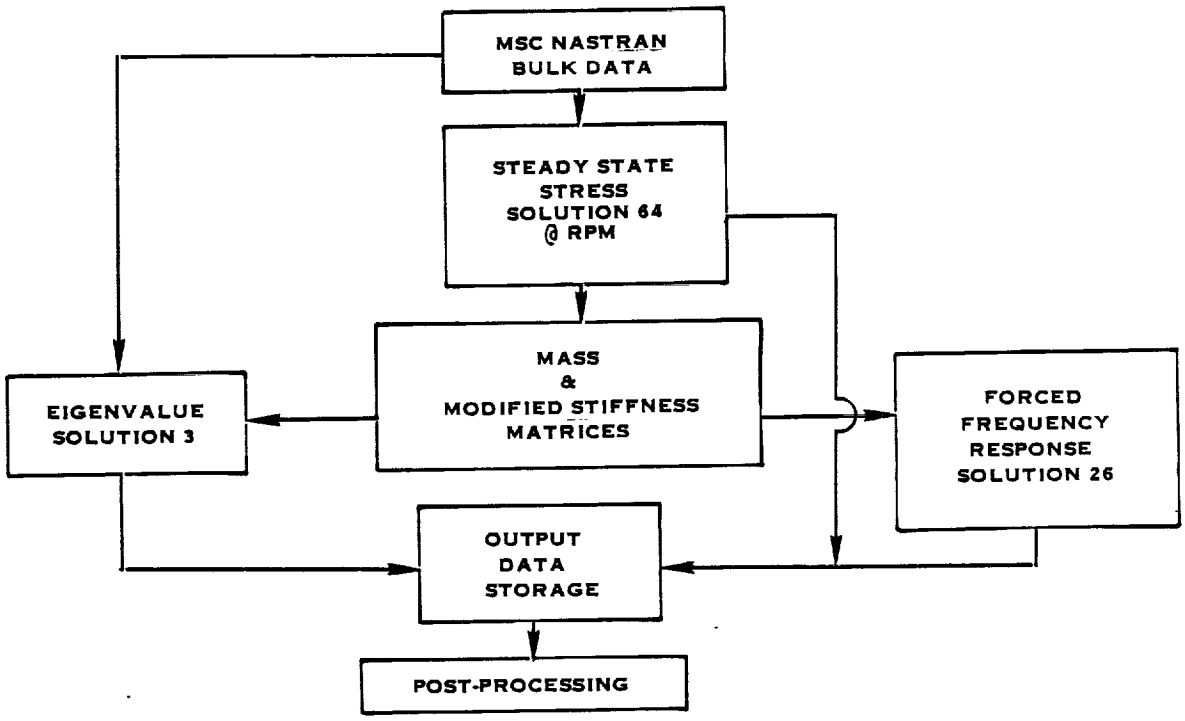

FIGURE 9.53 ANALYTICAL FLOWPATH

TABLE 9.20. BLADE LOAD CONDITIONS

		Design Cruise	Takeoff/ Climb
Shaft Power	Hp/ft^2 (Kw/m)	32.0 (257.0)	74.1 (595.0)
Flight Velocity	Mach #	0.80	0.20
Altitude	ft (m)	35,000 (10,675)	sea level
Tip Speed	ft/sec (m/sec)	800 (244)	800 (244)
RPM		1091	1091
Excitation Factor		4.5	4.5
Blade Angle	deg	57.57	38.26
Power	Hp (Kw)	6272 (4677)	14,520 (10,828)
thrust	lbf (N)	3463 (15409)	18560 (82560)

The air loads for these conditions are simulated by in-plane and out-of-plane, chordwise and spanwise distributed force components applied at the nodes of a model surface.

9.5.4.1 Natural Frequency - The natural frequency margin requirements established for the 9.0 foot (2.74 meter) aero-acoustic blade design at the tip speed of 800 ft/sec (244 m/sec), 1091 RPM are:

Excitation Order	Frequency Hz	Margin percent	Margin Band Hz	Margin Band RPM
2P	36.4	15.0%	5.5	164
3P	54.6	10.0%	5.5	109
4P	72.7	7.5%	5.5	82
5P	90.0	6.0%	5.5	65
6P	109.0	5.0%	5.5	55

The natural frequency characteristics for both blade concepts were calculated at the two load condition and blade angle positions for Climb and Cruise, statically, and at speed. The eigenvalue results for the first four modes listed in Table 9.21 were used to construct Campbell diagrams shown on Figures 9.54 thru 9.56 for margin requirement checking.

Normal mode shape deflection plots are shown on Figures 9.57 thru 9.61. As can be seen, not all margin requirements have been achieved with either concept. Mode 2 of concept #2 intersects the lower corner of the 3P diamond. This mode is sensitive to retention stiffness and this intersection could be altered by changing the retention geometry. Fine tuning of the blade was not pursued during this phase of the evaluation.

TABLE 9.21. NATURAL FREQUENCIES

CONCEPT #1
800 ft/sec (244 m/sec) v(tip) 1091 RPM
Retention stiffness = infinite for all degrees of freedom

Mode	Cruise	Margin	Climb	Margin
1	32.8 hz	-11%	32.8 hz	-11%
2	62.9 hz	+15%	59.3 hz	+ 9%
3	76.5 hz	+ 5%	79.9 hz	+ 7%
4	102.8 hz	+12%	110.9 hz	+14%

CONCEPT #2
800 ft/sec (244 m/sec) v(tip) 1091 RPM
Retention stiffness = 38500000 in-lb/rad In-plane
= 50500000 in-lb/rad Out-of-plane
= 48400000 in-lb/rad Torsion
= 17450000 lb/in Radial

Mode	Cruise	Margin	Climb	Margin
1	27.7 hz	-24%	29.3 hz	-19%
2	51.4 hz	- 6%	49.6 hz	- 9%
3	64.7 hz	-11%	66.0 hz	- 9%
4	95.1 hz	+ 5%	95.4 hz	+ 5%

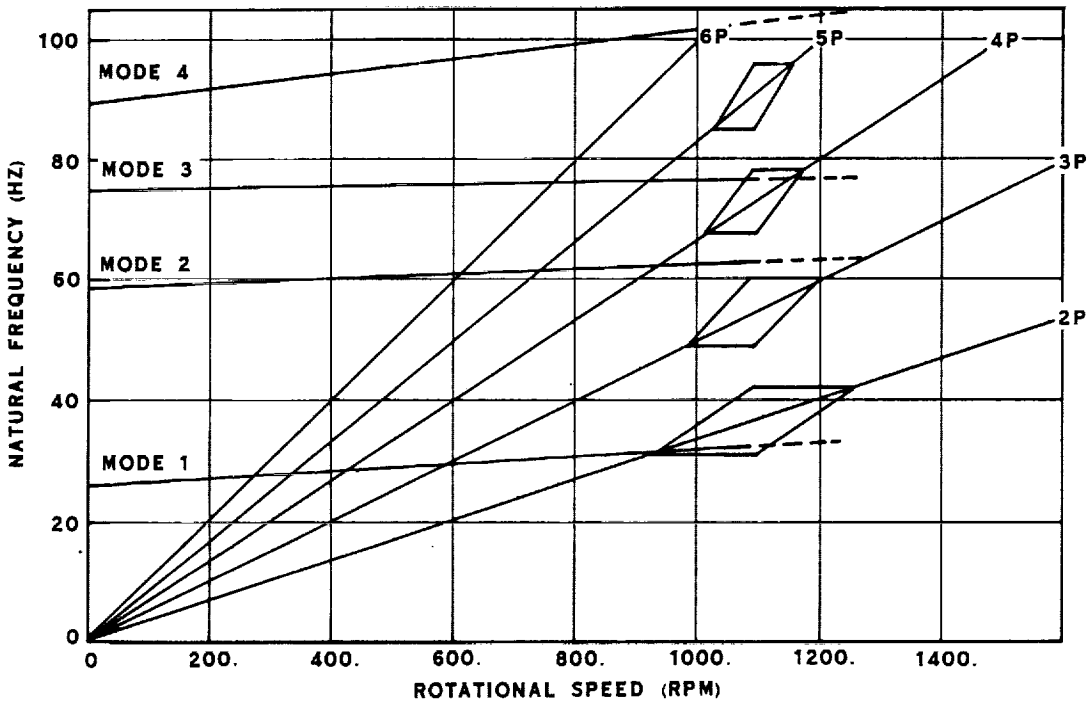

FIGURE 9.54 DIAGRAM CONCEPT # 1 CRUISE CONDITION

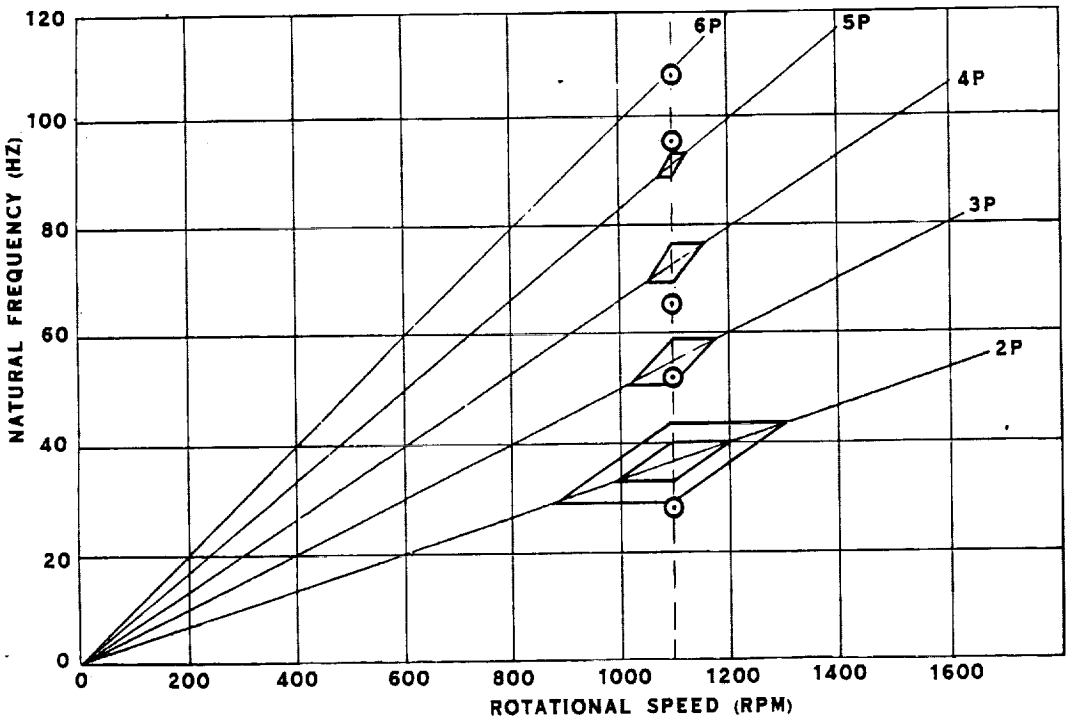

FIGURE 9.55 DIAGRAM CONCEPT # 2 CLIMB CONDITION

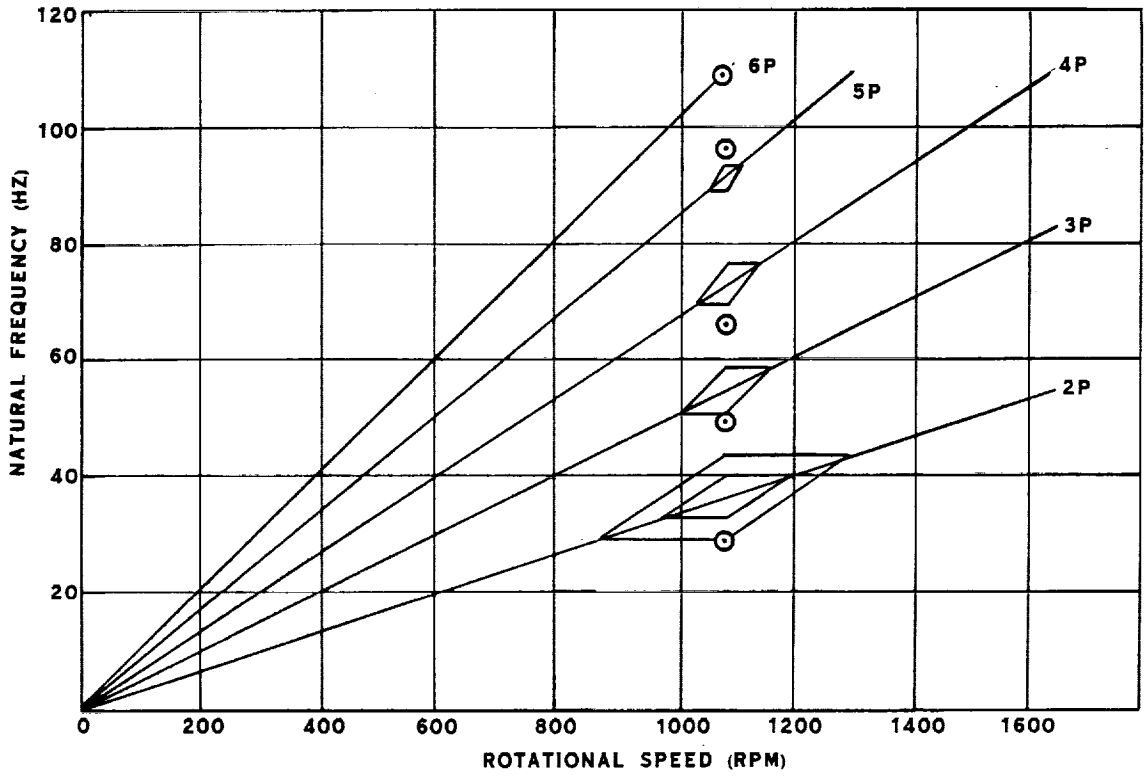

FIGURE 9.56 DIAGRAM CONCEPT # 2 CRUISE CONDITION

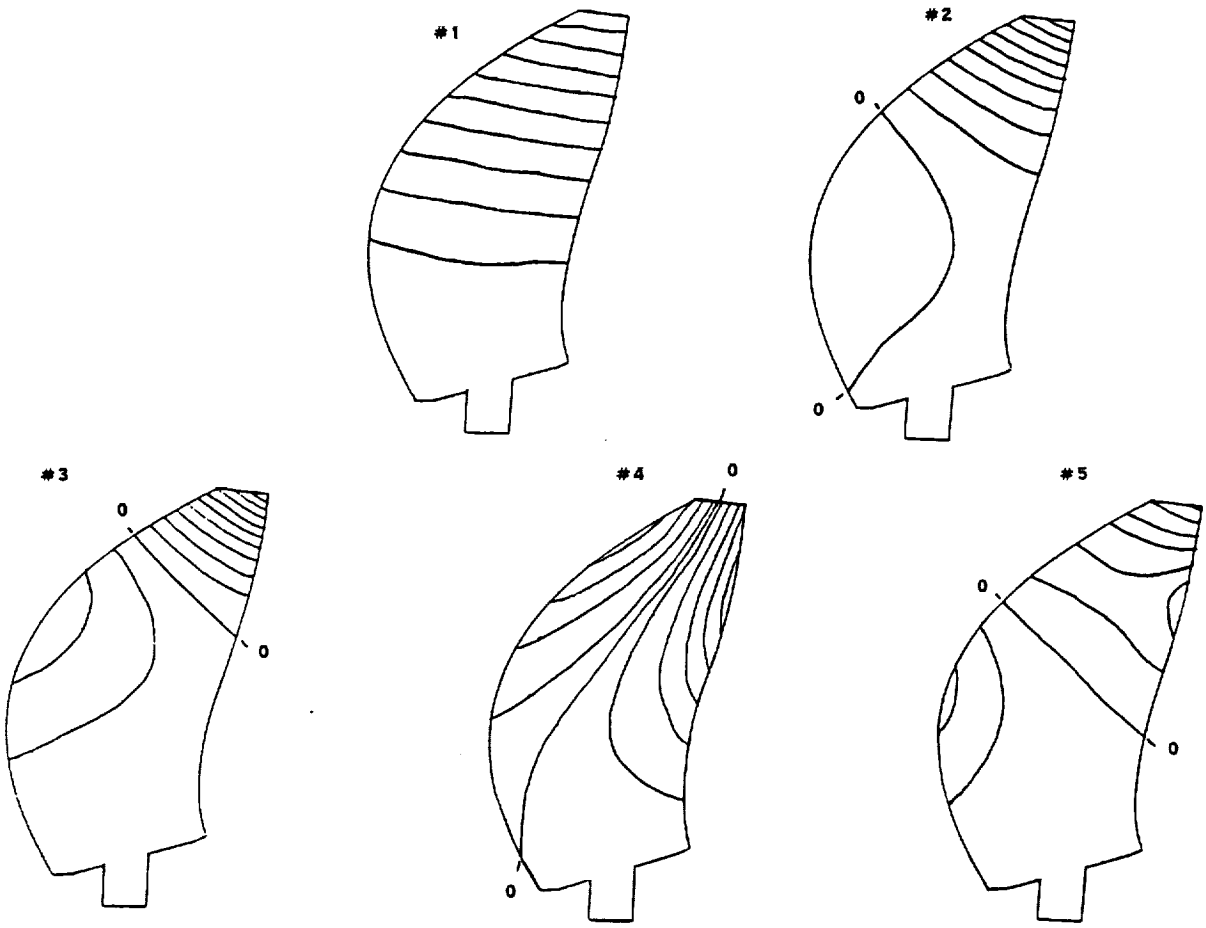

FIGURE 9.57 NORMAL MODE SHAPES - CONCEPT #2 - CRUISE CONDITION

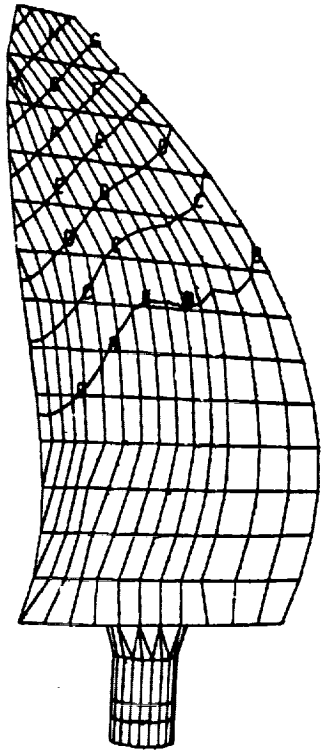

FIGURE 9.58 NORMAL MODE SHAPES - CONCEPT #1 - CRUISE CONDITION

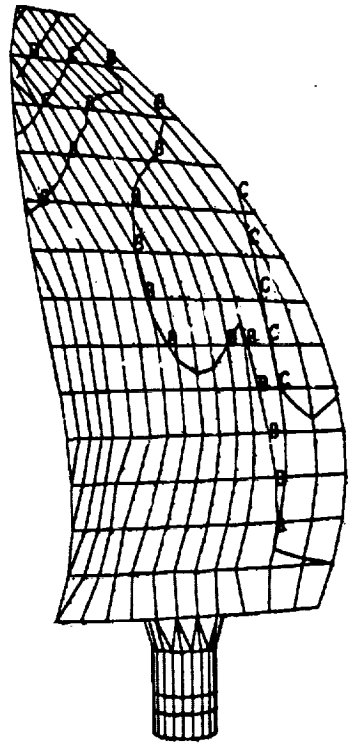

FIGURE 9.59 NORMAL MODE SHAPES - CONCEPT #1 - CRUISE CONDITION

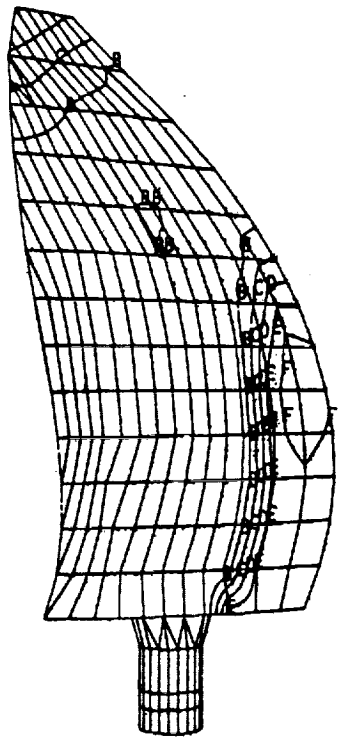

FIGURE 9.60 NORMAL MODE SHAPES - CRUISE CONDITION - CONCEPT #1

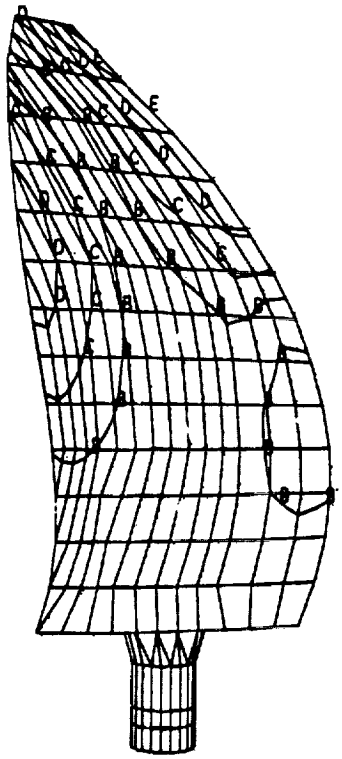

FIGURE 9.61 NORMAL MODE SHAPES - CONCEPT #1 - CRUISE CONDITION

9.5.4.2 Flutter - To evaluate the requirement for flutter free operation over the entire flight profile, the unstalled flutter characteristics for blade concepts #1 and #2 were calculated using an aeroelastic stability analysis, F203, specifically developed for Prop-Fan blades. The analysis utilizes the normal modes of vibration from the natural frequency calculation and linear, unsteady aerodynamics to calculate the viscous damping to critical damping ratio for specified modes of vibration at a particular condition. A negative ratio is the predictor of an instability.

Correlation of this analysis with wind tunnel model blade test data, primarily for mode 1 flutter, has been done.

The results of the stability calculation shown on Figures 9.62 thru 9.66 show an onset of flutter at 0.63 Mach number for concept #1 at the design cruise condition indicating it would be an unacceptable design for the flight profile. Concept #2 at the same condition, has a stability threshold of 0.96 Mach number, 19% higher than the design speed. Since Concept #1 was predicted unstable at the design condition, the sea level climb condition calculation was limited to Concept #2. A prediction of 0.65 Mach number threshold at the sea level climb condition for Concept #2 indicates this blade design to be free from unstalled flutter over the flight profile.

Low speed high power stall flutter was not analyzed for either concept during this evaluation. Since Concept #1 is unstable for high speed unstalled flutter, the stall flutter margin would be academic. Concept #2 exhibits the same vibration characteristics as the 9.0 foot (2.74 meter) design and would be acceptable for this criterion.

9.5.4.3 Stress - The simulated air loads were applied on the surface of the model as distributed force components parallel and perpendicular to the plane of rotation to create the chordwise and spanwise distribution of both the steady, and cyclic portions of the load. The two step solution sequence was then run to generate stress predictions for the blade components.

The results of these calculations shown on Figures 9.67 thru 9.72 indicate that Concept #1 has locally overstressed areas at the inboard and outboard regions of the shell suction surface for the Climb condition load case. These stresses may be influenced by the model but were considered correct for the concept evaluation. Concept #2, on the other hand, meets all the stress requirements imposed on the design.

As a by-product, the stress calculations generate the constraint loadings at the root of the blade that will be imposed on the rest of the propeller structure. Table 9.22 shows a listing of the steady portion of these loads.

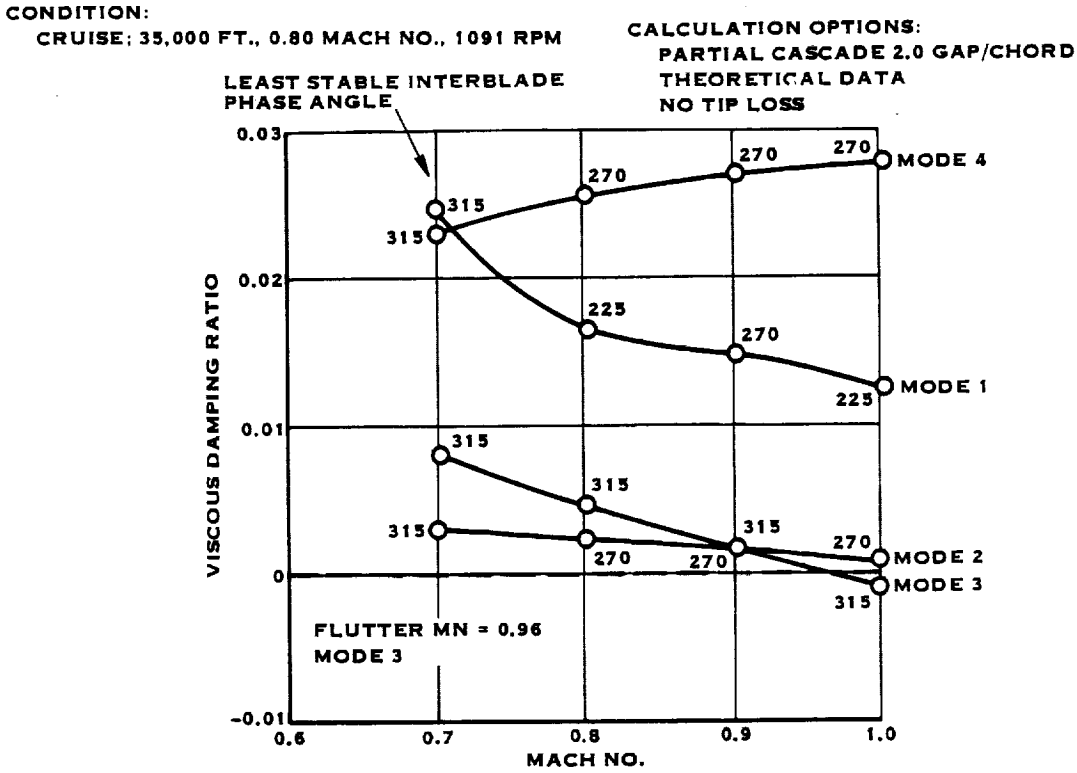

FIGURE 9.62 UNSTALLED FLUTTER STABILITY - CONCEPT #2

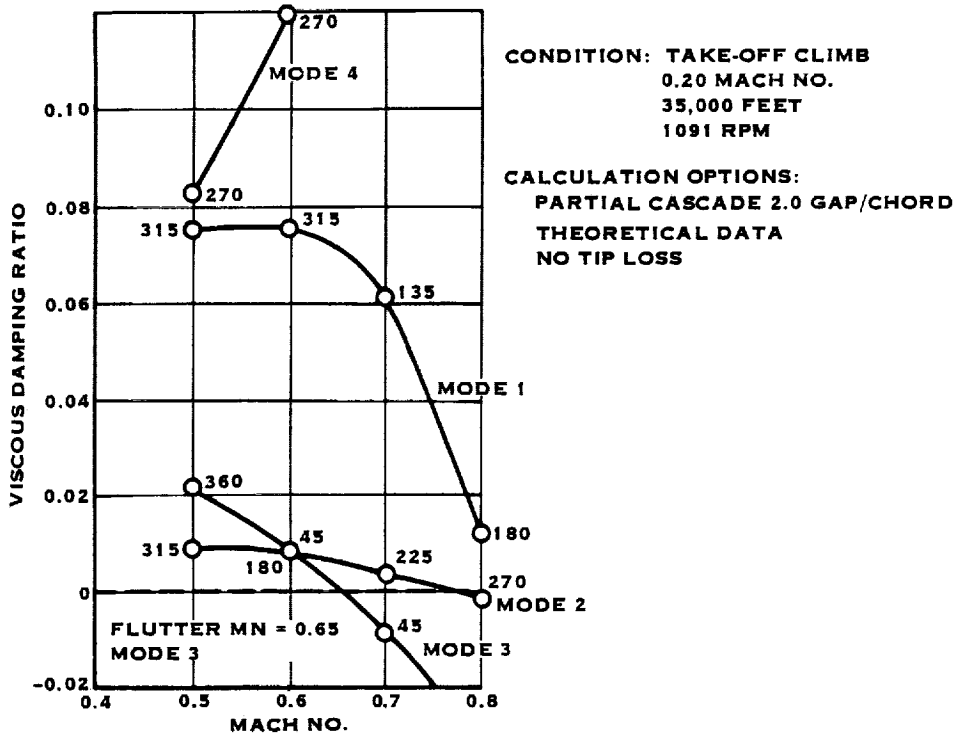

FIGURE 9.63 UNSTALLED FLUTTER STABILITY - CONCEPT #2

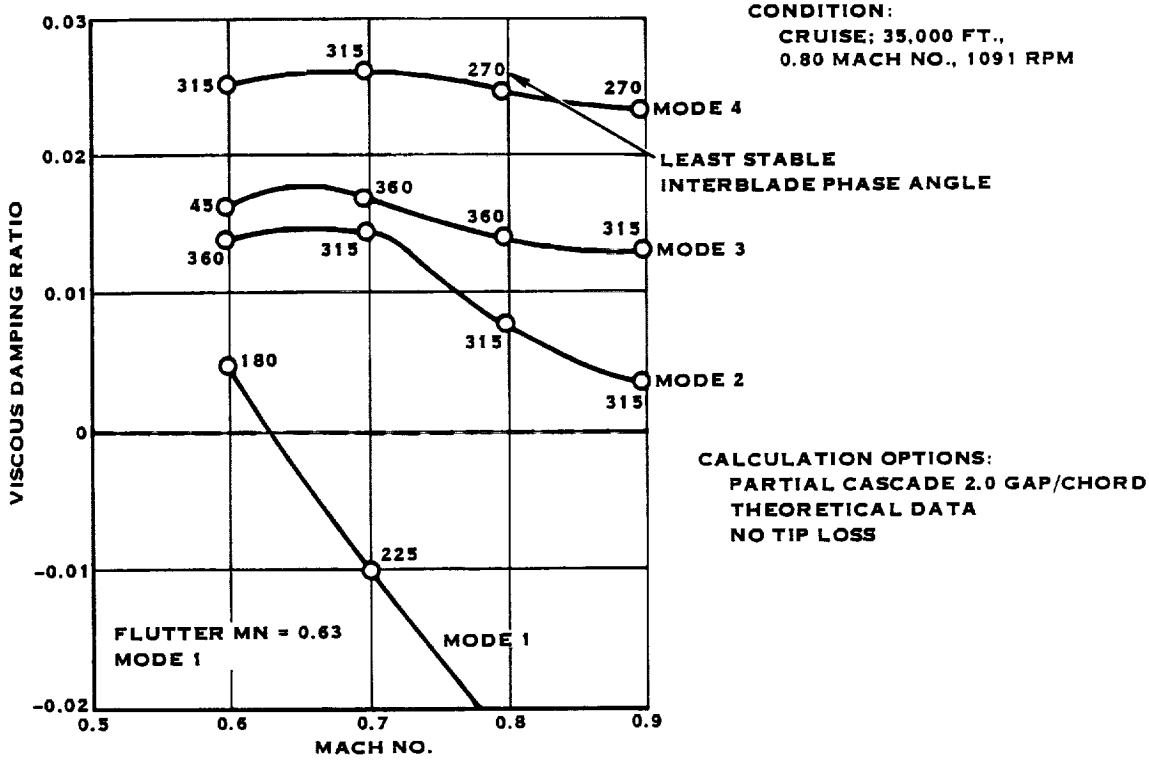

FIGURE 9.64 UNSTALLED FLUTTER STABILITY - CONCEPT #1

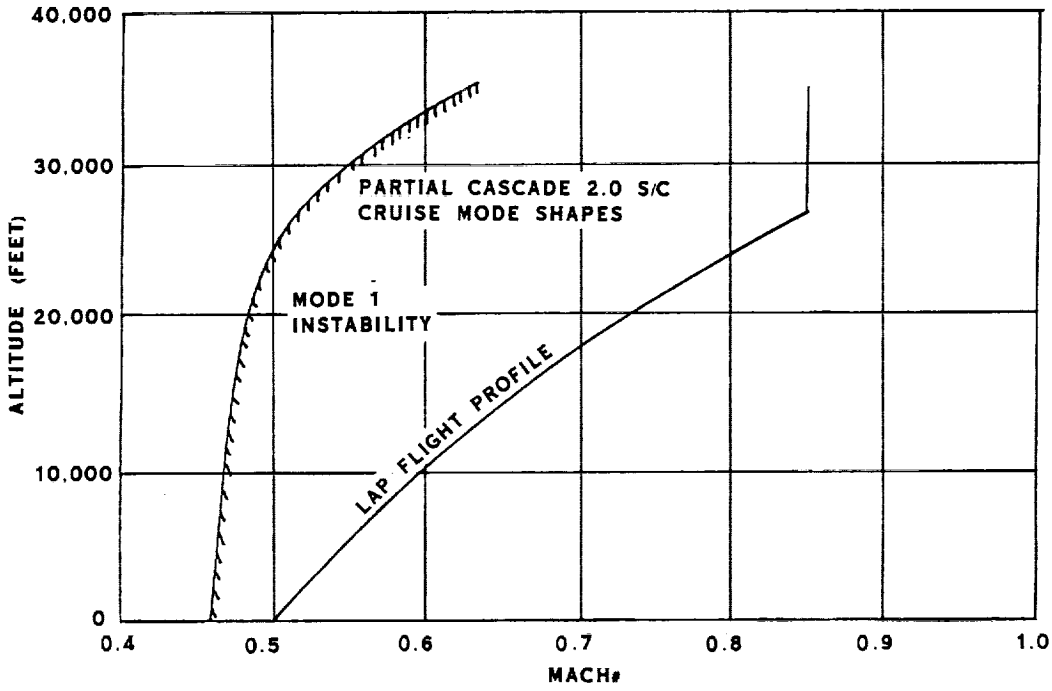

FIGURE 9.65 UNSTALLED FLUTTER STABILITY CONCEPT#1

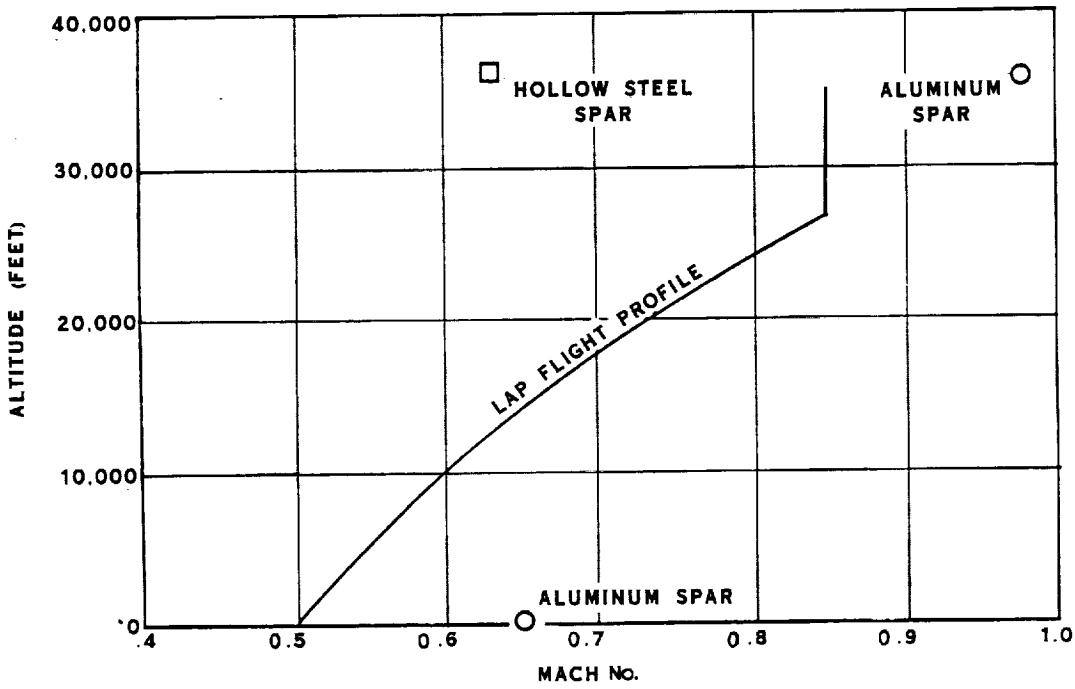

FIGURE 9.66 STABILITY SUMMARY

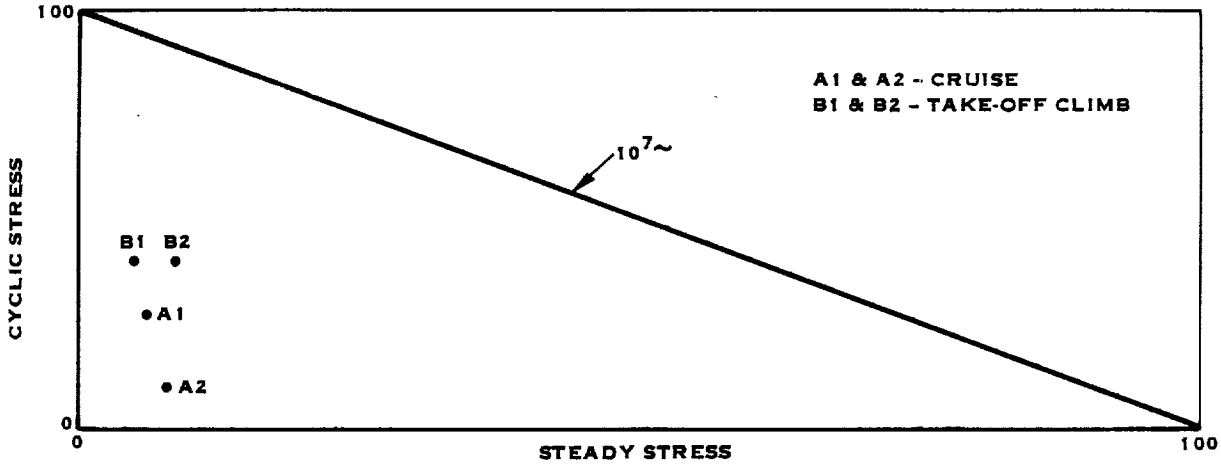

FIGURE 9.67 STRESS/STRENGTH COMPARISON - CONCEPT #1 - SPAR - AMS 6415, 40-44 HRC

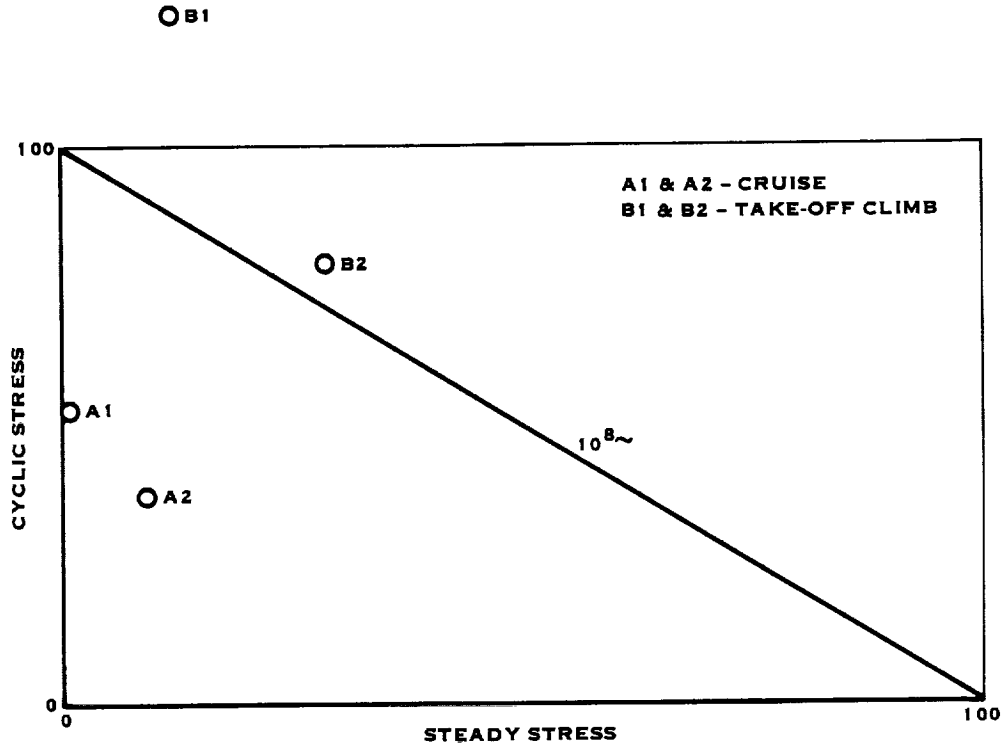

FIGURE 9.68 STRESS/STRENGTH COMPARISON - CONCEPT #1 - SHELL - 181 E-GLASS

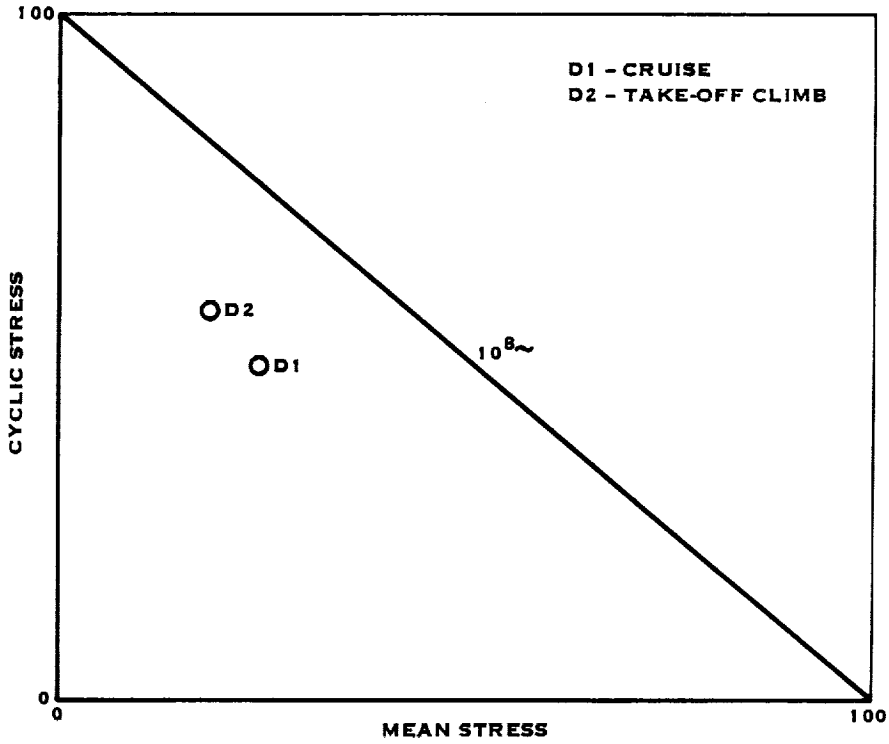

FIGURE 9.69 STRESS/STRENGTH COMPARISON - CONCEPT #2 - SPAR - ALUMINUM 7075-T73

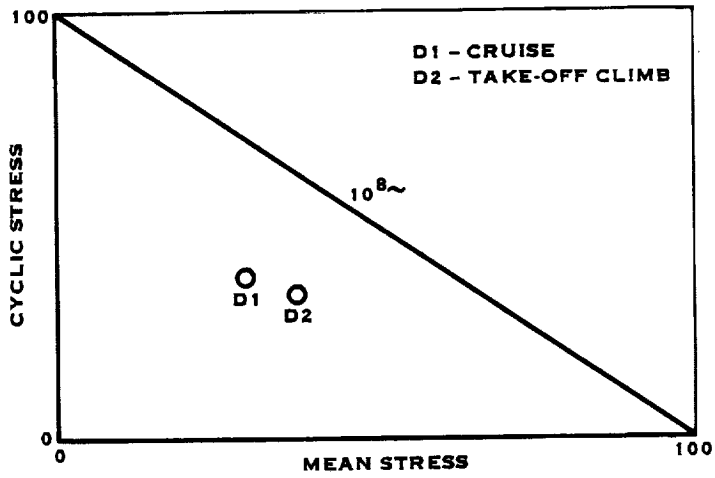

FIGURE 9.70 STRESS/STRENGTH COMPARISON - CONCEPT #2 - SHELL - 181 E-GLASS

C-3

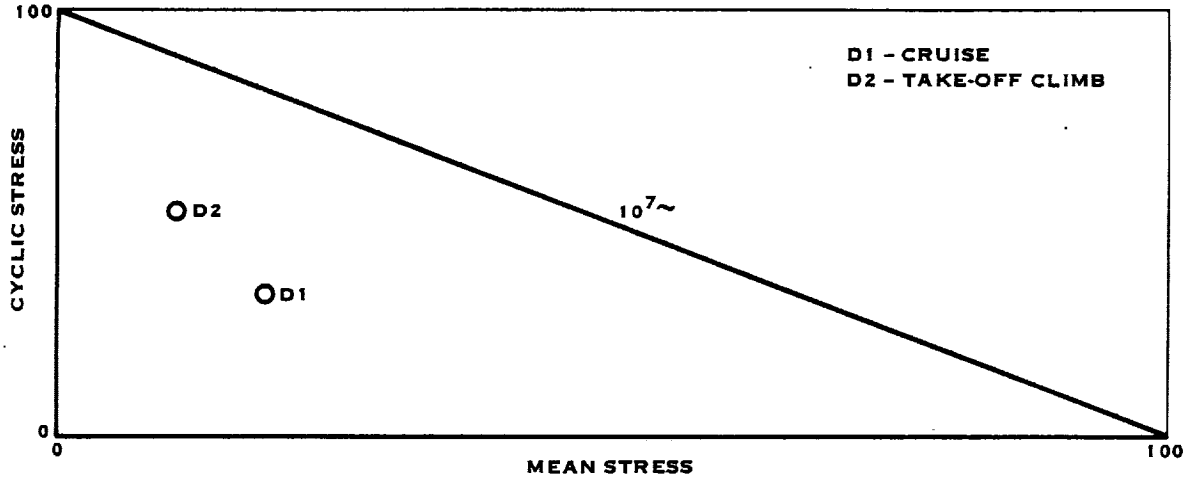

FIGURE 9.71 STRESS/STRENGTH COMPARISON - CONCEPT #2 - FILLER - 8 LB/FT^3 FOAM

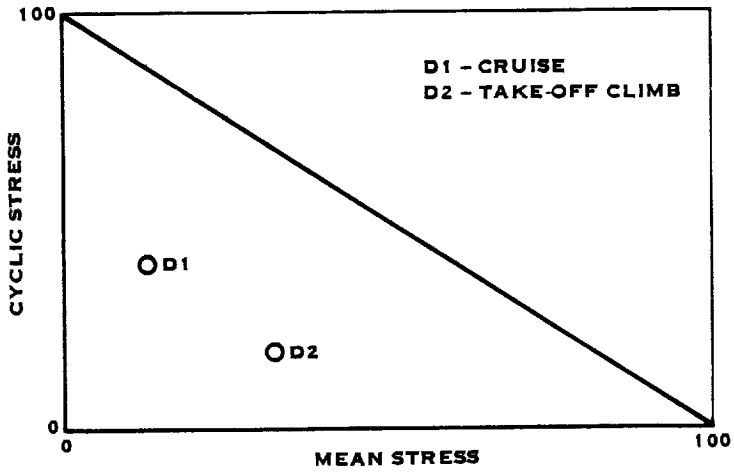

FIGURE 9.72 STRESS/STRENGTH COMPARISON - CONCEPT #2 - SHEATH - PLATED NICKEL

TABLE 9.22. STEADY RETENTION LOADS

800 ft/sec (244 m/sec) v(tip) 1091 RPM

	Concept #1		Concept #2	
	Cruise	Climb	Cruise	Climb
Shear - lbf (kn)				
In-Plane	2610 (11.6)	4013 (17.9)	9645 (42.9)	4698 (20.9)
Out-of-plane	433 (1.9)	2320 (10.3)	432 (1.9)	2248 (10.0)
Radial	162000 (721)	162000 (721)	192000 (854)	192000 (854)
Moments - in-lb (kn-m)				
In-plane	44000 (4.97)	104000 (11.8)	10400 (1.18)	46100 (5.21)
Out-of-plane	175000 (19.8)	235000 (26.6)	36600 (4.14)	44900 (5.07)
Torsion	44300 (5.01)	46100 (5.21)	66500 (7.51)	72300 (8.17)
Weight	159 lbs (72.2 kg)		157 lbs (71.3 kg)	
Radial c.g.	30.14 in (0.77 m)		36.31 in (0.92 m)	

9.5.4.4 Deflections - The deflections listed in Table 9.23 show Concept #2 to deflect to approximately the same position as the 9.0 foot (2.74 meter) blade, indicating that the pre-deflected position was acceptable for the scaled geometry.

Concept #1's angular untwist, shown on Figure 9.73, has a deflection of about 2.5 degrees at the tip. Due to the instability and over stressing in the shell, this effect was not investigated.

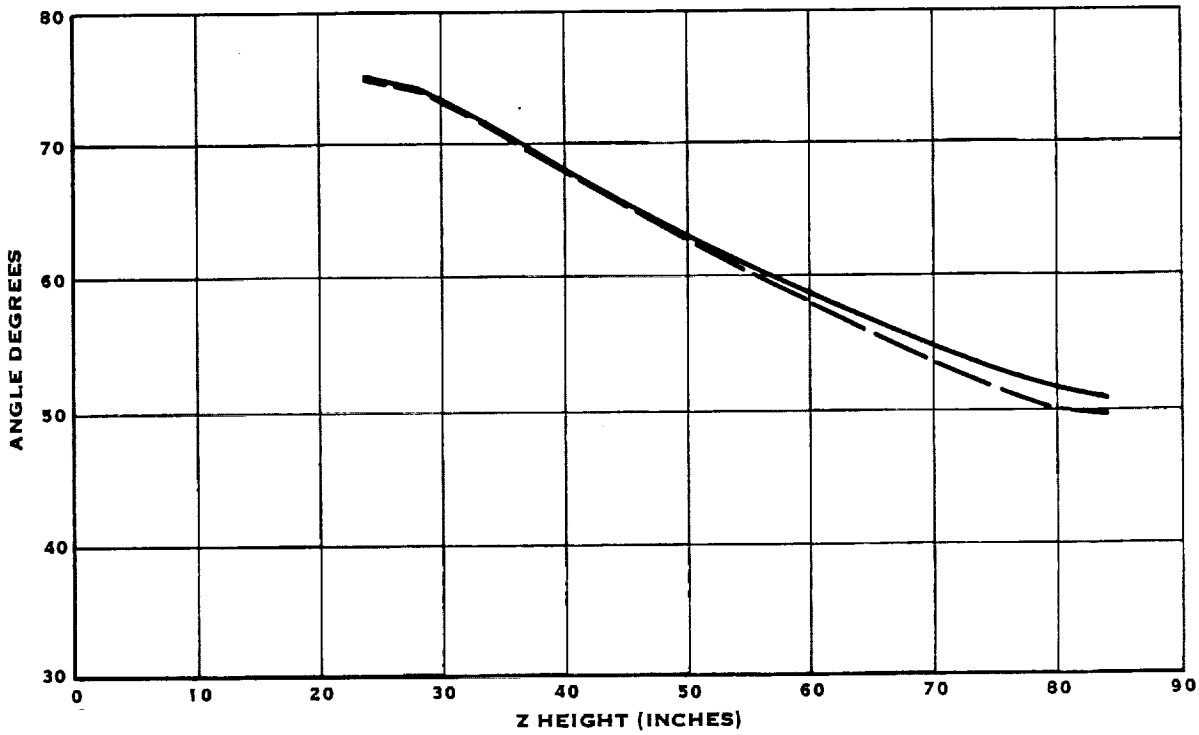

FIGURE 9.73 DEFLECTIONS - CONCEPT #1 - CRUISE CONDITION

TABLE 9.23. BLADE DEFLECTION - CONCEPT #2

	FLIGHT CONDITION	
Rotations, Deg	Design/Cruise	T.O. Climb
Mid Tip	3.3 deg	2.2 deg
T.E. 3/4 Rad	1.2 deg	1.1 deg

	FLIGHT CONDITION	
Translations	Design/Cruise	T.O. Climb
Mid Tip	-0.55 in	-1.21 in
T.E. 3/4 Rad	0.85 in	0.44 in

9.5.5 Conclusions

Concept #1 does not meet the design requirements. The shell is locally over-stressed in two regions and it has a low stability threshold for the design cruise condition.

Concept #1 does have a lower centrifugal force and pitch change torsion loads; section stacking modifications for reducing the in-plane and out-of-plane bending moments and increasing the stability threshold would produce a lower total system weight.

Concept #2 meets all the evaluation requirements imposed. Since Concept #2 is a scaled up version of the testbed size blade, the testbed size blade design is fully representative of a full size design.

References

1. Kraus, E.F. and Van Abkoude, J.C.: Cost/Benefit Trade-offs for Reducing the Energy Consumption of the Commercial Air Transportation System. Volume I: Technical Analysis, Volume II: Market and Economic Analysis and Summary Report, June 1976. NASA CR-137923, 4 & 5, Douglas Aircraft Company.

2. BCAC Preliminary Design Dept.: Energy Consumption Characteristics of Transports Using the Prop-Fan Concept. Final Report, October 1976 and Summary Report, November 1976. NASA CR-137937,8. Boeing Commercial Airplane Company.

3. Hopkins, J.P. and Wharton, H.E.: Study of the Cost/Benefit Trade-offs for Reducing the Energy Consumption of the Commercial Air Transportation System. Final Report and Summary Report, August 1976. NASA CR-137926,7. Lockheed California Company.

4. Revell, J.D. and Tullis, R.H.: Fuel Conservative Merits of Advanced Turboprop Transport Aircraft. NASA CR-152096, August 1977. Lockheed California Company.

5. Dugan, J.F., Gatzen B.S., Adamson, W.M.: Prop-Fan Propulsion. SAE Technical Paper 780995, November 1978.

6. Muehlbauer, J.S., et. al: Turboprop Cargo Aircraft Systems Study, Phase I. NASA CR-159355. November 1980. Lockheed-Georgia Company.

7. Lockheed Study Team: Advanced Turboprop Testbed Systems Study. April 21, 1981. Final Oral Briefing. Lockheed-Georgia Company.

8. Klotzsche, M. et. al: DC-9 Prop-Fan Feasibility Study. Final Oral Briefing, May 20, 1981. NAS2-10178 Contract Study. Douglas Aircraft Company.

9. Klotzsche, M. et. al: DC-9 Prop-Fan Testbed Study: Final Oral Briefing, April 22, 1981. NASA Contract NAS3-22347. Douglas Aircraft Company.

10. Schuetz, A.J.: Potential Applicability of Prop-Fan Propulsion to Maritime Patrol Aircraft. Oral Commentary to SAE National Aerospace Meeting, November 27, 1978. Lockheed California Company.

11. Welge, H.R., Crowder, J.P.: Simulated Propeller Slipstream Effects on a Supercritical Wing. NASA CR-152138, June, 1978. Douglas Aircraft Company.

12. Generalized Prop-Fan Performance and Weight, SP05A75, April 18, 1975. Hamilton Standard Division of United Technologies.

13. Prop-Fan Technology Study. Prepared for Naval Air Development Center under Contract No. N62269-77-C-0465. October 31, 1977. Hamilton Standard Division of United Technologies.

14. Prop-Fan Parametric Data Package. SP04A80. October, 1980. Hamilton Standard Division of United Technologies.

15. Analysis of Mach 0.8 Turboprop Slipstream Wing/Nacelle Interactions. July 9, 1981. NASA Contract NAS2-10881. Douglas Aircraft Company.

16. Black, D.M., Menthe, R.N. and Wainauski, H.S.: Aerodynamic Design and Performance Testing of an Advanced 30° Swept, Eight Bladed Propeller at Mach Numbers from 0.2 to 0.85. September 1978. NASA CR 3047. Hamilton Standard Division of United Technologies Corporation.

17. Metzger, F.B.: Progress and Trends in Propeller/Prop-Fan Noise Technology. AIAA Technical Paper 80-0856, presented May 6-8, 1980. Hamilton Standard Division of United Technologies Corporation.

18. Gatzen, B.S. and Adamson, W.M.: Prop-Fan Technical Progress Leading to Technical Readiness. Technical Paper AIAA-81-0810 CP. Presented at International Air Transportation Conference, May 26-28, 1981. Hamilton Standard.

19. Wainauski, H.S.: Aerodynamic Design and Performance Testing of an Advanced Unswept Eight Bladed propeller at Mach Numbers from 0.2 to 0.85. Prepared under Contract NAS3-20252 by Hamilton Standard. August 1977.

20. Rohrbach, C., F.B. Metzger, D.M. Black and R.M. Ladden: Evaluation of Wind Tunnel Performance Tests of an Advanced 45° Swept Eight Bladed Propeller at Mach Numbers from 0.45 to 0.85. NASA CR-3405, March, 1982.

21. Boctor, M.S., et al.: An Analysis of Prop-Fan/Airframe Aerodynamic Integration. NASA CR-152186, October 1978. Boeing Commercial Airplane Company.

22. Rohrbach, C. et al.: Aerodynamic and Acoustic Design Report: 10 Bladed, Highly Swept Prop-Fan for Cruise at 0.80 Mach Number. Prepared under contract NAS3-21724 by Hamilton Standard.

23. Memo to Cornell from LW. Smith - Trip Report - Visit to NASA-Lewis to discuss Prop-Fan Model Tests, June 22, 1981.

24. Baker, John E., "The Effects of Various Parameters including Mach Number on Propeller Blade Flutter with Emphasis on Stall Flutter." NACA RML50C12b.

25. "NASA-AMES Installed SR-2C Prop-Fan Model Flow Field and Response Calculations" letter report to O. Mehmed, Project Manager, NASA-Lewis Research Center, from B.P. Rosenthaler, Hamilton Standard, July 14, 1981. (Contract No. NAS 3-22755).

26. "On the Vortex Theory of Screw Propellers", S. Goldstein, Proceeding of Royal Society of Aviation, Vol. 123, 1929.

27. "Excitation Factor Sensitivity Study", Hamilton Standard, August, 1983, (NASA-LEWIS Contract NAS3-22394).

28. Hanson, D.B., "Near Field Frequency Domain Theory for Propeller Noise", AIAA Paper No. 83-0688, presented April 11-13, AIAA 8th Aero-Acoustics Conference, Atlanta, Georgia.

29. Large Displacements and Stability Analysis of Nonlinear Propeller Structures; Aiello, R.A., and Chamis, C.C.; LeRC, NASA TM 82850. Presented at the 10th NASTRAN User's Colloquium, New Orleans, LA, May 13-14, 1982.

APPENDIX D

UNITED TECHNOLOGIES
HAMILTON STANDARD

DESIGN REQUIREMENTS

FOR

ADVANCED TURBOPROP BLADES

SR-7

Prepared as Part of

Propeller Blade Structural Design Study

NASA Contract NAS3-22394

November, 1983

UNITED TECHNOLOGIES HAMILTON STANDARD

TABLE OF CONTENTS

UNITED TECHNOLOGIES HAMILTON STANDARD

I. INTRODUCTION

In recent years, considerable attention has been directed toward reducing aircraft fuel consumption. Studies have shown that the inherent efficiency advantage that turboprop propulsion systems have demonstrated at 0.65 Mn may now be extended to the higher cruise speeds of todays turbofan powered aircraft. In order to achieve this goal, new propeller designs will require advancements such as thin, high speed airfoils and aerodynamic sweep.

A program to conduct structural design studies of large scale blades of this type has been funded by NASA LeRC. This program includes the establishment of structural concepts for the fabrication of the SR-7 test bed Prop-Fan blade configuration, and the definition of it's structural properties.

This document contains a description of the design process, and a description of the analysis procedures which will be used during the study, and sets forth the requirements to which the blade will be designed. Since F.O.D. and stall flutter are not considered hard requirements for blade design based on todays technology, these two subjects will be addressed under Design Goals.

It is our intent to develop a document which allows for some flexibility.

II. APPROACH TO ANALYSIS

During the program, the SR-7 configuration will be analyzed using a finite element analysis method. This method is described below.

Finite Element Analysis Method (Ref. Figure 1)

The blade aerodynamic data, aerodynamic loads, external geometry and internal construction are entered into SHEDS (Structured Hierarchical Engineering Data Storage) using computer programs H250, H444, H882, H883 and H886 as indicated in the following manner.

The blade aerodynamic inplane and out-of-plane loads are calculated using a computer program (H444). The input to this program is the blade operating condition.

If composite laminates are used in the blade design, the elastic properties will be calculated using a composite material laminate analysis program, H250. This program has the capability to calculate the laminate stress allowable based on the orthotropic stress allowables of each layer.

The blade aerodynamic data, aerodynamic loads, and fabrication method are entered into a computer program (H882) which creates streamline airfoil sections. The airfoil sections are based on a "library" of airfoil coordinate data for many standard airfoils over a wide range of thickness ratios and camber levels. Internal cross-section geometry coordinates, where required, and lead edge sheath definitions are also created in H882. The streamline airfoil sections are then stacked relative to one another by computer program H883 to produce the aero-acoustically dictated three-dimensional blade shape. The blade shape is generated by fairing the streamline airfoil sections and internal blade geometry using spline curves in computer program H884. Orthogonal planes are cut through the faired blade geometry at desired radial locations for beam property calculations and manufacturing dimensional definition.

Blade section properties are calculated by computer program H886, based on the radial station cross-sections. Equivalent cross-sectional properties for non-homogenous blade components are also calculated using their elastic modulii and density ratios. Pertinent cross-sectional properties are then integrated along the blade span to determine weight, blade stiffness distribution, and mass distribution.

The finite element model is generated using program F018. This program utilizes the blade data from SHEDS and allows the designer to generate the model interactively on a computer terminal.

The finite element analysis will be performed using a computerized general purpose three-dimensional finite element program known as BESTRAN-H552. This is a program comprising several specialized subprograms which work together, based on the

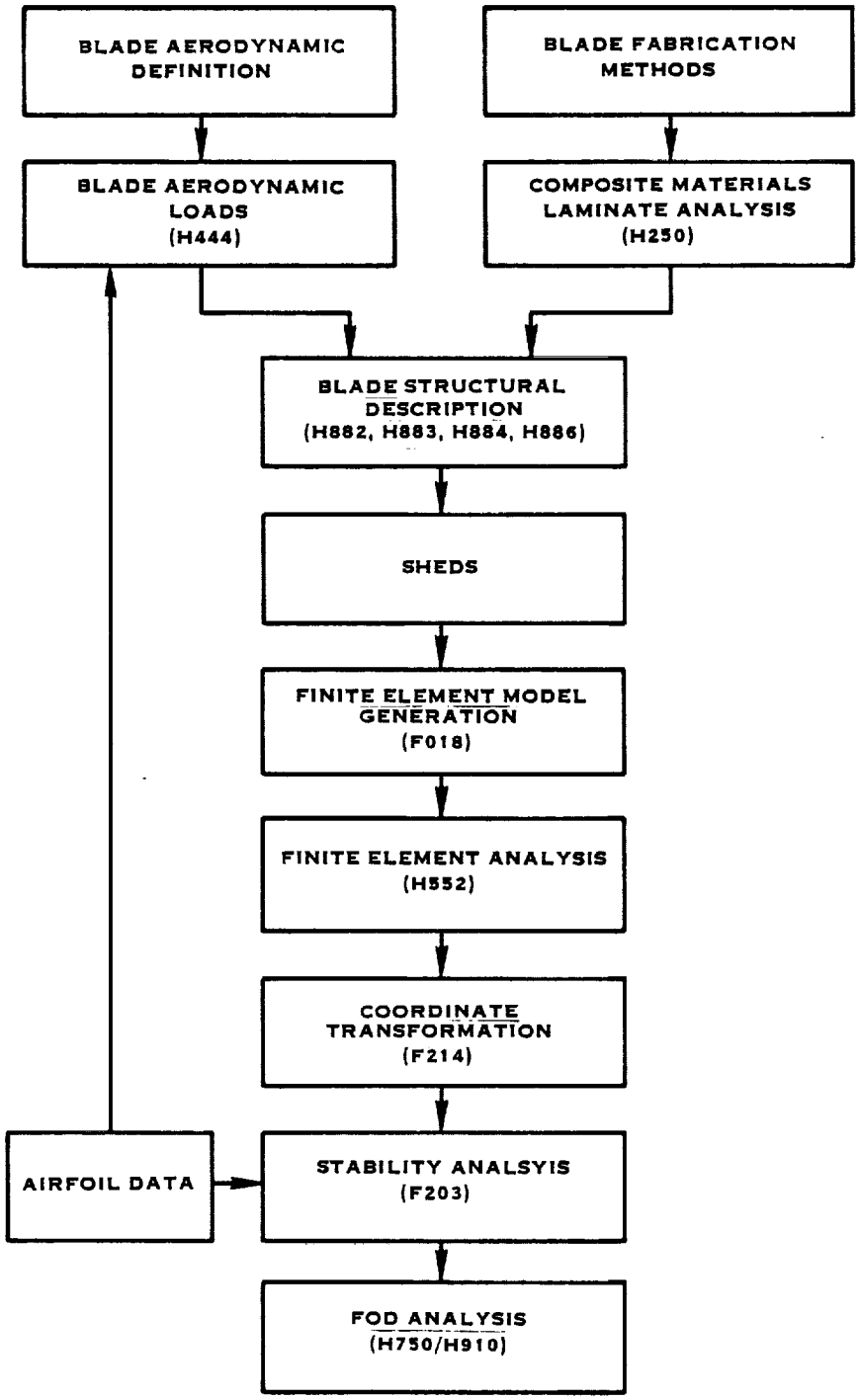

FIGURE 1. FLOW DIAGRAM - FINITE ELEMENT ANALYSIS

methods of finite element analysis. The analysis will calculate steady stresses and deflections at speed. Frequency, mode shape, and stress distributions will be calculated at rest and at speed and used to generate the Campbell Plot.

The frequencies, model masses and mode shapes are then input into a stability preprocessor (F214) that puts the data in a form that is compatible with the stability analysis (F203). There are two basic reasons for this conversion.. One is that in the finite element method, the blade is described by discrete elements that must be converted to a beam type coordinate system, and the mode shapes converted to a three-dimensional displacement system. This is to better describe the effects of sweep and twist. The second is a conversion to the blade section coordinator system. This latter system is necessary because of small angle approximations in the aerodynamics that are required by the linear analysis. This analysis will be used to predict stability for both classical and stall flutter, (See Section III F).

The blade design will then be subjected to a foreign object damage analysis using computer programs H750/H910. These programs are a three mode interactive blade impact analysis which utilizes a fluid missile model which is interactive with the dynamic model response of the blade.

Blade Aerodynamic Design Analysis

The Compressible Vortex Program, H409, will be used for the aerodynamic design and performance analysis of the SR-7 Prop-Fan. This program accounts for the effects of supersonic Mach number zone of influence and the swept lifting line on the induced velocities at the blades. The program utilizes two dimensional, compressible airfoil data which is corrected for blade sweep, cascade interference and the blade tip Mach cone.

Acoustic Analysis

An acoustic design analysis utilizing the Frequency Domain Near Field Noise Prediction Method will be used during the aerodynamic design phase.

UNITED TECHNOLOGIES HAMILTON STANDARD

III. DESCRIPTION OF ANALYSES

A. Aerodynamic Loads (H-444)

The once-per-revolution (1P) airloads are computed by means of the Hamilton Standard strip analysis program (Deck No. H444) utilizing two-dimensional compressible airfoil data. An operating condition is defined in terms of shaft horsepower, propeller rotational speed, pressure altitude, velocity, ambient temperature and inflow angle. These parameters in turn define the non-dimensional coefficients required to do a strip analysis, namely, advance ratio, J and power coefficient, Cp, defined as:

$$J = v/nD$$

$$C_p = P/\rho n^3 D^5$$

where v = true airspeed, feet per second

n = propeller speed, rps

D = diameter, feet

P = power, ft. lbs./second

ρ = density, lb. $sec.^2/ft.^4$

The advance ratio and inflow angle define the blade advance angle radially and azimuthally.

An iterative procedure is then utilized to calculate the blade angle at the given operating condition to absorb the proper power coefficient, C_p. For example, for the eight bladed Prop-Fan eight azimuthal positions are examined and the elemental power coefficient is integrated both azimuthally and radially until the required C_p is attained.

Once the blade angle is determined, the elemental in-plane force (Fr) and the elemental out-of-plane force (F_p) are calculated at the advancing and retreating positions. From these results, the change in in-plane and out-of-plane force ($F\alpha r$ & $F\alpha p$ respectively) are determined. These loads are then used in the multiazimuth analysis (H045) which is used in the determination of the excitation factor defined in IIID. The loads are also used as an input to the BESTRAN analysis (H552).

B. Mechanical Loads

1. Steady Tension (H-028 or H-552)

The most obvious load on a propeller blade is due to centrifugal force. Centrifugal force acts on blade mass elements to produce radial tensile forces which are additive from the blade tip, R, down to any radius, r_1, being studied. The total centrifugal load developed at radius r_1, is found by integrating as follows:

$$C.L. = \omega^2 \rho \int_{r_1}^{R} Ardr$$

where ω is the angular rotation speed, ρ is the mass density of the blade material, A is the blade cross sectional area and r_1 is the radius of the blade section. This force is a pure tensile load when the cross section mass centers are aligned on a single axis perpendicular to and passing through the axis of rotation. This is commonly called the "stacking axis".

2. Steady Bending (H-028 or H-552)

As a propeller blade rotates through the air, each portion of the blade produces a lift and drag force. The magnitude of these forces are determined by the specific characteristics of airfoil shape and its operating parameters as shown in Figure 2.

At any blade radial position, these aerodynamic forces, calculated with a strip analysis program, can be resolved into two vectors, thrust (T), and torque (Q), as shown in Figure 3. Also illustrated is the origin of a secondary aerodynamic steady load, aerodynamic twisting moment. This comes from the distance between the quarter chord point and the stacking axis which is commonly the centerline of the blade retention bearing and the axis about which the blade angle control mechanism torque is applied.

Summing these thrust and torque forces along the span of the blade yields the total thrust and torque per blade. These distributed forces produce bending moments in the cantilevered blade. From the preceding discussion of steady centrifugal loads, it is obvious that by offsetting the

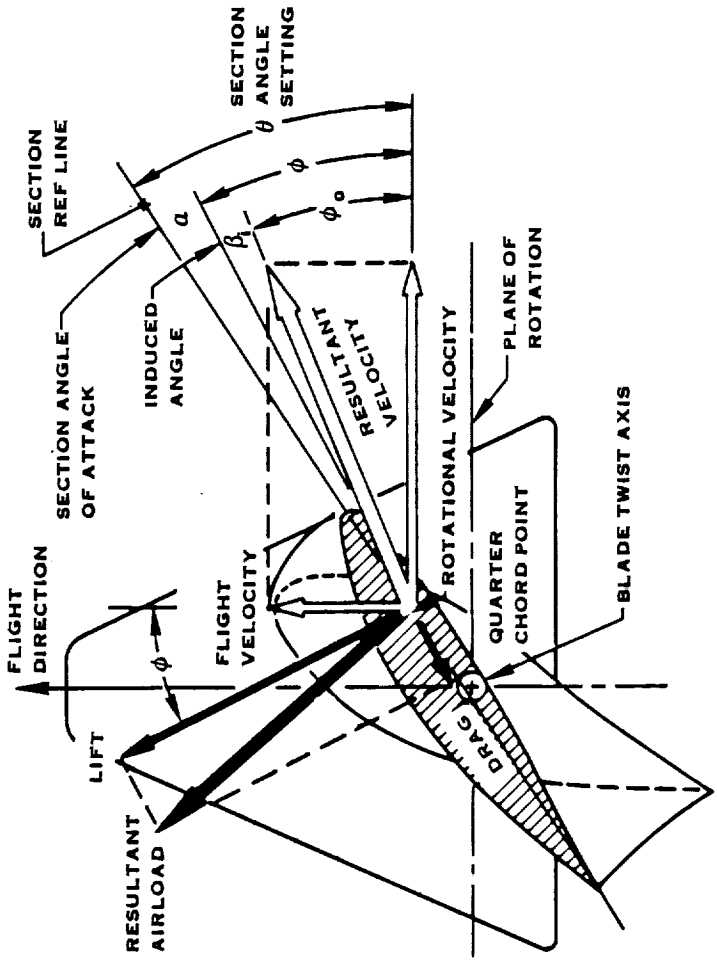

FIGURE 2. BLADE AERODYNAMIC LOAD RELATIONSHIPS

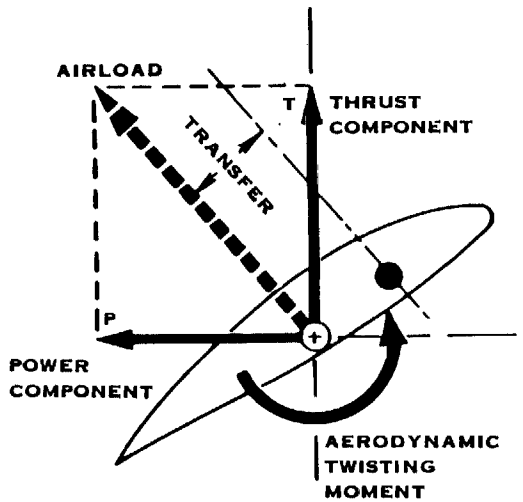

FIGURE 3. DEVELOPMENT AND RESOLUTION OF PROPELLER BLADE AIRLOADS

centers of gravity of the blade cross sections from the radial stacking axis in a systematic fashion, centrifugal bending moments can be developed in addition to the tensile loads. These moments are in a direction which tends to return the displaced mass center to the radial axis and are called centrifugal restoring moments. In some blades initial displacements along the local section chordline (sweep) and/or perpendicular to the local section chordline (offset) are built into the blade in order to generate restoring moments which reduce the aerodynamic bending moments.

3. Steady Untwist (H-886 or H-552)

Since a propeller blade operates in a radial centrifugal force field there are forces developed that tend to align the blade parallel to the plane of rotation. Resolution of these forces about the stacking axis into centrifugal twisting moments can be seen in Figure 4. In this figure the total cross sectional mass of a typical blade radial element is separated into two centers of mass, one for the leading edge portion of blade at distance "a" from the plane of rotation; and one for the trailing edge portion of the blade at distance "b" from the plane of rotation. Radial centrifugal force vectors, originating from the propeller rotational axis can be drawn through each of these mass centers. Each of these vectors may be separated into radial components parallel to the blade centerline and in-plane components, P_L and P_T, parallel to the plane of rotation.

The two components, at moment arms "a" and "b" generate a centrifugal twisting moment about the stacking axis which tries to align the section with the plane of rotation. This twisting moment for any specific section varies sinusoidally with the angular position of that section with respect to the plane of rotation. Consequently, the twisting moment about the stacking axis varies sinusoidally with section blade angle referenced to the plane of rotation over a period of 90°.

The twisting moments of each incremental cross section of a blade can be summed from tip to root resulting in a net twisting moment about the stacking axis at the blade root. In most operating conditions this centrifugal twisting moment is opposite in sense to the previously discussed aerodynamic twisting moment. The net twisting moment is a torque that must be carried by the blade angle control mechanism in order to maintain blade angle setting.

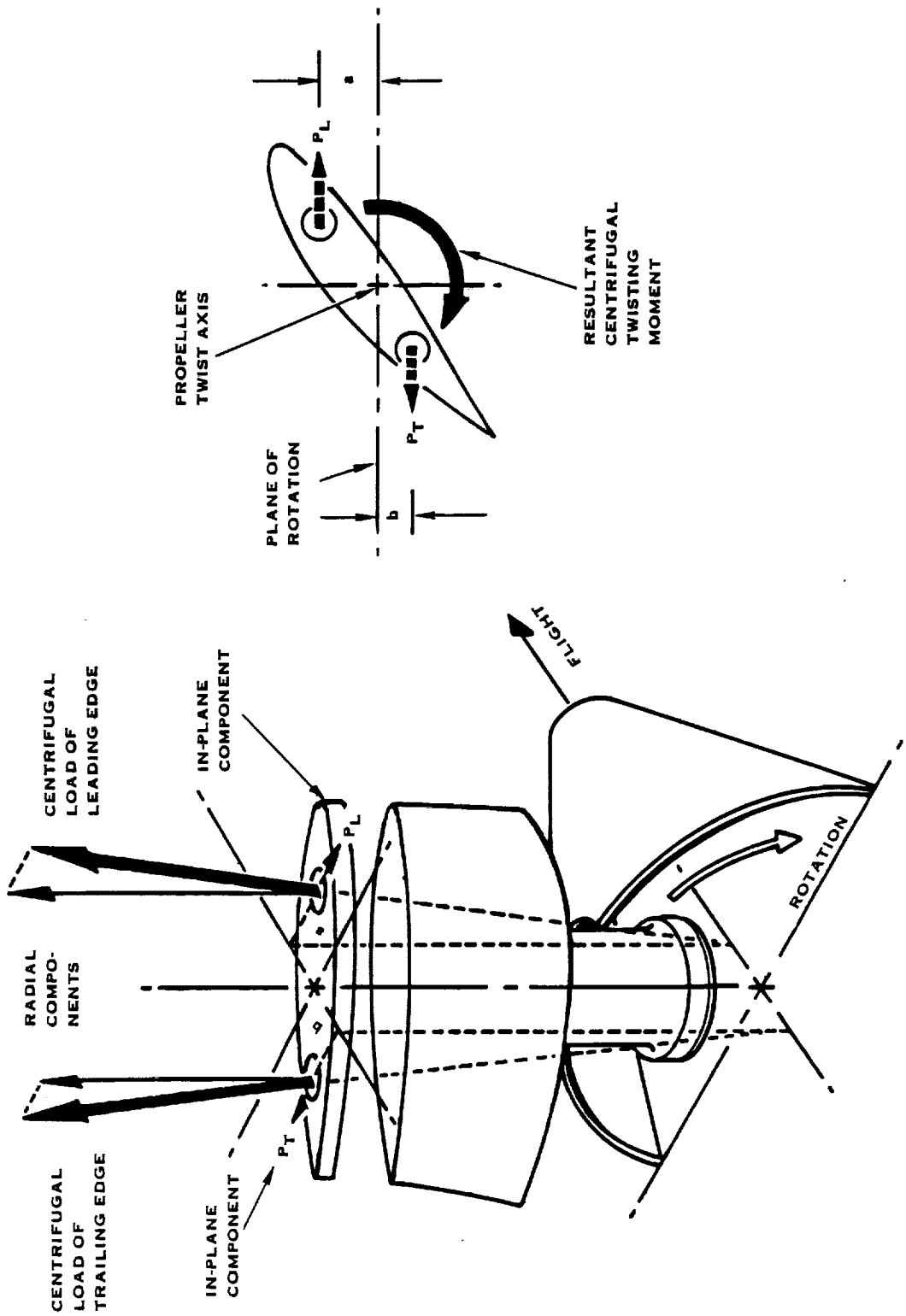

FIGURE 4. CTM DEVELOPMENT OF PROPELLER BLADE CENTRIFUGAL TWISTING MOMENT

These same offset mass forces lead to twisting moments within the blade even when the net root twisting moment is zero. This is because a blade has a built in twist distribution and there can be no single blade angle setting which results in a zero twisting moment for all incremental sections along its radial length. These internal centrifugal twisting moments, balanced by aerodynamic twisting moments, act to reduce the built in twist distribution of the blade, thus the common term "untwist". It is normal to correct for the untwist by building in a compensating amount of pretwist. As with sweep and offset, pretwist can only be exactly correct for one operating condition.

The basic explanation of the mechanical loading of a blade given above has been in beam theory terms. The blade is assumed clamped at some fixed location near the center of rotation. The classical beam section properties are calculated for an appropriate number of blade segments along the blade radial length. The radial increment between segments is chosen depending on the rapidity of geometric variation. These sections are then stacked in space relative to a radial line, the stacking axis, which passes through the axis of rotation. The mechanical body forces are then determined for the appropriate rotational speed by summing from tip to root. The mathematical description of a twisted, tapered, rotating beam subjected to distributed aerodynamic loading is a complicated process. The methods, however, are well established and proven by over forty years of application. The use of modern computers has made this task very straightforward.

All of the same mechanical loads can be calculated using finite element analysis methods. The method in common use at Hamilton Standard is called BESTRAN. BESTRAN is a broad based system written in FORTRAN language that is similar to but much less comprehensive than NASTRAN. Identical results have been obtained on comparative running of the two programs. BESTRAN is more commonly used at Hamilton Standard than NASTRAN because of a wide variety of pre- and post-processing methods that are keyed to BESTRAN.

An auxiliary program, ST570, is used for analyzing steady stresses and deflections in rotating structures. It applies to structures that can be modeled as plates or shells of arbitrary shape and thickness. The analysis recognizes centrifugal stiffening effect. There are eleven element types available which include types for isotropic or anisotropic materials. Several blade types have been analyzed using BESTRAN. Detailed comparisons with measured stresses and deflections confirm the applicability of this analysis method.

C. Critical Speeds (BESTRAN)

Every piece of rotating machinery has one or more "critical speeds". This critical speed results from the coincidence of some periodic, speed dependent forcing function and the natural frequency of the machine or some part of the machine. Certainly any bladed rotating device must be examined for critical speeds because of the many modes of resonant vibration the individual cantilevered blades can have and the various ways these blades modes can combine to produce rotor modes. The periodic forcing functions can be mechanical in origin such as gyroscopic precession, unbalance, engine firing torques, etc. or aerodynamic in origin such as an inclined flow field or a distroted flow field which becomes periodic to the propeller as it rotates through it. It is important to note that this discussion does not include "self excited" vibratory response - flutter phenomena. Flutter involves the interaction of the elastic motions of the blade and the aerodynamic loading and is discussed in Section F.

In propellers, the foundation of a critical speed study is the determination of the blade frequencies. Vibratory deflections that meet fatigue strength criteria are small enough so that aerodynamic coupling can be neglected. The hub to tip diameter ratios and the hub geometry is such that blade dynamic response is not influenced by hub dynamics. The blade retention stiffness and blade angle control mechanism stiffness must be considered as well as centrifugal stiffening effects.

The range of blade frequencies that are of interest is determined by the number of periodic forcing functions possible and the strength of those excitations. For Prop-Fans of eight blades or more, excitations up to 5 per revolution are judged to be significant. This judgement is preliminary and will be biased by the configuration and operating regime of each individual installation. Accepting the 5 per revolution judgement as appropriate for this study, all blade frequencies that fall above 5 per revolution at maximum operating speed need not be considered. This can be seen from Figure 5 which is an an example of a standard Campbell Plot. Here the first, second, and third modes would be studied for intersections with integer order exciting frequencies, but the fourth mode would not be considered because there is no critical speed near the operating regime.

The intersection of a blade frequency and an integer order excitation line is studied because it represents the possibility of excitation at resonance where the amplitude of response is limited only by the available damping. The location of the critical speeds can be altered by the possible modes of rotor vibration and the dynamic characteristics of the rotor mounting. Rotor modes can be divided into four basic categories.

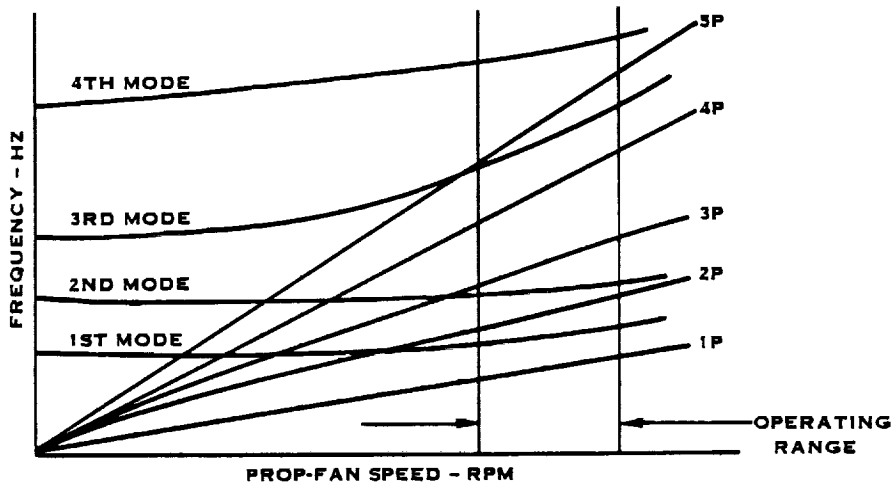

FIGURE 5. CAMPBELL PLOT

1. Those in which the sum of the vibratory out of plane moments on the propeller shaft is zero, but the sum of the forces is finite. This mode is called "symmetrical" and is characterized by in-phase bending of the blades which results in a fore and aft reaction on the rotor mounting.

2. Those in which the sum of the vibratory moments on the propeller shaft is finite, but the sum of the forces are zero. This mode is called "unsymmetrical" and is characterized by a lateral or whirling reaction on the rotor mounting.

3. Those in which neither a vibratory moment nor a vibratory force is transmitted to the rotor mounting. This mode is called "reactionless" since the forces and motions are confined to the propeller; no loads or motions are transmitted to the rotor mounting.

4. Those in which both moments and forces are transmitted to the rotor mounting. This mode can occur only at 1P frequency due to an inclined flow field or gyroscopic action. The 1P mode is unique in that it does not involve resonance although having blade frequencies near 1P will increase the stress response due to inertial magnification.

The above categories only consider the out-of-plane bending and neglect shaft torque effects. The first three categories are illustrated in Figure 6. The third category is of particular interest with eight and ten bladed Prop-Fans. The number of reactionless modes possible for an eight bladed rotor span the range from 2P to 6P, 7P and 9P are whirl modes and 8P is a symmetrical mode. Critical speeds for the first six exciting orders can be accurately predicted from a knowledge of the rotor alone. Critical speeds from 7P to 9P would require a knowledge of the rotor mounting impedance. As mentioned earlier, however, excitations beyond 5P are weak enough to be ignored. With a ten bladed rotor, the reactionless modes extend from 2P through 8P, 9P and 11P are whirl modes and 10P is a symmetrical mode.

The static and rotating blade frequencies can be calculated by beam theory or finite element analytical methods. The beam method will be discussed first.

For the theoretical analysis of the flexural vibration of a propeller blade, it must be constrained so that at some defined location near the center of rotation only uniform rotational motion is possible. This condition of end fixity was chosen to cover both symmetrical and unsymmetrical rotor modes. The system is furthermore assumed to be linear, with small vibratory

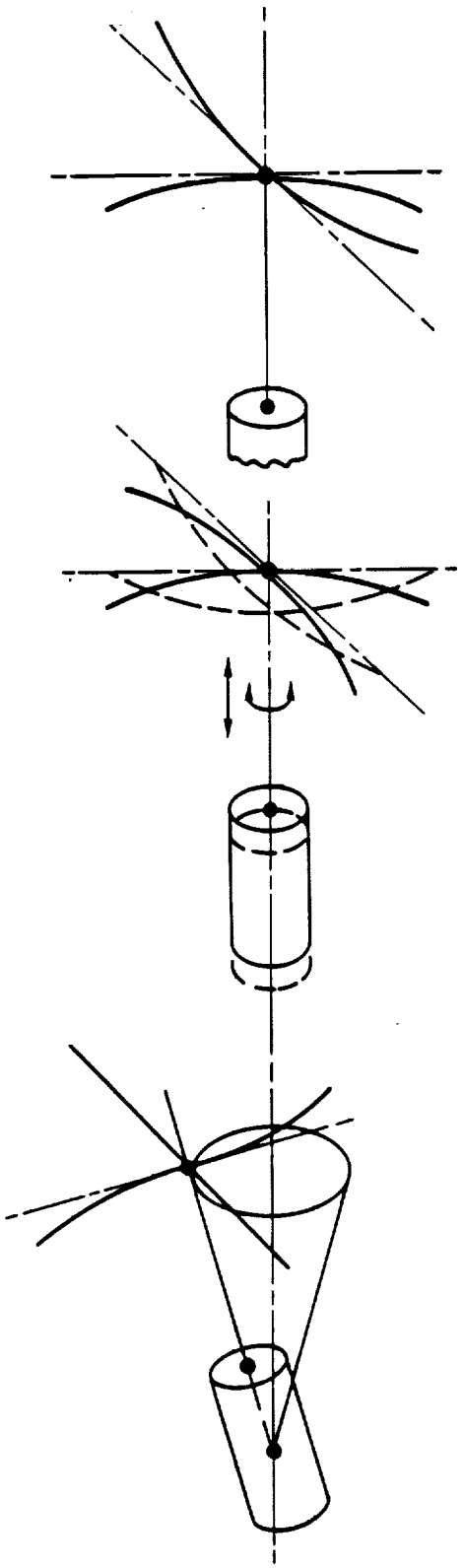

FIGURE 6. ROTOR VIBRATION MODES

displacements, and simple beam bending theory is used. The differential equations of equilibrium are first derived and transformed into integral equations, and they are then examined in the form of a matrix equation for a segmented blade, which permits the evaluation of vibratory response, critical speeds, and normal modes by simple classical methods.

The finite element program used for frequency determination is the same as described in Section III B. An auxiliary program, VIBR, is used that can perform vibration analysis of a wide variety of simple and complex structures. It determines vibratory response in the form of modal displacements for all possible degrees of freedom on systems excited by specified vibratory forces at the nodes or for specified vibratory frequencies. Problems involving bending, longitudinal and torsional vibrations, gyroscopic coupling effects, and combinations of effects can be solved. Resonant frequencies are found by a determinant search. Stress and deflection mode shapes can be generated and plotted out for any of the determinate cross-overs. Twenty-five element types are available to describe the blade which attests to broad based applicability of this analysis.

D. Aerodynamic Excitation (HO39 & HO45)

The primary source of vibratory stresses in a turbine-driven aircraft propeller is the periodic variation in aerodynamic forces caused by asymmetry in the direction and velocity of inflow to the propeller. Such periodic variations in force cause excitations at frequencies which are integer multiples of the propeller speed. These excitations are referred to as "P" orders - 1P, 2P, 3P, etc. The most important of these P-order excitations is the fundamental or 1P because it is, by far, the greatest in magnitude.

The unsymmetrical inflow to the propeller is caused by two major factors; 1) overall misalignment between the thrust axis and the incoming air velocity, and, 2) distortions to the free-stream flow due to the lift on the aircraft wing and distrubances due to flow past the other parts of the aircraft (fuselage, nacelle, etc.). The misalignment or angular inflow causes mostly 1P excitation while the distortions tend to cause both 1P and higher order excitations.

The aerodynamic excitations due to unsymmetric inflow are evaluated by first determining the pattern of flow coming into the propeller for various flight operating conditions. This is done by computerized analysis (H039) which calculates the distrubances caused by the individual structural components of the aircraft (wing, fuselage, nacelle, etc.) and superimposing them to give the total flow field seen by the propeller.

This program has the capability to handle three lifting surfaces (the wing, the pylon, and the tail surface) either separately or simultaneously. The lift for each of these surfaces is predetermined, with the total lift being equal to the aircraft gross weight. The propeller and nacelle can be located anywhere in the flow-field except on the centerline of any of the three lifting surfaces. The flow-field effects analyzed for the lifting surfaces are; circulation due to lift, cross flow and rectilinear flow. The effects of thickness and sweep of the surface are accounted for. The lifting surface velocity components are computed by standard vortex methods that assume the velocity is proportional to the circulation functions and is inversely proportional to radius as given by:

$$v_w = \frac{1}{4\pi} \int_{Sw} \frac{1}{r} d\Gamma$$

and

$$d\Gamma = \frac{dL}{\rho U}$$

where

v_w = Velocity component radius r

r = Radius from the center of the vortex

$d\Gamma$ = Circulation function or vortex strength element

S_w = Surface semi-span

dL = Incremental lift along the span

ρ = Air density

U = Local blade section velocity

The velocity component is determined in the plane of the propeller and assumes an elliptical spanwise lift distribution. The resulting velocity is an integrated effect that includes the bound vorticies as well as the trailing vortex sheet.

The cross flow effect is a flow disturbance caused by the component of the free stream normal to the lifting surface chord passing around the lifting surface planform. The surface is assumed to have an elliptical cross

section and the complex velocity potential is calculated for flow perpendicular to the major axis of the ellipse.

The lifting surface rectilinear flow is a flow distrubance caused by the finite thickness of the surface. The surface is again assumed to have an elliptical cross section and assumes that the chord and thickness are constant. The complex velocity potential is calculated for flow parallel to the major axis.

The flow field effects analyzed for the fuselage and nacelle are cross flow and rectilinear flow.

The cross flow is treated as a complex velocity potential where the equations are solved by treating the body as a number of equivalent cylinders. The potential function is determined by distributing doublets of unknown strength, oriented vertically, along the body axis. The doublet strength is then determined by setting the velocity potential equal to zero on the body surface.

For rectilinear flow, the body is assumed to be an asymetric rankine solid containing a single point source.

For each of the components (wing, fuselage, nacelle, etc.) the velocity perturbation is computed and superimposed on the free stream flow field in the plane of the Prop-Fan. Axial and tangential flow components are then calculated.

These flow components are then input to a multiazimuth airload program (HO45). This program accomplishes aerodynamic strip-analysis calculations at many azimuthal positions to obtain time-history variations of the aerodynamic loads. Harmonic analysis is then performed on these loads and the blade dynamic response is computed for each P-order harmonic.

Since the 1P aerodynamic excitation is the most important by virtue of its magnitude, it is a principal factor controlling the design of a propeller blade. It has been found that the magnitude of the 1P excitation is roughly proportional to the product of the inflow angle and the equivalent airspeed squared. Therefore a parameter called Excitation Factor (EF) was defined as $EF = \psi\left(\frac{Ve}{348}\right)^2$, where ψ is the inflow angle in degrees and Ve is the equivalent airspeed in knots. Excitation Factor is a convenient measure of the severity of 1P aerodynamic excitations, and the manner in which EF varies with flight conditions is an important consideration.

This method was used to estimate the excitations due to the flow fields for Prop-Fan installations on both Douglas and Boeing preliminary design aircraft. The results of these two studies along with a typical application utilizing an under the wing mounted Prop-Fan were used to generate an EF which could be input into our response program, HO26. As such, the results do not represent any one particular aircraft.

E. Response (HO26)

The response of a propeller to periodic unsteady aerodynamic loads as measured by stress or deflection amplitude is determined by four items:

1. The magnitude of the unsteady applied air loads.

2. The total stiffness of the blade which must include the centrifugal enhancement of the static stiffness.

3. The instantaneous elastic angular deflection of the blade since it is a first order influence on the angle of attack of the distributed airfoil sections. Bending motions and cross sectional distortion also affect the thrust and torque generated by a propeller blade. These latter two distortions are negligibly small because of the inherent stiffness and mass of a propeller blade relative to the magnitude of the cyclic air loads.

4. The proximity of a critical speed to a predominant harmonic of the unsteady airload.

For this study, it is desirable to define an excitation factor which is a measure of the total vibratory excitation, including the nP harmonics. The way a blade responds to nP excitations is dependent upon critical speed locations or nearness to resonance. In order to define an equivalent excitation factor, a magnification factor will be assumed and applied to the nP excitations.

With beam modeling, all four of these effects are handled. The method requires a complete multi-degree of freedom model of the rotating blade and a harmonic description of the unsteady air loading. The air loads are applied with proper periodicity as distributions of thrust and torque forces along the blade radial span. The twist deflections are iterated until equilibrium is achieved. The resulting modified radial airload distribution is then used to calculate the bending moments in the rotor coordinate and local blade coordinate systems. The moments are modified by applying a dynamic magnification factor based on the proximity of the harmonic content of the

unsteady loading and the critical speeds. This modified moment distribution is used to calculate blade deflection and stressing. The blade root moments and shear forces are also summed at the rotor attachment to predict rotor hub and attachment loadings.

The use of a finite element model of the blade results in a more exact description of the blade structure but the interaction of this model with the applied airload is not as well modeled as with the beam approach. This is not an inherent limitation of the finite element approach, the methodology has not yet been developed. For this study, the moments and forces as defined at the appropriate nodes along a line representing the center of pressure for each radial airfoil section will be represented by distributed loads across the respective blade chords. Stresses and deflections will be calculated for each load case and the maximum difference anywhere in the airfoil will be determined. This stress range will be combined with the appropriate steady stress and used for the fatigue life determination.

F. Flutter (F214 and F203)

In the past, flutter in the classical sense, has not been a problem for conventional propeller designs and conventional operating conditions. The Prop-Fan, however, with its high activity factor operated at dynamic pressures much greater than those found in the conventional propeller environment. The Prop-Fan also has more blade sweep and smaller thickness ratios than conventional propellers. These reduced thickness ratios may result in a reduction in stiffness without an equivalent reduction in airloads. Consequently, there is more concern with regard to blade stability. For this design study, both stall and classical flutter will be investigated using the recently developed stability analysis, F203. The analysis has a linear normal mode complex eigenvalue solution, which provides total damping at high subsonic Mach numbers on a single blade. The initial structural representation can be depicted by BESTRAN or NASTRAN finite element methods, where the response is described by modal deflections, modal frequencies and modal mass for each element. The modes are fully coupled and can be adjusted to account for steady displacements caused by the steady airloads defined by the blade aerodynamic load program, H444.

The flutter analysis, F203, requires that the structural description be transformed to a beam type coordinate system defined at the blade section where the modes are described in three dimensions. Since this is a linear analysis with the definition of the coordinate system as defined above, the inertial and centrifugal effects at large thrust and blade angles can be better approximated.

The transformation is accomplished in a preprocessor (F214) which uses the output from BESTRAN or NASTRAN and creates an input file for the flutter analysis.

The equations of motion are generalized in a normal modes approach and are fully coupled. The forcing functions which include quasi-steady and unsteady functions, the effective mass, damping and stiffness terms are generated using linear aerodynamics.

The quasi-steady terms are developed from the vibratory displacements and are provided in tables developed by Jordan, REF.1, along with the unsteady terms. These tables have been modified by methods similar to those used by Cunningham, REF.2, to account for sweep effects. The unsteady aerodynamics, including phase lag terms, are developed as a function of reduced frequency. Prandtl-Glauret corrections are applied to the lift and moment slopes to account for compressibility effects. Cascade effects are also included in this analysis in accordance with the theory of REF.3.

The solution is a linear complex eigenvalue one solved by the P-K method of REF.4. The aerodynamics are a function of frequency, and simultaneously have a strong effect on modifying the response frequency of the blade. Consequently, it is necessary to iterate the solution as it is modified by the aerodynamics. The results of the above methods produce the complex eigenvectors (or frequencies), and damping for all modes.

By applying Steinman's theory, REF.5, a method of approximating the aerodynamic forces and phase lag in the stalled region was obtained. The resulting new terms are then substituted for some of the aerodynamic terms in the present analysis, and the solution is carried out using the above mentioned methods. The Steinman aerodynamics uses the local lift and moment curve slopes. In our present analysis, the local lift and moment curve slopes are computed using the Hamilton Standard strip analysis program H444, so that the real aerodynamic effects will be considered.

Additionally, an energy approach to the structural response was also developed as a solution to the Steinman aerodynamics. Options are available to allow use of one or all of the above mentioned methods.

For all the options, the output is in the form of damping and eigen frequencies which are plotted as functions of airspeed, RPM, blade angle and altitude. The flutter boundaries can be determined from the points where the damping goes through zero. It is at these points where the response becomes unstable.

If the flutter boundary occurs outside the flight envelope, classical flutter will not be present. If the value of horsepower, obtained at the point where the damping ratio goes to zero, is larger than the power available, then stall flutter will not occur.

G. Foreign Object Damage Analysis (H750/H910)

The evaluation of foreign object impact resistance involves three steps:

1. The definition of the impact conditions;

2. The determination of the gross impact loads, blade response, and blade stressing from the gross structural blade characteristics; and

3. The determination of local stressing based on detailed local stress analysis.

The first step is fundamental to all of the blade designs since it depends only on the engine characteristics, size and density of the foreign object, the airspeed, and the radial impact position on the blade. For this program, the operating condition which previous analyses have shown to be the most severe will be used. A preprocessor determines the penetration of a cylindrical mass (representing the object) into the plane of the rotor and thus defines the fundamental impact parameters of size, weight, velocity and angle of impact of the slice of the ingested foreign object, which are needed for the second step of the analysis.

Having defined the impact conditions, the gross blade impact load, response, and stressing with time will then be calculated using the 3 dimensional (3 mode) computer program, H750/H910. The data stored in the SHEDS system for the blade designs are the structural characteristics that are used by H750/H910 in the FOD analysis.

The Three-Mode-Interactive Blade Impact Program utilizes a fluid missile model which is interactive with the dynamic modal response of the blade. This feature is essential to the analysis of FOD impacts, since the changing impact angle due to blade twist, the physical size of the missile, the changing rate at which it spreads on the blade surface during the impact event and the spreading mass thickness distribution have a large influence on blade response. The three-mode analysis uses the three beam-type modes of vibration to characterize the gross blade dynamics; i.e., the first flatwise bending, the first edgewise bending and the first torsional modes. Although

coupling between blade modes is accounted for in the dynamic characteristics input to the three-mode analysis, only the dynamic response of the blade flatwise and torsional modes are coupled in the impact. This makes the calculated blade response stresses slightly conservative.

The accuracy of the analytical methods has been confirmed by several tests. In addition, the pressure distribution as calculated for the fluid missile model used by the three-mode analysis correlates quite well with test data.

After defining the gross blade characteristics, and the resulting impact loads, gross stresses, and response with time for the various impacts, the blade will then be analyzed for local stressing in the impact region. This stress will be calculated using the impact load distribution and magnitude from the gross impact analysis. The gross blade stresses and the local blade stresses are then compared to appropriate material stress allowables and to the foreign object damage limits as defined in the Design Requirements Document to determine if the blade design satisfies all of the specified design requirements.

H. Blade Aerodynamic Design Analysis

For Prop-Fans, which are designed to operate at helical tip Mach numbers between 1.0 and 1.2; the relative velocity between the blade and wake vortex segment may be supersonic. Since the Prop-Fan is basically a rotating wing that creates a helical shaped wake, there are portions of the helix particularly in the near wake, where the Biot-Savart relation does not apply. Since this relation indicates that the near wake contributes most to the induced velocity at the blade, the predicted blade tip induced velocities are therefore lower than they would be for subsonic helical Mach numbers. Consequently higher loads will be carried to the blade tip region, since the induced losses are reduced. A correction is therefore applied to the two-dimensional airfoil data which negates some of the advantages offered by these lower induced losses. This correction lowers the lift and drag coefficients for the airfoils which are within the Mach cone and exhibit helical Mach numbers greater than or equal to one.

I. Acoustic Analysis

The near field noise will be calculated using the Hamilton Standard Prop-Fan noise calculation procedure. This procedure calculates thickness noise, loading noise and guadrupole noise contributions. The levels of five harmonics of blade passing frequency will be calculated for three tip clearances at the maximum noise location (i.e., plane of rotation).

The far field noise for the two propellers will be calculated in terms of EPNL for two operating conditions. This type of calculation will include unsteady loading effects due to angle of attack and wing upwash.

REFERENCES

1. Jordan, P.F., "Aerodynamic Flutter Coefficients for Subsonic, Sonic, and Supersonic Flow (Linear-Two-Dimensional Theory). Rep. No. Structures 141, British R.A.E., April 1953, ARC. R&M 2932-1953.

2. Barmby, J.G., Cunningham, H.J., and Garrick, I.E., "Study of Effects of Sweep on the Flutter of Cantilever Wings," NACA TN 2121, June 1950.

3. Smith, S.N., "Discrete Frequency Sound Generation in Axial Flow Turbomachines", Great Britain A.R.C. R&M No. 3709, 1971.

4. Hassig, Herman, "An Approximate True Damping Solution of the Flutter Equation by Determinant Iteration", J. Aircraft, Vol. 8, No. 11, November 1971.

5. Steinman, D.B., "Aerodynamic Theory of Bridge Oscillations," American Society of Civil Engineers Transactions, Paper No. 2420, October 1949.

UNITED TECHNOLOGIES HAMILTON STANDARD

IV. DESIGN REQUIREMENTS

A. Configurations

The configuration which will be structurally analyzed is listed in the following table.

BLADE DEFINITION

	SR-7
Tip Speed (ft/sec)	800
Tip Diameter (feet)	9
Number of Blades	8
Tip Sweep (degrees)	35.7
Activity Factor	227

B. Operating Conditions

This section defines the operating conditions to be used during the design study.

1. Load Spectrum

Condition	Altitude	Airspeed	SHP	Fan rpm
Min Climb	Seal Level	0.2Mn	6000	1698
Cruise	35,000 feet	0.8Mn	2592	1698
40% O'speed	35,000 feet	0.8Mn	0	2377

2. Foreign Object Damage

The foreign object damage analysis will be conducted at the take/off climb condition.

3. Excitation Factor

The maximum excitation factor was determined to occur at the following condition:

Condition	Altitude	Airspeed	Gross Weight
Climb	Sea Level	190 Knots	250,000 lbs.

4. Centrifugal Twisting Moment

The centrifugally induced twisting moment at the blade root about the blade retention bearing centerline will be calculated at maximum rated speed as a function of blade angle setting. This will permit scaling for other operating speeds and blade angles by the relationships discussed in Section III B.3. This twisting moment must be combined with aerodynamic and friction twisting moments in order to size the blade angle control mechanism.

5. Overspeed

All elements of the rotating propeller will be designed to withstand 125% overspeed or 150% centrifugal load with no inelastic deformation.

All elements of the rotating propeller will be designed to withstand 140% overspeed or 200% centrifugal load. This includes the blade, retention, disc, and blade angle control mechanism. Local inelastic deformation will be permitted in all of these elements at this overspeed but the propeller will be capable of changing pitch after exposure to 140% overspeed.

6. Flutter

The classical flutter boundary will be computed using the methods previously described for various operating conditions. The requirements are defined to be:

a. The calculated flutter Mach number must be greater than the flight profile given in the LAP RFP (Exhibit A, Figure 1).

b. At 14,000 ft. altitude, the calculated flutter Mach number must be greater than 0.8 at a test rig horsepower and RPM equivalent to the design power coefficient and advance ratio to allow testing in the Modane wind tunnel.

Stall flutter will be calculated for various horsepowers and propeller rpms.

7. Aerodynamic Loads

The aerodynamic loads will be determined for the conditions listed in IV B.1.

8. Mechanical Loads

a. Steady Tension

The steady tension loads will be determined at 100%, 125%, and 140% of maximum rated speed.

b. Steady Bending

The centrifugally induced steady bending loads will be determined at 100%, 125%, and 140% of maximum rated speed. The aerodynamically induced steady bending moment will be determined at maximum rated thrust and 100% speed only. Propeller overspeeds are generally associated with a loss in thrust due to a blade angle fault or application of negative torque, so that centrifugally induced bending moments are dominant at 125% and 140% overspeed conditions.

c. Steady Untwist

The centrifugally induced steady untwist stresses will be determined at 100%, 125%, and 140% of maximum rated speed. The aerodynamically induced twisting loads will be determined at maximum rated thrust and 100% speed only. The centrifugal loads would be dominant at the overspeed conditions.

d. Other

Other loads are present but, particularly for large commercial transport aircraft, the load limits set by the airframe and passenger comfort keep the resulting propeller stressing well within the capacity of the propeller. These loads include: gyroscopic, hard landings, gusts, etc.

C. Critical Speed Margins

The aerodynamically induced cyclic loads during crosswind operation on the ground are commonly more severe than experienced when the aircraft has forward airspeed. For the 2P excitation, the ground operation critical speed margin shall be a minimum of 20% of propeller speed and resonant frequency. The flight margin shall be a minimum of 10% of propeller speed and resonant frequency. This margin shall be reduced inversely as the exciting order is increased from 3P to 5P. No 1P critical speeds shall be

permitted in the propeller operating speed range and the minimum margin shall be 40% of maximum propeller operating speed. In determining these margins, the effect of blade angle on frequencies will be included.

D. Aerodynamic Excitations

The equivalent design 1P Excitation Factor (EF) will be 4.5. The basic EF due to 1P only is 3.30.

Normally, EF is only used as a measure of the 1P excitation. However, for design purposes it is desirable to define a quantity which is a measure of the total vibratory excitation, including the nP harmonics. The way a blade responds to nP excitations is dependent upon critical speed locations or nearness to resonance.

For simplicity, an equivalent design excitation factor was defined for the Prop-Fan, assuming a magnification factor of 1.0 for the 1P excitations and 3.0 for the nP excitations. The relative magnitude of the 1P and nP excitations, based on a typical installation, was therefore assumed to be:

	Relative Magnitudes	
Excitation Order	Unmagnified	Magnified
1P	1.00	1.00
2P	0.125	0.375
3P	0.037	0.111
4P	0.016	0.048
5P	0.008	0.024

Additionally, the higher orders were added in the worst vectorial phasing, which is inherently conservative for design purposes.

Comparisons made between measured and calculated 1P response stresses have shown a lack of correlation for swept blades. Since the measured stresses were higher than those calculated, a correction factor is being applied to the calculated values. Additionally, since the estimated effective stress obtained using NASTRAN is greater than that obtained using BESTRAN, a second correction factor is also being applied to the calculated values. The resultant correction factor, which is to be applied to the 1P stresses only for the SR-7 design, is indicated in Figure 7.

E. Distortion Criteria

During normal operation a propeller blade distorts elastically due to steady and cyclic loads. The cyclic deformations are small as compared with a helicopter blade, small enough so that accurate structural response can be determined without inclusion of aeroelastic coupling for all cyclic excitations except that at 1P frequency. At 1P frequency the aeroelastic effects commonly are less than 10% of the basic loading. Consequently, the elastic distortions due to cyclic loading will not be evaluated. Due to steady loads a propeller blade can change diameter, sweep, offset, twist and camber. Width and thickness changes are insignificant. Of these five geometric changes, only offset variations have no aero-acoustic effect. The magnitude of the other four distortions will be determined to permit comparisons between construction concepts.

No absolute limits will be set on distortion, other than those implied by stress and buckling limits. The acceptability of distortions within the stress and buckling limits should be determined by their affect on aero/acoustic performance over the operating range. In this program, the distortions will be used as an evaluation of the fabrication concept.

F. Flutter Margins

To provide a safety margin, classical flutter should clear the Modane test point of 14,000 ft. and the conditions of B6 above, with the blade natural frequencies degraded by 15% at all operating RPM's up to 105% of the normal maximum.

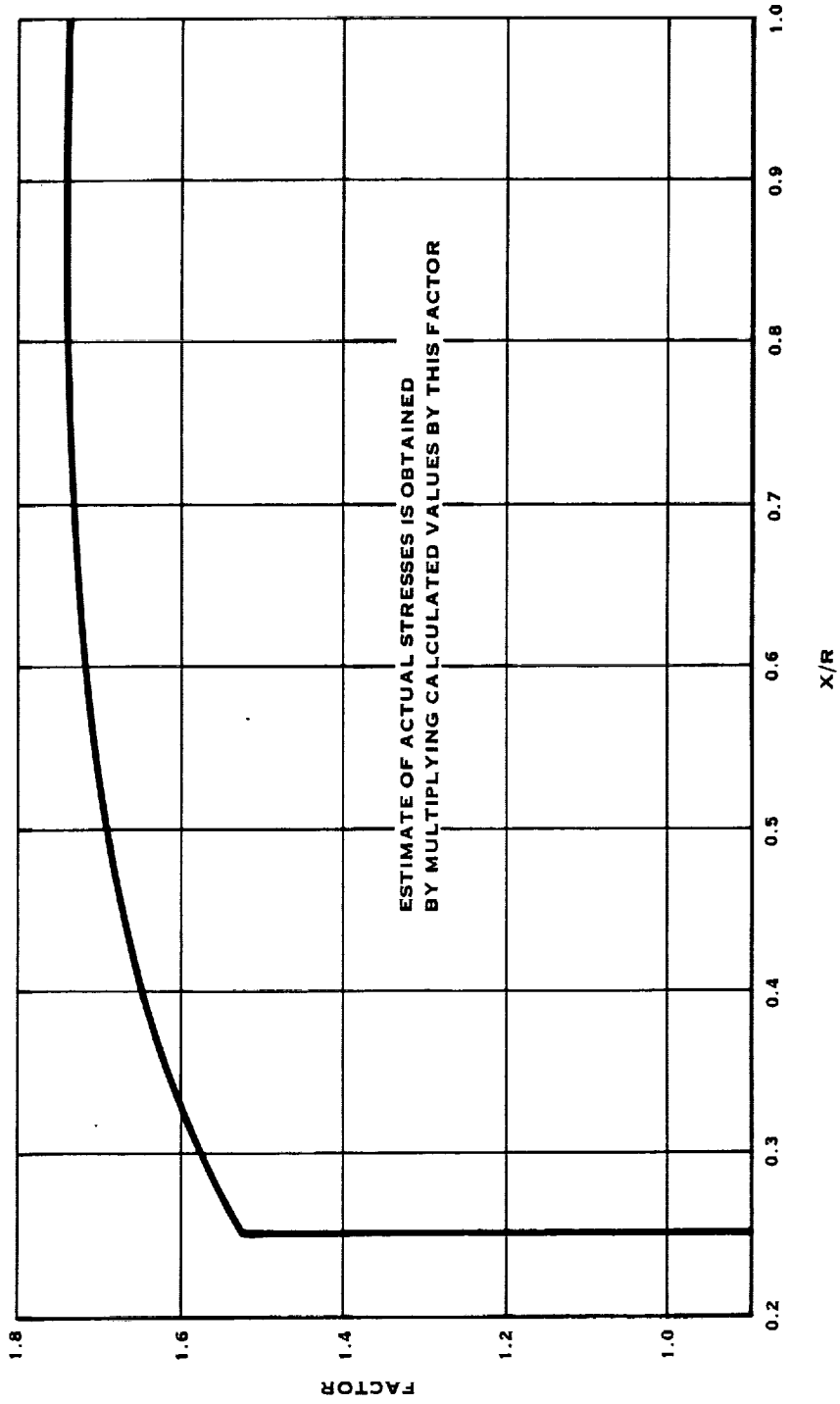

FIGURE 7. SR-7 1P STRESS CALCULATIONS USING BESTRAN

G. Stress Margins

The combined steady and cyclic stresses will be plotted on modified Goodman Diagrams for the materials of construction. The strength boundaries will represent a high probability of survival derived from experimental data on specimens and full scale structures. As a minimum, the boundaries will represent $\bar{x} - 3.5\sigma$ lines. The start-stop stress range will be reflected against a boundary for a life of 150×10^3 cycles. The high cycle combined stresses will be reflected against a boundary for 100×10^6 cycles or infinite life.

The maximum elastic (nominal x k_T) stressing due to a 120% overspeed and the nominal stressing due to a 140% overspeed will be kept below the 0.2% offset yield strength for homogenous metal materials. The change in elastic modulii will be kept below 5% for fiber reinforced resin material regarding these same overspeed requirements.

H. Features

1. Repairability

Consideration will be given to the use of materials in the blade which can be repaired in the field in the event of minor damage in service.

2. Replacement

The blade retention design will allow for the replacement of a single blade in a Prop-Fan assembly while installed on an engine.

3. Leading Edge Protection

The outer portion of the blade leading edge will be protected with a partial chord width metal sheath.

4. Lightning Protection (FAR part 25.581)

Lightning protection will be incorporated in the blade.

5. Ice Protection (FAR part 25 appecdix C)

The inner portion of the blade leading edge will contain an electric heater. However, the heater will not be connected and will therefore not be functional. The heater is present to allow evaluation of its effect, if any, on structural integrity.

6. Life and Reliability Goals

The blade will be designed for the following goals:

Maximum Continuous Stress Level	Infinite Life
Replacement Life	35,000 hours
Mean Time Between Unscheduled Blade Removals (8 blade set) (inherent)	50,000 hours

V. DESIGN GOALS

A. Stall Flutter

The propeller shall be free of stall flutter up to 100% of take-off power at 100% design speed for forward thrust, and up to 20% of take-off power at 100% design speed for reverse thrust.

B. FOD Criteria

The foreign objects are classified into three categories as follows: minor, moderate, and major impacts. Major and moderate impacts correlate with Group I and II definitions in FAR Advisory Circular 33-1B dated April 22, 1970. Minor impacts include sand, small stones, and birds up to about four ounces. Moderate impacts include two inch hailstones and birds up to two pounds. Major impacts include a single bird up to four pounds. The damage criteria are as follows:

Minor Impacts - No damage allowed to basic blade structure. Operation will continue without impediment.

Moderate Impacts - Damage can include loss of material or airfoil distortion. Operation shall continue at 75% power minimum for five minutes. No metal fragments shall be lost which can penetrate the aircraft fuselage pressure shell. Roughness shall be tolerable and as a guide, rotor unbalance force shall be kept below 5,000 pounds.

Major Impacts - Damage can include loss of material or airfoil distortion. Ability to feather the propeller must be maintained. A shutdown must be accomplished without catostrophic effects on airframe structure. As a guide, the rotor unbalance force shall be kept below 25,000 pounds. No metal fragments shall be lost which can penetrate the aircraft fuselage pressure shell.

APPENDIX E

DESIGN SELECTION DOCUMENT

FOR NASA LeRC

NAS3-22394

NOVEMBER, 1983

HAMILTON STANDARD

DIVISION OF UTC

WINDSOR LOCKS, CONNECTICUT

INTRODUCTION

In response to predicted energy shortages with the associated rising aviation fuel costs, NASA has sponsored studies of fuel conserving aircraft and propulsion systems since 1975.

One of these propulsion systems, Prop-Fan, is a small diameter, highly loaded, multibladed, variable pitch advanced turboprop. Because of the high speed flight regime of the Prop-Fan with cruise Mach numbers in the region of 0.7 to 0.8; the blades, spinner and nacelle must be carefully integrated to minimize the adverse effects of compressibility.

In various studies, the Prop-Fan has been found to offer significant reductions in fuel burned and direct operating cost when compared to turbo-fan powered aircraft. In view of the attractive fuel savings potential of the Prop-Fan propulsive system, NASA has included the Advanced Turboprop Project as part of the of the Aircraft Energy Efficiency Program.

As a result of this study project, the seventh of a series of single rotation (SR) Prop-Fans has been investigated and designated SR-7. The previous models, the SR-1, SR-1M, SR-2, SR-3, SR-5 and SR-6 have been tested in the NASA Lewis 2.44 by 1.83 M (8 x 6 ft.) supersonic wind tunnel. Each has been designed for a 0.8 Mach number cruise condition and an altitude of 10688 M (35000 ft.). Two of the models, the SR-1 and SR-2 were previously tested in the United Technologies Research Center's (UTRC) 2.44 M (8 ft.) high speed wind tunnel.

All of the previous models were designed to a specified tip speed and power loading. In designing the SR-7, the tip speed and power loading combination was selected to yield minimum fuel burned for a selected aircraft and mission.

This document describes the selection process that was used to define the SR-7 blade configuration for the Large Advanced Propeller (LAP) program.

- THE OBJECTIVES OF THE SR-7 TRADEOFF STUDY WERE TO PROVIDE A BASIS FOR SELECTION OF A PROP-FAN CONFIGURATION FOR USE ON A FULL-SIZE TRANSPORT, AND TO PROVIDE A SCALABLE PROP-FAN CONFIGURATION FOR A FLYING TESTBED.

- A SURVEY OF PUBLISHED LITERATURE AND AIRLINE, AIRFRAME AND ENGINE MANUFACTURER OPINION WAS REVIEWED TO DEFINE AN AIRCRAFT AND MISSION FOR THE SR-7 DESIGN, (FIGURE 1).

SR-7 DESIGN STUDY
BASELINE AIRPLANE

(Used in A/A tradeoff study, provided through NASA)

• Configuration	Low wing, twin
• Cruise mach no	0.80
• PAX	120
• TOGW	120,900 lbs
• OEW	80,900 lbs
• Design range	1200 nmi
• Study mission	500 nmi at 60% load factor
• Engine	Scaled STS 589-4
• Block fuel	4500 lbs (study mission)
• DOC	4.05¢/seat mi (study mission) at $1.50/gal fuel

FIGURE 1.

- THE TRADEOFF STUDY WAS CONDUCTED AT THIS CRUISE CONDITION BY VARYING BLADE GEOMETRIC PARAMETERS TO ESTABLISH THE PROP-FAN CONFIGURATION RESULTING IN THE MINIMUM AIRCRAFT FUEL BURNED AND DIRECT OPERATING COST. EACH BLADE DESIGN PARAMETER WAS EVALUATED RELATIVE TO A BASELINE BLADE. PARAMETERS STUDIED INCLUDED TIP SPEED, POWER LOADING, BLADE NUMBER AND DISTRIBUTIONS OF BLADE SWEEP, THICKNESS RATIO, PLANFORM, DESIGN LIFT COEFFICIENT, TWIST AND BLADE STACKING (DEFINED AS THE THREE-DIMENSIONAL HALF-CHORD LOCATION). (FIGURE 2.)

SR-7 TRADEOFF STUDY ~ BASIC MATRIX

Case no	Parameter	Tip speed	SHP/D^2	B	Λ	h/b	Planform	Des. C_L	Twist	Stacking line
1	Baseline	800	37.5	8	40°	TI	Baseline	Baseline	Baseline	On helix
2	Tip speed & SHP/D^2		30.0							
3			26.0							
4		700	37.5							
5			30.0							
6			23.0							
7		600	30.0							
8			26.0							
9			20.0							
10		850	37.5							
11			30.0							
12			26.0							

FIGURE 2.(CONTINUED)

SR-7 TRADEOFF STUDY ~ PARAMETER MATRIX

(CONTINUED)

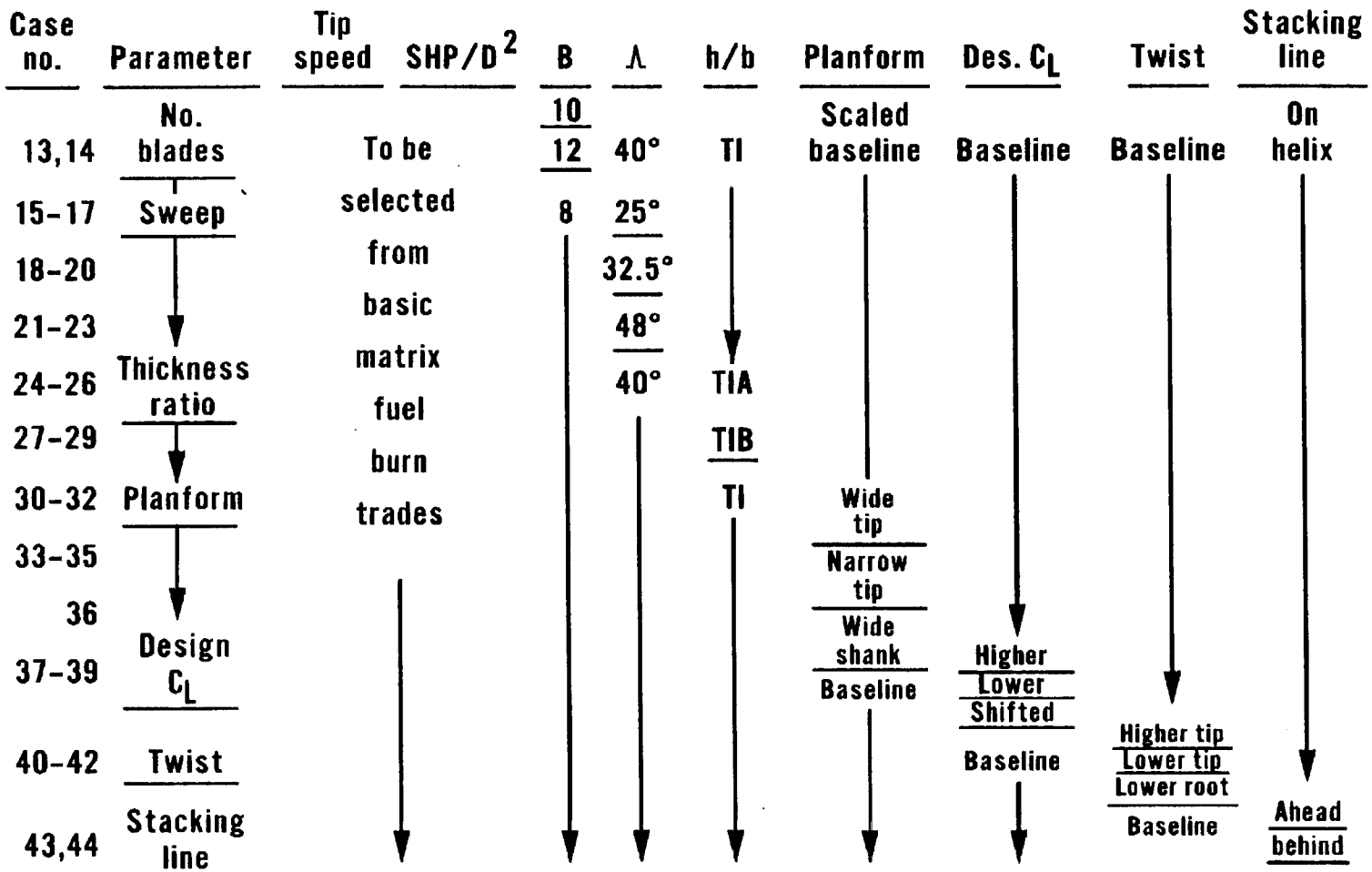

FIGURE 2.

- GEOMETRIC PARAMETERS THAT WERE MOST IMPORTANT IN INFLUENCING AIRCRAFT FUEL BURNED AND DIRECT OPERATING COST WERE BLADE NUMBER, SWEEP ANGLE, BLADE THICKNESS RATIO AND BLADE PLANFORM. (FIGURE 3.)

#	Case	Tip Speed M/S	Power Loading, kW/M²	Tip Speed Ft/Sec	Power Loading, HP/Ft²	No. Blades	Blade Tip Sweep, Deg	Thickness Ratio	Planform	Design Lift Coefficient	Twist	Stacking Line Related to helix	Net Efficiency	Peak Noise dB-BPF	Δ Fuel Burned Improvement, %	Δ Direct Operating Cost Improvement, %
—	Baseline	243.8	256.9	800	32	8	39.6	T1	Baseline (AF = 238)	Baseline (C_{L_i} = 0.214)	Baseline	On (Y/R_{tip} = 0.200)	0.796	143.2	0.00	0.00
—		259.1	264.9	850	33	8	39.6	T1					0.796	143.6	0.43	0.31
—		213.4	224.7	700	28	8	39.6	T1					0.790	140.2	-1.43	-0.80
13	Blade number	243.8	256.9	800	32	10	39.6	T1					0.804	141.0	2.92	1.80
14	Blade number	243.8	256.9	800	32	12	39.6	T1					0.811	139.2	4.81	2.92
15	Sweep	259.1	264.9	850	33	8	25.0	T1					0.776	147.8	-5.16	-2.99
16	Sweep	243.8	256.9	800	32	8	25.0	T1					0.765	147.7	-4.32	-2.78
17	Sweep	213.4	224.7	700	28	8	25.0	T1					0.786	146.8	-5.90	-3.94
18	Sweep	259.1	264.9	850	33	8	32.5	T1					0.785	146.2	-2.75	-1.57
19	Sweep	243.8	256.9	800	32	8	32.5	T1					0.790	145.8	-2.25	-1.44
20	Sweep	213.4	224.7	700	28	8	32.5	T1					0.786	144.3	-3.98	-2.55
21	Sweep	259.1	264.9	850	33	8	48.0	T1					0.803	138.7	3.17	2.06
22	Sweep	243.8	256.9	800	32	8	48.0	T1					0.796	138.5	1.76	1.28
23	Sweep	213.4	224.7	700	28	8	48.0	T1					0.787	139.3	-1.53	-0.77
24	Thickness ratio	259.1	264.9	850	33	8	39.6	T1A					0.775	143.8	-2.97	-1.33
25	Thickness ratio	243.8	256.9	800	32	8	39.6	T1A					0.774	143.2	-3.44	-1.62
26	Thickness ratio	213.4	224.7	700	28	8	39.6	T1A					0.768	142.8	-5.68	-3.02
27	Thickness ratio	259.1	264.9	850	33	8	39.6	T1B					0.736	143.7	-8.99	-4.15
28	Thickness ratio	243.8	256.9	800	32	8	39.6	T1B					0.736	143.2	-9.42	-4.44
29	Thickness ratio	213.4	224.7	700	28	8	39.6	T1B					0.729	141.7	-11.60	-5.77
30	Planform	259.1	264.9	850	33	8	39.6	T1	Wide tip (AF = 258)				0.791	144.1	-0.81	-0.37
31	Planform	243.8	256.9	800	32	8	39.6	T1					0.795	143.3	-0.30	-0.18
32	Planform	213.4	224.7	700	28	8	39.6	T1					0.794	141.3	-1.47	-0.98
33	Planform	259.1	264.9	850	33	8	39.6	T1	Narrow tip (AF = 217)				0.799	144.4	0.66	0.34
34	Planform	243.8	256.9	800	32	8	39.6	T1					0.799	142.7	1.82	0.58
35	Planform	213.4	224.7	700	28	8	39.6	T1					0.784	140.4	-2.15	-1.12
36	Planform	243.8	256.9	800	32	8	39.6	T1	Wide shank (AF = 240)				0.788	143.2	-1.22	-0.58
37	Design lift coefficient	243.8	256.9	800	32	8	39.6	T1	Baseline	Higher C_{L_i} = 0.273			0.788	143.2	-1.22	-0.58
38	Design lift coefficient	243.8	256.9	800	32	8	39.6	T1		Lower C_{L_i} = 0.163			0.794	142.2	-0.14	0.19
39	Design lift coefficient	243.8	256.9	800	32	8	39.6	T1		Shifted peak C_{L_i} = 0.171			0.792	143.4	-0.66	-0.34
40	Twist	243.8	256.9	800	32	8	39.6	T1		Baseline	Higher tip		0.784	145.5	-3.05	-1.78
41	Twist	243.8	256.9	800	32	8	39.6	T1			Lower tip		0.776	142.3	-2.72	-1.17
42	Twist	243.8	256.9	800	32	8	39.6	T1			Higher shank		0.783	142.8	-1.76	-0.78
43	Stacking line	243.8	256.9	800	32	8	39.6	T1			Baseline		0.795	144.3	-0.61	-0.44
44	Stacking line	243.8	256.9	800	32	8	39.6	T1				Off (Y/R_{tip} = 0.097)	0.800	145.9	-0.75	-0.76
45		243.8	256.9	800	32	10	48.0	T1				Off (Y/R_{tip} = 0)	0.804	139.4	3.37	2.13
46		243.8	256.9	800	32	10	25.0	T1				On	0.794	147.5	-1.46	-1.02
47		243.8	256.9	800	32	10	39.6	T1A					0.784	140.7	-0.20	0.36
48		243.8	224.7	800	28	10	32.5	T1					0.803	145.4	-0.08	-0.25
49		243.8	256.9	800	32	10	0.0	T1					0.784	150.4	-5.04	-3.26
50		243.8	256.9	800	32	8	36.0	T1 MOD	Narrow tip	Lower		Off (Y/R_{tip} = 0.096)	0.791	143.9	-0.75	-0.41
51		243.8	256.9	800	32	8	36.0	T1 MOD	Baseline	Baseline			0.794	144.2	-0.52	-0.35

FIGURE 3

- FOR THE RANGE OF BLADE NUMBER STUDIED, EIGHT TO TWELVE, TWELVE BLADES YIELDED THE LOWEST FUEL BURNED. TIP SWEEP ANGLE WAS VARIED BETWEEN 0 AND 48 DEGREES. THE HIGHEST SWEEP STUDIED PERFORMED BEST. INCREASING BLADE THICKNESS RATIO CAUSED SEVERE INCREASES IN FUEL BURNED AND DIRECT OPERATING COST. FOR THE BLADE PLANFORMS STUDIED, A NARROWER TIP CHORD PROP-FAN WAS THE BEST DESIGN. (FIGURES 4-7.)

EFFECT OF NO. OF BLADES ON FUEL AND D.O.C.

Base = 8 Blades, 32 shp/D^2, 40° sweep, 800 fps

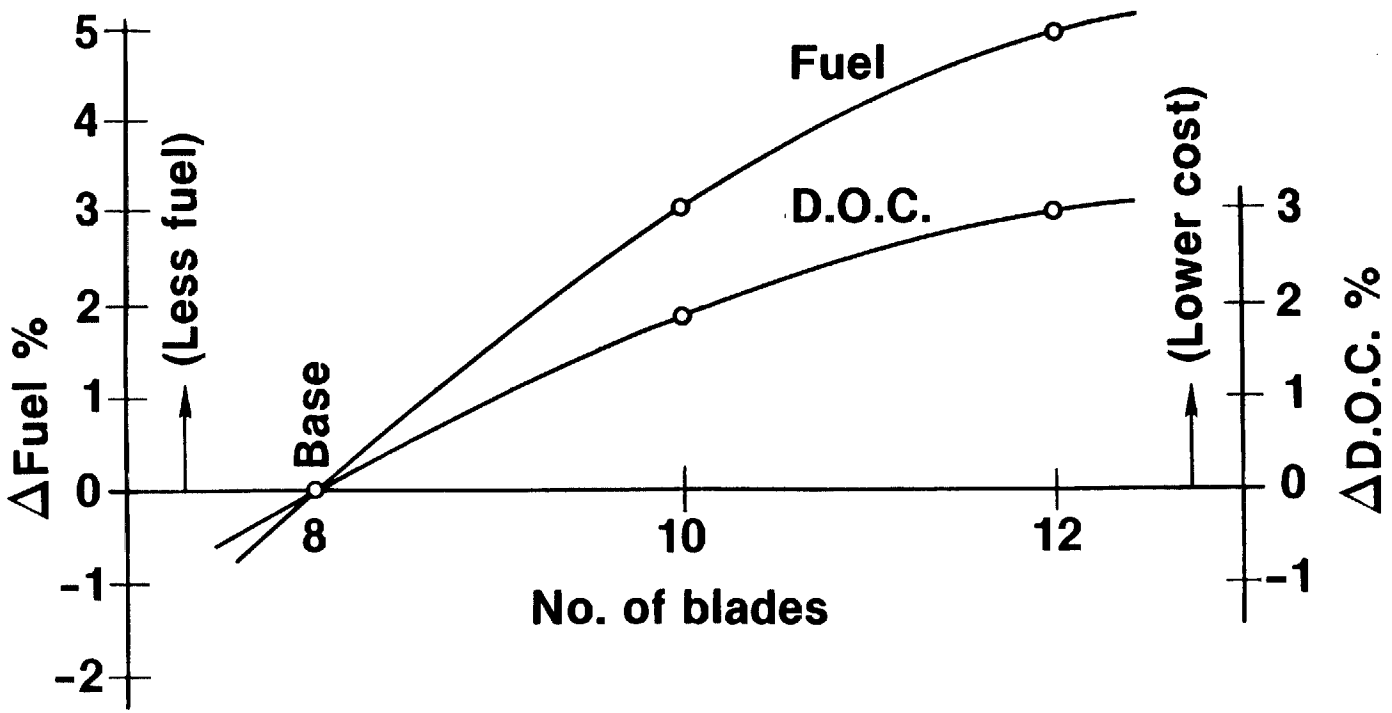

∴ More blades beneficial

FIGURE 4

EFFECT OF SWEEP ON FUEL & D.O.C.

Base = 8 Blades, 32 shp/D^2, 40° sweep, 800 fps

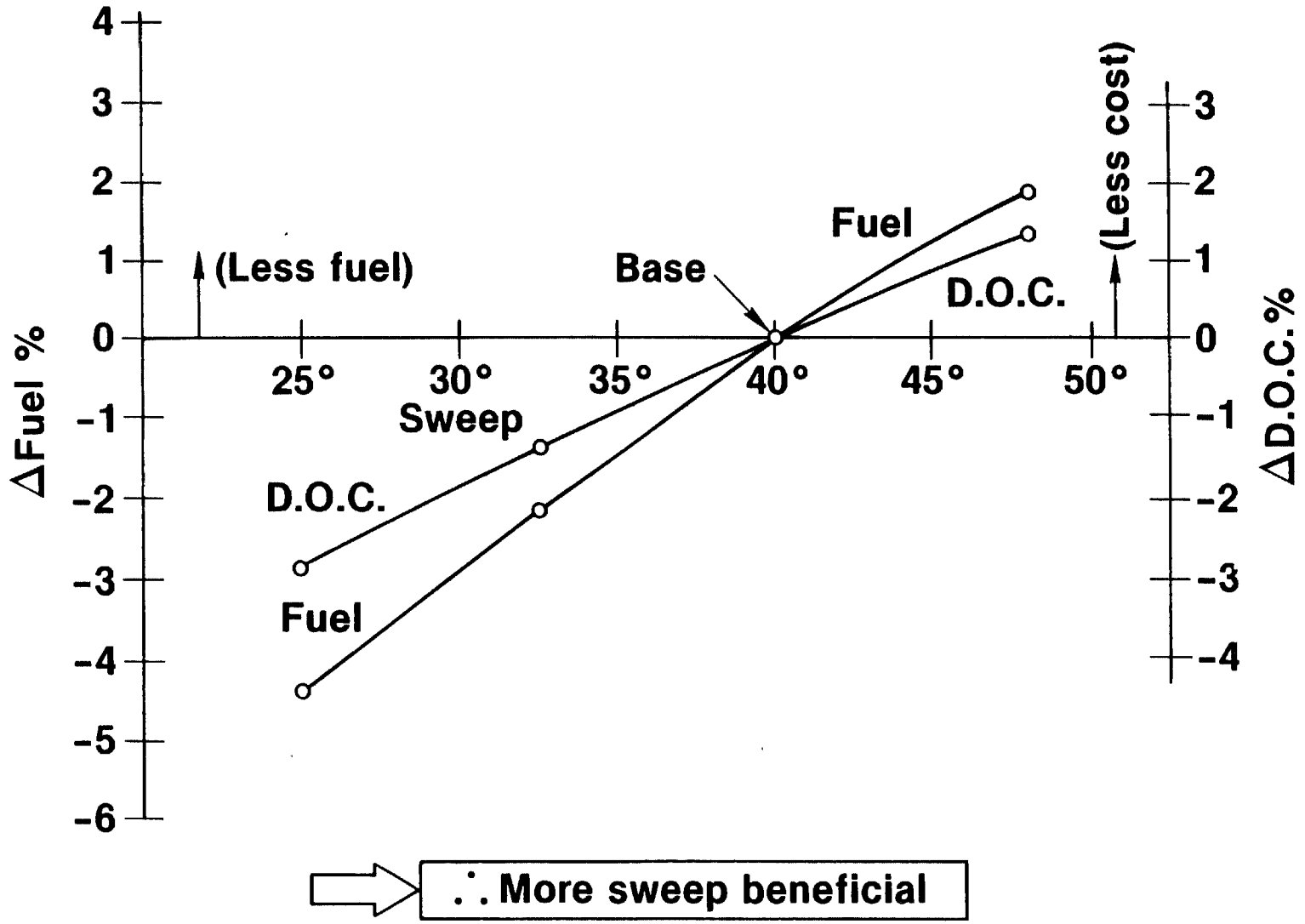

FIGURE 5

EFFECT OF BLADE THICKNESS ON FUEL AND D.O.C.

Base = 8 blades, 32 shp/D^2, 40° sweep, 800 fps

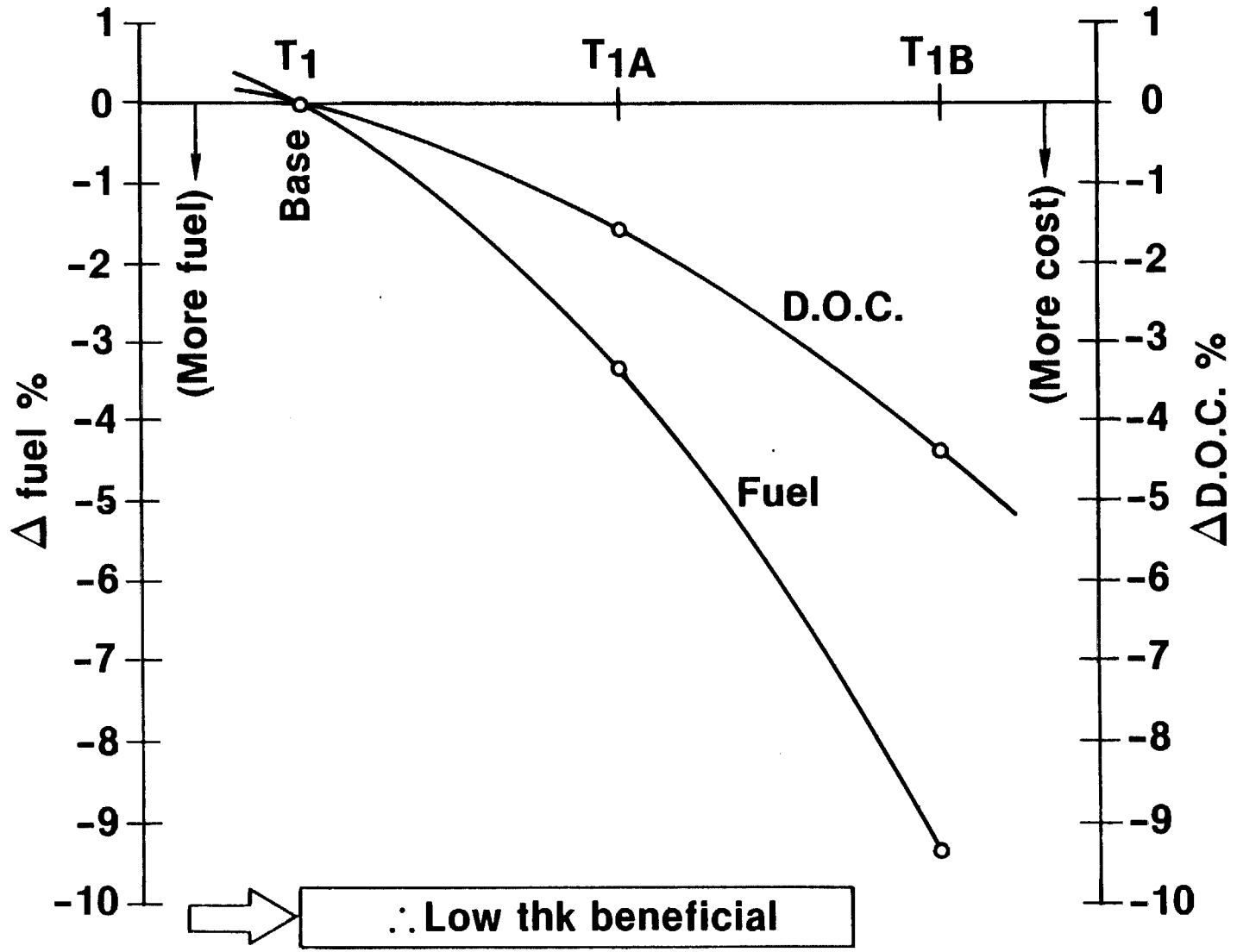

FIGURE 6

ECONOMIC STUDY SUMMARY

- More blades beneficial
- More sweep beneficial
- Low thickness beneficial
- Narrow tip chord beneficial
- Restacking has minimal effect

FIGURE 7.

- AERO/ACOUSTIC STUDY RESULTED IN THE INDICATED TRADEOFF STUDY BLADE BASED UPON 51 ITERATIONS WITH RESPECT TO PERFORMANCE. (FIGURE 8.)

- THE TRADEOFF STUDY REVEALED THAT THINNESS, INCREASED SWEEP, AND INCREASED NUMBER OF BLADES WAS GOODNESS.

TRADE OFF STUDY

	Baseline	A/A tradeoff study
Diameter (ft)	9.0	9.0
No. of blades	8	12
Activity factor	238	158.7
Integrated design C_L	0.214	0.214
Tip sweep (deg)	39.6	48.0
Blade layout	On helix	On helix

FIGURE 8.

- A FULL SCALE BLADE STUDY OF AN SR-5 (10 WAY), SR-3 (8 WAY, Λ = 39.6°), and SR-3 (10 WAY) INDICATED ALL HAD INADEQUATE FLUTTER MARGINS.

- TRADEOFF STUDY RESULTS WERE TEMPERED, BASED UPON SOME PRELIMINARY STRUCTURAL CONSIDERATIONS, RESULTING IN BLADE SR-7-1. (FIGURE 9.)

  - TWELVE BLADES REDUCED TO EIGHT TO PROVIDE A HIGH DEGREE OF CAPACITY FOR CARRYING 1P STRESSES

  - EIGHT BLADES ARE MORE STABLE THAN TEN (BASED UPON SR-3 AND SR-5 (Λ = 48°) MODEL TESTS)

- WE, THEREFORE, FELT THAT THE REDUCTION IN BOTH THE NUMBER OF BLADES FROM TWELVE TO EIGHT AND THE SWEEP TO 36° WAS NECESSARY.

- THE SR-7-1 WAS FURTHER MODIFIED THROUGH NUMEROUS ITERATIONS TO ACHIEVE BOTH STRESS AND CLASSICAL FLUTTER MARGINS. THESE MODIFICATIONS RESULTED IN BLADE SR-7-21. (FIGURE 9.)

SR-7 DESIGN STUDY
PROP FAN

	A/A tradeoff	SR-7-1 (Input to struct)	SR-7-21
Diameter (ft)	9.0	9.0	9.0
No. of blades	12	8	8
Activity factor	158.7	217	227
Integrated design C_L	0.214	0.214	0.214
Tip sweep (deg)	48.0	36	35.7
Blade layout	On helix	Off helix	Off helix

FIGURE 9.

- FIGURE 10 INDICATES THE SPECTRUM OF BLADE THICKNESS RATIOS THAT WERE INVESTIGATED IN DETERMINING AN ACCEPTABLE BLADE. THICKNESSES T1A AND T1B ARE OFFSHOOTS OF THICKNESS T1, WHICH IS OF THE T1, T2, T3 FAMILY OF BLADES.

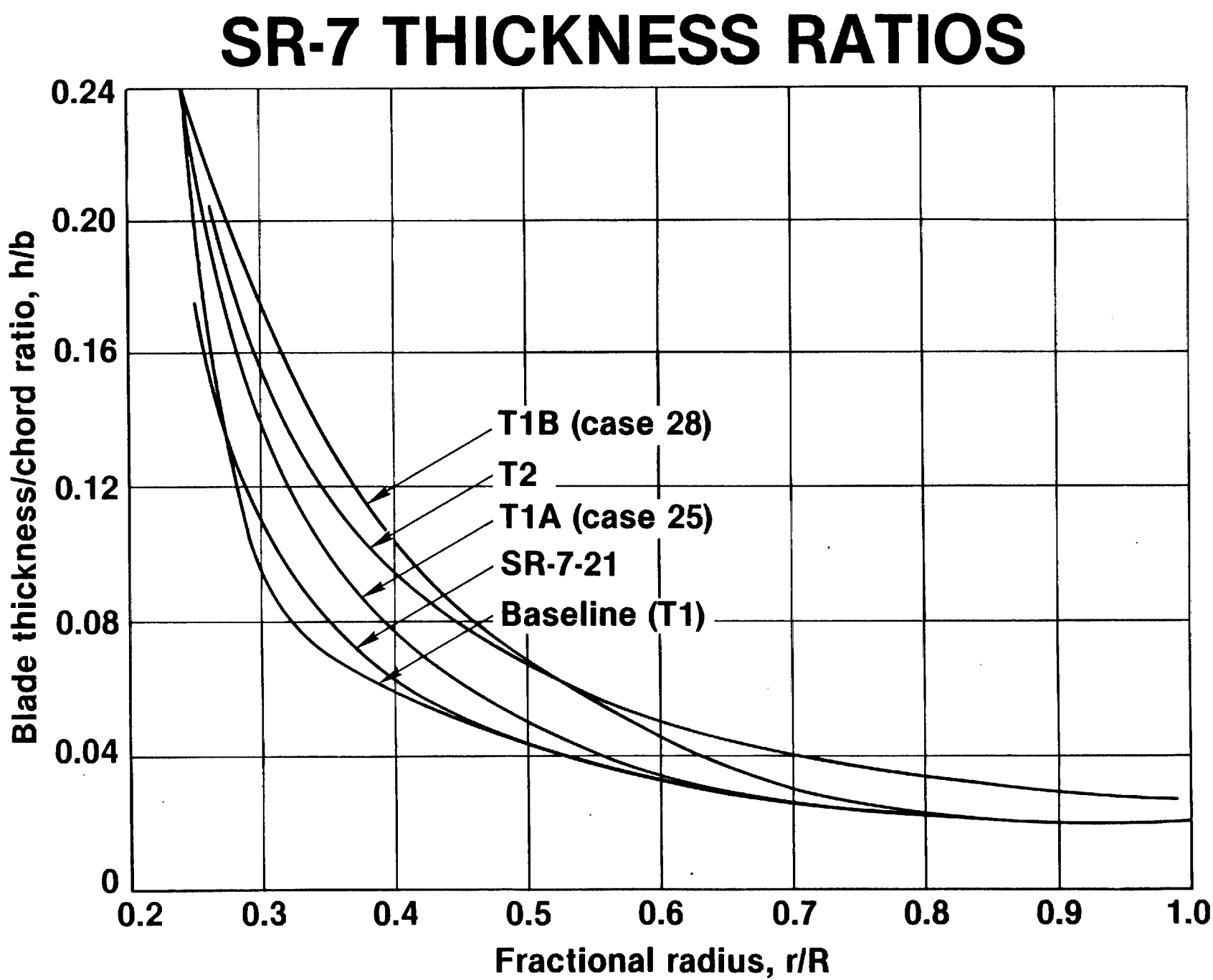
SR-7 THICKNESS RATIOS
Blade thickness/chord ratio, h/b
0.24
0.20
0.16
0.12
0.08
0.04
0
0.2
0.3
0.4
0.5
0.6
0.7
0.8
0.9
1.0
Fractional radius, r/R
T1B (case 28)
T2
T1A (case 25)
SR-7-21
Baseline (T1)

FIGURE 10

- FIGURE 11 DEPICTS THE COMPROMISES THAT WERE MADE FOR THE SR-7-21 DESIGN:

  - REDUCED TIP SWEEP

  - OFFSET DICTATED BY STABILITY

  - LOCAL INCREASE IN THICKNESSES

- FIGURES 12 - 16 INDICATE THE COMPARISON OF THE PLANFORM, OFFSET, SWEEP, BLADE CHARACTERISTICS AND SWEEP LINE COORDINATES, RESPECTIVELY, FOR THE SR-3 AND THE SR-7-21 BLADE CONFIGURATIONS. ALSO INCLUDED FOR REFERENCE IS THE SR-7 BASELINE.

COMPROMISES FOR SR-7-21 DESIGN

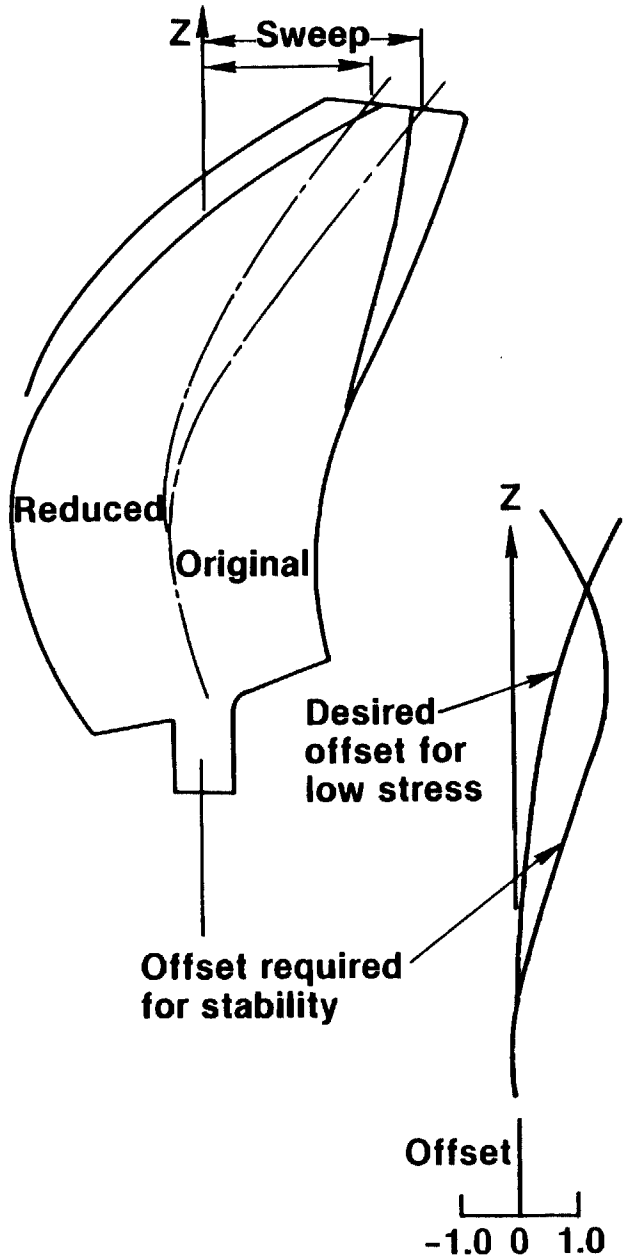

Tip speed reduced

Offset dictated by stability requirements

Thickness ratio increased slightly

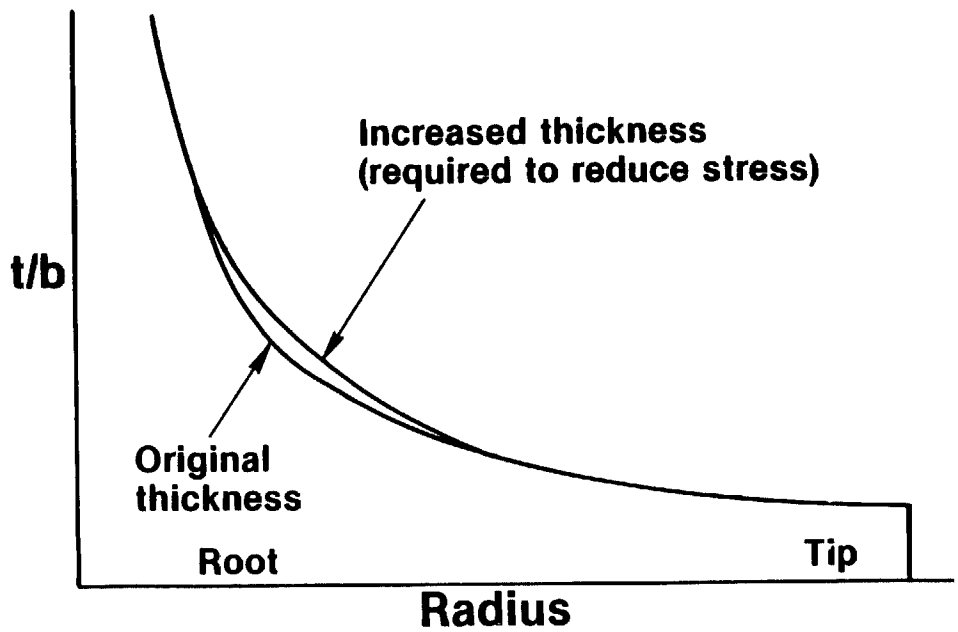

FIGURE 11

PLANFORM COMPARISON
(Aero-Acoustic Definition, No Cone Angle Shown)

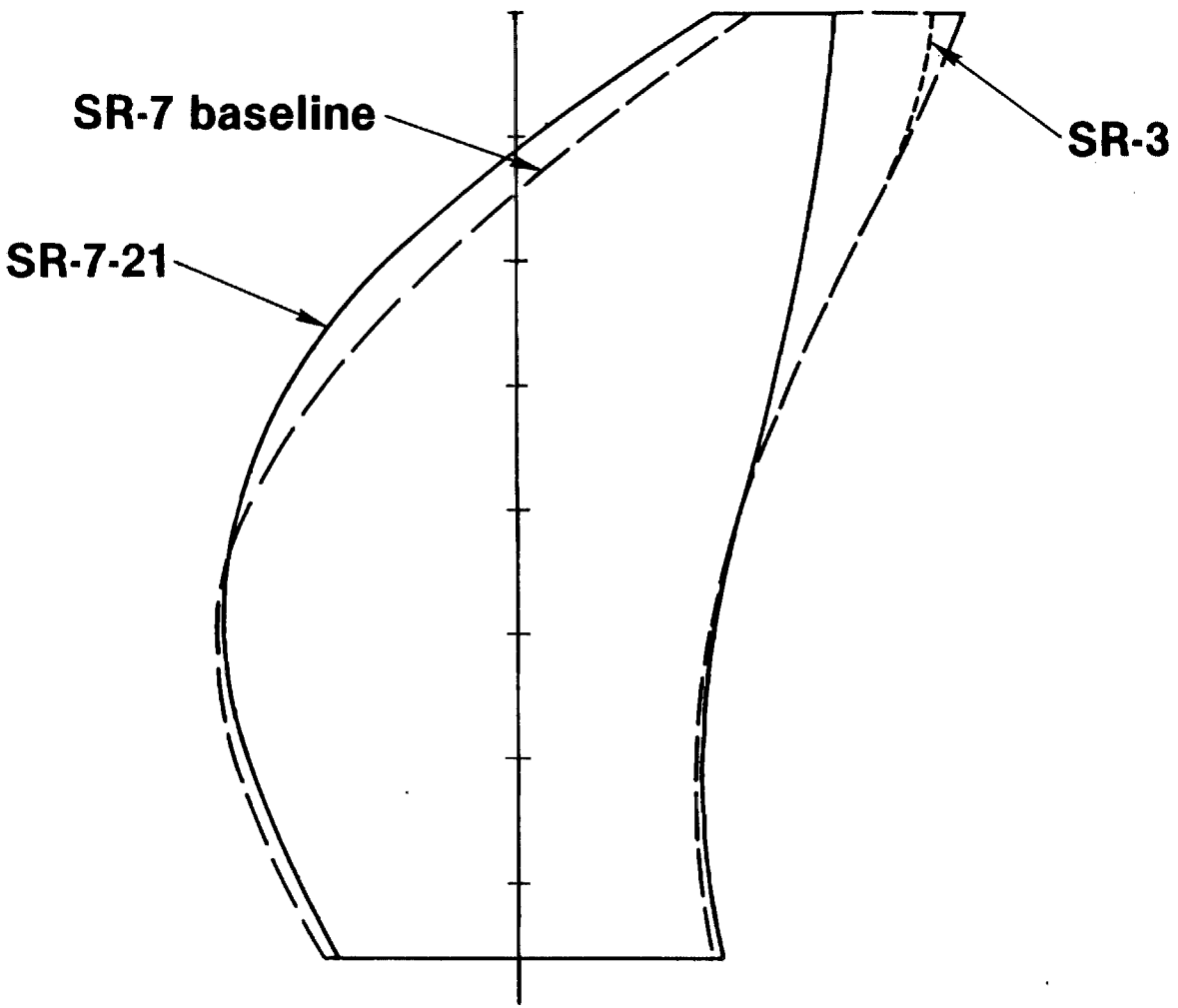

FIGURE 12

BLADE OFFSET COMPARISONS*

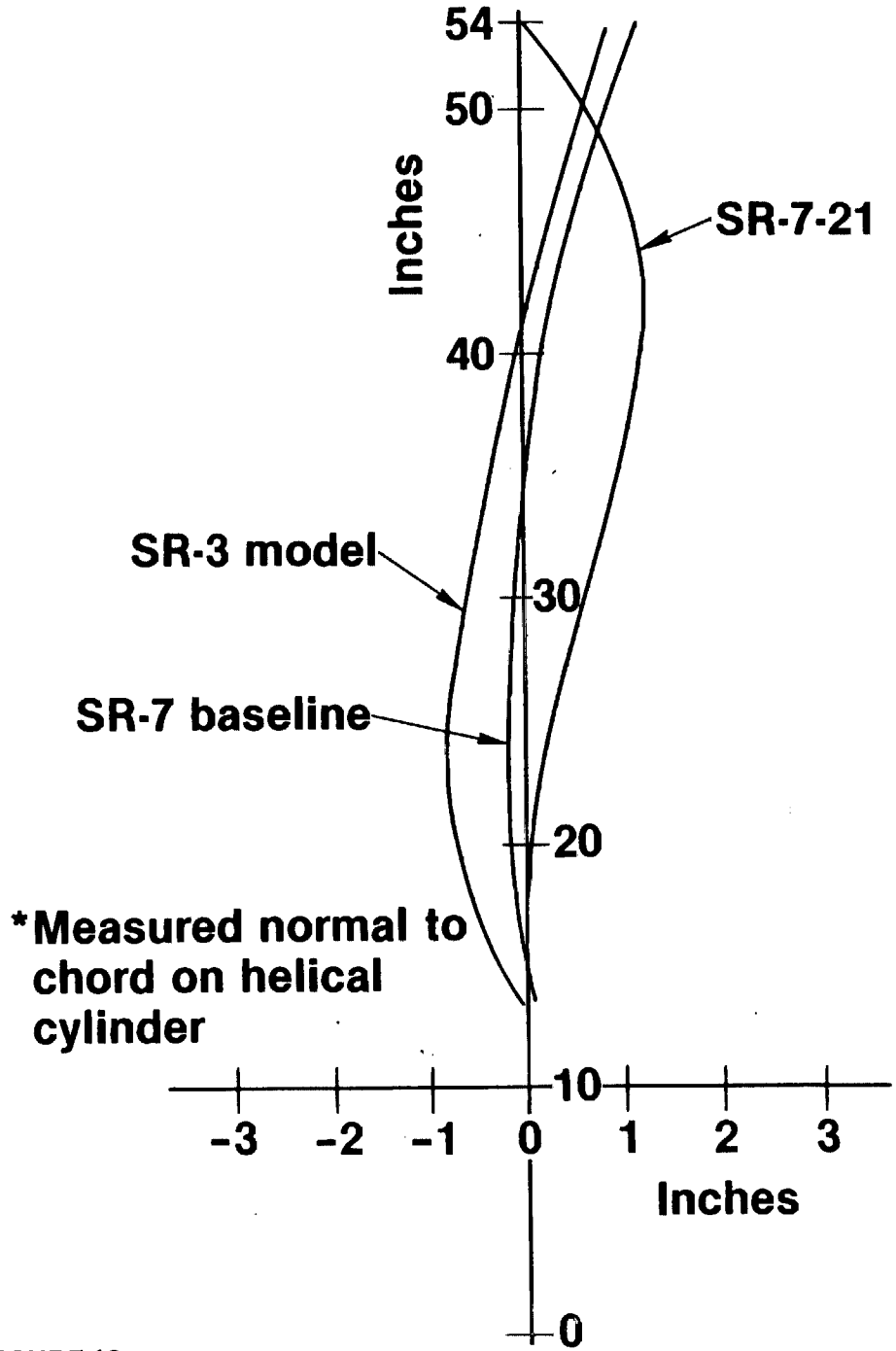

FIGURE 13

BLADE SWEEP COMPARISON*

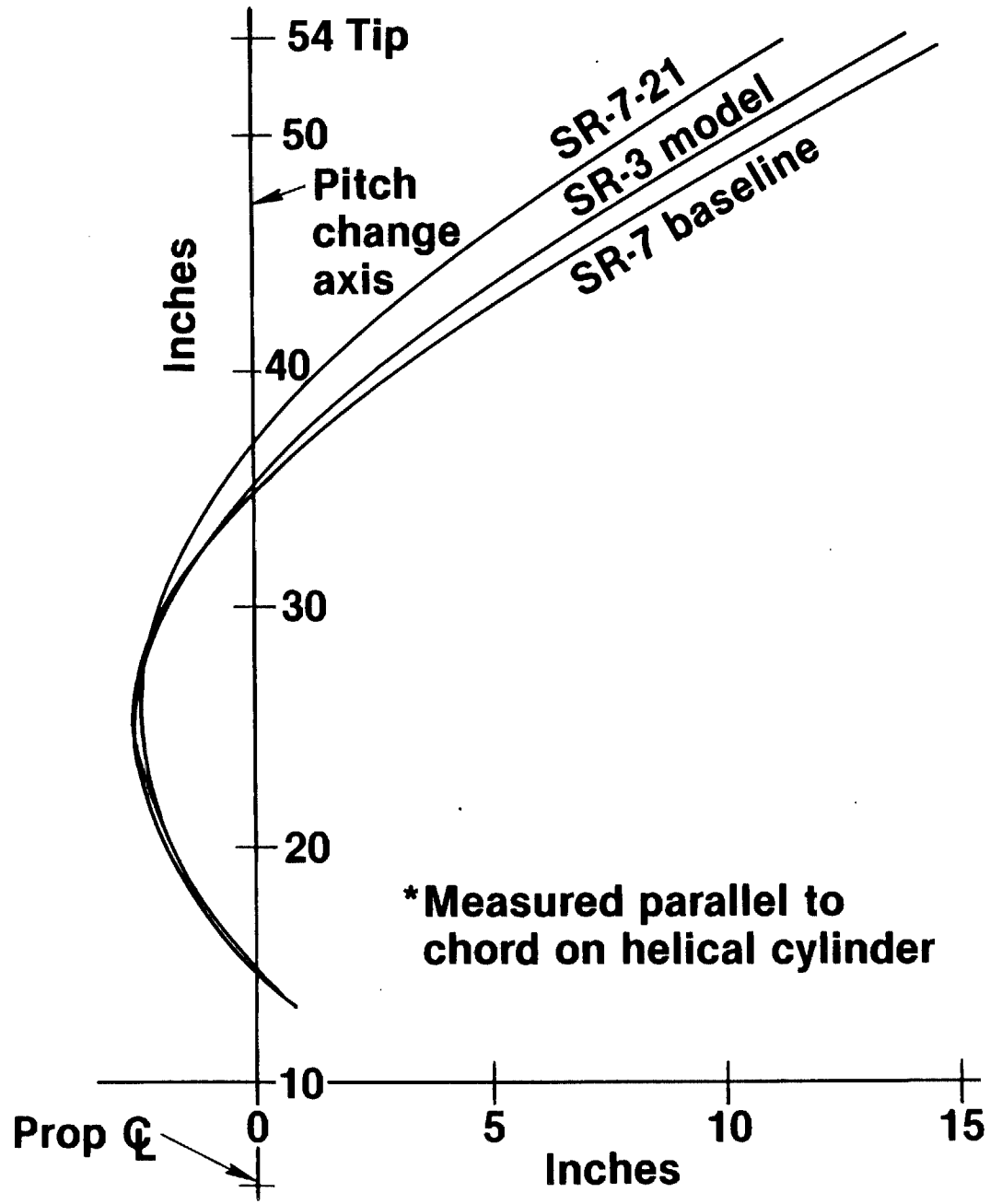

FIGURE 14

BLADE CHARACTERISTICS

SR-7-21 — 8 Blades
Dia = 9.0 ft.
AF = 224
C_{Li} = 0.214

SR-3 – – – 8 Blades
Dia = 24.5 in.
AF = 235
C_{Li} = 0.241

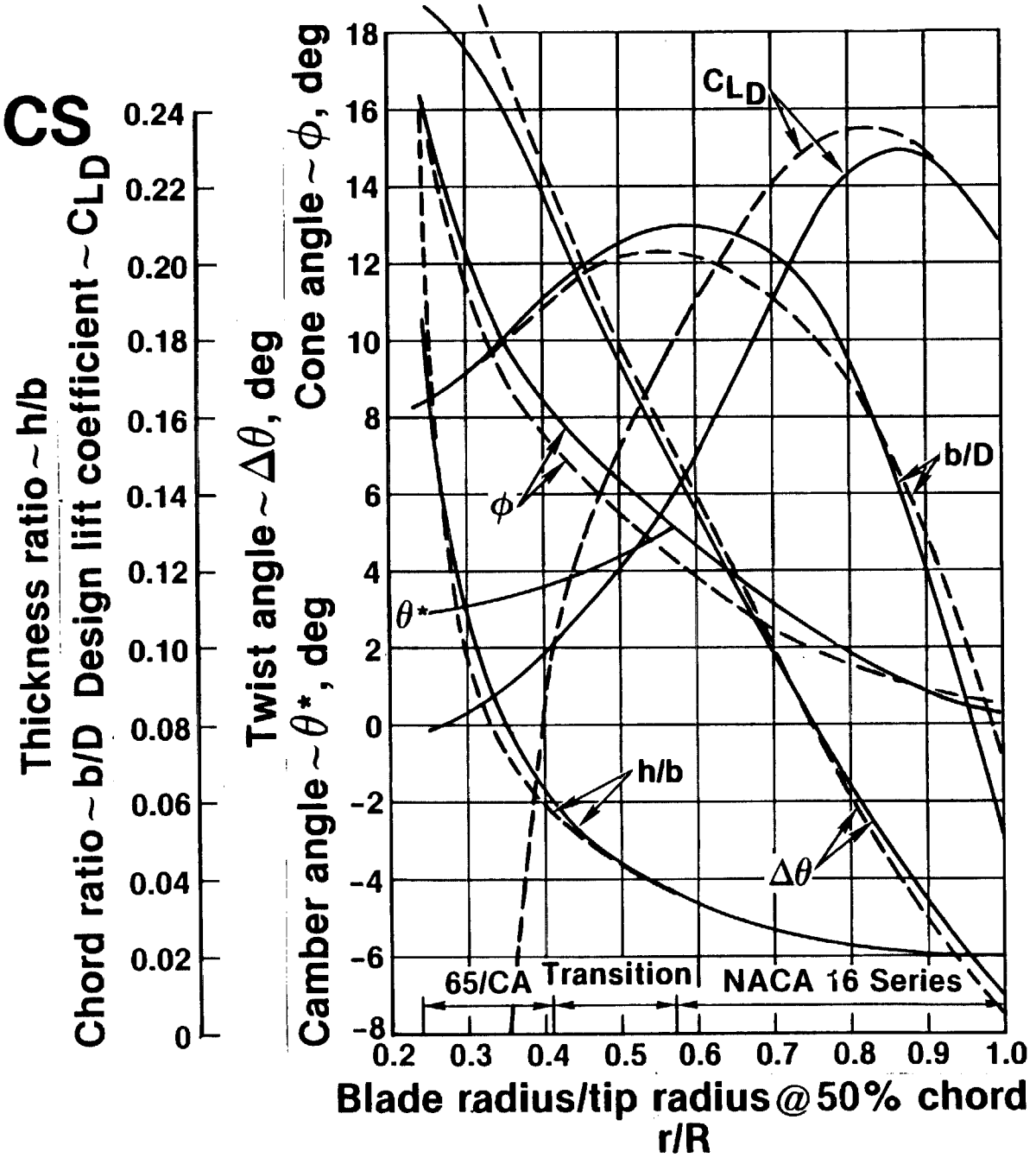

FIGURE 15

SWEEP LINE COORDINATES

SR-7-21 ——— 8 Blades
Dia = 9.0 ft.
AF = 224
C_{Li} = 0.214

SR-3 — — — 8 Blades
Dia = 24.5 in.
AF = 235
C_{Li} = 0.241

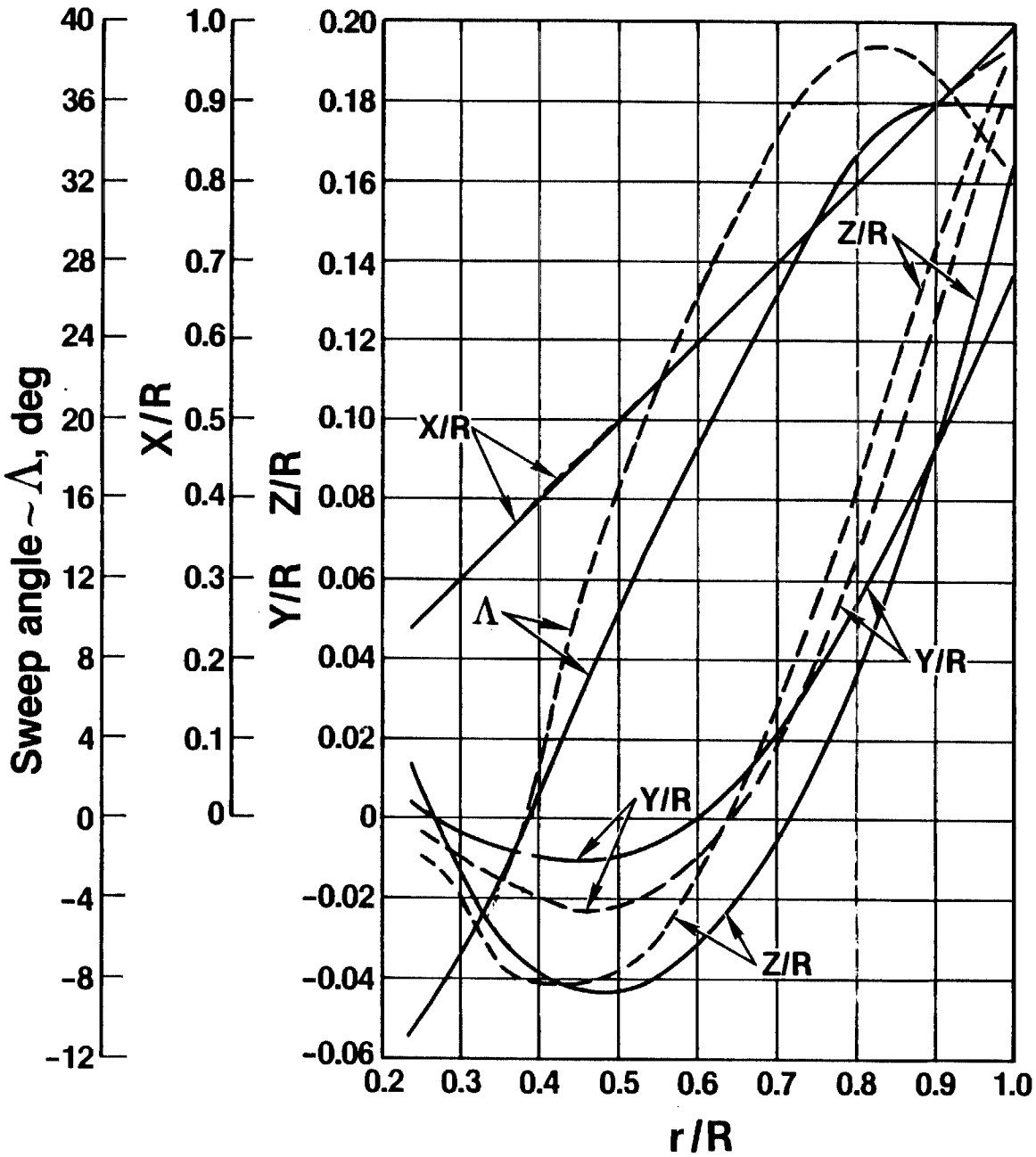

FIGURE 16

SR-7-21 PLANFORM VIEW

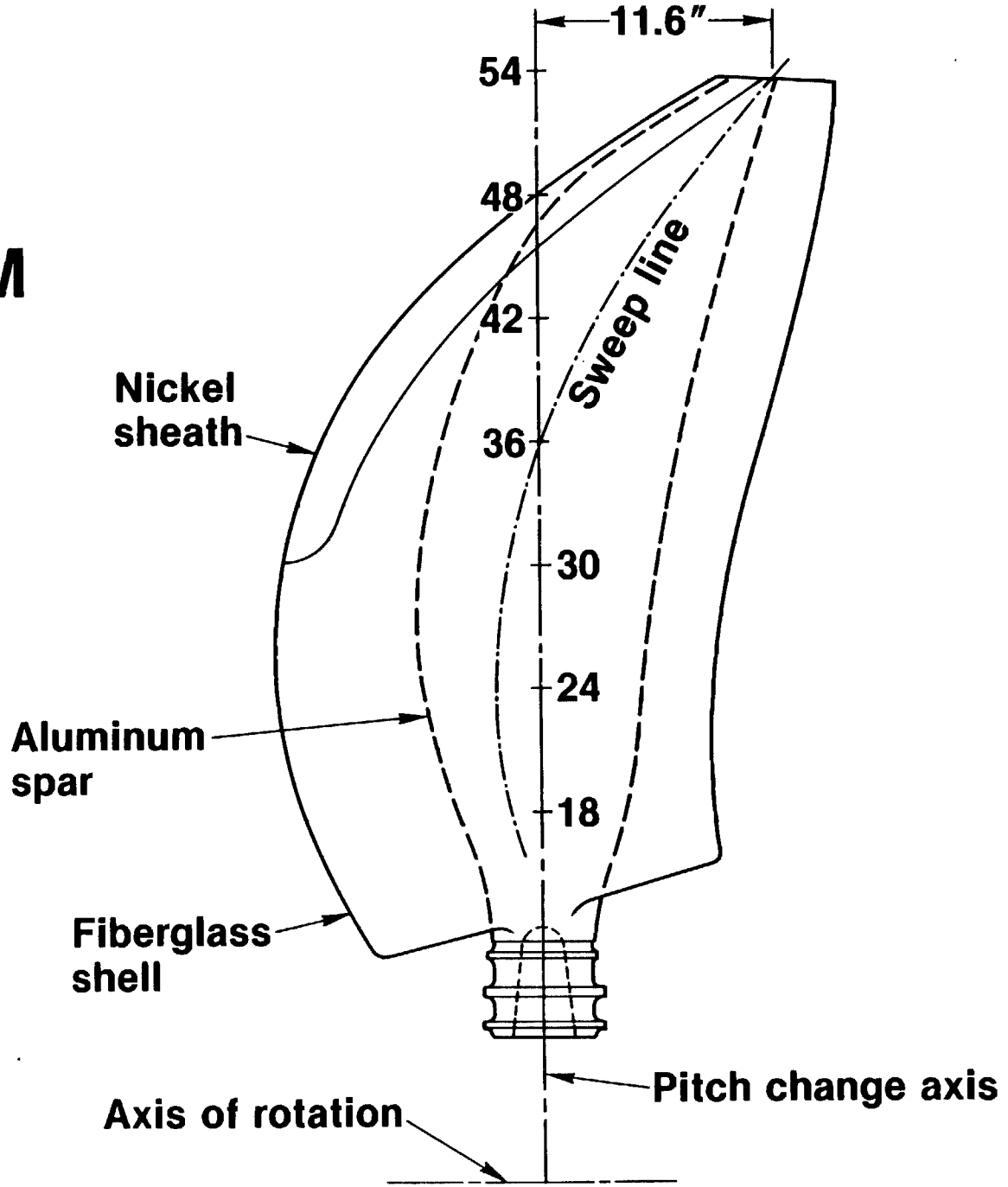

FIGURE 17

- FIGURE 17 DEPICTS THE SR-7-21 BLADE PLAN-FORM VIEW WITH THE SPAR LOCATION AND MATERIAL SELECTION INDICATED.

- AS INDICATED, THE BASELINE BLADE AND THE SR-3 BLADE ARE AERO-ACOUSTICALLY SIMILAR. (FIGURE 18.)

- FOR THE 0.8 Mn DESIGN CRUISE CONDITION, THE SR-7-21 (WHICH IS THE RESULTANT OF A BLADE MODIFICATION TO ACHIEVE BOTH STRESS AND CLASSICAL FLUTTER MARGINS) EXHIBITS A DROP IN EFFICIENCY OF 1.3 POINTS, AN INCREASE IN NOISE OF 1.4 dB, AND AN INCREASE IN FUEL BURN AND DOC OF 2.59% AND 1.39%, RESPECTIVELY, OVER THE BASELINE BLADE. (FIGURE 18.)

PERFORMANCE COMPARISON AT DESIGN CRUISE CONDITION

0.8 M_N /35,000FT/800fps/32 SHP/D^2

	SR-3	Baseline	SR-7-21
Efficiency, η_{NET}	0.796 (0.794)*	0.796	0.783
Noise, dB_{BPF} at 0.8D	143.6	143.2	144.6
Δ FB, %	-	0	+2.59
Δ DOC, %	-	0	+1.39
Sweep, deg	33	39.6	35.7

* Test

FIGURE 18.

- THE ESTIMATED BREAKDOWN FOR THE SR-7-21 PERFORMANCE LOSS AT Mn = 0.8, DUE TO INCREASED THICKNESS RATIO, MODIFIED PLANFORM, REDUCED SWEEP AND MOVING OF THE BLADE LAYOUT OFF THE HELIX CAN BE APPROXIMATED AS INDICATED IN FIGURE 19.

SR-7 PERFORMANCE LOSS BREAKDOWN (ESTIMATED)

0.8 M_N/35,000FT/800fps/32 SHP/D^2

	η	dB	FB	DOC
Baseline Prop-Fan	0.796	143.2	0.0	0.0
• Increased t/b	-0.004	-	+0.63	+0.30
• Modified planform	+0.001	-0.4	-0.45	-0.28
• Reduced sweep	-0.004	+1.2	+1.10	+0.68
• Off helix	-0.006	+0.6	+1.31	+0.69
SR-7 Prop-Fan	0.783	144.6	2.59	1.39

FIGURE 19.

- FOR THE 0.7 Mn DESIGN CRUISE CONDITION, IT CAN BE SEEN THAT THE SR-7-21 BLADE EXHIBITS A DROP IN EFFICIENCY OF 0.5 POINT, AN INCREASE IN NOISE OF 1.2 dB, AND A NEGLIGIBLE INCREASE IN FUEL BURN AND D.O.C. OVER THE BASELINE BLADE. (FIGURE 20.)

PERFORMANCE COMPARISON OF SR-7 WITH BASELINE ON 0.7 M_N AIRCRAFT AT DESIGN CRUISE CONDITION

(0.7 M_N /35,000FT/800fps/28 SHP/D^2)

	Baseline	SR-7-21
Efficiency, η_{NET}	0.824	0.819
Noise, dB_{BPF} at 0.8D	137.9	139.1
Δ FB, %	0	+0.75
Δ DOC, %	0	+0.36

FIGURE 20.

- FIGURE 21 INDICATES THE FUEL SAVINGS FOR BOTH A 0.8 Mn AND A 0.7 Mn PROP-FAN POWERED AIRCRAFT RELATIVE TO A TURBOFAN POWERED AIRCRAFT, USING THE SAME CARE TECHNOLOGY.

FUEL SAVINGS FOR PROP-FAN POWERED AIRCRAFT RELATIVE TO TURBOFAN POWERED AIRCRAFT WITH SAME CORE TECHNOLOGY*

35,000 FT/800 fps/500 NMi/60% payload

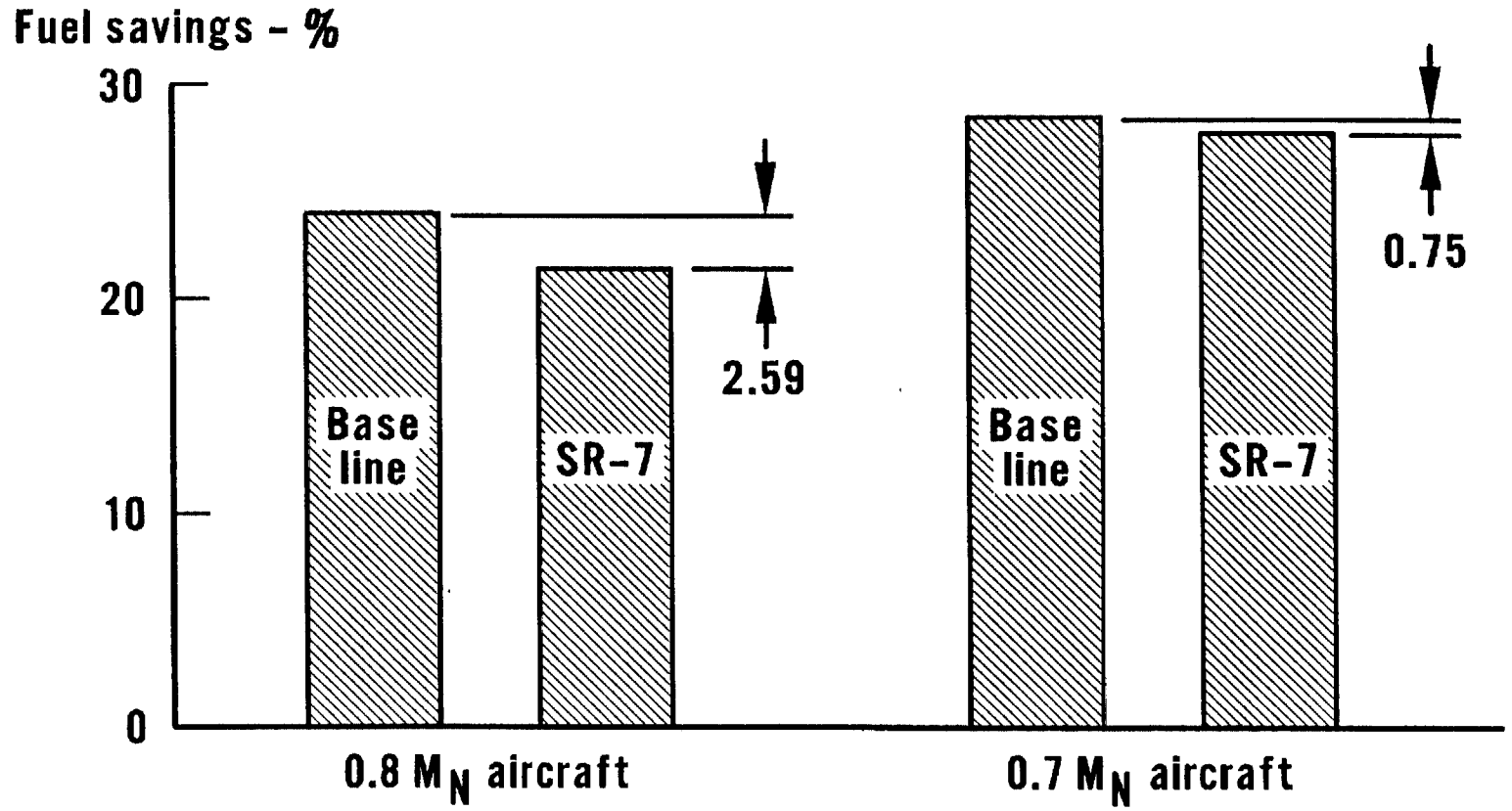

*LeRC ATP data

FIGURE 21.

- THE DESIGN CRITERIA RESULTED IN A BLADE EXHIBITING THE HIGHEST PERFORMANCE, AND AT THE SAME TIME WAS CONSISTENT WITH FREQUENCY PLACEMENT, STRESSING, FLUTTER MARGIN AND CURRENT MANUFACTURING TECHNOLOGY.

  THE BLADE WILL BE NEAR OPTIMUM, BASED UPON MATERIALS AND CONSTRUCTION, AND IS CONSISTENT WITH THE TECHNOLOGY FOR BUILDING PROPELLER BLADES WITHOUT INVOLVING H.S. IN A MATERIAL/FABRICATION DEVELOPMENT PROGRAM. (FIGURE 22.)

BLADE DESIGN CRITERIA

- Flutter free over flight envelope and at $M_N = 0.8$ in Modane
- Stress (steady + cyclic) less than design allowables for spar & shell
- Meet critical speed margins

OTHER CONSIDERATIONS

- Low deflection, FB, DOC

- High performance blade consistent with structural criteria and current manuf. technology

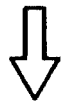

- Consistent with lap objectives

BLADE DESIGN CRITERIA

- FLUTTER FREE OVER FLIGHT ENVELOPE & AT M_N=0.8 IN MODANE
- STRESS (STEADY+CYCLIC) LESS THAN DESIGN ALLOWABLES FOR SPAR & SHELL.
- MEET CRITICAL SPEED MARGINS

OTHER CONSIDERATIONS

- LOW DEFLECTION, FB, DOC

- HIGH PERFORMANCE BLADE CONSISTENT WITH STRUCTURAL CRITERIA & CURRENT MANUF TECHNOLOGY

- CONSISTENT WITH LAP OBJECTIVES

SR-7-21 IS AN ADVANCED BLADE

- Offers high performance/low noise
- Uses key technologies
  - Sweep
  - Thinness
- Meets design criteria
- Acceptable for lap

FIGURE 23.

SR-7-21 IS BEST DECISION FOR LAP BLADE

- Safe design - meets criteria
  - Reasonable margins for P order response
  - Reasonable flutter margin. Stability very sensitive to blade deflection & mode shapes. Inaccuracies < 10% estimated
- Uses known mat'l/fabr technology

FIGURE 24.

RISK REDUCERS & SAFEGUARDS

- Stiffer composites improve flutter margin

- UTRC vacuum test, SR-3C & SR-7A programs provide earlier insight into SR-7L results

- Increased thickness improves flutter & response margins - can be added very late in program

FIGURE 25.

1. Report No.	2. Government Accession No.	3. Recipient's Catalog No.
CR 174993		

4. Title and Subtitle	5. Report Date
Large Scale Prop-Fan Structural Design Study Volume II - Preliminary Design of SR-7	6. Performing Organization Code 73030

7. Author(s)	8. Performing Organization Report No.
L.C. Billman R.M. Ladden J.E. Turnberg C.J. Gruska D.K. Leishman	HSER 11518
	10. Work Unit No.

9. Performing Organization Name and Address	11. Contract or Grant No.
Hamilton Standard Division United Technologies Corporation PO Box 1000 Windsor Locks, Connecticut 06096	NAS3-22394
	13. Type of Report and Period Covered Contractor Report
12. Sponsoring Agency Name and Address National Aeronautics and Space Administration Washington, DC 20546	14. Sponsoring Agency Code

15. Supplementary Notes

Project Manager, David A. Sagerser Advanced Turbo Prop Project Office NASA Lewis Research Center Cleveland, Ohio 44135

16. Abstract

In recent years, considerable attention has been directed toward improving aircraft fuel consumption. Studies have shown that the inherent efficiency advantage that turboprop propulsion systems have demonstrated at lower cruise speeds may now be extended to the higher speeds of today's turbofan and turbojet-powered aircraft. In order to achieve this goal, new propeller designs will require features such as thin, high-speed airfoils and aerodynamic sweep, features currently found only in wing designs for high-speed aircraft.

The purpose of the effort described in Volume I of this report was to establish structural concepts for such advanced propeller blades, to define their structural properties to identify any new design, analysis, or fabrication techniques which were required and to determine the structural tradeoffs involved with several blade shapes which were selected primarily on the basis of aero/acoustic design considerations. The feasibility of fabricating and testing dynamically scaled models of these blades for aerolastic testing was also established. In addition, the preliminary design of a blade suitable for flight use in a testbed advanced turboprop was conducted and is described in Volume II.

17. Key Words (Suggested by Author(s))

Prop-Fan
Blade
Structural Design

of this information in whole or in part. Date for general release August, 1989.

19. Security Classif. (of this report)	20. Security Classif. (of this page)	21. No. of Pages	22. Price*
		192	

[redacted]

NASA-C-168 (Rev 10-75)